Neuropilin-2 as a Novel Angiogenic Player:

Deciphering the contributions of neuropilin-2 during developmental and pathological angiogenesis

---

Christopher J. Benwell

A thesis submitted for the degree of Doctor of Philosophy (Ph.D.) in Biomolecular Science.

University of Easy Anglia
School of Biological Sciences

Quadram Institute Bioscience
Gut Microbes and Health

Abstract

Angiogenesis, the growth of neovasculature from pre-existing vessels, is driven by the stimulation of endothelial cells (ECs) by pro-angiogenic factors to invade the surrounding tissue and expand the vascular network. The extracellular matrix (ECM) component fibronectin (FN), and its canonical receptors, α5β1 and αvβ3 integrins are upregulated on angiogenic vasculature. Historically, the selective targeting of these FN receptors was postulated to provide directed anti-angiogenic therapy against pathologies typified by uncontrolled vascular growth such as cancer and retinopathy. Genetic ablation of these integrins however, proved not to inhibit the development of excessive vascularisation, and in some cases even accelerated the pathological phenotype. It is now believed that the failure of such integrin-based therapies can be attributed to the action of VEGF co-receptors, such as neuropilin-1 (NRP1) and neuropilin-2 (NRP2), to rescue and promote a pro-angiogenic phenotype. Unlike NRP1, far less is known about NRP2's role in microvascular ECs during angiogenesis, and therefore we sought to characterise NRP2's interaction with α5β1 integrin in ECs and investigate whether a dual contribution with NRP1 exists to promote developmental and pathological angiogenesis. To achieve this, we implemented siRNA-mediated depletion *in vitro*, and developed and employed genetically modified mouse models (GEMMs) *in vivo* to study the angiogenic consequences of inducing EC specific deletion of NRP2 alone, or in tandem with α5 integrin or NRP1. Our results indicate that NRP2 promotes polarised EC migration and adhesion to FN by directing the cellular trafficking of α5 integrin-phospho-focal adhesion kinase (*p*-FAK) complexes in a Rab11-dependent manner. By utilising both physiological and pathological models of angiogenesis, we also provide evidence that NRP2 promotes the formation of stable cell-matrix interactions to facilitate tip cell sprouting in the postnatal retina, and is essential for tumour vascularisation. In addition, by targeting both endothelial NRPs we were able to successfully arrest tumour angiogenesis completely.

Contents

List of figures

List of tables

Acknowledgements

It would not have been possible to write this doctoral thesis without the support and encouragement selflessly given by so many in my life, for which my mere expression of gratitude will never suffice. I will, nevertheless, attempt in this section to thank those closest to me, and those who have made my PhD one of the most rewarding experiences of my life so far.

First and foremost, I would like to thank my parents, for all you do for me, I am the person I am today thanks to your unequivocal love and support. It is to you both that this thesis is dedicated, for without your unwavering dedication to me and my aspirations, I would have fallen short in so many avenues of my life. To Dan, no doubt that this piece of work comes as a direct result of striving to improve in everything I do, a quality I owe to always being able to look up to a big brother.

The Robinson lab, past and present, are without doubt a wonderful group of individuals, all of whom I have the privilege to call my good friends. Dr Stephen Robinson, I could not wish for a kinder, more caring PhD supervisor than you. Never once pushing unnecessary deadlines, or putting your own needs above ours, your ability to motivate us all through words of encouragement (and supplies of coffee) is what makes you both a great boss, but also a loved one. Alastair Mckee, James Taylor and Dr Wesley Fowler, time spent around you never felt like work at all. Always up for a coffee break, or to converse entirely in Lord of the Rings quotes, half my day was usually spent doubled over laughing, over the most random of things. Chris Price, (other Chris), your dedication to your work, the guild of magicians, and to the humble chicken goujon wrap is something to be admired, I wish you all the best for your final year. Alicia Nicklin, although you are only just beginning your PhD, it is obvious already that you have a bright career in research, should you wish to pursue it. Good luck for the years to come! Thank you to Nancy Teng for always being a bright and cheerful presence in the lab. Dr's Rob Johnson, Alex Gontarczyk, Jordi Lambert, and Kate Makin, thank you for all of your help throughout my first and second years, you always found the time to answer my steady stream of questions, despite being busy yourselves. All of your shared input into my work has proven invaluable. Dr Sally Dreger, thank you for all the help you have given me over the course of my PhD, and for all you do for the lab to run smoothly, including the regular bringing in of cake! And finally, Dr Abdullah Alghamdi, you were the first to welcome me into the lab, and to offer your help. I hope I have done justice to your story, and to your highest of standards.

I would also like to take this opportunity to thank Professor Samuel Fountain, for all of your feedback and critique over the years, you helped me take ownership of my project, and to appraise

my work with the same steely consideration as you did. Your guidance on how to progress my research always gave me the confidence to push forward.

Finally, I would like to thank my beautiful girlfriend and best friend, Mia, your love and support throughout is something I will always be thankful for. Despite often finding yourself snowed under with your own work, you put mine first, always stopping to listen, to offer advice, or share in my excitement when I found myself thinking aloud or when an experiment yielded a new, interesting result. Keep being brilliant, that which you can never accept you are.

1 Introduction

1.1 Preface

Angiogenesis is the process by which new blood vessels form from pre-existing vasculature. Its regulation is essential during both embryonic and postnatal development, in addition to the maintenance of healthy physiological processes. Its dysregulation however, can contribute to the progression of a series of pathologies, including cancer, diabetic retinopathy and chronic wound healing. This thesis will initially examine how two endothelial receptors: neuropilin-2 (NRP2), and α5β1 integrin interact in the presence of a FN-rich extracellular matrix (ECM) to regulate key angiogenic mechanisms. Whilst NRP2 and α5β1 integrin have already been reported to interact, their dual contributions during angiogenesis are largely undescribed. The existence of a complex tripartite interaction between NRP2, α5β1 integrin and neuropilin-1 (NRP1) in coordinating developmental and pathological angiogenesis will then be considered. The subsequent introduction will discuss what is currently known about these receptors and their roles in mediating angiogenesis, starting with an overview of the vascular system itself.

1.2 The vascular system

The vascular system is the first organ to develop during embryogenesis [1] and can be subdivided into four dynamic and multifunctional components: the arterial, capillary, venous and lymphatic systems. The arterial, capillary and venous circuits, the foci for this report, are often preferentially defined as the cardiovascular microcirculation, which serves as the major zone of exchange between the circulating blood and the peripheral tissues in the body [2]. As such, embryo development is intrinsically linked to the ability for the cardiovascular microcirculation to expand and mature, enabling oxygen and nutrient transport, immune and mechanical function [3], [4].

In the cardiovascular system, blood circulates via a 'closed loop' through two circulatory systems, systemic and pulmonary. In this process, deoxygenated blood residing in the heart is pumped from the arteries to the arterioles, and then into the lung capillaries of the pulmonary system to be oxygenated. Radiating vessels then supply the organs and tissues of the body with oxygen and nutrients whilst simultaneously allowing for the secretion of metabolic waste products, such as carbon dioxide (CO_2). Blood is subsequently returned to the heart though the venules and veins of the systemic circulatory system.

As conduits of the cardiovascular system, blood vessels mediate blood flow throughout the body, but also perform discrete physiological functions suited to the needs of the tissue they reside in. That being said, the vast majority of vasculature is composed of three histological layers: the tunica intima, the tunica media and the tunica adventitia. The innermost layer, the tunica intima, consists of a single endothelial monolayer stabilised by a basement membrane (BM). The tunica media is located between the tunica intima and the outermost layer and is composed of organised layers of vascular smooth muscle cells (VSMCs) and elastic fibres. Finally, the tunica adventitia is the outermost layer, consisting of fibro-elastic connective tissue that acts to strengthen the vessel and anchor it to the surrounding tissue. Whilst capillaries are composed only of the tunica intima, supported only by associated pericytes, larger vessels are composed of all three layers to support the high-pressured flow-through of blood, particularly through the arterial vessels [4], [5] (**Figure 1.1**).

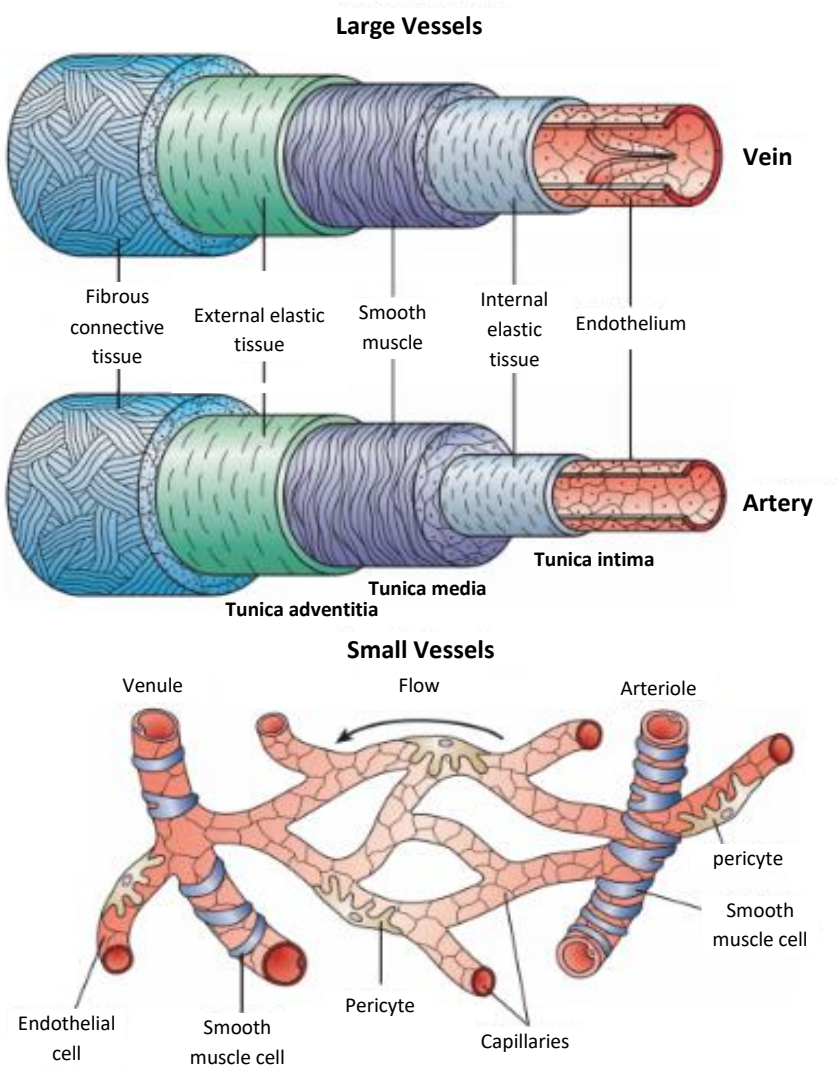

Figure 1.1 Vessel architecture of the cardiovascular system. Vessels of the cardiovascular system are mainly comprised of three histological layers: the tunica intima, the tunica media and the tunica adventitia. The innermost layer, the tunica intima, is composed of a layer of ECs, a basement membrane and an internal elastic layer. In comparison, the tunica media is composed of multiple layers of VSMCs and elastin, whilst the tunica adventitia is composed of an external fibro-elastic connective tissue layer. Whilst capillary vessels only consist of the tunica intima, large blood vessels (arteries, arterioles, veins and venules) consist of all three layers (Figure adapted from [5]).

1.3 The endothelium and the endothelial extracellular matrix

The innermost layer of all blood vessels, the tunica intima, consists of a single endothelial monolayer stabilised by an underlying BM. This monolayer is composed of endothelial cells (ECs), which whilst are typically inert in large vessels, are highly dynamic in capillary vessels, mediating the exchange of oxygen and nutrients to the surrounding tissues. Their ability to undergo significant structural remodelling also enables ECs to respond to angiogenic cues, for example hypoxia [6]. Despite exhibiting a certain degree of homology, ECs across the vascular system are remarkably heterogeneous in their structure and function. Most noticeably at the morphological level, the endothelium can be sub-divided into three types: continuous, fenestrated, or discontinuous, each suited to regulating the passage of different macromolecules to and from the blood [7]. More recently however, studies have also considered that different organ-specific EC populations exhibit discrete metabolic rates and angiogenic potentials [8].

Supporting the endothelium is the endothelial extracellular matrix (ECM), which can be classified into two distinct compartments: the BM and the interstitial matrix (IM). Forming sheet-like structures that lie directly beneath the endothelium, the BM is composed of type IV collagen, laminin, nidogen and heparan sulphate proteoglycans, and is the primary anchor point for quiescent ECs [9]. Upon receiving pro-angiogenic signals however, the BM matrix is degraded, allowing ECs to extravasate and adhere to the IM, which is found in the interstitial space between cells and mainly composed of fibrillar collagens and glycoproteins such as fibronectin (FN). Once adhered, ECs can then migrate over the IM towards the angiogenic stimuli [10].

1.3.1 Fibronectin

FN is a ubiquitous ECM glycoprotein that is secreted and assembled into fibrillar matrices in all tissues, mediating communications between the intra and extracellular environment [11]. Composed of two homologous ~250 kDa subunits that are linked by a pair of disulphide bonds near the C-terminus, each subunit comprises of a series of repeating domains that dictate fibril elasticity and mechanical stability. The vast majority of these domains are constitutively contained within the mature FN structure, however specific ligand affinities can be affected by alternative splicing of the FN gene [12], [13]. Indeed, alternative splicing results in the formation of two major FN isoforms, extra domain-A (EDA)-containing FN (EDA-FN), and extra domain-B (EDB)-containing FN (EDB-FN). The FN gene can also undergo splicing at its variable (V) region, during which the V domain undergoes either partial inclusion or exclusion, also known as exon subdivision [13].

These FN isoforms are commonly classified into two groups; soluble plasma FN (pFN) which is synthesised by hepatocytes in the liver [14], and circulates through the blood, and cellular FN (cFN). Whilst pFN usually lacks EDA- and EDB-FN sequences, cFN constitutes a more heterogeneous variety of splice variants, including EDA-, EDB-FN and V region isoforms [12], and is commonly overexpressed in numerous cancer subtypes to promote matrix stiffness [15], [16].

1.4 Development of the vascular system

The formation of a vascular network in the developing embryo is implemented by two distinct events, vasculogenesis and angiogenesis. In the following sub-sections, the mechanisms of both will be outlined and discussed.

1.4.1 Vasculogenesis

Vasculogenesis, the formation of *de novo* blood vessels, occurs during embryogenesis and establishes the first primitive vascular plexus inside the embryo and its surrounding membranes [17]. This occurs by the *in-situ* differentiation of mesodermal derived hemangioblasts into hematopoietic stem cells (HSCs) and angioblasts, the progenitors of ECs [18]. Following the migration of angioblasts to distant sites throughout the embryo, they aggregate to form endothelial tubes, which give rise to primitive arteries and veins. This initial vascular network then undergoes significant remodelling via processes of angiogenesis and vessel regression, establishing the complex vascular networks required to sustain the body [1], [19].

1.4.2 Angiogenesis

Angiogenesis is the growth of new blood vessels from the pre-existing vasculature. Whilst vasculature is typically quiescent in adults, angiogenesis is essential during development, and is activated to maintain healthy physiological processes, and under pathological conditions such as during the re-vascularisation of tissues following an injury, diabetic retinopathy, or tumour growth [20]–[22]. During embryonic development, vasculogenesis occurs, whereby a primitive vascular network is laid via the *in-situ* differentiation of pluripotent mesenchymal progenitors [1], [23]. Subsequently, new blood vessels grow from sprouting capillaries derived from this vascular network toward an ischemic region deficient in oxygen. This process, termed angiogenesis, is orchestrated by the activation, proliferation and migration of ECs, which mediate vessel sprouting, remodelling and growth [21]. The establishment of new blood vessels requires ECs to be able to respond to a wide variety of extracellular signals that activate receptors responsible for growth, differentiation, adhesion and migration [24]. With its central roles in development and wound healing, in addition to being implicated in a range of diseases, delineating the control mechanisms behind the angiogenic cascade has extensive therapeutic capacity.

1.4.2.1 The angiogenic cascade

Vessel quiescence is maintained by the activity of mural cells, namely vascular smooth muscle cells (vSMCs) and pericytes, found ensheathing the vascular network. In addition to providing mechanical support to the vessel, mural cells also mediate the formation and maintenance of tight junctions in the endothelium by promoting the expression of endothelial barrier proteins such as VE- and N-cadherins, and claudins [25]. As such, mural cells play an essential role in modulating adherens junction stabilisation to regulate vascular permeability [26], [27].

Quiescence is alleviated following the detection of pro-angiogenic stimulation by ECs. For example, upon the accumulation of hypoxia inducible factors (HIFs) within hypoxic tissues, growth factors such as vascular endothelial growth factor (VEGF) and fibroblast growth factor (FGF) are expressed and released (VEGFs are discussed in detail in chapter 1.5) [28]. Following such stimulation, ECs begin to preferentially express angiopoitin-2 (ANG-2) which competitively antagonises complex binding between angiopoietin-1 (ANG-1) and endothelial tyrosine-protein kinase receptor-2 (Tie-2). This sequestration of Tie-2 away from ANG-1 by ANG-2 subsequently stimulates the detachment of pericytes from the vessel, enabling the increase in vascular permeability required to promote ECM remodelling [29]. During this remodelling phase, the increase in vascular permeability elicited by pericyte detachment enables the secretion of matrix metalloproteinases (MMPs) from ECs. MMP-mediated proteolysis of the BM then allows ECs to dissociate and proliferate to form sprouts that migrate into the IM away from the existing vessel along an angiogenic signalling gradient [30]–[32].

ECs in the nascent sprout adopt two discrete cellular phenotypes, tip and stalk cells. Located at the end of vascular sprouts, tip cells are characterised by long and dynamic filopodia that mediate their highly migratory behaviour. By integrating certain directional cues, for example a hypoxic environment, tip cells are responsible for defining the route along the new, angiogenic-competent, matrix. Following the tip cell are stalk cells, which are highly proliferative and function to establish adherent and tight junctions to stabilise the new sprout as it forms the vascular lumen [29], [32], [33]. To moderate the angiogenic response to pro-angiogenic stimulation, and thereby to prevent hypervascularisation of tissues, differentiation into tip cells is tightly regulated by competing VEGF/Notch-Delta-like-ligand-4 (DDL-4) signals [34]. Upon VEGF stimulation, DLL-4 becomes expressed on the surface of ECs and activates Notch-1 receptor on adjacent stalk cells. Notch-1 signalling subsequently supresses vascular endothelial growth factor receptor 2 (VEGFR-2) and neuropilin-1 (NRP1) expression to prevent VEGF-induced tip cell characterisation in stalk cells. In

addition, the expression of Jagged-1 receptor on the surface of stalk cells inhibits the membrane localisation of Notch-1 in tip cells, further defining their distinction from their counterparts [35], [36].

The process of two migrating tip cell sprouts joining to form a loop in the perivascular stroma is termed anastomosis, and is mediated by macrophage activity to promote the formation of new VE-cadherin^{+} tight junctions [37]. As the new vessel perfuses, nutrient exchange and oxygen transfer reduces the expression of VEGF, restoring homeostasis in the vessel microenvironment, and removing the angiogenic stimulus. In response, PDGFβ and TGF-β are secreted by ECs, stimulating the recruitment of overlaying pericytes that provide physical stabilisation of the newly fused loop. Concomitantly, collagens IV, XV and XVIII are synthesised to establish the new extracellular basement membrane [38], promoting vascular quiescence and inducing the expression of tissue inhibitors of MMPs (TIMPs) to relieve any further ECM degradation. The differentiation into venous and arterial vasculature is subsequently coordinated by repulsive ephrin-Eph receptor interactions, defining the spatial boundaries of the developing vascular bed (**Figure 1.2**) [33], [39]–[42].

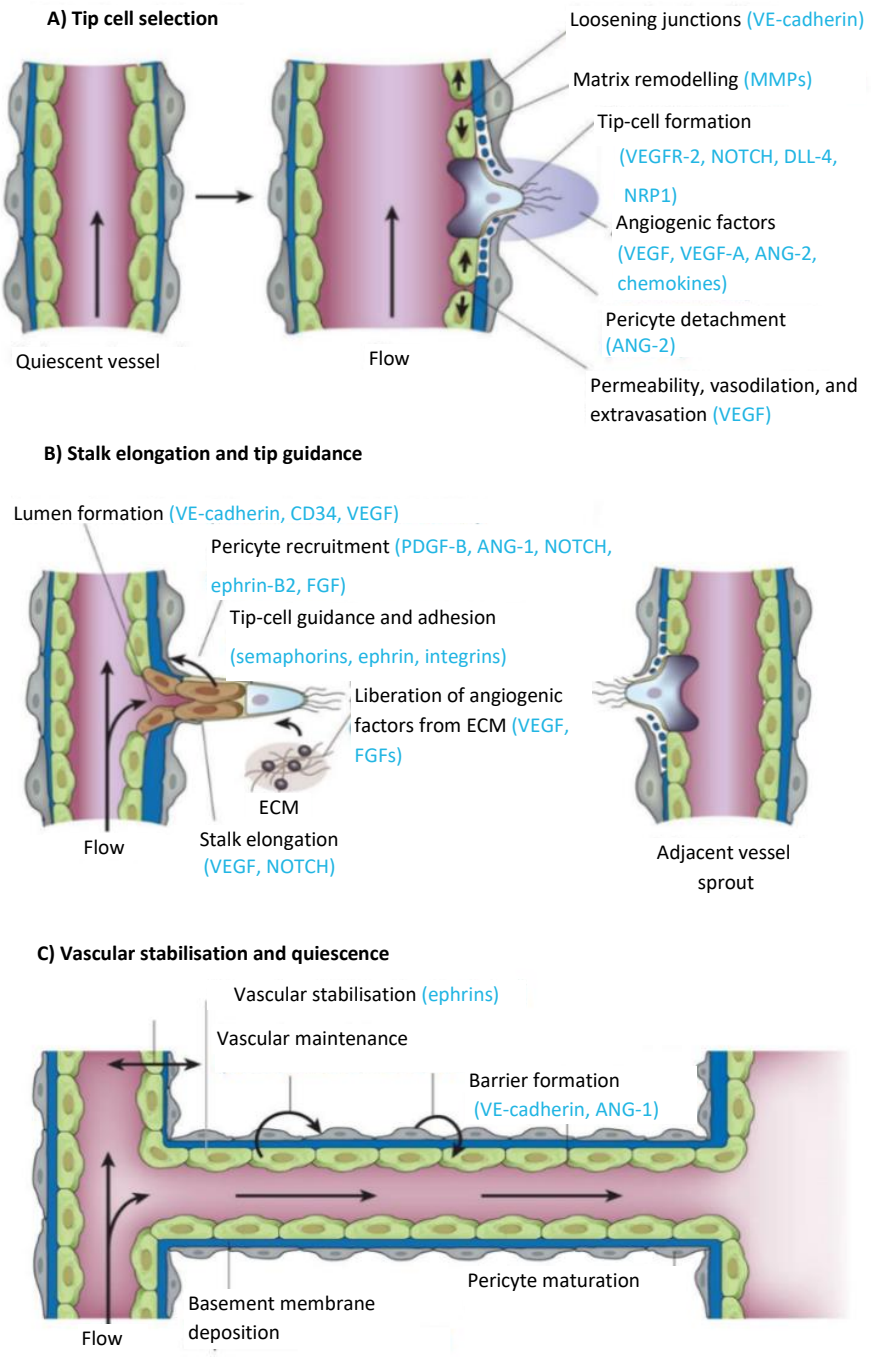

Figure 1.2 Angiogenic vessel remodelling. A) Selection of tip cells: angiogenic activating signals induce BM remodelling via MMP-mediated proteolysis, ANG-2 mediates pericyte detachment, ECs dissociate and proliferate to form sprouts, and a tip cell is selected via integrated VEGFR-2/Notch-DLL-4 signalling. **B**) Stalk elongation and tip guidance: continued angiogenic signals guide the tip cell, whilst supporting stalk cells remodel the ECM. **C**) Vascular stabilisation and quiescence: two tip cells meet, ephrins mediate vascular differentiation and stabilisation, a new BM is deposited by ECs lining the nascent vessel, and pericytes are recruited to restore quiescence (Figure adapted from [29]).

1.5 VEGFs and VEGFRs: principal regulators of angiogenesis

Whilst numerous molecules play a role in regulating angiogenesis, VEGF-VEGF receptor (VEGFR) signalling is customarily considered its principal driver. Following the onset of hypoxia, accumulating HIFs complex with HIF-1b to become a transcription factor for the pro-angiogenic growth factor VEGF. As a result, the expression of VEGF is upregulated 30-fold, restoring normoxia to the affected tissue through interactions with associated VEGFRs present on the endothelial cell surface [29], [43].

VEGF-A is the best characterised of the VEGF family members and is the most widely described soluble factor with roles regulating angiogenesis [22], [44]–[46]. VEGF-A can exert the activation of various downstream pro-angiogenic signalling cascades by interacting with high affinity to two transmembrane bound cell surface receptor families; the VEGFR family of tyrosine kinase receptors, notably VEGFR-1 and VEGFR-2, both of which are selectively expressed on vascular ECs, or the neuropilin (NRP) family of receptors, NRP1 and NRP2 [29], [47]. In vertebrates, VEGF-A is broadly expressed, and confers a crucial role not only in the formation, maintenance and function of the vascular system, but also in other organ systems, including the central nervous system (CNS) and during lung and liver development [48]. It is unsurprising therefore, that early *in vivo* mouse studies report the genetic deletion of even a single allele of the VEGF-A gene to cause embryonic lethality at embryonic day 9.5 (E9.5), resulting from severe vascular defects, impaired blood-island formation, and cardiovascular abnormalities [45], [49]–[52]. Initiation of the VEGF signalling pathway is promoted upstream by the FOXF1 protein via direct transcriptional activation. Predictably, conditional knockdowns of the *foxf1* gene were also demonstrated to elicit an embryonic lethal phenotype with analogous growth retardation, cardiac hypoplasia and vascular abnormalities to mouse embryos lacking the VEGF-A allele. Depletion of FOXF1 protein from ECs in culture was also shown to reduce EC proliferation and abrogate VEGF signalling, emphasising the essential role of VEGF-A in developmental angiogenesis [53].

VEGFR-2 is recognised as the principle VEGF receptor for mediating the pro-angiogenic effects of VEGF-A [54], and is known to induce capillary sprouting and endothelial tube formation [55]. Binding of VEGF-A to the extracellular domain of its cognate VEGF receptor initiates receptor homodimerization or heterodimerization, and subsequently the trans-autophosphorylation of numerous tyrosine (Tyr) residues within the receptor's intracellular tyrosine kinase domain, including: Tyr^{951}, Tyr^{1054}, Tyr^{1059}, Tyr^{1175} and Tyr^{1214}. In response, a cascade of downstream signalling is initiated, responsible for mediating pro-angiogenic processes such as cell proliferation, migration

and survival [56]. This occurs both via the activation of VEGFR-2's kinase domain, but also through SRC homology 2 (SH2) domain-mediated recruitment of signalling and scaffolding molecules to VEGFR-2's cytoplasmic tail. The downstream activation of signalling pathways such as the extracellular signal-regulated kinase (ERK)/mitogen-activated protein kinase (MAPK) pathway to promote EC proliferation, the phosphoinositide-3 kinase (PI3K)/Akt pathway to promote EC survival and the Src/focal adhesion kinase (FAK) pathway to promote EC migration then function to potentiate VEGF-VEGFR-2 signalling to drive angiogenesis [46], [57]–[60]. Owing to its importance, VEGFR-2 signalling is tightly regulated at numerous biological levels, including its expression, availability, and binding affinity for its various soluble ligands. In addition, signal duration and amplitude is explicitly influenced by the rate at which receptors are endocytosed and trafficked in the cell. Once internalised into the cytoplasm, VEGFR-2 can either be shuttled to lysosomes for degradation, or undergo dynamic recycling back to the membrane to initiate a new angiogenic response [48].

Unlike VEGFR-2, VEGFR-1 acts as a negative regulator of angiogenesis, regulating embryological vasculogenesis by sequestering VEGF. VEGFR-1 can exist as either a homodimer or as a heterodimer when complexed with VEGFR-2, depending on its bound VEGF ligand. Despite binding to VEGF-A with a high affinity, VEGFR-1 tyrosine phosphorylation and the induction of downstream signalling is comparatively weak compared to VEGFR-2, and therefore VEGFR-1 is commonly viewed as a decoy receptor to moderate the amount of available VEGF-A capable of promoting a pro-angiogenic response. In doing so, normal physiological levels of tissue vascularisation are maintained. Correspondingly, VEGFR-1 null mouse embryos die at E8.5, suffering from uncontrolled EC proliferation and the formation of disorganised vascular beds [48], [61]. VEGFR-3 can also bind VEGF-A, however is typically associated with lymphangiogenesis and early vasculogenesis through its binding of unprocessed VEGF-C and D [49]. Despite VEGFR-3's prominent expression on sprouting endothelial tip cells following VEGF-A stimulation, where it activates Notch signalling to promote stalk cell differentiation, its expression is made redundant by the dominant actions of VEGFR-2 [62] (**Figure 1.3**).

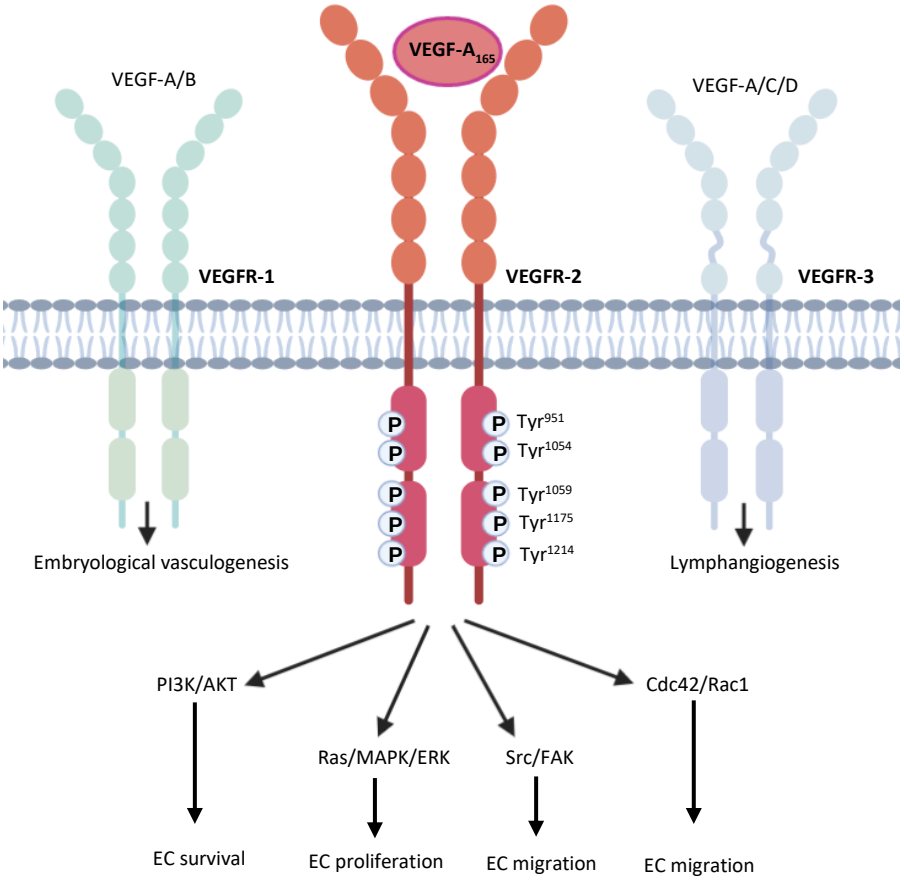

Figure 1.3 VEGF-mediated signalling cascades induce angiogenic responses in ECs. VEGF ligand isoforms bind the extracellular domain of specific VEGFRs in response to a hypoxic event. Ligand binding induces receptor dimerization, enabling trans-autophosphorylation of cytoplasmic tyrosine residues. Phosphorylation of these residues initiates numerous downstream signalling cascades that mediate EC survival, proliferation and migration (Figure adapted from [60], generated using BioRender).

1.6 Neuropilins as VEGF coreceptors

It is becoming increasingly accepted that VEGF-mediated angiogenic signalling is regulated, to some extent, through the direct interaction with NRPs [63]. NRPs are membrane-bound multifunctional non-tyrosine kinase receptors, composed of a single large extracellular region consisting of five domains, a single helical transmembrane domain and a short cytoplasmic tail [64], [65]. First identified in the nervous system of Xenopus embryos, NRPs were initially described for their roles in regulating axon guidance and neuronal pattern development through binding members of the class 3 Semaphorin (SEMA3) family [66], [67]. SEMA3s bind to a complex composed of NRPs and Plexin-A1, a co-receptor for SEMA3s, at the cell membrane. This complex formation is necessary for signal propagation and subsequent axon guidance, cytoskeletal remodelling and cell migration [68]. SEMA3s have also been shown to act as competitive inhibitors of VEGF-mediated EC proliferation and migration, labelling them as promising anti-angiogenic effectors [6], [69]. For example, tumours that overexpress either SEMA3E or SEMA3F exhibit reduced vascularisation and metastatic capability [70]–[72], attributed to the collapsing integrity of both tumour cell and EC cytoskeletons. In this state, the cell suffers rapid depolymerisation of its stress fibres, alongside a loss of adhesion and contractility [73], [74].

In addition to complexing with SEMA3s, NRPs act as co-receptors for VEGF ligands, playing an essential role in sprouting angiogenesis [64], [66]. During angiogenesis cascade initiation, NRPs have been shown to induce optimal binding between VEGF-A and VEGFR-2 to promote receptor phosphorylation. It has also been demonstrated that NRP1-VEGFR-2-VEGF-A trimeric complexes subsequently cluster with other nearby complexes to further amplify the VEGF-induced signalling cascade, enhancing cellular migration and survival. As such, NRPs are considered to act in a pro-angiogenic manner when in complex formation with VEGF-A and VEGFR-2 [75]–[77]. Nevertheless, due to their truncated cytoplasmic tails, which confer no catalytic activity, NRPs cannot transduce any anti- or pro-angiogenic intracellular signals on their own, but only when complexed with SEMA3s or VEGFRs respectively [78].

1.6.1 Neuropilin 1

NRP1 is a 130 kDa transmembrane glycoprotein with specificity for VEGF-A, VEGF-B, VEGF-E and phosphatidylinositol-glycan F protein-2 (PlgF-2), as well as SEMA3A [6], [79]–[81]. These pleiotropic interactions are enabled by a large extracellular region, divided into five domains labelled a1, a2 (CUB), b1, b2 (FV/FVIII), and c (MAM): a and b domains are involved in ligand binding [82] whilst the c domain promotes oligomerisation [83], [84]. A cytoplasmic tail occupying SEA motif, capable

of recognising the PDZ domain (SEA-COOH) of other cytoplasmic scaffolding proteins, also enables NRP1 to interact with other receptors to mediate or enhance signal transduction (**Figure 1.4**). For example, binding between NRP1 and the PDZ domain of GAIP interacting protein C-terminus member-1 (GIPC1) [85], followed by the recruitment of its intracellular binding partner synectin, has been shown to be necessary for stabilising complex formation between NRP1 and VEGFR-2, enhancing the activation of VEGFR-2 and the potency of the resulting downstream signalling cascade [86], [87]. NRP1-mediated partner binding between GIPC1 and synectin has also been reported to modulate endocytic trafficking [88]–[91], whereby upon signal propagation, GIPC1 mediates ligand-dependent internalisation of NRP1-VEGFR-2 complexes in ECs [92]. More recently, it has been demonstrated that following receptor internalisation, NRP1, through its interactions with GIPC1, mediates VEGFR-2 recycling back to the cell surface membrane via Rab5, Rab4 and Rab11 associated vesicles [91]. The transit of VEGFR-2 through Rab11 associated recycling endosomes was shown to be suspended in ECs lacking the GIPC1 binding motif of NRP1, attenuating VEGFR-2 mediated signalling completely [90].

NRP1 expression is prominent during developmental angiogenesis, in particular on ECs of capillaries, arteries, and veins of the postnatal retina and in capillaries of the embryo hindbrain in mice [93]–[95]. Its importance during embryonic vascular development was first described in overexpression studies in mouse embryos, whereby elevated NRP1 levels subsequently led to an equivalent upregulation of VEGFR-2 expression. The following dysregulated angiogenic surge resulted in the excessive development of leaky and haemorrhagic vessels however, and conferred an embryonic lethal phenotype [96]. Conversely, global NRP1 knockout mice exhibit diminished vessel sprouting and cardiac abnormalities and become embryonic lethal between E10.5 and E14.5 [93], [97], [98]. Whilst these reports highlight the importance of carefully regulating endothelial NRP1 expression, they have also underwritten studies promoting NRP1 as an ideal therapeutic target for vascular disorders. For example, Fernandez-Robredo *et al.,* demonstrated that depleting endothelial NRP1 in an inducible manner post embryogenesis attenuates pathological neovascularisation in the developing retina [99].

When directly evaluating the importance of NRP1-mediated complex formation between VEGF and VEGFR-2 during vascular development however, a conflict arises. $Nrp1^{Y297A/Y297A}$ mice mutants exhibiting a point mutation in the VEGF binding pocket, do not display any of the severe embryonic vascular defects of full or EC-specific NRP1 null mice [91]. This point mutation has previously been identified as essential for a strong binding affinity between NRP1 and VEGF [100], [101], and therefore alludes to NRP1 possessing VEGF-independent roles during angiogenesis that have been

suggested to cooperate with its annotated role as a VEGFR2 coreceptor during embryonic development [6]. Indeed, Raimondi *et al*., demonstrated this to be the case, revealing that integrin ligand binding to FN stimulates actin remodelling and paxillin phosphorylation in a VEGF/VEGFR-2 independent, but NRP1 dependent manner [102]. Subsequent studies have evidenced NRP1 to play a key role during postnatal angiogenesis and arteriogenesis of the heart and retina, in addition to pathological revascularisation [103].

1.6.2 Neuropilin 2

NRP2, an ortholog of NRP1, shares a very similar domain structure to its counterpart, exhibiting an overall 44% amino acid homology (**Figure 1.4**). Like NRP1, the expression and functionality of NRP2 has been identified in many cell types, including nerve cells, ECs, epithelial cells, osteoblasts and tumorigenic cells [65], [104], [105].

Whilst their role as VEGFR coreceptors has annotated both NRPs as being implicated in influencing endothelial cell adhesion, migration and permeability during angiogenesis, under both physiological and pathological conditions, these studies have focused almost exclusively on NRP1 however [106]–[108]. This focus may have arisen from the fact that whilst global deletion of the NRP1 gene confers an embryonic lethal phenotype [93], NRP2-null mice are viable with no apparent cardiovascular defects, only that they display fewer venous/lymphatic vessels [109]. Whilst these early transgenic studies speculated a predisposal for NRP1 to be preferentially expressed on arteries, arterioles and capillaries, and NRP2 to be expressed on veins, venules and lymphatic vessels [109], [110], subsequent studies have revealed that both NRPs are expressed on the surface of cardiovascular and lymphatic associated ECs, each playing essential roles in regulating the development of both vasculature networks [111]–[113]. This has been made apparent from NRP1/NRP2 global knockout mice studies, where NRP1/NRP2-null mice exhibit more severe vascular defects than NRP1-null mice, resulting in lethality at E8.5 [114].

Regarding NRP2's role in ECs during development, it has been shown to interact with both VEGFR-2 and VEGFR-3 to promote human EC survival and migration following stimulation by VEGF-A and VEGF-C respectively [115]. Compared to NRP1 however, there is a 50-fold weaker binding affinity between VEGF-A and NRP2 in ECs. This interaction is mediated by specific electronegative motifs in exon 7 and exon 8 of VEGF-A, and the L1 loop of the NRPs, which extends from their b1 domain. Importantly, differences in the amino acid composition of NRP2's L1 loop results in a direct electrostatic repulsion during VEGF-A binding, which has steered the focus of many to annotate the roles of NRP1 over NRP2 during VEGF-driven angiogenic processes [116]. In addition to VEGF-A

however, NRP2 is known to interact with VEGF-C and VEGF-D during their complex formation with VEGFR-3 in lymphatic ECs [117]. This was later shown to promote lymphatic EC sprouting, work that complemented the findings of Shen *et al*., who demonstrated that NRP2 deficiency suppressed VEGF-induced neovascularisation of the retina [118]. It remains unclear however the precise mechanism(s) through which endothelial NRP2 integrates VEGF-induced signalling to influence angiogenesis, if they exist.

1.6.2.1 Neuropilin 2 and disease

Despite the endothelial-specific contributions of NRP2 during vessel development have been, for the most part, unexplored, numerous investigations have been made into its multifunctional roles during disease. Upregulation of NRP2 expression is consistent with cancer progression in a number of cell types (e.g. neuroblastomas [119], non-small cell lung carcinoma (NSCLC) [120], human prostate carcinoma, melanoma [105], lung cancer [120]–[122], myeloid leukaemia [123], breast cancer [124] and pancreatic cancer [125]). Conversely, NRP2 knockdown has been demonstrated to significantly inhibit both VEGF-A and VEGF-C-induced hMVEC migration [115], human colorectal tumour invasiveness and metastasis [126], human pancreatic adenocarcinoma cell migration [127], and aggressive squamous cell carcinoma (OSCC) migration and invasion [128]. More recent investigations in pancreatic neuroendocrine tumour (PNET)-associated human umbilical vein ECs (HUVECs) ectopically overexpressing NRP2 have demonstrated this increased invasive potential to likely arise from an augmented upregulation of cofilin activity, propagating increased rates of actin polymerisation at the leading edges of cells [129]. Supporting *in vivo* studies have also shown NRP2 knockdown to decrease pancreatic adenocarcinoma tumour volume and disrupt tumour vasculature. Further investigation found this to arise due to a reduction in Jagged-1 expression [127], suggesting that NRP2 may regulate tip cell selection during pathological angiogenesis.

Both *in vitro* and *in vivo* studies have revealed mounting evidence that NRP2 is involved in numerous other signalling networks that drive EC migration and survival-associated cascades during cardiovascular disease. In a colon-cancer epithelial cell line, it was shown that NRP2 expression activates transforming growth factor β (TGFβ)-induced epithelial to mesenchymal transition (EMT), a process defined by loss of cell-cell and cell-ECM contact and increased migratory activity. Subsequent investigation found this to arise due to the constitutive phosphorylation of the Smad2/3 complex and the inhibition of E-cadherin. Furthermore, co-immunoprecipitation and surface plasmon resonance studies revealed that NRP2 directly binds TGFβ-1 to mediate an enhanced complex interaction with TGFβR1 to positively regulate EMT [130]. In addition to

modulating EMT, NRP2 has also been implicated in regulating vascular permeability through its interactions with angiopoietin-like-4 protein (ANGPTL4). This interaction was found to stimulate the activation of the RhoA/ROCK signalling cascade, mediating the dissociation of EC-EC junctions and subsequent vascular leakage in the retina [131] (**Figure 1.5**). Taken together, there is mounting evidence indicating that NRP2 could be employed not only as a biomarker for the progression of a number of different cancers and disorders, but also act as a potential pharmacological target.

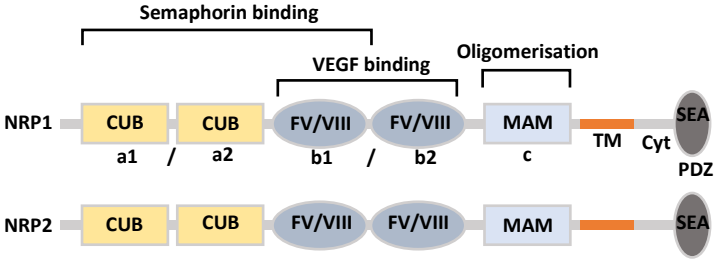

Figure 1.4 Neuropilin family structures. NRP1 and NRP2 both consist of a large extracellular region comprised of two SEMA binding CUB domains (a1 and a2), two VEGF binding domains (b1 and b2), and an adhesive MAM domain that promotes oligomerisation. The cytoplasmic tail of both NRPs contains an SEA motif that is capable of binding proteins with a PDZ domain, such as GIPC1 and synectin (Figure adapted from [104]).

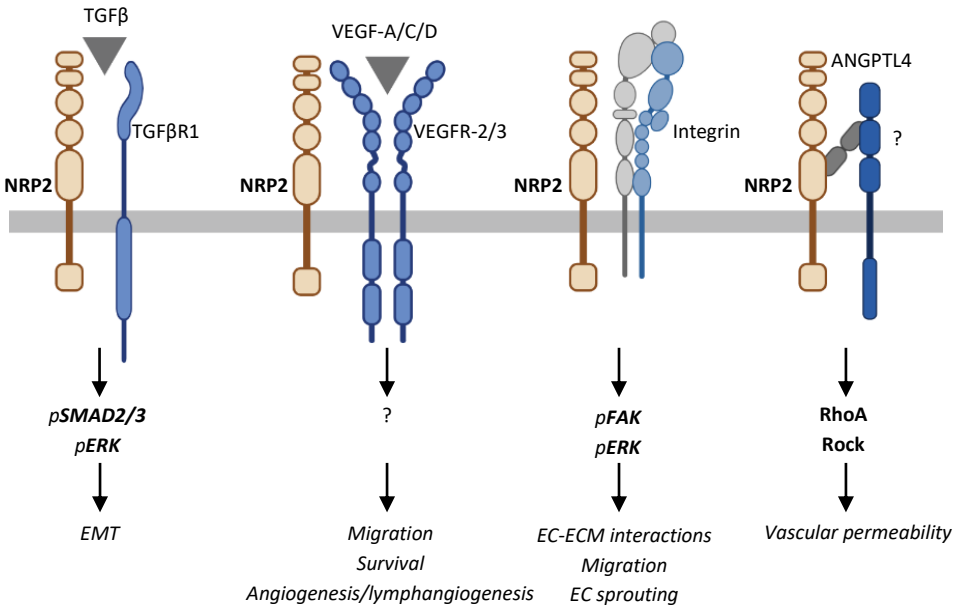

Figure 1.5 NRP2-mediated signalling cascades. NRP2 has been implicated in a number of key signalling cascades to regulate migration, survival and vascular permeability. From left to right, NRP2 has been shown to mediate complex formation between TGFβR-1 and TGFβ to promote EMT, in addition to mediating interactions between VEGFRs and VEGF-A, VEGF-C and VEGF-D. NRP2 can also bind ANGPTL4 to activate the RhoA/ROCK signalling cascade to drive the breakdown of EC-EC junctions to increase vascular permeability. Interactions between NRP2 and integrins will be discussed in subsequent chapters (Figure adapted from [132]).

1.7 Integrins: molecular anchors to the ECM

Angiogenesis relies on the ability for ECs to adhere to and migrate over the ECM in response to angiogenic stimuli [133], [134]. Cell-ECM interactions are mediated via integrins, heterodimeric type I transmembrane glycoprotein receptors that integrate the cellular cytoskeleton with the underlying ECM [24]. As such, integrins have commonly been reported as principal regulators of angiogenesis [135]. These studies have defined their essential roles in embryonic development, in addition to their ability to regulate cellular behaviour under both physiological and pathological conditions [136].

Integrins exist as non-covalently associated α β heterodimers, each subunit consisting of: 1) a large extracellular domain, typically in the range of between ~80-150 kDa, which can be divided into an N-terminus headpiece, and a tailpiece. Whilst the headpiece is required for extracellular ligand binding, the integrin tail subdomain mediates receptor activity by regulating its conformational shape [24]. When active, the integrin heterodimer is extended and able to bind its matrix ligand, however upon loss of ligand binding, it undergoes bending into an inactive state. Integrin subunits also possess: 2) a single membrane-spanning coiled-coil α helix transmembrane domain, and: 3) a short non-catalytic cytoplasmic domain. These domains are involved in the receiving and transmission of bi-directional signals, allowing integrin receptors to modulate a range of cellular events through their coordination of signalling cascades [137]–[139].

This is controlled, in part, by the selective pairing of α and β subunits, as not every α subunit is capable of forming a heterodimer with every β subunit. ECs express at least 11 different integrin heterodimers, (α1β1, α2β1, α3β1, α4β1, α5β1, α6β1, αvβ1, αvβ3, αvβ5, α5β8 and α6β4), their diverging compositions and promiscuities determining their individual ligand specificity [140]. For example, α1β1 and α2β1 heterodimers bind collagen matrices, α3β1, α6β1 and α6β4 heterodimers bind laminin matrices, α4β1 and α5β1 heterodimers bind FN matrices, whilst αvβ3 and αvβ5 heterodimers bind vitronectin matrices. Despite the existence of some overlap in ligand specificity, each integrin subunit is known to perform a discrete non-redundant function in the cell. This has been demonstrated in mouse models whereby the depletion of individual subunits has resulted in distinct perturbated phenotypes. Furthermore, by comparing the expression profiles of different integrins on quiescent versus angiogenic vasculature, it has been purported that specific integrins are more essential than others when mediating cell-ECM associations during angiogenesis [24] (**Figure 1.6**).

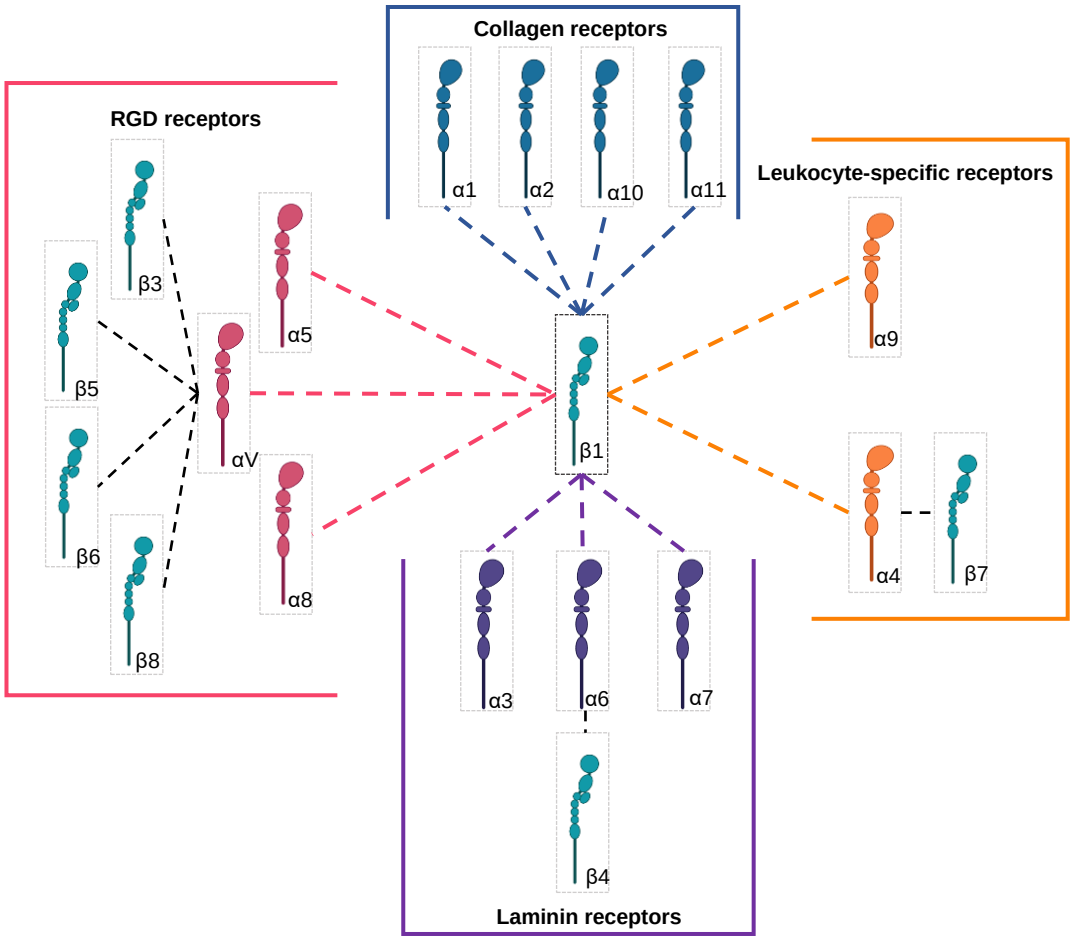

Figure 1.6 Integrin subfamilies and their specificities. Schematic representation of integrin ligand specificity, showing RGD-motif (fibronectin and vitronectin), laminin, collagen, and leukocyte specific receptors. ECs express at least 11 integrin heterodimer receptors (α1β1, α2β1, α3β1, α4β1, α5β1, α6β1, αvβ1, αvβ3, αvβ5, α5β8 and α6β4), enabling their interaction and adhesion to a broad range of matrix ligands [140]. (Figure generated using BioRender).

1.7.1 Integrins and focal adhesion formation

An important mechanism by which ECs regulate integrin function is through their ability to control rapid and reversible changes in integrin extracellular domain conformation. This permits for tight spatial and temporal control of integrin activation, and allows cells to regulate their affinity for different extracellular matrix ligands [141]–[143]. A characteristic profile of integrins is that they mediate bi-directional signalling, transducing signals across the plasma membrane in both directions, either by inside-out or outside-in signalling. Integrins therefore have multidisciplinary roles in regulating cellular survival, proliferation, migration, adhesion and apoptosis [137], [139]. During inside-out signalling, intracellular proteins bind to the cytoplasmic tails of the integrin heterodimer in order to transmit signals to influence integrin extracellular domain interactions with ligands in the extracellular environment. In contrast during outside-in signalling, ligand binding to the extracellular domain of integrins transmits signals to the intracellular space to influence actin cytoskeleton organisation and adhesion complex formation [144].

Depending on integrin maturity, subcellular distribution and ECM composition, their activation propagates the assembly of various adhesion complexes that mediate the aforementioned cellular processes [145], [146]. Upon ligand binding, integrins recruit numerous cytosolic scaffolding proteins such as paxillin, adaptor proteins such as talin and vinculin, and signalling proteins such as kinases and Rho family GTPases in order to initiate a cellular response. This occurs alongside the simultaneous clustering of the integrin heterodimers themselves, amplifying the response by promoting the accumulation of such cytosolic proteins at sites of adhesion to form focal adhesions (FAs) [24], [140], [147]. When cells first adhere to a substrate, they assemble small, highly tyrosine phosphorylated, nascent adhesions otherwise referred to as focal contacts (0 – 2.5 μm^2). These dynamic structures often translocate by simultaneously extending centripetally and contracting peripherally, and are rapidly turned over to promote migration [148]. As these adhesions mature and become influenced by actomyosin-driven forces, they then transition to large macromolecular assemblies referred to as focal complexes or FAs (2.5 - 5 μm^2), which localise to the leading edge of migrating cells. During this transition, vinculin, or the Rap1-GTP-interacting adaptor molecule RIAM compete to engage the C-terminal rod of talin in a mutually exclusive manner, stimulating talin activation and membrane localisation. Talin recruitment to assembling integrin complexes subsequently promotes integrin activation and linkage to the actin cytoskeleton [149]–[151]. This is followed by the RhoA-mediated elongation of actin into linear stress fibres, which requires further complexation with the adaptor proteins zyxin, tensin and VASP [152].

As FAs mature and turnover, their integrin composition changes to reflect the cell's migratory potential. Whilst α5β1 integrin is recruited early during focal contact assembly to mediate transient interactions between the cytoskeleton and the ECM, αvβ3 integrin is recruited later during focal complex assembly, anchoring the adhesion site to the actin cytoskeleton to mediate more stable mechanical changes within the cell [153], [154]. Stress-fibre-associated FAs can further mature into fibrillar adhesions after approximately 24 to 48 hours, whereby engaged α5β1-integrin is translocated along actin cables centripetally towards the cell body. These elongated beaded structures become increasingly enriched with the actin-binding protein tensin-1 as they extend from the medial ends of stationary FAs, and act to funnel the necessary actomyosin tension required to unfold and integrate secreted FN dimers into an extracellular fibrillar network. By mediating both FN fibril formation and their remodelling, fibrillar adhesions are also involved in guiding the subsequent deposition of other matrix components such as collagens, fibrillin, and tenacin-C to promote ECM expansion [152]–[155]. Fibrillar adhesion formation is therefore characteristic of a reduced motility and increased cell stability (**Figure 1.7**).

Our understanding of how integrins mediate dynamic attachments with the ECM and the subsequent development of adhesion structures is, for the majority, based on studies conducted on planar 2D substrates. In reality, more recent investigations have demonstrated that classic focal and fibrillar adhesions represent exaggerated precursors of *in vivo* 3D-matrix adhesions. In comparison to readily detectable protein aggregates, 3D-matrix adhesions are often visualised as more diffusely distributed throughout the cell, display a less redundant integrin composition, and mediate enhanced adhesion activity ([156]–[158]. Substantiating *in vitro* conclusions with live or fixed imaging in 3D *in vivo* model systems is therefore important when assessing cell-matrix interactions and how they are influenced.

1.7.1.1 Focal adhesion kinase

By clustering with protein kinases, integrins overcome the limits imposed by the absence of enzymatic or kinase activity in their cytoplasmic tails [137]. One of the core protein kinases recruited to FAs is focal adhesion kinase (FAK), a non-receptor tyrosine kinase that is recruited and subsequently activated upon VEGF-dependent integrin-mediated adhesion to the ECM [159], [160]. FAK is composed of a central kinase domain, flanked by an N-terminal FERM domain, and a FA targeting C-terminal domain. Owing to its analogous structure with that of cytoskeletal proteins such as talin, FAK'S FERM domain has been proposed to mediate interactions with integrins and growth factor receptors. The C-terminal domain of FAK also contains proline-rich docking sites that

enable interactions with SH3 domain-containing proteins such as p130cas, which act to recruit additional signalling proteins [161]. Combined with its ability to mediate interactions with SH2 domain-containing proteins such as SRC and PI3K through its autophosphorylation site at Tyr^{397} (**Figure 1.8**), which exposes additional binding sites on its surface, FAK is crucial for potentiating numerous signalling cascades following integrin engagement [159], [162]. One such signalling cascade is the activation of Rho family GTPases Rac1 and Cdc42 by modulating the availability of GTPase activating proteins (GAPs) and guanine nucleotide exchange factors (GEFs). Whilst active Rac1 drives the protrusion of lamellipodia, actin rich projections at the leading edge of cells, active Cdc42 promotes the extension of filopodia, microspike actin projections localised to the tips of lamellipodia. Both these GTPase proteins are subsequently involved in activating the Arp2/3 complex to promote the nucleation and polymerisation of actin stress fibres, enabling the dynamic cytoskeletal remodelling required to foster cell spreading and migration. FAK facilitates the involvement of these Rho family GTPases by stimulating their translocation to assembling nascent FAs upon activation [144], [162]–[164] (**Figure 1.9**). Studies utilising mutant HUVECs have also elucidated an important role for FAK's Tyr^{407} residue during VEGF-stimulated signalling to promote EC migration. For example, mutations in the b1 domain of NRP1, resulting in the complete loss of VEGF binding, cause a significant attenuation of VEGF-dependent FAK phosphorylation at Tyr^{407}, without significantly affecting other major signalling pathways [101].

FAK's involvement in the dynamic remodelling of the actin cytoskeleton runs parallel to the rapid disassembly and re-assembly of nascent FAs, which utilise actin highways to coordinate integrin transport and trafficking to promote their turnover. Studies have since revealed that integrins endocytosed and recycled with phosphorylated FAK are maintained in their active conformation, promoting polarised reassembly of nascent FAs to promote directional migration [165]. It has also been alluded to that FAK-coupled integrin internalisation potentiates various intracellular integrin-mediated signalling cascades to promote cellular adhesion and survival [166]. Accordingly, FAK is regarded as a key integrator of both integrin-mediated signal propagation and transport, facilitating mechanical linkage to the actin cytoskeleton as the cell migrates.

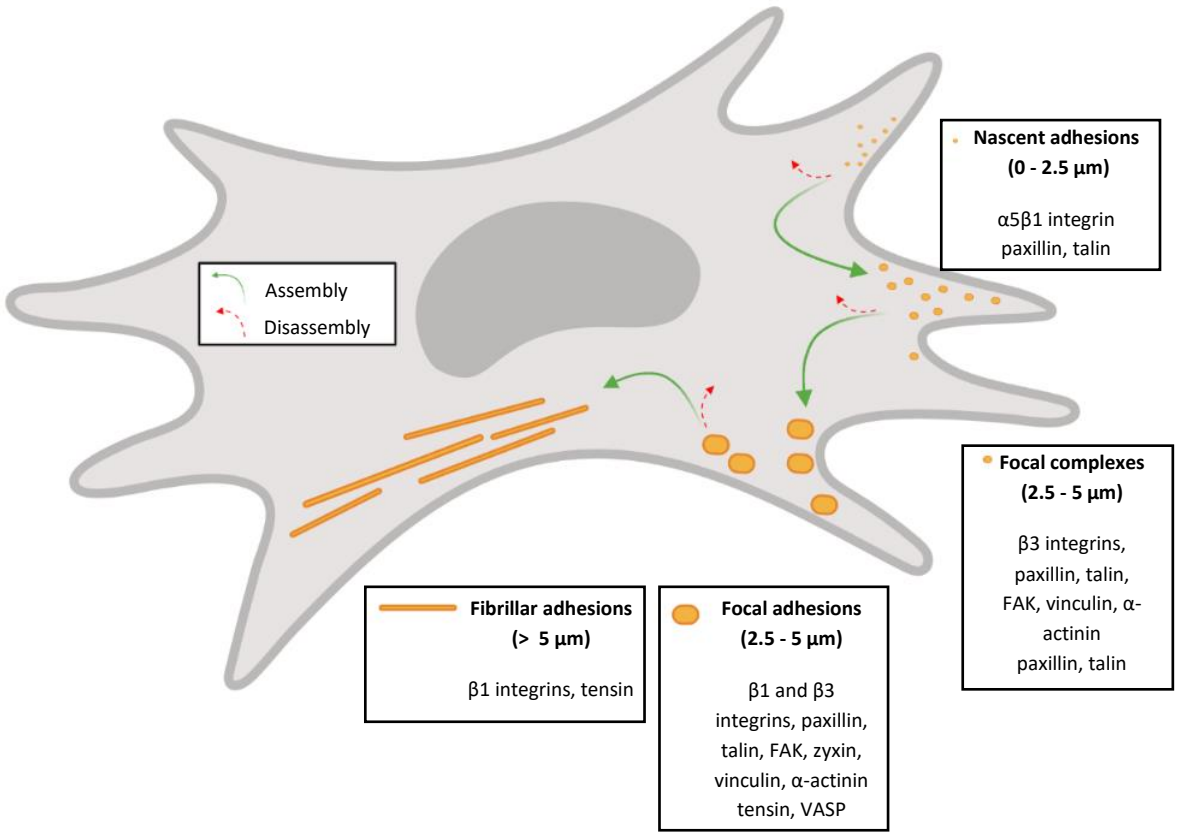

Figure 1.7 Focal adhesion structures and their composition. It is accepted that four classical subtypes of adhesion complex exist: nascent adhesions, focal complexes, FAs, and fibrillar adhesions. Depending on their composition, these structures alter their localisation, and are characterised by their size and rate of turnover. Whilst nascent adhesions are composed of α5β1 integrin, mature FAs are composed for the majority of β3 integrins complexed with a wide range of adaptor, scaffolding, and signalling proteins. In comparison, fibrillar adhesions are characterised by their long fibril structures which are enriched with translocating α5β1 integrin and tensin-1 (Figure adapted from [167], generated using BioRender).

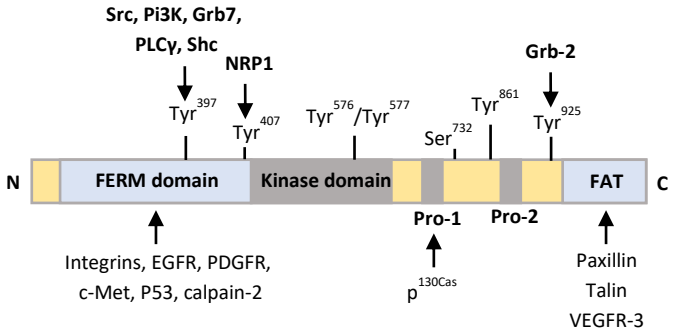

Figure 1.8 Structural features and interacting proteins of FAK. FAK is composed of a central kinase domain, an N-terminal FERM domain and a C-terminal FAT sequence. Whilst the FERM domain mediates interactions with integrins and other surface receptors, its FAT domain targets FA scaffolding proteins such as paxillin and talin. In addition, major autophosphorylation sites such as Tyr^{397} expose binding sites on SH2 domain-containing signalling proteins to further amplify FA-associated signalling cascades [162].

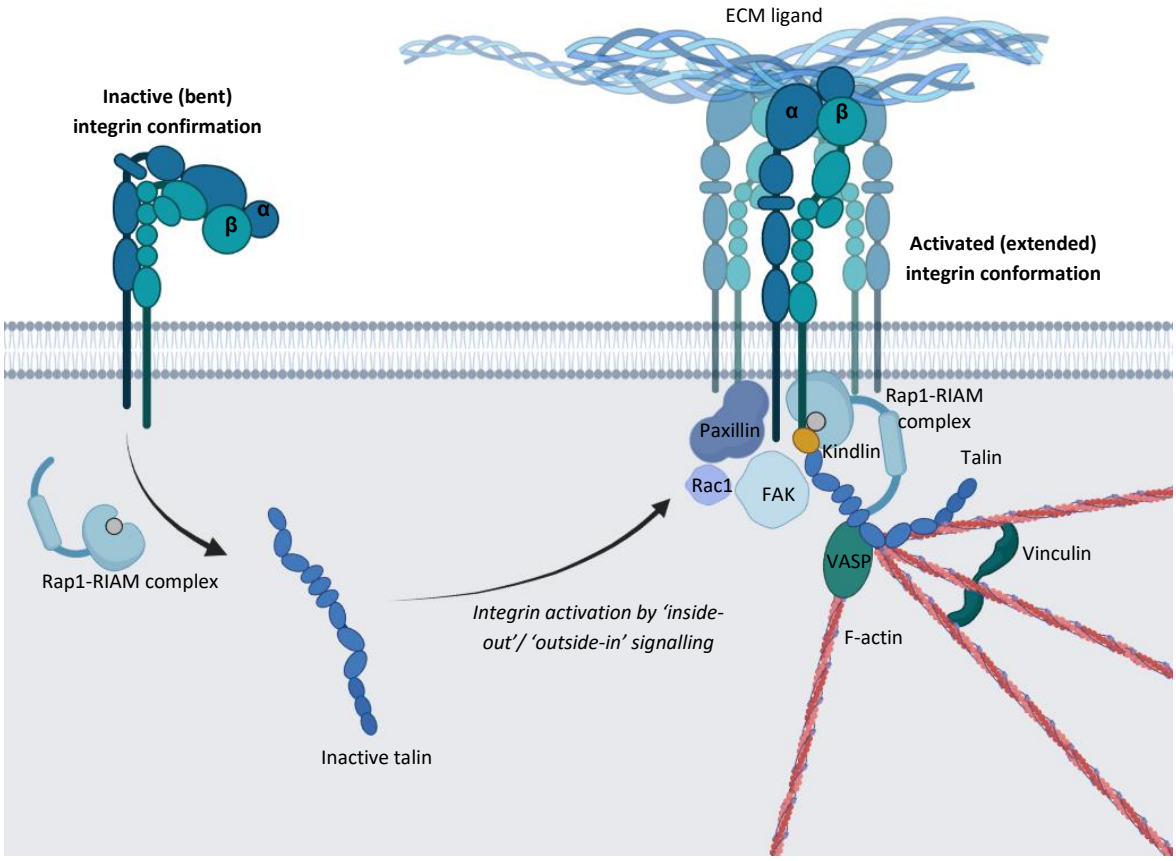

Figure 1.9 Integrin activation and FA formation. Integrin activation, involving conformational changes in both α and β subunits, transitioning the receptor from an inactive bent state to an active erect state, propagates the assembly of FAs that mediate cellular migration across the ECM. Integrins tether the migrating cell to the ECM through their affinity for specific ECM ligands, and recruit a module of intracellular proteins, including FAK, paxillin, actin adaptors and Rho GTPases to anchor the FA complex to the cytoskeleton to mediate mechanical changes in the cell. The recruitment and activation of both integrins and FAK are required for FA complex assembly, and to drive EC survival, proliferation and migration [24], [162]. (Figure generated using BioRender).

1.7.2 Integrin trafficking

FA turnover relies on the ability for integrin heterodimers to be trafficked to and from the cell surface membrane. The more efficiently integrins can transit through the cell's trafficking machinery, the faster new sites of ECM attachment can form [145], [168]. In turn, the endocytosis and recycling of active integrins; those bound to their respective ECM fragment, facilitates the turnover and replenishment newly synthesised matrix components [169]. Once bound to the ECM, β1 integrins are known to stimulate the release of biochemical signals that establish and maintain the apico-basal polarity that enables directional migration in ECs. Once this axis has been defined, FN-bound active α5β1 integrin is responsible for directing the secretion of freshly synthesised and unfolded FN towards the abluminal basolateral surface of ECs. Cycles of active α5β1 integrin traffic therefore preserve a self-sustaining signalling cascade to maintain cell polarity [155], [170].

Integrins are known to be internalised from disassembling FAs either by clathrin-dependent or clathrin-independent endocytosis, their subsequent recycling back to assembling FAs at the leading edge of the cell via sorting and recycling endosomes regulating dynamic cytoskeletal changes that drive cellular migration [145]. Integrin endocytosis is initiated by the clustering of endocytic coat proteins at the inner leaflet of the plasma membrane. Once assembled, the membrane invaginates to form a clathrin-coated pit, which is released following the recruitment of scission proteins such as dynamin-2 (Dyn-2) [171]. Depending on the site of internalisation and integrin composition, endocytosing vesicles transit through either Rab21 or Rab5 small GTPases until contact is made with the early endosome (EE), prior to which the protein coat disassembles, leaving the nascent cargo-filled vesicle to undergo recycling or degradation. Within the EE, active α5β1 also promotes the GTP-loading of intracellular Rac1, stimulating its polarised relocation to assembling adhesions to support lamellipodium-driven cell motility. This is thought to coincide with the subsequent activation of FAK to suppress anoikis [169], [172], [173] .

Whilst a fraction of the internalised integrin pool is degraded into lysosomes, the majority is recycled back to the plasma membrane to facilitate nascent adhesion formation. Integrins can either be recycled via a fast 'short-loop' route, which occurs in the presence of growth factor stimulation; Akt activity induces the inhibition of glycogen synthase kinase-3 (GSK-3) which otherwise obstructs fast recycling, or via a basal, slow 'long-loop' pathway, which occurs in the absence of growth factor stimulation [169], [174]. Unlike αvβ3 integrin, which solely undergoes fast recycling in $Rab4^+$ vesicles [175], α5β1 integrin has been found to transit via both fast and slow routes. Whilst active α5β1 integrin is known to recycle via a short loop pathway within $Rab5^+$

vesicles in a NRP1-dependent manner [108], the turnover of α5β1 integrin within fibrillar adhesions occurs via a slow recycling route [155]. Here, α5β1 integrin is transported to the perinuclear recycling compartment (PNRC) via Rab21 [176], [177]. Rab21 is then displaced by p120RasGAP, stimulating the release of the integrin-containing vesicle from the perinuclear region. From the PNRC, α5β1 integrin is then recycled back to nascent adhesions via $Rab11^{+}$ vesicular endosomes [178] (**Figure 1.10**). Whilst it remains less than intuitive as to why specific integrins rely more or less on fast or slow recycling routes [179], it is understood that during suppression of short-loop-dependent αvβ3 integrin recycling in fibroblasts, the rate of long loop α5β1 integrin recycling is upregulated to compensate. Indeed, by utilising dominant-negative Rab4 mutants to compromise short-loop recycling of αvβ3 integrin, White *et al*., demonstrated that the rate of α5β1 integrin recycling increased by at least two-fold, and as a result, migratory persistence was supressed by promoting ROCK-dependent cofilin phosphorylation. It was further shown that the converse overexpression of αvβ3 integrin profoundly impaired the ability for α5β1 integrin to return to the cell surface. Indeed, the ability for the cell to balance integrin signals and thereby favour directional migration over random migration is essential when responding rapidly to directional cues [180].

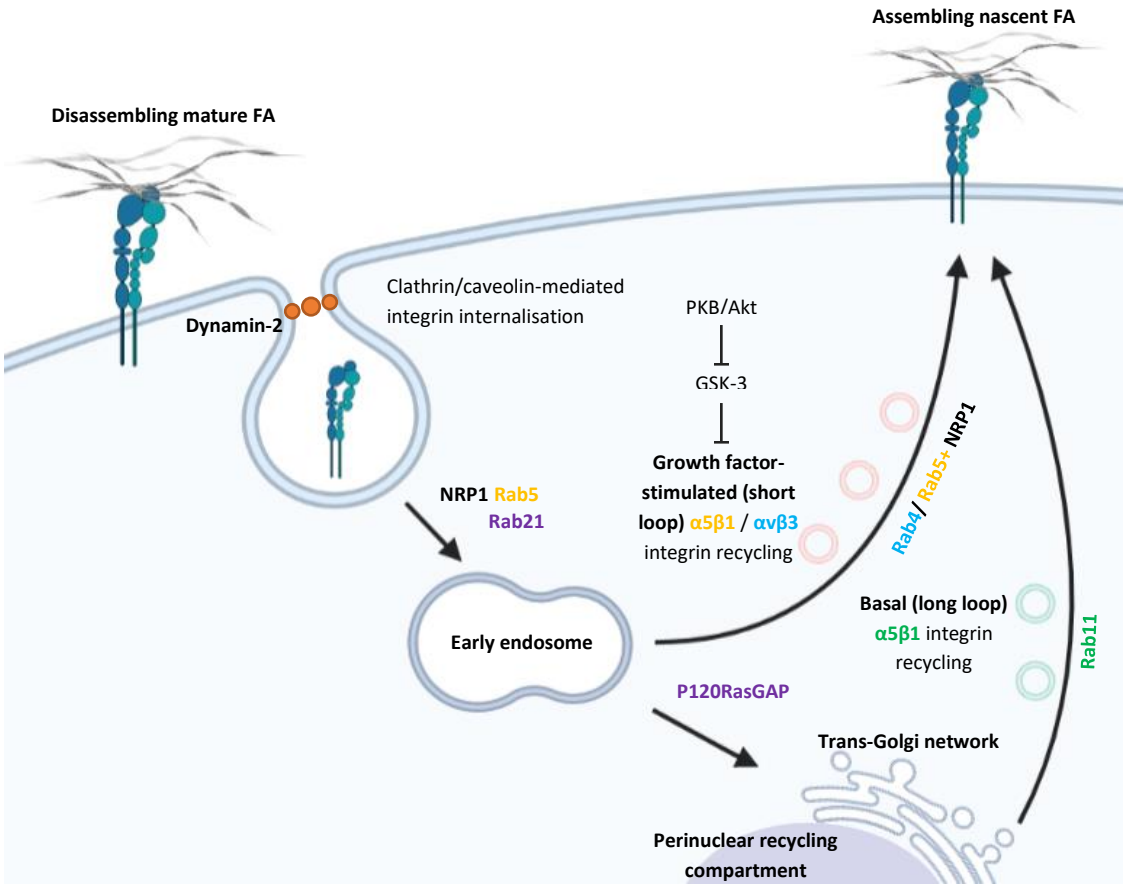

Figure 1.10 Integrin trafficking. Rapid FA turnover is driven by the internalisation of integrin complexes by clathrin-dependent or independent (caveolin-dependent) endocytosis to the early endosome (EE), and the subsequent recycling back to assembling nascent FAs. αvβ3 integrin is recycled via a Rab4-dependent 'short loop' pathway, whilst α5β1 can either be recycled via a Rab11-dependent 'long loop' pathway through the perinuclear recycling compartment (PNRC) or via a Rab5-dependent pathway mediated by NRP1 [108], [178], [181] (Figure generated using BioRender).

1.8 Interactions between neuropilins and integrins

It is known that clustered integrins can cross talk with VEGFRs and their NRP coreceptors to regulate EC behaviour during angiogenesis [182]. Whilst several studies have implicated all aforementioned integrin heterodimers in regulating angiogenesis [170], [182]–[184], the canonical FN-specific integrin receptors α5β1 and αvβ3 have become of principle interest in recent years [185], [186]. The expression of both α5β1 and αvβ3 integrin is upregulated on angiogenic neovasculature compared to quiescent, mature vasculature, which quickly led them to be considered as candidates for anti-angiogenic therapies [184], [187], [188]. Other studies have also demonstrated that both receptors interact with and cross talk with NRP1 [107], [108], [189], [190].

1.8.1 αvβ3 integrin crosstalk with neuropilin 1

In mouse models, αvβ3 integrin expression is upregulated in sprouting capillaries during both physiological and pathological angiogenesis, suggesting that it acts in a pro-angiogenic manner [184], [185], [187]. In defence of this, upon binding to the ECM, and in the presence of VEGF, αvβ3 integrin interacts with, and enhances, the activation of VEGFR-2, promoting EC proliferation and migration [191], [192]. In response, the small cyclic peptide inhibitor Cilengitide was developed as a highly specific antagonist against αvβ3 integrin, shown to inhibit pathological angiogenesis in *in vitro* bovine aortic endothelial (BAE) angiogenesis assays and *in vivo* animal models [193], [194]. Unfortunately, Cilengitide did not progress through phase III clinical trials, conferring no benefit for patient survival [195]. Subsequent studies have since purported that low concentrations of such RGD-mimetic inhibitors paradoxically promote tumour growth and tumour angiogenesis by enhancing VEGF-induced phosphorylation and trafficking of VEGFR-2 [196]. Further investigation surrounding the function of αvβ3 integrin revealed that its anti-tumorigenic efficacy was dependent upon the duration of its depletion. Whilst tumour growth was impeded during the first 2 weeks of depletion, long-term depletion provided no protective response [197].

The race to define αvβ3 integrin as either pro- or anti-angiogenic has since progressed to examining the effects of altering the expression of the β3 integrin subunit only. For clarification, to best investigate the endothelial functions of αvβ3 integrin, the β3 subunit should be examined in isolation as it is specific only to the αv subunit. On the contrary, the intrinsic promiscuity of the αv subunit enables it to pair with any of the following: β1, β3, β5 or β8. Therefore, when disrupting the expression of the αvβ3 integrin heterodimer, you also indirectly perturb the expression of αvβ1, αvβ5 and αvβ8 integrin [24]. Whilst global loss of β3 confers no obvious defects in developmental angiogenesis, β3-null mice exhibit enhanced tumour growth, vascular permeability, EC migration

and proliferation, resulting from the overexpression of VEGFR-2 [198], [199]. More recently, it has been reported that in the absence of β3, tumour growth becomes sensitised to Rac1 inhibition. Usually activated through α5β1 integrin containing nascent adhesions to drive EC migration [200], Atkinson *et al.,* demonstrated that loss of β3 integrin promotes the association between Rac1 and α5β1 integrin by altering microtubule stability [201].

Cross talk between β3 integrin and NRP1, facilitated by a physical interaction, has since been elucidated to restore the angiogenic impediment elicited by the short-term depletion of β3 integrin. This interaction would later be defined to reveal β3 integrin as a negative regulator of NRP1-VEGFR-2 complex formation, whereby inhibition of NRP1 only impairs neovascular formation when endothelial β3 integrin is also lost. Subsequent studies, utilising β3 integrin heterozygous (β3-HET) mice in an attempt to avoid any pre-existing angiogenic phenotype produced as an artefact of complete β3 deletion, confirmed this finding, demonstrating that both tumour growth and VEGF-induced sprouting were significantly inhibited following the additional endothelial specific depletion of NRP1 [107]. Co-depleting these receptors, and thereby sensitising pathological angiogenesis to NRP1 disruption, may therefore provide an effective anti-angiogenic therapeutic strategy.

1.8.2 Neuropilin 1 and α5β1 integrin

Like αvβ3, the expression of α5β1 integrin is specifically upregulated on angiogenic vasculature [184], [188]. Investigation into the roles of α5β1 integrin can also performed, in a similar manner to αvβ3 integrin, by focusing on the α5 integrin subunit in isolation. Not only does the α5 subunit regulate the heterodimer's canonical specificity for FN, but is also only capable of pairing with β1 integrin in ECs [202]. In comparison to the monogamous nature of α5 integrin, the β1 subunit is capable of pairing with six other α subunits [24], and therefore whilst global depletion of either subunit results in severe vascular deformity, embryonic lethality resulting from loss of β1 integrin occurs at E6.5 compared to E11 (following loss of α5 integrin) [203]–[207].

As a canonical receptor for the matrix ligand FN, it is unsurprising that α5β1 integrin is found in the FAs of ECs allowed to adhere on FN *in vitro* [186]. By mediating EC adhesion to FN matrices, α5β1 integrin has been widely reported to promote EC migration and survival during developmental and pathological angiogenesis [184], [188]. Whilst loss of α5β1 integrin impairs adhesion to FN, this phenotype is transient, with ECs rescuing their ability to adhere over time. It was not until Van der Flier *et al*., demonstrated that depletion of both α5 and αv integrin prevented the ability for ECs to form FAs whatsoever, observing a severely reduced level of adhesion to FN matrices, was a

compensatory cross talk between α5 and αv integrin first truly considered. Constitutive depletion of α5 and αv integrin had however previously been shown to induce early mesenchymal abnormalities and lethality at E14.5 resulting from severe vessel remodelling defects [186], [203].

In addition to interacting with αvβ3, NRP1 is also known to interact with α5β1 integrin, as demonstrated by co-immunoprecipitation in pancreatic cancer cells and by fluorescence resonance energy transfer (FRET) analysis in human umbilical artery ECs (HUAECs) [106], [108]. The cross talk between NRP1 and α5β1 integrin has since been elucidated to regulate α5β1-mediated adhesion to FN matrices, as loss of NRP1 elicits a reduction in FN-dependent EC adhesion. It is also known that the binding of the endocytic adaptor GIPC1 to the cytoplasmic SEA domain of NRP1 selectively stimulates the direct and rapid endocytosis of active α5β1 integrin from mature FA complexes (or fibrillar adhesions). This alternative endocytic transport mechanism occurs via myosin VI directed shuttles that actively traffic α5β1 along the actin cytoskeleton to the EE in a Rab5 dependent manner [108].

1.8.3 Integrins and neuropilin 2

Like NRP1, NRP2 has also been reported to share physical interactions with integrins. Given NRP2's previously established role as a biomarker for cancer progression, its interactions have, for the majority, been described as promoting cancer development. For example, in $EpCAM^+$ epithelial cells isolated from human breast tumours, NRP2 has been shown to direct FAK-mediated adhesion via α6β1 on laminin matrices by propagating the activation of the proto-oncogene protein kinase C (PKC). Immunofluorescence microscopy substantiated the co-localisation between NRP2 and active FAK within α6β1-containing FAs at the leading edge of cells [208]. Further evidence alluding to a regulatory nexus between NRP2 and FAK was shown in colorectal carcinoma, where the expression of NRP2 in lymphatic ECs promoted migration, sprouting and tubulogenic capacity via binding to α9β1 integrin, stimulating FAK and ERK activation [209]. Other studies employing an *in vivo* pancreatic cancer model, demonstrated that an upregulation of NRP2 enhanced cellular adhesion between a highly metastatic pancreatic cancer cell line (ASPC-1) and ECs via trans-binding to α5 integrin. Knockdown of NRP2 in this cell line was also shown to confer a reduced extravasation ability compared to control cells in a zebrafish extravasation model. Similarly, although transplanted NRP2 deficient ASPC-1 cells were shown not to confer a significantly reduced rate of primary tumour growth, metastatic nodules found in the lung were far fewer compared to those found in control mice. A significantly reduced rate of cancer cell liver metastasis in a SCID mouse xenograft model has also been reported [210].

By mediating cancerous cell adhesion to the endothelium, tumours can extravasate from the vessel and subsequently invade distant metastatic sites. Targeting the interactions between NRP2 and adhesion receptors, such as α5 integrin, may therefore provide an alternative anti-tumorigenic therapeutic strategy by inhibiting the migratory capability of cancer cells. Furthermore, given the high level of structural homology between NRP2 and NRP1, in addition to its emerging interactions with key pro-angiogenic receptors such as α5 integrin, it is possible that endothelial NRP2 may modulate integrin-mediated EC-ECM and EC-EC interactions to regulate angiogenic signalling cascades , fine-tuning cell behaviour to respond to changes in their environment. It is clear however that the multidisciplinary roles of endothelial NRP2 during developmental and pathological angiogenesis warrants further investigation.

1.9 Research aims and objectives

Previous research (unpublished) conducted in our laboratory has revealed that a complex tripartite cross talk exists between NRP1, α5β1 integrin and αvβ3 integrin during both pathological and developmental angiogenesis. In this network, angiogenesis is regulated by the pro-angiogenic actions of NRP1 and αvβ3, whereby NRP1 promotes angiogenesis both through its interactions with VEGFR-2, and through the inhibition of α5β1, which in turn inhibits the pro-angiogenic actions of αvβ3.

Given the structural and functional similarities between NRP1 and NRP2, in particular with regard to NRP2s emerging role in regulating α5 integrin, this thesis sets out to investigate the contributions of endothelial NRP2 during developmental and pathological angiogenesis. It follows a descriptive set of pilot data previously generated in the Robinson laboratory (unpublished), which identified: **1:** siRNA-mediated transfection as an efficient method to transiently deplete NRP2 in mouse-lung microvascular ECs (mLMECs); **2:** NRP2 promotes EC migration over FN matrices but unlike NRP1, does so independently of VEGFR-2 signalling or β3 integrin involvement; **3:** NRP2 directly interacts with α5 integrin in mLMECs, and **4:** NRP2 depletion impairs total α5 subunit recycling, attenuating the rate of FA turnover. From these observations, this thesis will cover the following aims:

1. To further characterise the cellular and molecular consequences of genetically manipulating endothelial NRP2 and α5 integrin expression in cultured mLMECs to assess whether a complex regulatory interaction exists.

2. To generate genetically engineered mouse models with which the inducible depletion of endothelial NRP2, individually or in combination with α5 integrin or NRP1, can be examined *in vivo*.

3. To utilise such genetically engineered mouse models to examine the contributions of endothelial NRP2 during pathological angiogenesis, and during normal physiological angiogenesis in the postnatal retina model.

Based on the evidence discussed above, and taking into account the unpublished work produced by the Robinson Lab, we hypothesise that NRP2 regulates FN-dependent migration, adhesion and signalling pathways in ECs by controlling cellular trafficking of α5 integrin.

2 Materials and methods

2.1 Chemicals and antibodies

All chemicals, unless otherwise stated, were purchased from ThermoFisher Scientific (Loughborough, UK). All primary and conjugated secondary antibodies purchased for use in this report, including host, reactivity, application, supplier, and catalogue/clone number, are provided in **Table 2.1** and **Table 2.2** respectively.

Table 2.1 List of primary antibodies

Antigen	Reactivity	Host	Application	Supplier	Cat#/Clone#
α5 integrin	Mouse	Rabbit	WB/IP	CST	4705S
α5 integrin	Mouse	Rat	IF	Abcam	Ab25251
α-SMA	Mouse	Rabbit	IF	Abcam	Ab124964
AKT	Mouse	Rabbit	WB	CST	9272
AKT(phospho-Ser^{473})	Mouse	Rabbit	WB	CST	4060
Biotin	Mouse	Mouse	WB/IP	JI	3D6.6
Caveolin-1	Mouse	Mouse	WB/IP	Abcam	Ab18199
Claudin-5	Mouse	Rabbit	WB	Abcam	Ab131259
Clathrin heavy chain-1	Mouse	Rabbit	WB/IP	Abcam	Ab21679
Collagen IV	Mouse	Rabbit	IF	Abcam	Ab19808
Dynamin-2	Mouse	Rabbit	WB/IF	Abcam	Ab3457
EDA-FN	Mouse	Mouse	WB/IF	Sigma	F6140
EEA1	Mouse	Rabbit	ICC	Abcam	Ab2900
Endomucin	Mouse	Rat	WB/ECS	SCB	Sc-65495
ERG	Mouse	Rabbit	WB	Abcam	Ab92513
ERK	Mouse	Rabbit	WB	CST	4695
ERK(phospho-Thr$^{202/204}$)	Mouse	Rabbit	WB	CST	9101
FAK	Mouse	Rabbit	WB	CST	3285
FAK(phospho-Tyr$^{397/407}$)	Mouse	Rabbit	WB/IF	CST/Abcam	8556/Ab4814
GAPDH	Mouse	Mouse	WB	Proteintech	60004-1-1g
GM130	Mouse	Rabbit	ICC	NB	NBP2-53420
HSC70	Mouse	Mouse	WB	SCB	B-6/sc-7298
Lamp1	Mouse	Rabbit	ICC	Abcam	Ab24170
NRP1	Mouse	Rabbit	WB/IP	CST	3725S
NRP1	Mouse	Goat	IF	R&D	AF566
NRP2	Mouse	Rabbit	WB/IP	CST	D39A5
NRP2	Mouse	Mouse	IF	SCB	sc-13117
Paxillin	Mouse	Rabbit	IF	Abcam	Ab32084
Pecam-1	Mouse	Rabbit	WB	eBioscience	48-0311-80
Prox-1	Mouse	Rabbit	WB	Abcam	Ab11941
Rab11	Mouse	Rabbit	WB/IP	Abcam	Ab3612
Rab11Fip5	Mouse	Rabbit	WB/IP	Abcam	Ab153843

Rac1	Mouse	Mouse	WB/IP	Millipore	23A8
Tensin-1	Mouse	Rabbit	WB/IF	NB	NBP1-84129
Antigen	**Reactivity**	**Host**	**Application**	**Supplier**	**Cat#/Clone#**
VE-cadherin	Mouse	Rabbit	WB	Abcam	Ab205336

Application key: WB: Western Blotting, **IP**: Immuno-precipitation, **IF**: Immuno-fluorescence, ECS: EC sorting

Supplier key: CST: Cell Signalling Technology, **SCB**: Santa-Cruz Biotechnology, **JI**: Jackson Immuno-research, **NB**: Novus Biologicals

Table 2.2 List of conjugated secondary antibodies

Host	Anti-	Application	Conjugate	Supplier	Cat#/Clone#
Rabbit	Goat	IF	Alexa®-488	Invitrogen	A-21222
Rabbit	Goat	IF	Alexa®-594	Invitrogen	A-21223
Donkey	Rabbit	IF	Alexa®-488	Invitrogen	A-21206
Goat	Rabbit	IF	Alexa®-647	Invitrogen	A-21244
BS-1 lectin	Blood-vessel	IF	FITC	Sigma	L9381
Sheep	Rat	ECS	Dynabeads	Invitrogen	A-21100
Goat	Rabbit	WB	HRP	Dako®	P 0448
Rabbit	Mouse	WB	HRP	Dako®	P 0260
Rabbit	Goat	WB	HRP	Dako®	P 0449

2.2 Animals

All experiments were performed in accordance with UK home office regulations and the European Legal Framework for the Protection of Animals used for Scientific Purposes (European Directive 86/609/EEC), prior to the start of this project. The study was also approved by the Animal Welfare and Ethical Review Board (AWERB) committee at the University of East Anglia, School of Biological Sciences.

2.2.1 Breeding and generation

NRP2 floxed ($NRP2^{flfl}$) mice [211] were purchased from Jackson Laboratories (Bar Harbour, Maine, USA), and were generated by gene target insertion of embryonic stem cells, resulting in the insertion of loxP sites flanking exon 1 of the NRP2 gene. Mice floxed for either α5 integrin ($\alpha5^{flfl}$) [186] or NRP1 ($NRP1^{flfl}$) [212] were generated in a similar manner by gene target insertion of embryonic stem cells, resulting in the insertion of loxP sites flanking either exon 1 of the α5 integrin gene, or exon 2 of the NRP1 gene; $\alpha5^{flfl}$ mice were provided for by Richard Hynes (Massachusetts Institute of Technology, USA) and $NRP1^{flfl}$ mice were purchased from The Jackson Laboratory (Bar Harbour, Maine, USA). loxP-tauGFP FRT-flanked neo cassettes were inserted via homologous recombination. Heterozygous animals were crossed to an flp recombinase transgenic line for

removal of the neo cassettes. Transgenic mice expressing a tamoxifen-inducible PDGFb-iCreER^{T2} allele [213] were provided by Marcus Fruttiger (UCL, London, UK), and were generated by substituting the exon 1 of the PDGFb gene by the iCreER^{T2}-IRES-EGFP-pA sequence.

NRP2^{flfl}, α5^{flfl}, and NRP1^{flfl} mice were bred with PDGFb.iCreER^{T2} mice to generate NRP2^{flfl}; PDGFb.iCreER^{T2}, α5^{flfl}; PDGFb.iCreER^{T2} and NRP1^{flfl}; PDGFb.iCreER^{T2} animals respectively. NRP2^{flfl}; PDGFb.iCreER^{T2} mice were subsequently bred with either α5^{flfl}; PDGFb.iCreER^{T2} or NRP1^{flfl}; PDGFb.iCreER^{T2} mice to generate animals floxed for both NRP2 and α5 integrin (NRP2/α5^{flfl}; PDGFb.iCreER^{T2}), or both NRP2 and NRP1 (NRP1/NRP2^{flfl}; PDGFb.iCreER^{T2}). PDGFβ-iCreER^{T2} expression was maintained exclusively on breeding males, thereby ensuring the generation of both Cre-negative and positive offspring and enabling the use of littermate controls. All animals were bred on a pure C57/BL6 background.

2.2.2 Genotyping

DNA genotyping was performed on ear biopsies taken from all animals to ensure correct gene floxing and PDGFβ-iCreER^{T2} expression. All PCR reactions were run on a 1.8 % agarose gel, before being imaged using a BioDoc-IT Transilluminator (UVP).

2.2.2.1 DNA preparation

Biopsies were taken from the ears of weaned mice, and digested overnight at 56 °C in tissue lysis buffer (Tris-HCL (50 mM, pH 8.5), EDTA (10 mM, pH 8.0), NaCl (100 mM) and SDS (0.2 %)) supplemented with proteinase K (100 µg/ml) (Sigma). DNA was subsequently precipitated by the addition of isopropanol (100 µl), and collected by centrifugation at 1400 x g for 30 minutes. DNA was then resuspended in TE buffer (Tris-HCl (10 mM, pH 7.5) and EDTA (1 mM).

2.2.2.2 PCR reactions

Analysis of floxed alleles (NRP2, α5 integrin and NRP1) and PDGFβ-iCreER^{T2} expression was performed using the following PCR reaction: DNA (0.6 µl), MegaMix-Blue (10 µl) (Microzone: a 1.1X reaction buffer containing Taq polymerase, 2.75 mM $MgCl_2$, 220 µM dNTPs and blue agarose loading dye), and 0.08 µl forward (F) and reverse (R) primers (diluted from a 100 µM stock solution). PCR reaction mixes were loaded into 96-well PCR plates before being placed in a 96-well block thermal cycler (Bioer Technology) under the conditions outlined below in **Table 2.3:**

Table 2.3 Primers and amplification programmes for PCR analysis of target gene floxing and PDGFb.iCreER status

Gene	Primers		Amplification Programme		
NRP2	F (WT) a	5' – CAGGTGACTGGGGATAGGGTA – 3'	**94°C**	2mins	
	Common a+b:	5' – AGCTTTTGCCTCAGGACCCA – 3'	**94°C**	20secs	**10x Touch down**
			65°C (-0.5°C**)**	15secs	
	F ($^{fl/fl}$) b	5'-CCTGACTACTCCCAGTCATAG -3'	**68°C**	10secs	
			94°C	15secs	
			60°C	15 secs	**28x**
			72°C	10secs	
			72°C	2mins	
			16°C	Indefinitely	
α5 integrin	HT030:	5' –GCAGGATTTTACTCTGTGGGC– 3'	**95°C**	5mins	
	HT0311:	5' –TCCTCTGGCGTCCGGCCAA– 3'	**94°C**	30secs	
	HT032:	5' –GAGGTTCTTCCACTGCCTCCTA– 3'	**60°C**	90secs	35x
			72°C	1min	
			72°C	10mins	
			16°C	Indefinitely	
NRP1	F:	5' –AGGTTAGGCTTCAGGCCAAT– 3'	**94°C**	3mins	
	R:	5' –GGTACCCTGGGTTTTCGATT– 3'	**94°C**	30secs	
			65°C	1min	35x
			72°C	1min	
			72°C	10mins	
			16°C	Indefinitely	
PDGFb-iCreER^{T2}	F:	5'–GCCGCCGGGATCACTCTC–3'	**94°C**	4mins	
	R:	5' –CCAGCCGCCGTCGCAACT–3'	**94°C**	30sec	
			57.5°C	45sec	34x
			72°C	1min	
			72°C	10mins	
			4°C	Indefinitely	

2.3 Mouse-lung microvascular EC isolation and immortalisation

Mouse lung microvascular ECs (mLMECs) were isolated from mice between 3 to 6 weeks of age and prepared as previously described [214]. Typically, lungs were aseptically removed from 3 animals at a time and collected in mouse-lung EC (MLEC) media (1:1 mixture of Ham's F-12-DMEM medium (low glucose) (Invitrogen) supplemented with 20 % foetal bovine serum (FBS) (Invitrogen), penicillin/streptomycin (pen-strep): 100 units/ml (Invitrogen), glutamax: 2 mM (Invitrogen), heparin: 50 μg/ml, and endothelial mitogen: 25 mg (AbD Serotech), rinsed in 70 % ethanol (EtOH)

and returned to fresh MLEC media. Subsequently, lungs were minced with scalpels and digested at 37 °C for 1 hour in a PBS + Ca^{2+} and Mg^{2+} (both at 1 mM concentrations) solution containing 0.1 % collagenase I (Invitrogen) and 0.01 % DNase I (Invitrogen), with agitation every 15 minutes. The cellular digests were expelled through a 19G needle 3 times, a 21G needle once and then filtered through a 70 µm sterile strainer (Fisher Scientific) before the filtrate was centrifuged for 3 minutes at 300 x g. The resulting pellet was gently resuspended in MLEC media, seeded into a T75 flask, pre-coated with a solution of 0.1 % gelatin containing FN (10 µg/ml) and collagen (COL I) (10 µg/ml), and incubated at 37 °C, 5 % CO_2, 95 % humidity. The following day, red blood cells were removed by performing two washes with PBS, before being replaced with fresh MLEC media. When the flask was near confluence, ECs were positively selected for through their expression of endomucin by magnetic activated cell sorting (MACS) as previously described [214]. Cells were placed at 4 °C for 20 minutes prior to incubation with rat-anti-mouse endomucin (Santa Cruz) (1:1000 in PBS) at 4 °C for 30 minutes. Post incubation, cells were washed once in PBS before being incubated with sheep-anti-rat IgC coated magnetic beads (Invitrogen) (1:1000 in MLEC media) at 4 °C for a further 30 minutes. After 3 PBS washes, cells were detached using 0.25 % trypsin-EDTA (Invitrogen) and neutralised with MLEC media before being collected into a 15 ml Falcon centrifuge tube and placed into a magnetic tube stand for 3 minutes. The supernatant was discarded, and the EC attached to the beads were resuspended in fresh MLEC media, and seeded into a T25 flask coated as described previously. Once cells neared confluency, a second positive sort for endomucin (as described above) as a marker for ECs was performed to enhance EC purity.

To immortalise primary ECs, they were treated with polyoma-middle-T-antigen (PyMT) by retroviral transfection as previously described [189]. Briefly, following the second endomucin positive selection, primary ECs were treated with PyMT conditioned media supplemented with polybrene (8 µg/ml) for 6 hours at 37 °C, before being returned to MLEC media. The same procedure was repeated the following day, however once the conditioned media was discarded, cells were cultured in immortalised microvascular mouse-lung EC (IMMLEC) media (modified MLEC media recipe whereby FBS was only supplemented to 10 % and endothelial mitogen was excluded) before being expanded and frozen down, ready for *in vitro* use.

2.4 IMMLEC tissue culture

ECs were grown on tissue culture flasks pre-coated with 0.1 % gelatin in IMMLEC media. All cell culture was performed under the following conditions: 37 °C, 5 % CO_2 and 95 % humidity.

Once the ECs had reached a state of near confluency, the IMMLEC media was removed, and the ECs were washed once using pre-warmed PBS, before being detached using 0.25 % trypsin-EDTA for 2 minutes. Following trypsinisation, trypsin-EDTA was neutralised with pre-warmed IMMLEC media, and the cell suspension transferred to a suitable gelatin-coated tissue culture flask. Immortalised ECs were used for experiments between passages 5 and 28.

2.5 TAT-Cre recombinase nucleofection

To excise our genes of interest, ECs were nucleofected with TAT-Cre recombinase (70 units) (Sigma), before being allowed to recover for two days. After which ECs were nucleofected again in the same manner.

2.6 siRNA nucleofection

Transfection of ECs was performed by nucleofection, according to the Lonza general nucleofection protocol, using the Lonza 4D Core/X Unit Nucleofector™. ECs were resuspended in a homemade nucleofection buffer HEPES: 200 mM, NaCl: 137 mM, KCl: 5 mM, D-glucose: 6 mM, Na_2HPO_4: 7 mM), (100 µl per $1x10^6$ ECs). To target NRP2, ECs were nucleofected with SMARTpool siRNA duplexes (#03, #04) purchased from Dharmacon. To target Rab11a and Rab11b, ECs were nucleofected with SilencerSelect siRNA purchased from Thermo Fisher Scientific. All nucleofection reactions were ran alongside a non-targeting control pool (Ctrl) siRNA reaction. siRNA pellets were resuspended as described by the manufacturer at a concentration of 40 µM, with 5.6 µl being used per $1x10^6$ ECs (for a final siRNA mass of 3 µg).

2.7 Western blotting

Protein samples were obtained by lysing cells in electrophoresis sample buffer (ESB) (Tris-HCL: 65 mM pH 7.4, sucrose: 60 mM, 3 % SDS). Lysed cells were scraped from their tissue culture plate using an Eppendorf tip, transferred to safe-lock Eppendorf tubes containing acid-washed glass beads (Sigma), homogenised in a Tissue Lyser (Qiagen) at 50 Hz for 2 minutes and finally centrifuged at 16,500 x g for 10 minutes to remove any bubbles. Lysates were analysed for protein concentration using the BioRad DC protein assay (BioRad), and added to NuPAGE 10X sample reducing agent and 4X LDS sample buffer (Life Technologies), at a final concentration of 1X. Protein samples were then boiled on a dry block thermostat at 95 °C for 5 minutes, before being loaded (20-30 µg) onto 8 % polyacrylamide gels with molecular mass protein markers, and subjected to SDS-PAGE for 2 hours at 100 volts. Separated proteins were then transferred to a 0.45 µm Amersham Protran® nitrocellulose membrane (GE Healthcare, Amersham) at 30 volts for 3 hours, before being blocked for 1 hour in 5 % milk powder in PBS 0.1 % Tween-20 (PBST 0.1 %), and incubated overnight in

primary Ab (unless otherwise stated at a 1:1000 dilution in 5 % BSA/PBST 0.1 % solution) at 4 °C. Following 3 washes, 5 minutes per wash, in PBST 0.1 %, membranes were incubated in an appropriate horseradish peroxidase (HRP)-conjugated secondary Ab (unless otherwise stated at a 1:2000 dilution in 5 % milk/PBST 0.1 % solution) for 2 hours at room temperature (RT). Membranes were then washed 3 times, 5 minutes per wash, with PBST 0.1 % and treated with 1:1 solution of Pierce ECL Western Blotting Substrate (Thermo Scientific). Chemiluminescence was detected on a ChemiDoc™ MP Imaging System darkroom (BioRad). Densitometric readings of band intensities for blots were obtained using Image J™.

2.8 Stripping nitrocellulose membranes

Membranes were stripped for additional probing using 2 x 10 minute incubations with a mild (pH 2.2) stripping buffer (glycine: 15 g, SDS: 1 g, Tween-20: 10 ml, buffer made up to 1 L in ultrapure water), followed by 2 x 10 minute washes in PBS, and 2 x 5 minute washes in PBST 0.1 %, before being re-blocked in 5 % milk powder in PBST 0.1 %. Membranes were then incubated in primary antibody as described in section 2.7.

2.9 Random migration assays

ECs were subject to nucleofection as described in section 2.6, seeded into 10 cm tissue culture dishes pre-coated with 10 µg/ml FN, and incubated for 24 hours. ECs were then washed twice with PBS, trypsinised, seeded into 24-well tissue culture plates pre-coated with 10 µg/ml FN at a density of $7x10^3$ ECs/well, and allowed to adhere for 180 minutes. EC migration was captured by timelapse microscopy: fixed images of multiple field/well of each condition were taken every 20 minutes for 16 hours using an inverted Axiovert (Zeiss) brightfield microscope in one phase contrast. Individual cell migration was manually tracked using the ImageJ™ MTrackJ plugin. Random migration speed of individual cells was calculated in µm/second.

2.10 Scratch-wound assays

ECs were subject to nucleofection as described in section 2.6, seeded into 10 cm tissue culture dishes pre-coated with 10 µg/ml FN, and incubated for 24 hours. ECs were then washed twice with PBS, trypsinised, seeded onto acid-washed, oven sterilised glass coverslips pre-coated with 10 µg/ml FN at a density of $1x10^5$ ECs/coverslip, and allowed to adhere overnight. Confluent cell monolayers were then scratched using a P1000 pipette tip and allowed to recover for a period of 8 hours. Phase contrast brightfield images were taken immediately after scratches were made, and again following 8 hours incubation. ECs were then incubated in 4 % paraformaldehyde (PFA) for 10

minutes at RT, followed by two washes in PBS before being processed for immunofluorescence imaging as described in section 2.11.

2.11 Immunocytochemistry

ECs were subject to nucleofection as described in section 2.6, seeded into 10 cm tissue culture dishes pre-coated with 10 µg/ml FN, and incubated for 24 hours. ECs were then washed twice with PBS, trypsinised, seeded onto acid-washed, oven sterilised glass coverslips pre-coated with 10 µg/ml FN for the indicated timepoint at a density of $2.5x10^4$ ECs/coverslip. Coverslips were washed twice with PBS before being incubated in 4 % PFA for 10 minutes at RT. Coverslips were then washed twice with PBS to remove any remaining PFA, before being blocked and permeabilised with 10 % goat serum, PBS 0.3 % triton X-100 for 1 hour at RT, and incubated in an appropriate primary antibody in PBS overnight at 4°C. Coverslips were washed 3 times with PBS, and incubated in an appropriate Alexa-fluorescent secondary antibody diluted 1:200 in PBS for 2 hours at RT in the dark. F actin staining was performed by incubating coverslips in phalloidin-568 diluted 1:40 in PBS for 2 hours at RT during the secondary antibody incubation. Coverslips were washed 3 times in PBS, before being mounted onto cover-slides with Prolong® Gold containing DAPI (4',6-diamidino-2-phenylindole- nuclear DNA stain) (Invitrogen). Images were captured using a Zeiss AxioImager M2 microscope (AxioCam MRm camera) at 63x or 40x magnification (with oil immersion), or using a Zeiss LSM880 Airyscan Confocal microscope at 63x magnification (with oil immersion). FA number and size was quantified using ImageJ™ software as previously described by Lambert *et al*. [215] using a FA size lower detection limit of 0.8 microns.

2.12 SOAX software analysis

SOAX software was employed to show azimuthal angles of actin stress fibres and measure stress fibre length in mLMECs. Analysis was performed as described previously [216]. Briefly, Images were exported into SOAX software in Tif. format, and '*snakes'* labelled. File images showing azimuthal angles (the horizontal angle displaced perpendicularly away from the point of interest in the spherical coordinate system) were produced using the azimuthal angle tool, colouring snakes based on their orientation. Stress fibre length was measured by computing snake length.

2.13 Immunocytochemistry including primaquine pre-treatment

Immunocytochemistry studies were performed as described in section 2.11, with the exception that prior to fixation, ECs were pre-incubated with 0.3 mM primaquine (PMQ) solution in PBS for 10 minutes. (Primaquine is widely known to inhibit endosomal recycling by accumulating in trafficking endosomal compartments where it neutralises endosomal pH [217]).

2.14 Rac1 pulldown assays

ECs were subject to nucleofection as described in section 2.6, seeded into 10 cm tissue culture dishes pre-coated with gelatin, and incubated for 48 hours. ECs were then washed twice with PBS, trypsinised, seeded into 10 cm tissue culture dishes pre-coated with 10 µg/ml FN and incubated for 180 minutes at a density of $2x10^5$ ECs/dish. ECs were lysed on ice with 1X $Mg2^+$ lysis/wash buffer (MLB) (diluted to 1X with sterile water containing 10 % glycerol and 1X Halt™ protease inhibitor cocktail (Thermo Scientific). Protein lysates were then cleared of insoluble cell debris by centrifugation for 5 minutes at 14,000 x g at 4 °C, before a 0.5 ml sample aliquot of each cell extract was added to a new microcentrifuge tube. Per 0.5 ml aliquot, 10 µl (10 µg) of Rac1/Cdc42 Assay Reagent (300 µg of Pak-1 PBD in 150 µl of glutathione magnetic beads, provided as a 50 % beads slurry in PBS containing 50 % glycerol for a final volume of 300 µl) was added, and allowed to incubate for 45 minutes at 4°C with gentle agitation. The beads were then pelleted using a magnetic tube stand, and the supernatant discarded. The beads were washed 3 times in MLB (per sample, per wash, 0.5 ml MLB was added, mixed by gentle pipetting, and beads pelleted using the magnetic tube stand). Beads were resuspended in 40 µl of NuPAGE 10X sample reducing agent and 4X LDS sample buffer, at a final concentration of 2X, and heated to 95 °C for 5 minutes. Samples were then subject to Western blotting as described in section 2.7. Nitrocellulose membranes were immunoblotted using 1 µg/mL of anti-Rac1, clone 23A8 (Sigma).

2.15 VEGF-stimulated signalling assays

ECs were subject to nucleofection as described in section 2.6, and seeded into 6-well tissue culture plates pre-coated with 10 µg/ml FN at a density of $3x10^5$ ECs/well for 48 hours. ECs were then washed twice with PBS and incubated in serum-free medium (OptiMEM®; Invitrogen) for 3 hours. ECs were then incubated with VEGF at a final concentration of 30 ng/ml/well for the indicated timepoints. Stimulation was suspended at the indicated timepoints by placing ECs on ice. ECs were then washed twice with PBS and lysed in ESB. At this point, lysates were prepared and subject to Western Blotting as described in section 2.7.

Vascular endothelial growth factor-A (VEGF-A_{164}: the mouse equivalent of VEGF-A_{165}) was made in-house as previously described by Krilleke *et al.,* [218].

2.16 Co-immunoprecipitation assays

ECs were subject to nucleofection as described in section 2.6, seeded into 10 cm tissue culture dishes pre-coated with 10 µg/ml FN, and incubated for 48 hours at a density of $2x10^6$ ECs/dish. ECs were then lysed on ice with lysis buffer as previously described [108] in the presence of 100X Halt™

protease inhibitor cocktail, and protein quantified using the DC BioRad assay. 400 µg protein samples were incubated with protein-G Dynabeads® (Invitrogen) resuspended in PBS 0.02 % Tween-20 (PBST 0.2%) coupled to an appropriate primary antibody on a rotator overnight at 4°C. Beads were then washed 3 times with lysis buffer in the presence of 1X Halt™ protease inhibitor (per sample, per wash, 0.5 ml lysis buffer was added, mixed by gentle pipetting, and beads pelleted using the magnetic tube stand), and once in PBS to elute any immunoprecipitated complexes. Samples were added to NuPAGE 10X sample reducing agent and 4X LDS sample buffer at a final concentration of 1X, heated to 95 °C for 5 minutes, and subject to Western Blotting as described in section 2.7.

2.17 Co-immunoprecipitation assays including primaquine pre-treatment

Co-immunoprecipitation studies were performed as described in section 2.16, with the exception that prior to lysis, ECs were pre-incubated with 0.3 mM primaquine (PMQ) solution in PBS for 10 minutes.

2.18 Biotinylation assays

2.18.1 Internalisation assays

ECs were subject to nucleofection as described in section 2.6, and seeded into 10 cm tissue culture dishes pre-coated with 10 µg/ml FN at a density of $2x10^6$ ECs/dish for 48 hours. ECs were then incubated in serum-free OptiMEM® for 3 hours, before being placed on ice for 5 minutes, then washed twice with Soerensen buffer (SBS) pH 7.8 (14.7 mM KH_2PO_4, 2 mM Na_2HPO_4, and 120 mM Sorbitol pH 7.8) as previously described [219]. EC cell surface proteins were labelled with 0.3 mg/ml biotin (Thermo Scientific) in SBS for 30 minutes at 4 °C. Unreacted biotin was quenched with 100 mM glycine for 10 minutes at 4 °C. ECs were then incubated in pre-warmed serum-free OptiMEM® for the indicated time points. A sample of ECs were maintained at 4 °C for use as positive/negative (+/- Mesna) controls. Following incubation, dishes were immediately placed on ice, washed twice with SBS pH 8.2, and incubated with 100mM Mesna (Sigma) for 75 minutes at 4°C (with the exception of Mesna control plates, which were lysed in lysis buffer (25 mM Tris-HCl, pH 7.4, 100 mM NaCl, 2 mM MgCl2, 1 mM Na_3VO_4, 0.5 mM EGTA, 1% Triton X-100, 5 % glycerol, and protease inhibitors), and placed on ice). Following Mesna incubation, excess Mesna was quenched with 100 mM iodoacetamide (Sigma) for 10 minutes at 4 °C, then ECs were washed twice with SBS pH 8.2 and lysed. Lysates were cleared by centrifugation at 12,000 x g for 20 minutes at 4 °C. Supernatant proteins were then quantified using the DC BioRad assay, and subsequently immunoprecipitated with Dynabeads™ Protein G (Invitrogen) coupled to mouse anti-biotin antibody overnight at 4 °C.

Immunoprecipitated biotin-labelled proteins were separated by SDS-PAGE and subjected to Western blot analysis as described in section 2.7. The level of internalised α5 integrin at each time of incubation was normalised to the (- Mesna) control.

2.18.2 Recycling assays

After surface labelling, ECs were incubated in pre-warmed serum free OptiMEM® for 20 minutes to allow for internalisation. A sample of ECs were maintained at 4 °C for use as positive/negative controls. The remaining dishes were subsequently placed on ice, washed twice with SBS pH 8.2, and any un-internalised biotin-labelled proteins were stripped off using 100 mM Mesna in Tris buffer for 75 minutes at 4°C. The internalised fraction of proteins was then allowed to recycle to the membrane by incubating the ECs for the indicated time points in serum-free OptiMEM®. Following the indicated times of incubation, dishes were placed on ice, washed twice with SBS pH 8.2, and subjected to Mesna incubation for 75 minutes at 4 °C. (-Mesna) treatment dishes at each timepoint were used as respective controls for each sample. All subsequent stages were performed in the same manner as the internalisation assay. The level of the recycled α5 integrin was determined by normalising the amount of α5 integrin quantified from dishes treated with Mesna, to the total α5 integrin on the membranes of the Mesna-untreated cells in the same period of incubation.

2.19 Deoxycholate (DOC) buffer-extraction

ECs were subject to nucleofection as described in section 2.6, seeded into 10 cm tissue culture dishes pre-coated with 10 µg/ml FN, and incubated for 16 hours. ECs were then lysed in DOC lysis buffer (20 mM Tris, pH 8.5, 1 % sodium deoxycholate, 2 mM iodoacetamide, 2 mM EDTA) in the presence of 100X Halt protease inhibitor cocktail, cleared by centrifugation, and the insoluble fraction isolated. Insoluble fractions were separated by SDS-PAGE and subjected to Western blotting as described in section 2.7.

2.20 *In vivo* CMT19T tumour growth assays

Mice received intraperitoneal (IP) injections of tamoxifen (75 mg/kg bodyweight, 2 mg/ml stock) (Jackson Laboratory Protocol, Bar Harbor, Maine, USA) thrice weekly (Monday, Wednesday, Friday) for the duration of the experiment(s) from D-4 to D17 to induce Cre-recombinase activity. CMT19T lung carcinoma cells (CR-UK Cell Production) were prepared in PBS ($1x10^6$ per 100 µl) and implanted subcutaneously (SC) into the flank of mice at D0 and allowed to grow until D18. Tumour growth was tracked using callipers from D7 until the day of harvest. On D18, mice were sacrificed, tumour sizes measured, and tumour samples fixed in 4 % PFA for blood vessel density analysis. Tumour

volumes were calculated according to the formula: length x width^2 x 0.52 [220]. Tamoxifen injections were delayed from D-4 to D7 during intervention experiments.

CMT19T cells were cultured in high glucose DMEM, supplemented with 10 % FBS and pen-strep (100 units/ml). CMT19T cells were SC implanted on D10 after a total of 3 passages for repeatability purposes.

2.21 *In vivo* PyMT-BO1 tumour growth assays

PyMT-BO1 cells (1x10^5 in matrigel) were implanted orthotopically into the inguinal mammary fat pad under anaesthesia, and allowed to develop until D15. Mice received intraperitoneal (IP) injections of tamoxifen (75 mg/kg bodyweight, 2 mg/ml stock) thrice weekly (Monday, Wednesday, Friday) for the duration of the experiment from D7 to induce target deletion. Tumour growth was tracked using callipers from D7 until the day of harvest. On D15, mice were sacrificed, tumour sizes measured, and tumour samples fixed in 4 % PFA for blood vessel density analysis.

2.21.1 Immunofluorescence analysis of tumour sections

Frozen tumours were sectioned (6 µm) using a Crystat HM-560 (Microm) and mounted onto positively charged slides. Slides were then air dried for 10 minutes, before being fixed in 4 % PFA for 10 minutes at RT. Slides were washed twice in PBS 0.3 % triton-X100, twice in PBLEC (1x PBS, 1% Tween 20, 0.1 mM $CaCl_2$, 0.1 mM $MgCl_2$, 0.1 mM $MnCl_2$) and incubated in Dako protein block serum free (Agilent). Sections were then incubated overnight at 4 °C in primary antibody (diluted in PBS). Following primary antibody incubation, sections were washed again twice in PBS 0.3 % triton-X100 and PBLEC before being incubated in the appropriate Alexa fluor secondary antibody for 2 hours at RT. Sections were then blocked in Sudan black (0.1 % in 70 % EtOH) for 5 minutes (in order to quench auto-fluorescence), briefly rinsed in dH_2O before being mounted with Fluoromount-G™ with DAPI and imaged at 20x magnification using a Zeiss AxioImager M2 microscope. Blood-vessel density was assessed by counting the number of endomucin-positive vessels per mm^2 from 3 representative ROIs/ section, averaged over 3 sections/tumour. Analyses are presented as relative values against corresponding Cre-negative control values.

Quantification of the % of *p*-FAK^{Tyr407}-positive blood vessels was calculated by counting the number of endomucin-positive, *p*-FAK^{Tyr407} positive vessels, and dividing by the total number of endomucin-positive vessels from 5 representative ROIs/ tumour, 3 tumours per group.

2.22 *In vivo* retina assays

Tamoxifen-induced activation of Cre-recombinase was employed via 2 regimes: juvenile mice either received subcutaneous (SC) injections of tamoxifen (50 µl, 2 mg/ml stock) on postnatal (P) days 2 and 3, followed by intraperitoneal (IP) injections of the same dose on P4 and 5 before retinas being harvested at P6, or mice received IP injections of tamoxifen (50 µl, 2 mg/ml stock) on postnatal (P) days 7 to 10 before retinas being harvested at P12. After dissection, retinas were fixed in ice-cold methanol for 30 minutes before being prepared for blocking and immuno-staining. First, retinas were permeabilised in PBS 0.25 % triton-X100 for 30 minutes at RT, before being washed twice in PBLEC and then blocked in Dako protein block serum free for 1 hour. Retinas were then incubated in primary antibody. Following primary antibody incubation, retinas were incubated in the appropriate secondary antibody for 1 hour at RT, before being washed twice in PBS 0.1 % triton-X100 and mounted using Fluoromount-G™. Images were captured using a Zeiss LSM880 Airyscan Confocal microscope.

2.22.1 *In vivo* retina analysis

A range of measurements were taken from both the proliferative and remodelling zones of the mouse retina (Figure 2.1A).

2.22.1.1 Vascular extension

Vascular extension analysis was performed using ImageJ™, by measuring the length of the growing superficial vascular plexus from the optic nerve. A total of 3 lengths were taken per retinal leaf, which were then averaged to produce a mean length of vascular extension per leaf. The averages of each leaf were subsequently averaged to produce a retina mean.

2.22.1.2 Vessel density and branch points

Vessel density and number of vessel branching points were measured using AngioTool™ from 350 x 350 micron ROIs captured at the proliferative zone (**Figure 2.1A-B, E**). A total of 1 ROI was taken per retinal leaf. These values were averaged to produce a retina mean. The density of ERG positive EC nuclei was captured using ImageJ™, by manually counting the number of ERG positive EC nuclei in 200 x 200 micron ROIs taken 100 microns from the vascular front (**Figure 2.1C**). A total of 3 ROIs were measured per retinal leaf, which were then averaged to produce a mean density per leaf. The averages of each leaf were subsequently averaged to produce a retina mean.

Vessel density, vessel branching points and the number of descending vessels in retinas harvested at P12 at both the superficial plexus and the deep plexus layers were measured from 850 x 850 micron ROIs. A total of 1 ROI was taken per retina (**Figure 2.1D**).

2.22.1.3 Vessel regression

Vessel regression was measured by counting the number of BS-1 lectin negative, collagen IV positive vessels within 200 x 200 micron ROIs taken mid-way between the vascular front and the optic nerve (**Figure 2.1C**). A total of 3 ROIs were taken per retinal leaf, which were then averaged to produce a mean value of regressed vessels per leaf. The averages of each leaf were subsequently averaged to produce a retina mean.

2.22.1.4 Vessel diameter

Vessel diameter was analysed by measuring the diameter of 5 vessels within 350 x 350 micron ROIs taken at the proliferative zone (**Figure 2.1A-B**). Each vessel was measured at its centre point, and the values averaged to produce a mean diameter per ROI. A total of 3 ROIs were measured per retina, and the mean values combined to produce a retina mean.

2.22.1.5 Tip cell and filopodia enumeration

Number of tip cells at the vascular front was measured by manually counting the number of sprouting ECs at the vascular front per leaf, before dividing by the length of the vascular front (**Figure 2.1C, E**). A retina mean was then calculated from averaging leaf values. Filopodia number was measured by manually counting the number of filopodia per sprouting tip cell. The filopodia of a total of 50 tip cells were counted from at least 5 retinas per genotype. Filopodial tortuosity was calculated by measuring the linear distance between filopodial start and end points, before dividing by the total length of filopodial tracks. A total of 50 filopodia were counted from at least 5 retinas per genotype. *p*-FAK^{Tyr407} intensity within tip cells relative to stalk cells was calculated by measuring the corrected total cell fluorescence (CTCF- QBI, The University of Queensland, Australia). CTCF was calculated according to the formula: IntDen - area * background IntDen. Tip cell CTCF values were subsequently made relative to stalk cell CTCF values. A total of 50 tip cells were counted from at least 5 retinas per genotype.

With the exception of vessel regression, filopodial tortuosity, and *p*-FAK intensity within tip cells, all retina analyses are presented as relative values against corresponding Cre-negative control values.

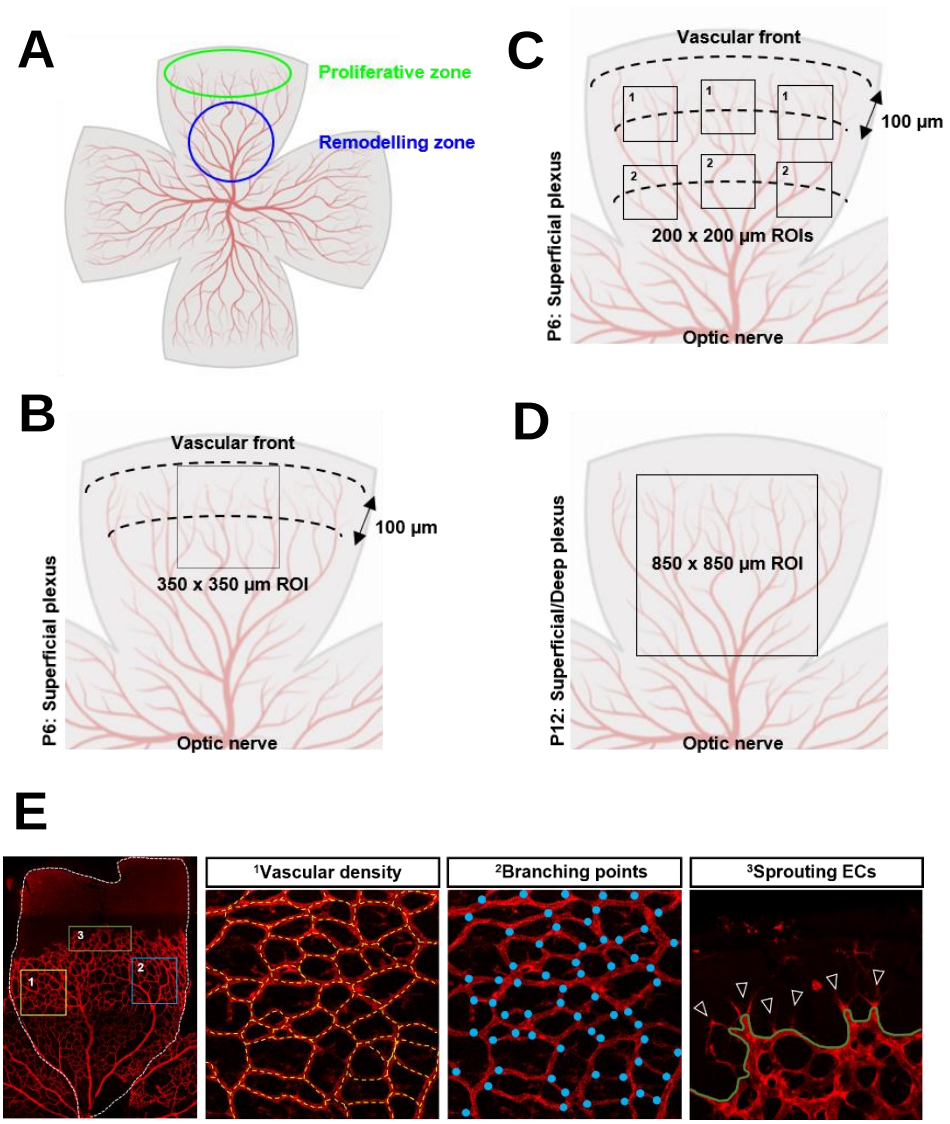

Figure 2.1 Schematics showing locations of retina analysis. A) Schematic image of a murine retina showing the locations of both proliferative and remodelling zones. **B**) Schematic image of a retinal leaf showing the location of the 350 x 350 micron ROI taken at the proliferative zone to measure vessel density, vessel branching points and vessel diameter. **C**) Schematic image of a retinal leaf showing the locations of 200 x 200 micron ROIs taken either at the proliferative zone, 100 microns from the vascular front to measure the density of ERG positive nuclei (1), or at the remodelling zone, mid-way between the optic nerve and the vascular front to measure vessel regression (2). **D**) Schematic image of a retinal leaf showing the location of the 850 x 850 micron ROI taken to measure vessel density, vessel branching points and number of descending vessels in retinas harvested at P12 at both the superficial plexus and deep plexus layers. **E**) Retinal flat mount images indicating areas of analysis for vascular density (1), branching points (2), and sprouting ECs (3). (Figure generated using BioRender).

2.23 Statistical analysis

The graphic illustrations and analyses to determine statistical significance were generated using GraphPad Prism 9 software. Unless otherwise stated, unpaired (two-tailed) Student's t-tests (with, or without multiple comparisons as appropriate) were performed to analyse differences between mean values.

When evaluating *in vivo* results, statistical analysis comparing *in vivo* Cre-positive mean values to their respective Cre-negative counterpart mean values, was performed using unpaired (two-tailed) Student's t-tests. Statistical analysis comparing two or more independent Cre-positive animal groups was performed using one-way ANOVA.

All bar charts show mean values and the standard error of the mean (± SEM). Asterisks indicate the statistical significance of P values: $P > 0.05$ = ns (not significant), * $P < 0.05$, ** $P < 0.002$, *** $P < 0.0005$ and **** $P < 0.0001$.

Power calculations from previous preliminary datasets were used to inform the required numbers of n values for *in vivo* experimental analyses.

3 Results

3.1 Generating the tools to study the interplay between endothelial NRP2, NRP1 and a5 integrin during angiogenesis

To examine how the interactions between NRP2, α5β1 integrin and NRP1 regulate angiogenesis at the cellular and molecular level, we required a model with the ability to induce discrete temporal deletion of our genes of interest, individually and in duplicate, specifically within the endothelium. The Robinson Laboratory has historically employed the Cre-LoxP system to genetically excise genes in this manner [107], [189], [198]. To refine the endothelial specificity of our deletion, we and others have utilised the Cre-loxP system alongside the endothelial specific PDGFb.iCre promoter, isolating Cre expression to the endothelium [221]. Employing such promoters also enables the user to overcome the embryonic lethal phenotypes observed from constitutive knockout models, such as Tie1.Cre and Tie2.Cre [212].

Further advances in the design of this system have since allowed researchers the ability to control the activity of Cre-recombinase temporally. This was achieved by incorporating an estrogen receptor within the Cre gene construct that possesses a mutated ligand binding domain, ER^{T2}. This blocks the nuclear localisation signal (NLS) necessary for nuclear translocation, and therefore Cre recombinase remains sequestered within the cytoplasm following transcription. $CreER^{T2}$ activity is exogenously inducible through the administration of tamoxifen, which is subsequently metabolised to 4-hydroxytamoxifen (4-OHT) by circulating hepatocytes. 4-OHT then binds the estrogen receptor ER^{T2} domain, revealing the NLS, thereby allowing the translocation of $CreER^{T2}$ into the nucleus [222]. Floxed gene(s) are consequentially removed from the genomic DNA by Cre-mediated recombination that occurs between LoxP sites. By administering tamoxifen in excess, issues surrounding partial mosaic Cre-LoxP recombination; the incomplete genetic depletion of multiple floxed genes, are also avoided [223].

3.1.1 Breeding strategy for the generation of genetically modified mouse models

Upon commencing this project, the $\alpha5^{flfl}$ and $NRP1^{flfl}$ single knockout genetically engineered mouse models expressing $PDGFb.iCreER^{T2}$ on a pure C57/BL6 background to selectively induce α5 and NRP1 depletion following tamoxifen administration had already been generated by the combined efforts of Dr Tim Ellison, Dr Samuel Atkinson and Dr Robert Johnson. We therefore only needed to generate the $NRP2^{flfl}$ single knockout and both $NRP1^{flfl}$/$NRP2^{flfl}$ and $NRP2^{flfl}$/ $\alpha5^{flfl}$ double knockout models. Briefly, the generation of these models required crossing the $PDGFb.iCreER^{T2}$ promoter with mice floxed for NRP2 (flanked by loxP sites), followed by crossing the single $NRP2^{flfl}$ knockout

model with either the $\alpha5^{flfl}$ or the $NRP1^{flfl}$ single knockout models to generate both double knockout models (**Figure 3.1.**). To maintain a heterozygous expression of PDGFb.iCreER^{T2} in the progeny of these knockout models, and thereby utilise Cre-recombinase 'negative' (Cre-negative) offspring as littermate controls in all experiments, we limited its expression to breeding males only. Using this littermate control strategy subsequently accounted for any experimental variance that may have arisen from using multiple breeders for each knockout model.

In addition to confirming the genetic floxing of all our experimental animal breeders, alongside expression of PDGFb.iCreER^{T2} in breeding males (**Figure 3.2.**), we also confirmed the genetic identity of every animal born to those breeders. This breeding strategy to minimise unintentional floxing or PDGFb.iCreER^{T2} expression arose from the chance identification of incorrect heterozygous floxing in one of our breeding colonies. Furthermore, all PDGFb.iCreER^{T2} PCR reactions were ran with an internal β2-microglobulin loading control to avoid false negative results.

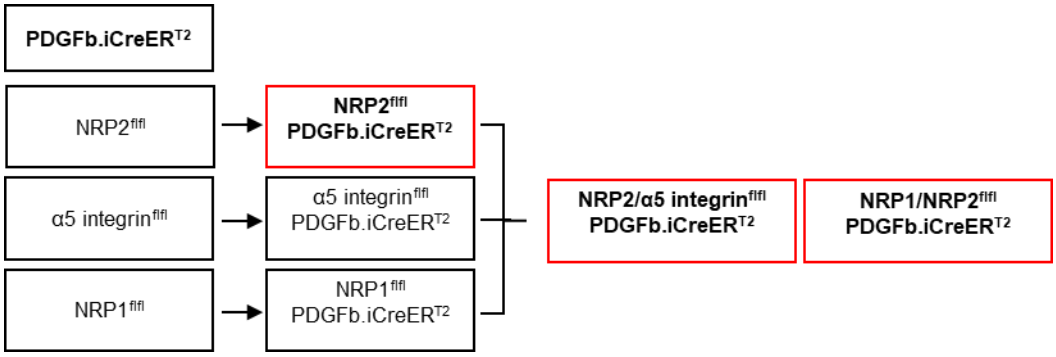

Figure 3.1 Breeding schematic to generate NRP2^{flfl} single knockout and both NRP1^{flfl}/NRP2^{flfl} and NRP2^{flfl}/ α5^{flfl} double knockout models. Tamoxifen-inducible deletion of our target genes was achieved by crossing mice expressing the endothelial-specific promoter of Cre-recombinase PDGFb.iCreER^{T2}, with mice floxed for either NRP2, α5 or NRP1. Subsequent crosses were made to establish both NRP1^{flfl}/NRP2^{flfl} and NRP2^{flfl}/ α5^{flfl} double knockout models. Throughout this breeding process, the expression of PDGFb.iCreER^{T2} was limited to breeding males in order to maintain its heterozygous identity in resulting progeny.

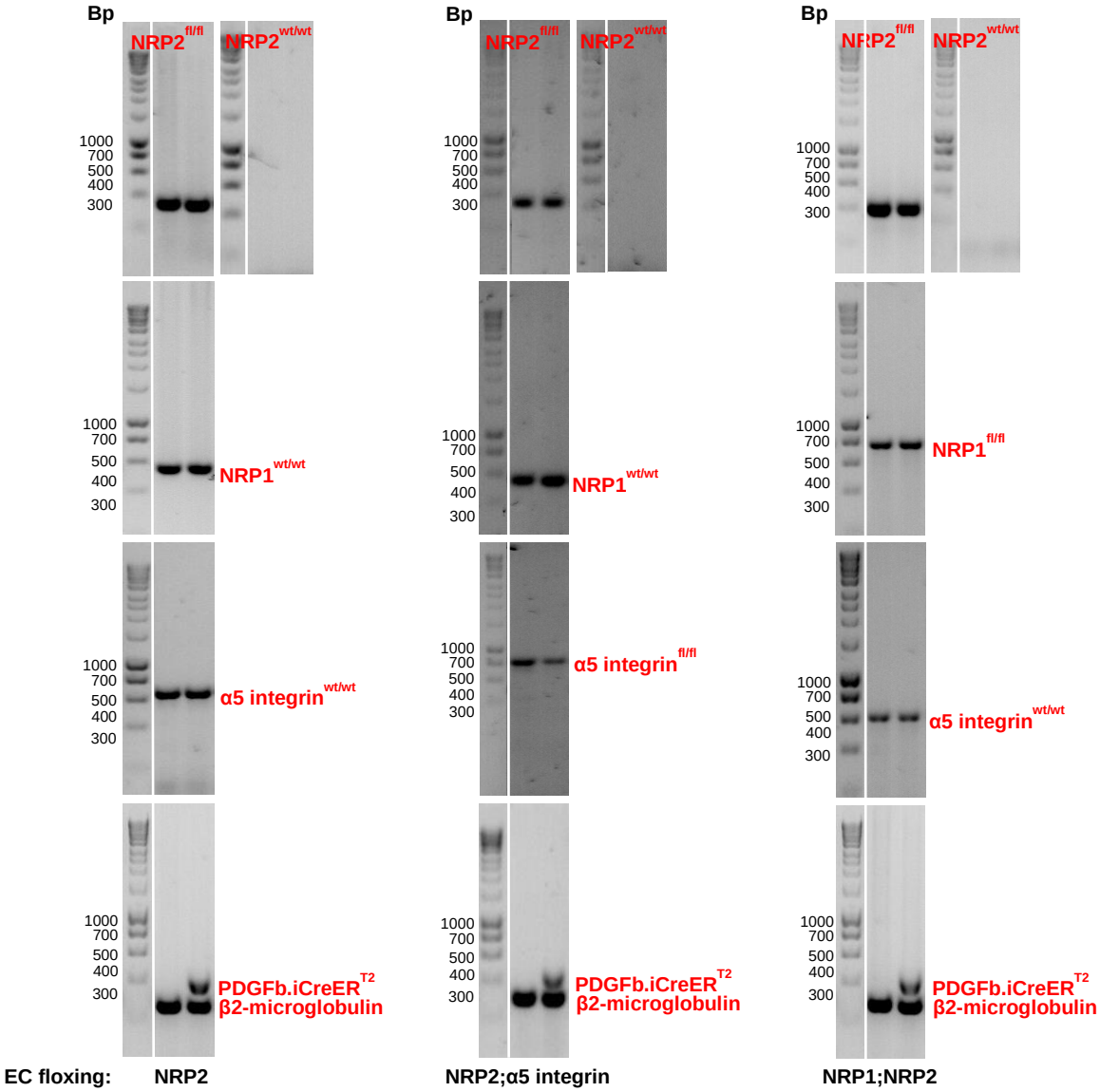

Figure 3.2 Representative PCR analysis confirming target gene floxing and PDGFb.iCreER^{T2} expression in all knockout models. PCR reactions were performed on DNA from ear tissue biopsies in order to confirm genetic floxing of target genes in addition to the expression of PDGFb.iCreER^{T2}. Shown are two representative DNA samples per knockout model demonstrating the heterozygous expression of PDGFb.iCreER^{T2} in each floxed line. The PDGFb.iCreER^{T2} PCR reaction is shown with a β2-microglobulin loading control.

3.1.2 siRNA-based silencing in floxed endothelial cell lines enables the study of multiple knockout phenotypes *in vitro*

In the period taken to generate the NRP2^{flfl} single knockout and both NRP1^{flfl}/NRP2^{flfl} and NRP2^{flfl}/α5^{flfl} double knockout models, we required EC lines with which we could begin to understand the complex interplay between our three target receptors and how they regulate angiogenesis. Prior to commencing this project, both the α5^{flfl} and NRP1^{flfl} single knockout mLMEC lines had already been generated by isolating primary ECs from the lung microvasculature of their respective animals. These primary ECs had subsequently been immortalised using the polyoma-middle-T-antigen (PyMT) retrovirus as previously described [189], [197], [224], in an effort to avoid using the unethical number of animals required for various complex biochemical assays. Inducing target deletion by directly transfecting Cre-recombinase (TAT-Cre-recombinase) into a pool of genetically identical immortalised mLMECs rather than to isolate ECs from tamoxifen-induced floxed animals also enabled us to maximise the use of our animals. Briefly, each knockout line began as a population of immortalised mLMECs floxed for their specific target/targets. From this population, a subpopulation underwent two rounds of nucleofection with TAT-Cre-recombinase to induce highly efficient target deletion, which was subsequently confirmed by western blotting over the course of their passaged lifespan. This technique also left a population of ECs whose genetic floxing remained intact, and therefore acted as a control to which experimental findings could be compared.

Without the NRP2^{flfl} single and double knockout models however, respective EC lines to compare against the α5^{flfl} and NRP1^{flfl} single knockout lines were yet to be generated. In their place, we utilised siRNA-mediated knockdown to induce temporary depletion of NRP2 in either TAT-Cre-recombinase 'negative' mLMECs, or in either α5^{flfl} or NRP1^{flfl} TAT-Cre-recombinase 'positive' mLMECs. To my benefit, Dr Abdullah Alghamdi of the Robinson laboratory had already identified two different mouse-specific NRP2-siRNAs (Dharmacon Cat# D-040423-03 and # -04) that induced between 90 - 95 % suppression of NRP2 expression for at least 72 hours from the day of nucleofection. Importantly, these siRNA constructs showed no cross reactivity to NRP1. Historically, the laboratory has employed electroporation (utilising the Amaxa Nucleofector II^{TM}) to efficiently induce siRNA-mediated knockdown in PyMT-immortalised mLMECs [215], [225]. This method is fast, highly efficient and replicable, however upon starting this project the Amaxa Nucleofector II^{TM} had been replaced with the Lonza 4D Core/X Unit Nucleofector^{TM}. To confirm the efficiency of our NRP2-specific siRNAs using the Lonza 4D Core/X Unit Nucleofector^{TM}, we performed a series of optimising nucleofection reactions using 15 different unit programs, all at a final siRNA

concentration of 40 µM, 5.6 µl per reaction (for a final mass of 3 µg), as previously described [225]. Of these 15 reactions, we identified a program (EO100) that induced a ~95 % depletion of NRP2 that lasted 72 hours from the day of nucleofection (**Figure 3.3A-B**), without altering the expression of either α5 integrin or NRP1. All subsequent NRP2 siRNA nucleofection reactions, unless stated otherwise, were completed using siRNA#3 at a final mass of 3 µg under the EO100 program using the Lonza 4D Core/X Unit Nucleofector™ alongside a control pool (Ctrl) siRNA.

This method enabled us to quickly produce EC lines in which NRP2 was depleted individually (*si*NRP2) or in combination with either α5 integrin (α5*KO si*NRP2) or NRP1 (NRP1*KO si*NRP2) respectively. These NRP2 siRNA-treated ECs were subsequently compared to their respective internal control pool siRNA-treated EC population during analyses (**Figure 3.3C**).

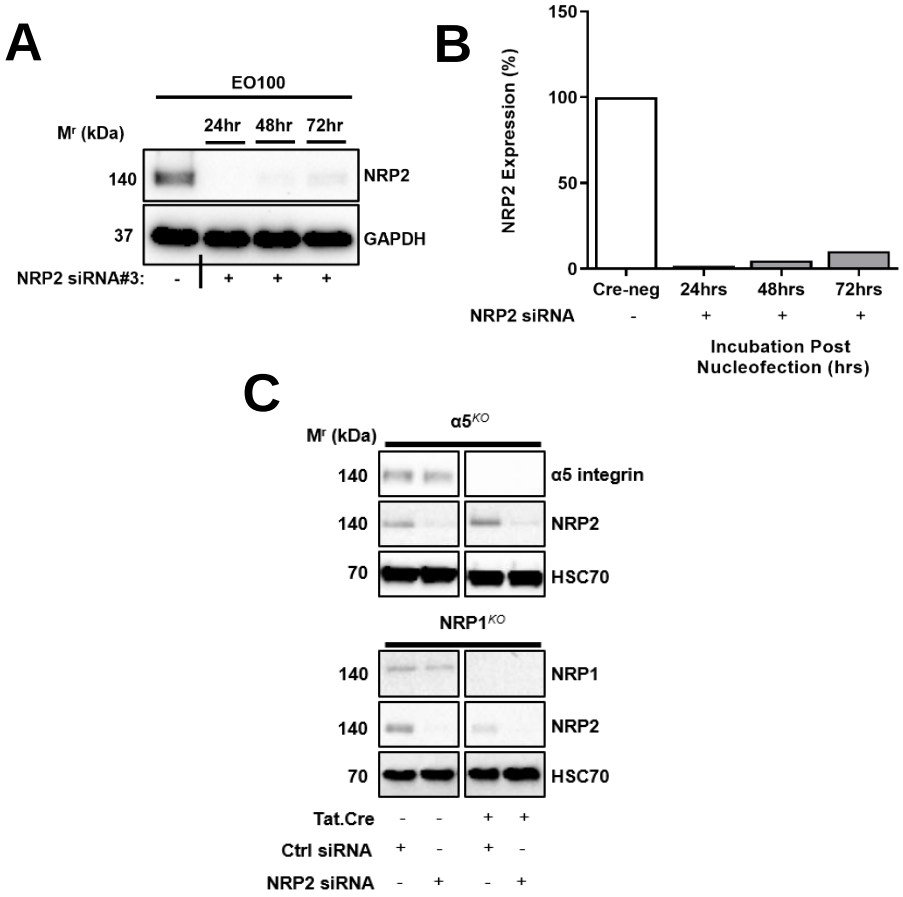

Figure 3.3 Confirming the efficiency of NRP2 depletion by siRNA-mediated nucleofection. A) 1x10^6 ECs were nucleofected with either Ctrl siRNA or NRP2 siRNA#3 and seeded on 10 cm dishes pre-coated with gelatin for the indicated time (24, 48 or 72 hours) at 37 °C in a CO_2 incubator. ECs were lysed in ESB and subjected to the DC protein assay before being analysed by Western blotting. GAPDH was used as a loading control. Bands were quantified using ImageJ^{TM} densitometric analysis. **B)** Accompanying densitometric analysis. **C)** siRNA silencing in floxed endothelial cell lines enables the study of multiple knockout phenotypes. α5 floxed and NRP1 floxed Cre negative and positive ECs were nucleofected with either Ctrl siRNA or NRP2 siRNA and seeded into 6-well plates pre-coated with 10 µg/ml FN at a density of 3x10^5 ECs per well, before being incubated at 37 °C in a CO_2 incubator for 48 hours. ECs were lysed in ESB and subjected to the DC protein assay before being analysed by Western blotting. Blots images show NRP2 depletion in both Cre negative and positive floxed lines. HSC70 was used as a loading control.

3.1.3 Endothelial identity is preserved following PyMT-induced immortalisation

Despite now having established a method by which we could study the effects of depleting each of our targets individually or in duplicate using siRNA-based silencing in a combination of immortalised floxed EC lines, prior to their use, we thought it necessary to confirm how comparable immortalised ECs are to their primary counterparts. Cell immortalisation has become an attractive tool to overcome the limited proliferative capacity of primary cells, enabling the generation of cell numbers required for large and complex biochemical assays. Furthermore, the repeated isolation and characterisation of primary cell cultures from animal donors is often argued as both untenable and unethical. We and others have previously shown that PyMT-immortalised ECs are a good model to study key angiogenic mechanisms *in vitro*, demonstrating that transformation does not alter their underlying cellular mechanics or phenotypic traits [189], [197], [215], [224], [225]. That being said, an in depth assessment comparing the behaviour of primary mLMECs and PyMT-immortalised mLMECs remains lacking in the scientific field.

Firstly, we isolated two mature populations of ECs, confirming their endothelial identity against lysate collected from the fibroblast 3T3 cell line using ERG and claudin-5 [226]–[228]. Their expression also remained stable following the depletion of NRP2 (**Figure 3.4A**). Whilst demonstrated previously, we then thought it pertinent to once more confirm that the endothelial identity of our mLMECs was maintained following immortalisation with the PyMT retrovirus [225], for completeness. Despite our isolation procedure involving two independent sorts using endomucin, a marker for mature ECs, to positively select for ECs, it has been previously speculated that the immortalisation process alters endothelial identity. For this reason, lysates from three wild-type (WT) immortalised EC lines were assayed for their expression of several other key endothelial markers, including VE cadherin and pecam-1, in addition to ERG and claudin-5 [226]–[228]. We also probed for the expression of the lymphatic marker prox-1, to assess the purity of our EC populations [229]. All three lines were confirmed to express all endothelial markers, and only very minimal prox-1 expression, demonstrating that our mLMECs retain their endothelial identity post PyMT-induced immortalisation (**Figure 3.4B**).

In addition to confirming endothelial identity, we went on to assess any differences in the migration speed and FA development of our mLMECs on FN matrices, following immortalisation. These two processes are essential during angiogenesis, for without the ability to rapidly assemble adhesive structures to provide mechanical anchorage to the ECM, the migrating sprout would fail to track along its angiogenic signalling gradient [21]. To examine this, we isolated three discrete primary

mLMEC populations, and assayed their random migration speed over FN for a 16 hour period. We also measured the mean size of FAs in ECs allowed to adhere on FN for either 90 minutes or 16 hours. FAs were visualised in fixed cells by immunostaining for the FA marker paxillin. We subsequently immortalised the same three primary mLMEC populations and repeated our investigations, measuring both migration speed and FA size. In doing so we hoped to minimise any variation that may have arisen from using three different primary EC preparations. Despite observing no significant alterations in FA area between primary and immortalised mLMECs at 90 minutes, immortalised ECs exhibited significantly larger paxillin^{+} FAs after adhering to FN for 16 hours (**Figure 3.4C**). Concomitantly, immortalised ECs migrated significantly slower across a FN matrix than their primary counterparts, likely due to their accelerated production of larger, more stable adhesions, which undergo turnover less frequently (**Figure 3.4D**). Whilst it is important to consider that a greater degree of variation is likely to occur within a 16-hour period compared to only 90 minutes, it also highlighted the importance of potential changes immortalisation may incur on a cell's behaviour. We therefore endeavoured to repeat and confirm key experimental findings using primary mLMECs throughout the duration of this study.

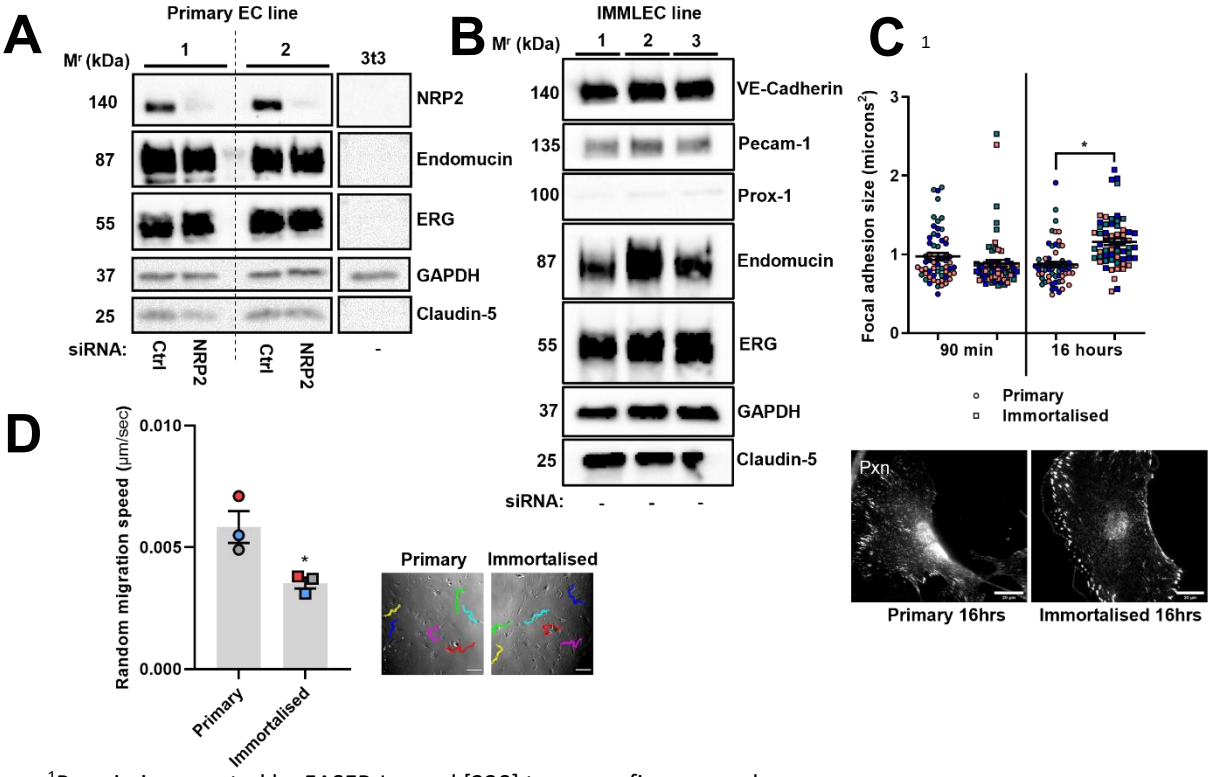

[1]Permission granted by FASEB Journal [230] to re-use figure panels.

Figure 3.4 A comparative analysis between primary and PyMT-immortalised mLMECs. Lungs from 10 WT C57 mice were digested in 0.1% collagenase solution for 1 hour at 37°C before being passed through a 19G needle 3 times, and subsequently a 21G needle into a 70 µm strainer. The resulting solution was then centrifuged, and the pellet resuspended in fresh media, before being seeded into three T75 culture flasks pre-coated with 0.1% gelatin, 10 µg/ml FN and 10 µg/ml collagen type 1 and incubated at 37°C overnight. Two successive primary EC sorts were then performed using rat primary antibody against Endomucin and anti-rat IgC coated magnetic Dynabeads to positively select for ECs. A subpopulation of each primary EC population was then immortalised using the PyMT viral vector by retroviral transfection. **A**) $1x10^6$ ECs from two primary populations were lysed in ESB and subjected to the DC protein assay before being analysed by Western blotting to confirm endothelial identity. The expression of the following endothelial markers were assessed compared to a 3T3 fibroblast control lysate pool: endomucin, ERG and claudin-5. GAPDH was used as a loading control. **B**) $1x10^6$ ECs from three independent WT immortalised lines were lysed in ESB and subjected to the DC protein assay before being analysed by Western blotting to assess endothelial identity and purity. GAPDH was used as a loading control. **C**) Three independent populations of primary and immortalised ECs were seeded at a low density onto acid-washed, oven sterilised coverslips pre-coated with 10 µg/ml FN and incubated for either 90 minutes or 16 hours. Coverslips were fixed in 4% PFA, blocked and permeabilised. ECs were then incubated with anti-paxillin primary antibody overnight at 4°C. Following two washes to remove any unreacted primary antibody, ECs were incubated with donkey anti-rabbit Alexa 488 secondary antibody at RT for 1 hour. Coverslips were mounted with Prolong Gold. Graph shows mean FA size/cell (μm^2). Error bars show mean ± SEM; N = 3 (n ≥ 60); colours indicate experimental repeat; *=P<0.05, unpaired students t-test (two-tailed) performed on mean values. Bottom panels show representative images of primary and immortalised ECs at 16 hours adhesion to FN immuno-stained with paxillin (Pxn). **D**) EC migration was captured by timelapse microscopy: fixed images of multiple field/well of each condition were taken every 20 minutes for 16 hours at 37°C and 5% CO_2 using an inverted Axiovert (Zeiss) microscope in one phase contrast. Individual cell migration was manually tracked using the ImageJ™ MTrackJ plugin. Random migration speed of individual cells was calculated in µm/sec. Error bars show mean ± SEM; N = 3 (n ≥ 250); colours indicate experimental repeat; *=P<0.05, unpaired students t-test (two-tailed) performed on mean values. Panels show representative phase contrast images.

3.1.4 Employing Label Free-Quantitative Mass Spectrometry analysis as a tool to identify candidate interactions

In addition to identifying the means to efficiently deplete NRP2 by siRNA-transfection, Dr Abdullah Alghamdi had also performed Label-Free Quantitative (LFQ) mass spectrometry and peptide identification (using MaxQuant software based on the Andromeda peptide database as described by Schiller et al., [231]. This data set had identified proteins immunoprecipitating with NRP2 at a significantly increased fold-change compared to proteins immunoprecipitated from NRP2 knockdown lysates in two WT mLMEC lines, each analysed with three technical repeats [225]. By analysing immunoprecipitated proteins in this manner, it was possible to ignore any false-positive protein hits (anything immunoprecipitated by the anti-NRP2 antibody in cells treated with NRP2-siRNA would be non-specific and therefore ignored). These analyses were performed with the aim of identifying cellular networks directly or indirectly regulated by NRP2, and to identify potential unknown candidate binding partners in an unbiased manner.

Previously, only protein hits detected in both WT lines had been considered as candidate binding partners of NRP2, including four microvascular EC specific markers: Pcam1, Mcam, endoglin and plasmalemma vesicle-associated protein [232]–[236], and three fibronectin receptors: α5 integrin, αV integrin and β1 integrin [24]. This informed the decision for Dr Abdullah Alghamdi to examine the interactions between NRP2 and α5 integrin, which forms the basis for this project. In an attempt not to overlook possible binding partners only identified in one of the two WT cell lines, the functions of all 1,080 peptide hits (**Appendix 1**) were re-annotated by literature review. Ingenuity Pathway Analysis software (kindly donated by Dr Naiara Beraza) was subsequently employed to arrange these proteins by the cellular pathways they support, placing NRP2 and its roles within the cell into a more comprehensive and visible context. Selecting the first 10 highest confidence pathways (**Appendix 2**) revealed that a large number of proteins immunoprecipitating with NRP2 regulated cellular adhesion or intracellular trafficking. These proteins were ordered hierarchically by calculating Log2(average fold-change) values, which are shown in **Table 3.1**. Adhesion-associated and intracellular trafficking-associated proteins are shown separately in **Figure 3.5**, generated using STRING software, arranged by their interaction confidence values. These candidate binding proteins will serve as a reference point for subsequent chapters and will be examined in more detail throughout this report.

There are, of course, caveats associated with co-immunoprecipitation-based proteomics analyses that should be considered when appraising this data. Firstly, inadequate incubation periods to allow

for binding, and the use of extensive washing steps, may prevent the detection of certain low affinity or transient protein-protein interactions. Furthermore, upon cell lysis, large numbers of non-specific proteins usually separated by cell boundaries will inevitably come into contact to give false-positive interactions. Optimising the ionic strength of lysis and wash buffers to account for, and reduce unspecific binding would therefore be advised for future immunoprecipitation-based proteomics. As a large proportion of candidate interactions were found with proteins regulating the cell's trafficking machinery, it would also be appropriate to include an additional internal transferrin control alongside immunoprecipitated complexes originating from NRP2 siRNA treated lysates, as described previously [237]. This would enable comparisons to a normalised baseline value rather than zero.

Table 3.1 LFQ mass spectrometry analysis identifying proteins immunoprecipitating with NRP2. Proteins referenced in the text of this thesis are highlighted in yellow. Annotated protein functions were taken from the RefSeq website at url: https://www.ncbi.nlm.nih.gov/refseq/. (Data generated by Dr Abdullah Alghamdi).

Gene name:	Average fold-change (Log2* LFQ Ctrl siRNA-NRP2 siRNA)	Protein name/function
Actb;Actg1	27.352935	*Actin (subunits)*
Actbl2	26.91196	*Beta actin like protein 2*
Vim	26.34357	*Vimentins: class III intermediate filaments- can link to focal adhesions*
Myh9	24.38293	*Myosin 9- during cell spreading, promotes cytoskeletal reorganisation, focal contact formation and lamellipodium retraction*
Capza1	23.21312	*F actin capping protein subunit*
Myh10	22.79844	*Myosin 10- Conventional non-muscle actin myosin- actin dependent motor promoting cytokinesis, cell motility and polarity*
Tpm4	22.57404	*Tropomyosin A4- stabilises actin filaments*
Tjp1	22.57389	*Tight junction protein ZO-1- promotes cell migration by targeting cdc42BPB to the leading edge of migrating cells*
Capza2	22.33849	*F actin capping protein subunit alpha2*
Pecam1	22.25224	*EC marker*
Tjp2	22.24607	*Tight junction protein - component of tight junctions and adherens junctions*
Twf1	22.19763	*Twinfilin-1 actin binding protein- inhibits actin polymerisation by sequestering G actin, caps barbed ends to regulate motility, promotes CME*
Arpc2	22.09911	*Actin related protein 2/3 complex subunit 2*
Ckap4	21.97439	*Cytoskeletal associated protein 4*
Arpc4	21.86602	*Actin related protein 2/3 complex subunit 4*
Tpm1	21.71132	*Tropomyosin alpha1 chain-binds to actin filaments, stabilises actin filaments*
Lima1	21.59035	*LIM domain and actin binding protein1- binds to actin monomers and filaments, increases numbers and size of stress fibres, inhibits membrane ruffling, inhibits filament depolymerisation*
Dbn1	21.52365	*Drebrin1- plays roles in cell migration and plasticity of dendrites, required for actin polymerisation at immunological synapses*
Tmod3	21.511345	*Tropomodulin-3 blocks elongation and depolymerisation of actin filaments at the pointed end*
Capzb	21.04462	*F actin capping protein subunit beta*
Mcam	21.00387	*Cell surface glycoprotein MUC18- plays roles in cell adhesion- acts as a surface receptor for phosphorylation of FAK*
Dab2	20.8565	*Disabled homolog 2- adaptor protein that functions as a clathrin associated sorting protein (CLASP) required for CME of proteins*
Arpc1b	20.82736	*Actin related protein 2/3 complex subunit 1B- functions as a component of ARP2/3 complex, regulates actin polymerisation*
Cav1	20.54872	*Caveolin-1*
Cfl1	20.52987	*Cofilin-1- binds F actin and exhibits pH sensitive F actin depolymerisation activity- regulates cytoskeletal dynamics*
Add1	20.48766	*Alpha adducin- membrane cytoskeletal associated protein that promotes assembly of spectrin actin network- binds to calmodulin*
Myo1c	20.41087	*Myosin 1c- actin based motor*
Rac1;Rac2;Rac3	20.33898	*Rac GTPases*
Map4	20.29954	*Microtubule associated protein 4- promotes microtubule assembly*
Actr2	20.16754	*Actin related protein 2- regulates actin polymerisation*
Actg1	20.1117	*Actin (subunits)*
Cav2	20.05977	*Caveolin-2- scaffolding protein in caveolar membranes*
Itga6	20.0482	*Integrin α6*
Itgb1	19.99879	*Integrin β1*
Eps15l1	19.98542	*EGFR substrate 15 like 1- constitutive component of clathrin coated pits, required for receptor mediated endocytosis*
Ap2m1	19.94502	*Clathrin adaptor*
Icam1	19.91639	*EC marker*
Pcdh1	19.81745	*Proto-cadherin 1*
Ptrf	19.77045	*Caveolae associated protein 1*
Tpm1	19.5741	*Tropomyosin alpha 1 chain- binds and stabilises actin filaments*
Itga3	19.19916	*Integrin α3*

Arpc5l	19.19293	*Actin related protein 2/3 complex subunit 5 like protein*
Ybx3;Igf2bp3	19.06616	*Insulin like growth factor 2 mRNA binding protein 2- RNA binding factor- binds to beta-actin transcripts*
Snx9	19.04328	*Sorting nexin 9- regulates endocytosis and intracellular vesicle trafficking*
Col18a1	18.94963	*Collagen alpha1 (XVIII) chain- plays a major role in determining retinal vascular development*
Ap2s1	18.87728	*AP2 clathrin adaptor*
Plcb4	18.86502	*Phospholipase C beta4*
Cttn	18.84761	*Src substrate cortactin- contributes to organisation of actin cytoskeleton and cell shape, promotes tumour metastasis, plays a role in focal adhesion assembly and turnover*
Actc1;Acta2;Actg2;Acta1	18.728625	*Actin (subunits)*
Ablim1	18.72782	*Actin binding LIM protein 1- may regulate retinal vascular development*
Actr3	18.68072	*Actin related protein 3- ATP binding component of Arp2/3 complex, involved in regulation of actin polymerisation*
Itga5	18.66171	*Integrin α5*
Plec	18.63159	*Plectin- interlinks intermediate filaments with microtubules and microfilaments and anchors intermediate filaments to desmosomes*
Cd44	18.60012	*Involved in cell migration, tumour growth, and progression*
Msn	18.52815	*Moesin- involved in connections to major cytoskeletal structures to the membrane, regulates proliferation, migration and adhesion*
Vasp	18.36514	*Vasodilator stimulated phospho protein- promotes actin filament elongation and FAK phosphorylation*
Cdh13	18.36345	*Cadherin 13- calcium dependent cell adhesion proteins*
Sdpr	18.27245	*Caveolae associated protein 2- regulates caveolae morphology by inducing membrane curvature within caveolae- required for formation of caveolae in lung endothelium*
Dyn-2	18.22985	*Dynamin2- plays important role in vesicular trafficking*
Tuba1b;Tuba4a	18.161405	*Tubulin (subunits)*
Arpc5	18.14685	*Actin related protein 2/3 complex subunit 5- functions as component of Arp2/3 complex- regulates actin polymerisation*
Wdr1	18.12918	*WD repeat containing protein 1: actin cytoskeleton regulation*
Rala	18.082035	*Ras related protein Ral-A- GTPase involved in cell migration, proliferation and membrane trafficking*
Rab11fip5	18.07134	*Recycling adaptor for Rab11*
Shank3	18.04178	*Links to the actin cytoskeleton*
Tmed10	18.03238	*Transmembrane emp24 domain containing protein 10- involved in vesicular protein trafficking*
Ralb	17.968125	*Ras related protein Ral-B- multi functional GTPase involved in cell migration, proliferation, membrane trafficking*
Mmrn2	17.95231	*Multimerin-2- inhibits EC motility, negatively regulates angiogenesis by sequestering VEGFA and preventing it from binding VEGFR-2*
Tmod2	17.90464	*Tropomodulin-2 blocks elongation and depolymerisation of actin filaments at the pointed end*
Ap2b1	17.88544	*AP-2 clathrin adaptor*
Add3	17.723735	*Gamma adducin- membrane cytoskeletal associated protein that promotes the assembly of spectrin actin network, binds calmodulin*
Rab6a;Rab6b	17.7023	*Recycling GTPase*
Rab14	17.70072	*Involved in membrane trafficking between Golgi and endosomes during early embryonic development*
Ehd4	17.67049	*EH domain containing protein 4- plays a role in early endosomal transport*
Pdcd10	17.649975	*Programmed cell death protein 10- promotes cell proliferation, important for cell migration, structural integrity of Golgi, required for normal angiogenesis vasculogenesis and haematopoiesis during embryonic development*
Esam	17.52096	*Endothelial cell selective adhesion molecule (EC marker)*
Myo6	17.50802	*Unconventional myosin-VI: actin based motor molecules- functions in variety of intracellular processes such as vesicular membrane trafficking and cell migration*
Emd	17.48906	*Emerin- stabilises and promotes formation of nuclear actin cortical network- stimulates actin polymerisation*
Tnc	17.48901	*Tenacin- Stimulates angiogenesis in tumours by elongation, migration and sprouting of ECs*
Pcdh1	17.46153	*Protocadherin-1*
Vapa	17.45271	*Vesicle associated membrane protein - stimulates rRas signalling attenuating integrin β1 activation at the cell surface*
Rab18	17.37967	*Recycling GTPase*
Cdc42ep1	17.34617	*Cdc42 effector protein 1- involved in organisation of actin cytoskeleton*

Flna	17.30314	*Filamin-A actin binding protein that promotes orthogonal actin filament branching and links actin filaments to membrane glycoproteins*
Cct4	17.25002	*T-complex protein 1 subunit delta- involved in actin folding*
Vti1b	17.2326	*Vesicle transport through interaction with t-SNAREs homolog 1B; vesicle trafficking*
Bcam	17.20623	*Basal cell adhesion molecule / laminin α5 receptor*
Tmem2	17.13397	*Regulates angiogenesis by mediating degradation of extracellular hyaluronan, thereby regulating VEGF signalling*
Picalm	17.13025	*Phosphatidylinositol binding clathrin assembly protein- recruits clathrin and AP-2 to cell membranes at sites of coated pit formation and clathrin vesicle assembly*
Vamp7	17.12582	*Vesicle associated membrane protein 7: involved in targeting of transport vesicles to their target membrane during transport of proteins from early endosome to lysosome*
Adam9	17.1037	*Disintegrin and metalloproteinase domain containing protein 9- cleaves and releases TEK, KDR, EPHB4, CD40, VCAM1 and Cdh5 to regulate tumorigenesis and angiogenesis*
Stx6	17.08659	*Syntaxin-6, involved in intracellular vesicle trafficking*
Rab35	17.0683	*Recycling GTPase*
Gm17087	17.0524	*Member of the actin family*
Ncstn	17.052	*Nicastrin- involved in proteolytically processing Notch*
Tpm1	17.04772	*Stabilises cytoskeletal actin filaments*
Scamp3;Tu52	17.040355	*Endocytic trafficking post Golgi recycling pathways*
Rab7;Rab7a	17.02443	*Rab7- late endosome marker*
Triobp	17.00441	*TRIO and F actin binding protein, may regulate actin cytoskeletal organisation, cell spreading , coordinates number of stress fibres*
Synpo	16.99803	*Actin associated protein, plays a role in modulating actin based shape and motility of dendritic spines*
Vamp3;Vamp2	16.97365	*Vesicle associated membrane protein 2/3: involved in targeting of transport vesicles to their target membrane during transport of proteins from early endosome to lysosome*
Myo5a	16.95829	*Processive actin based motor*
Myl12a	16.95068	*Myosin light chain 12A*
Twf2	16.94795	*Twinfilin2- actin binding protein- inhibits actin polymerisation - caps barbed ends of filaments to regulate motility*
Ppp1r9b	16.89936	*Neurabin-2- scaffolding protein in multiple signalling pathways- binds actin (F actin) filaments and shows cross linking activity*
Cdh5	16.8382	*Cadherin 5 - calcium dependent cell adhesion protein*
Ldlr	16.837325	*Regulator of CME*
Rras	16.78979	*Ras related protein- regulates organisation of actin cytoskeleton*
Sdcbp	16.789785	*Syntenin-1- trafficking transmembrane proteins, promotes tumorigenesis*
Ehd1	16.74583	*EH domain containing protein 1- regulates membrane trafficking between endosomes by mediating equilibrium between cell surface associated and cell surface dissociated caveolae*
Palm	16.74272	*Paralemmin-1 involved in membrane dynamics and cell process formation- necessary for axonal and dendritic filopodia induction*
Pdlim7	16.62921	*PDZ and LIM domain protein 7- PDZ domains bind to actin filaments, but can also regulate trafficking via GIPC1 domain*
Sec22b	16.56748	*Vesicle trafficking protein*
Tpm1	16.56535	*Tropomyosin alpha 1 chain- binds actin filaments- stabilises actin filaments*
Itgb3	16.55691	*Integrin β3*
Epn2	16.55035	*Epsin-2- plays a role in formation of clathrin coated invaginations and endocytosis*
Arpc3	16.54422	*Actin related protein 2/3 complex subunit 3*
Marcksl1	16.49389	*MARCKS related protein- controls cell movement by regulating actin cytoskeleton homeostasis and filopodium/ lamellipodium formation*
Grb2	16.43816	*Ras adaptor*
Scamp2	16.37087	*Functions in post Golgi recycling pathways- acts as a recycling carrier to the cell surface*
Iqgap1	16.32632	*Ras GTPase activating like protein IQGAP-1- binds to activated Cdc42 but does not stimulate its GTPase activity, regulates actin cytoskeletal reorganisation*
Rab5c	16.27054	*Early endosome marker*
Ap2a1	16.248185	*AP-2 complex subunit α1*
Flot1	16.2365	*Flotillin-1: scaffolding protein within caveolar membranes*
Epn1	16.21974	*Epsin-1- modifies membrane curvature and facilitates formation of clathrin coated invaginations- regulates receptor mediated endocytosis*
Epha2	16.21529	*Ephrin type A receptor 2- activated by the ligand ephrin-A1 to regulate migration, integrin mediated adhesion- regulates cell adhesion and differentiation through DSG1*

Ktn1	16.17446	*Kinectin- receptor for kinesin thus involved in kinesin driven vesicle motility, accumulates in integrin based adhesion complexes upon integrin aggregation by FN*
Fscn1	16.16555	*Fascin- organises filamentous actin into bundles - plays a role in organisation of actin filament bundles and formation of actin microspikes, ruffles and stress fibres*
Ap2a2	16.04031	*AP-2 complex subunit α2*
Actn4	15.90556	*Alpha actinin-4 F actin cross linking protein*
Marcks	15.88345	*Filamentous F actin cross linking protein*
Add2	15.80156	*β-adducin- membrane cytoskeletal associated protein that promotes the assembly of spectrin actin network, binds calmodulin*
RhoA;RhoB;RhoC	15.73653	*Rho GTPase family members*
Ptk7	15.70356	*Inactive tyrosine protein kinase 7- regulator of Wnt signalling, functions in cell adhesion, migration, polarity, actin cytoskeletal reorganisation*
Tubb5;Tubb2b;Tubb2a;Tubb3	15.68854	*Tubulin (subunits)*
Mapre1	15.64087	*Microtubule associated protein family member 1- regulates microtubule cytoskeleton dynamics- promotes nucleation and elongation*
Actr1a	15.54383	*Actin related protein*
Eps15	15.532455	*EGFR substrate 15 involved in cell growth regulation, acts as a clathrin adaptor for post Golgi trafficking*
Rdx	15.48895	*Radaxin- binds barbed end of actin filament to plasma membrane*
Clta	15.45988	*Clathrin light chain A*
Cltc	15.445875	*Clathrin heavy chain C*
Ctnnd1	15.38476	*Catenin (cadherin associated protein)*
Ehd2	15.366515	*EH domain containing protein 2- regulates membrane trafficking between endosomes by mediating equilibrium between cell surface associated and cell surface dissociated caveolae*
Flot2	15.32638	*Flotillin-2: scaffolding protein within caveolar membranes*
Specc1l	15.30421	*Cytospin-A involved in actin cytoskeleton organisation, cell adhesion and migration*
Clint1	15.28675	*Clathrin interactor 1- roles in transport via clathrin coated vesicles from trans golgi network to endosomes- stimulates clathrin assembly*
Eng	15.13457	*Endoglin-vascular endothelium glycoprotein- regulator of angiogenesis- required for normal structure and integrity of adult vasculature, regulates migration of vascular ECs, may play a role in the binding of ECs to integrins*
Itgav	15.084215	*Integrin αV*
Scamp1	15.082605	*Functions in post Golgi recycling pathways- acts as a recycling carrier to the cell surface*
Sh3gl1	15.05388	*Endophilin-A2- implicated in endocytosis*
Ctnna1	15.026255	*Catenin α1- associates with cadherins- cadherin/catenin complexes associate with the actin filament network*
Ctnnb1	15.02593	*Catenin β1 - key downstream component of Wnt signalling pathway- involved in the regulation of cell adhesion*
Rap1b	14.92447	*Ras related protein Rap-1b- GTPase- establishes EC polarity*
Htra1	14.8882	*Serine protease- targets/cleaves fibronectin*
Vps13b	14.86762	*Vacuolar protein sorting associated protein 13B- may be involved in protein sorting post Golgi membrane traffic*
Map1b	14.83246	*Microtubule associated protein- cytoskeletal regulation*
Sdc3	14.67728	*Syndecan 3- organisation of cell shape by affecting cytoskeleton*
Golim4	14.59475	*Golgi integral membrane protein 4- plays a role in endosome to Golgi protein trafficking*
Rab1b	14.23007	*Recycling regulator*
Icam2	13.61156	*EC marker*
Grasp	13.39968	*Receptor for phosphoinositide 1 associated scaffold protein-promotes intracellular trafficking*
Cope	13.03227	*Coatomer subunit epsilon- Golgi trafficking*
Cct3	12.96404	*Involved in actin folding*
Notch1	12.79969	*Negatively regulates sprouting angiogenesis - inhibits migration and angiogenic sprouting in tip cells*
Golga7	12.51175	*Regulates transport from Golgi to cell surface*
Smtn	12.48062	*Smoothelin- structural protein of the cytoskeleton*
Plvap	11.9327435	*Plasmalemma vesicle associated protein- involved in formation of caveolae, may function in microvascular permeability*
Myo18a	11.90463	*Unconventional myosin-XVIIIa: may link Golgi membranes to cytoskeleton and participate in the tensile force required for vesicle budding from the Golgi*
Psen1	11.015	*Presenilin- involved in proteolytically processing Notch*

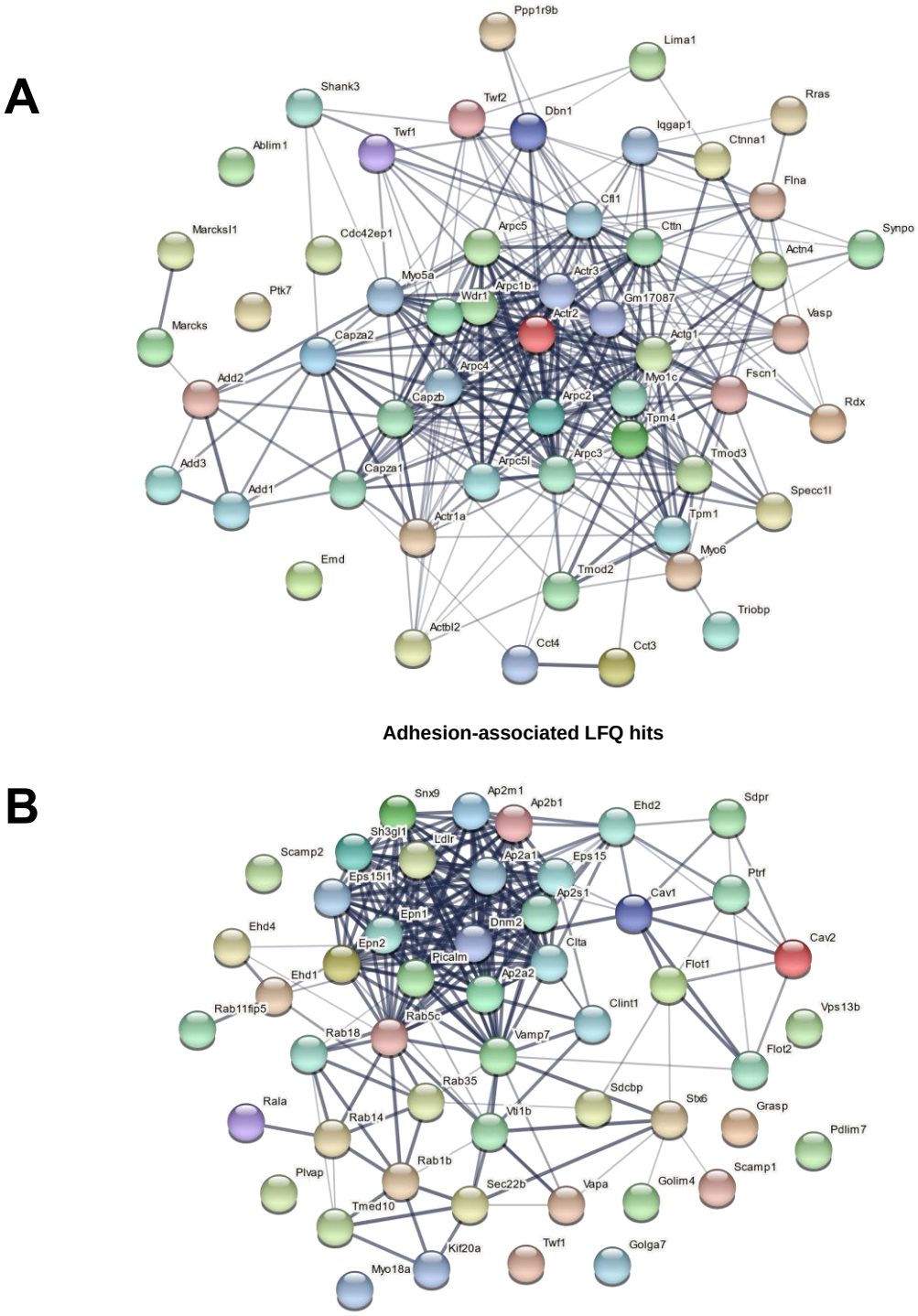

Figure 3.5 NRP2-associated proteins identified from Label-Free quantitative (LFQ) mass spectrometry analysis. LFQ mass spectrometry hits identified as proteins immunoprecipitating with NRP2 at a significantly increased fold change compared to proteins analysed from NRP2 knockdown cell lysates. **A**)/ **B**) Adhesion-associated and intracellular trafficking-associated protein hits and their interactions. Line width correlates with interaction confidence, measured according to the STRING mouse database. Diagrams generated using STRING built-in online tool set to default parameters. (Data generated by Dr Abdullah Alghamdi).

3.2 NRP2 differentially regulates the contributions of α5 integrin during endothelial adhesion to fibronectin

Preliminary studies previously carried out in the Robinson laboratory by Dr Abdullah Alghamdi found that NRP2 and α5 integrin co-immunoprecipitate in our immortalised mLMECs. It was subsequently identified that ECs depleted for NRP2 display impaired adhesion and migration to FN matrices, owing to a reduced rate of α5 integrin recycling [225]. These findings support the work of Cao *et al*., who demonstrated that an upregulation of NRP2 expression enhanced the cellular adhesion between metastasising pancreatic ASPC-1 cancer cells and ECs via trans-binding to α5 integrin [210]. Similarly, NRP1 is also known to interact with α5 integrin directly, it's cytoplasmic tail regulating active α5β1-integrin trafficking to mediate EC adhesion and migration on FN [108]. Indeed, previous members of our laboratory have shown that a complex regulatory mechanism exists between NRP1 and α5 integrin in ECs, whereby the deleterious effects elicited by the depletion of either receptor individually are somewhat ameliorated when depleted in combination. For example, whilst the loss of α5 integrin substantially impaired the ability for ECs to adhere to FN, cell adhesion was significantly restored upon depleting both α5 integrin and NRP1 receptors. Not only does this suggest a regulatory link between α5 integrin and NRP1, but also that a compensatory mechanism exists to mediate a recovery phenotype in the event that both targets are lost.

With this in mind, and given NRP2's candidate interactions with α5 integrin, we sought to investigate whether an analogous regulatory mechanism exists in mLMECs. From our LFQ analysis, the majority of proteins identified to interact with NRP2 were those involved in regulating cellular adhesion and migration, either via mediating cytoskeletal contact to the ECM or through their ability to facilitate intracellular trafficking. We began therefore, by examining the effects of depleting either NRP2 or α5 integrin individually, or in combination, during cellular processes governed by the ability of ECs to adhere and migrate over the ECM. During these experiments, we assayed the ability of our mLMECs to perform such processes on plasticware coated with 2 μg/ml FN, a concentration which has previously been shown to fall within the linear range of endothelial adhesion.

Whilst 2D monolayer culture systems such as this have provided a wealth of information on fundamental biological processes, it would be inappropriate not to appraise their limitations alongside more modern, complex, 3D culture methods however. Tissue microenvironments enable simultaneous cellular interactions with a range of ECM components: glycoproteins (e.g. fibronectin), glycosaminoglycans (e.g. heparan sulphates), ECM-sequestered growth factors, and

proteolytic enzymes, each providing discrete stimuli that regulate cellular behaviour. Any changes to the composition of the underlying ECM are often accompanied by fluctuations in matrix rigidity and mechanical stiffness, properties that hugely affect the ability for cells to potentiate downstream signals, polarise, and migrate appropriately along a concentration gradient. Not only do more complex 3D cell culture models integrate various ECM constituents, but they also enable the user to provide interactions with other relevant cell-types, such as stromal cells (e.g. fibroblasts) to provide mechanical support, and immune cells to stimulate cytokine release. 3D polymeric scaffolds can also be incorporated to recapitulate physiological tissue structures and cellular contacts, considerations that are lacking in 2D monolayer systems [238], [239]. Unfortunately, this study was limited to evaluating the actions of NRP2 in ECs grown in 2D monolayers, which does not necessarily reflex the complex microenvironment cells respond to and interact with in a tissue. Going forward therefore, it would be pertinent to substantiate our findings using more physiologically relevant culture systems to more accurately support our *in vivo* datasets.

3.2.1 NRP2 promotes polarised migration over fibronectin matrices

Angiogenesis relies on the ability of ECs to sense, integrate and disseminate signals they receive from the ECM and from secreted growth factors in order to adhere and migrate towards an angiogenic stimulus [133], [134]. EC migration is essential for nascent sprouts to form, and is directionally regulated by chemotactic, haptotactic and mechanotactic stimuli [21]. A recent investigation into the role of NRP2 during PNET-associated angiogenesis found that it promoted HUVEC migration via a VEGF-VEGFR-2-independent pathway [129]. The Robinson laboratory has also previously demonstrated that NRP2 depletion in mLMECs confers a deleterious effect on migration over a FN matrix, which, in direct conflict with NRP1, occurs independently of both VEGF signalling and β3 integrin expression [107], [225]. In this case, siRNA-mediated depletion of NRP2 in ECs expressing a heterozygous deletion of β3 integrin elicits no compounded response when compared to the migration rate of ECs depleted for NRP2 only [225].

Whilst NRP2 was shown not to exhibit any co-dependence on β3 integrin expression during EC migration over FN, a physical regulatory interaction was found between NRP2 and α5 integrin in mLMECs [225]. The α5β1 integrin heterodimer is largely considered as the principle receptor mediating initial EC adhesion to FN, promoting the assembly of nascent adhesions and mediating interactions between the cytoskeleton and the ECM. Naturally it has been demonstrated to promote adhesion and EC survival during angiogenesis [108], [186]. We therefore chose to instead consider the effects of depleting both NRP2 and α5 integrin in combination on the rate of EC migration in the same manner as studied previously. By doing so, we hoped to ascertain whether a similar regulatory nexus exists between NRP2 and α5 integrin, as it does between NRP1 and α5 integrin.

As others have shown before, the speed of randomly migrating ECs over FN was impaired following siRNA-mediated depletion of NRP2 (*si*NRP2), compared to their control pool siRNA-treated counterparts (Ctrl) [129], [225]. Equally, ECs depleted for both NRP2 and α5 integrin (α5*KO siNRP2*) exhibited a comparable reduction in migration rate. In comparison, those depleted for α5 integrin only (α5*KO*), showed no defect (**Figure 3.6A**). Whilst this confirms that NRP2 is required for WT levels of EC migration over FN, it is also suggestive that NRP2 functions independently of α5 integrin, its additional loss stimulating no compensatory mechanism to promote a recovery phenotype.

As *si*NRP2 ECs migrated significantly slower than Ctrl ECs over FN, we next chose to evaluate the role of NRP2 in establishing cell polarity during directional migration by employing the scratch-

wound assay. Confluent monolayers of Ctrl and NRP2 siRNA-treated ECs were scratched before being allowed to recover over an 8 hour period. EC polarisation was subsequently assessed by examining Golgi-apparatus positioning at the wound margin [240]–[242]. Indeed, not only did NRP2 depletion impair directional migration into the scratch site compared to Ctrl ECs (**Figure 3.6B-C**), but also resulted in a loss of Golgi-apparatus polarisation towards the leading edge. NRP2 depleted ECs also exhibited a reduced number of dorsal stress fibres and lamellipodial projections directed into the avascular space (**Figure 3.6D-F**). Based on this data, it is likely that NRP2 promotes polarised EC migration, possibly by influencing actin cytoskeleton remodelling.

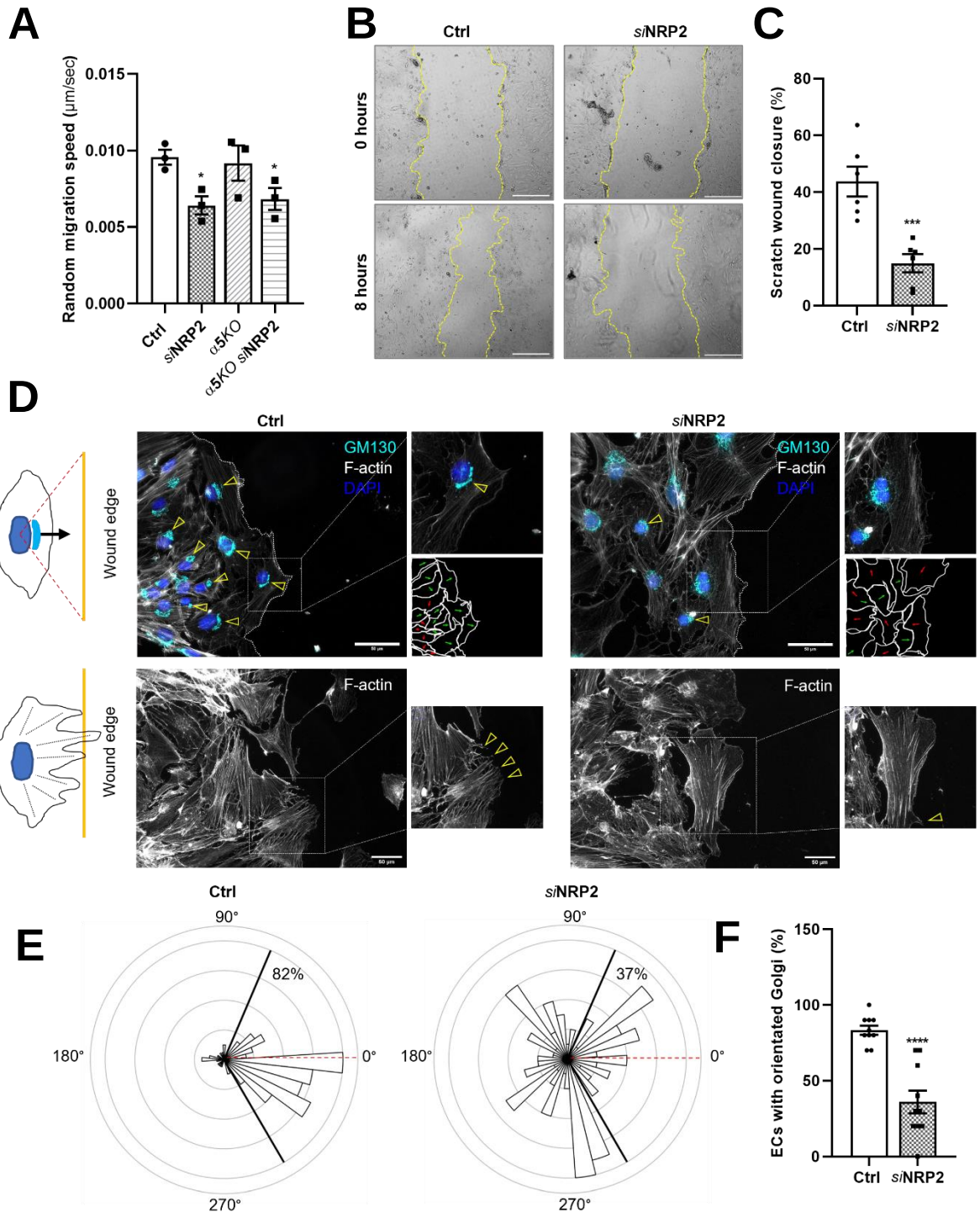
A
Random migration speed (μm/sec)
0.015
0.010
0.005
0.000
Ctrl
siNRP2
α5KO
α5KO siNRP2
B
Ctrl
siNRP2
0 hours
8 hours
C
Scratch wound closure (%)
80
60
40
20
0
Ctrl
siNRP2
D
Ctrl
siNRP2
GM130
F-actin
DAPI
Wound edge
E
Ctrl
siNRP2
90°
180°
0°
270°
82%
37%
F
ECs with orientated Golgi (%)
150
100
50
0
Ctrl
siNRP2

Figure 3.6 NRP2 promotes polarised migration over FN matrices. $1x10^6$ α5 Cre negative and positive ECs were nucleofected with either Ctrl siRNA or NRP2 siRNA and seeded on 10 cm dishes pre-coated with 10 µg/ml FN at 37°C in a CO_2 incubator for 24 hours. ECs were then trypsinised and re-seeded at a low density of $7x10^3$ per well of a 24 well plate pre-coated with 10 µg/ml FN and incubated for 180 minutes at 37°C to allow ECs to adhere. EC migration was captured by timelapse microscopy: Fixed images of multiple field/well of each condition were taken every 20 minutes for 16 hours at 37°C and 5% CO_2 using an inverted Axiovert (Zeiss) microscope in one phase contrast. Individual cell migration was manually tracked using the ImageJ™ MTrackJ plugin. **A**) Random migration speed of individual cells was calculated in µm/sec. Error bars show mean ± SEM; N = 3 (n ≥ 50); *=P<0.05, unpaired students t-test (two-tailed). **B**) $1x10^6$ ECs were nucleofected with either Ctrl siRNA or NRP2 siRNA and seeded on 10 cm dishes pre-coated with 10 µg/ml FN at 37°C in a CO_2 incubator for 24 hours. ECs were then trypsinised and seeded at a high density of $1x10^5$ cells/well onto acid-washed, oven sterilised coverslips pre-coated with 10 µg/ml FN and incubated overnight. Scratches were made using P1000 pipette tips, before being allowed to recover for 8 hours. Phase contrast images were taken immediately after making the scratch and again following 8 hours incubation. Panels show representative phase contrast images at hour 0 and following 8 hours incubation. **C**) Quantification of scratch-wound closure (%). Error bars show ± SEM; N = 6; ***=P<0.0005, unpaired students t-test (two-tailed). **D**) Scratch-wound coverslips were fixed in 4% PFA, blocked and permeabilised. ECs were then incubated with anti-GM130 primary antibody overnight at 4°C. Following two washes to remove any unreacted primary antibody, ECs were incubated in anti-rabbit Alexa 488 secondary antibody and phalloidin-568 at RT for 1 hour. Coverslips were mounted with Prolong Gold with DAPI. Panels show representative images of Ctrl and *si*NRP2 wound margins showing $GM130^+$ Golgi-apparatus positioning (top panels) and lamellipodial protrusions (bottom panels). Yellow open arrowheads indicate correctly orientated Golgi apparatus (top panels) and correctly positioned dorsal stress fibres (bottom panels). Green and red arrows in schematic diagram indicate correctly and incorrectly orientated Golgi apparatus respectively. Scale bars show 50 µm. **E**) Histogram plots showing Golgi apparatus distribution, (n ≥ 100). **F**) Quantification of correctly orientated Golgi-apparatus (%). Error bars show ± SEM; n = 10 fields of view; ****=P<0.0001, unpaired students t-test (two-tailed).

3.2.2 NRP2 and α5 integrin act cooperatively to promote dynamic actin pattern development and remodelling of stress fibres

Organised remodelling of the cytoskeleton acts as a convergence point for numerous canonical signalling networks, and is essential for polarised cell migration [136]. In ECs, actin is the most abundant and active cytoskeletal element, continuously undergoing rhythms of polymerisation and depolymerisation to form dynamic filopodial and lamellipodial projections at the leading edge of the cell [144], [164][165]. Actin cytoskeleton remodelling requires the activation of the Arp2/3 complex, which subsequently mediates the nucleation and polymerisation of long linear actin stress fibres. In addition to directing cell motility, morphogenesis, and both contractile and non-contractile forces within the cell, the actin cytoskeleton also acts as a highway for endocytic and intracellular transport [108], [243].

As the depletion of NRP2 impaired polarised EC migration over FN, we proceeded to assess the effects of NRP2 silencing, individually or in combination with α5 integrin, during actin cytoskeleton remodelling. In recent investigations by Luo *et al*., it was revealed that HUVECs overexpressing NRP2 formed larger, actin-rich lamellipodial protrusions at the cell periphery compared to control ECs. It was subsequently demonstrated that NRP2 overexpression induced the dephosphorylation of cofilin, a major regulator of actin depolymerisation at slow growing filament ends. In turn, increased rates of actin polymerisation at the leading edges of the cell were observed [129]. Furthermore, hMVECs depleted for NRP1 were observed to exhibit fewer stress fibres and actin microspikes at their periphery, in addition to a rounded cell phenotype characteristic of reduced adhesion and motility [244]. In support of this, our LFQ dataset indicated that a large percentage of NRP2-associated target proteins shared functions associated with regulating actin dynamics. Of note were those involved in stabilising the spectrin actin network such as tropomyosin alpha-chain-4 and 1, members of the Arp2/3 complex, including cortactin, which regulates branch nucleation and polymerisation, and proteins involved in coordinating stress fibre development, such as vasodilator-stimulated phosphoprotein (VASP), cofilin-1, fascin and TRIO-binding protein [129], [243], [245]–[247]. Unlike cofilin-associated proteins and TRIOBP, VASP is known to act as a potent regulator of stress fibre linearity. Following initial adhesion to FN, the actin cytoskeleton becomes organised into peripheral rings composed of circumferential actin bundles that proceed to grow radially inwards towards the cell body. These radial bundles then tilt anti-clockwise to form characteristic chiral distributions, before linearising to form long stress fibres [248] (**Figure 3.7**). In fibroblasts, the absence of VASP expression has been demonstrated to result in premature actin

rings failing to transition to the long linear stress fibres that are required by the cell to support the growth of dynamic protrusions during cell adhesion to FN [247], [249].

To assess the contributions of NRP2 and α5 integrin during actin cytoskeleton remodelling, ECs were fixed following 90 or 180 minutes adhesion to FN, and their cytoskeletal morphology compared by immunocytochemistry. In a similar manner to Jalal *et al.,* ECs were sorted based on which of the four stages of actin pattern development: circular, radial, chiral and linear, they resembled most [248]. At 90 minutes, the vast majority of Ctrl ECs exhibited either a chiral or a linear actin morphology, characterised by the presence of long linear stress fibres. In contrast, we observed a far greater proportion of both *si*NRP2 and α5*KO si*NRP2 ECs presenting with a circular phenotype, characterised by an array of circumferential transverse fibres orientated orthogonally to the growth of radial fibres, and parallel to the cell edge. Accordingly, far fewer ECs depleted for NRP2, either singly or in combination with α5 integrin, exhibited long linear stress fibres. When α5 integrin was depleted individually, we observed a less severe delay in ECs transitioning from a circular phenotype to a linear one, suggesting that whilst NRP2 is indispensable for promoting actin pattern development during initial adhesion to FN, α5 integrin's role is less essential. When we compare these findings to our 180 minute timepoint, the above phenotypes are maintained, all Ctrl ECs displaying long linear stress fibres, and ECs depleted for NRP2 exhibiting the highest proportion of circular actin rings at their periphery (**Figure 3.8A-B**).

Further analysis revealed that the depletion of either NRP2 or α5 integrin, individually or in combination, resulted in ECs exhibiting a higher degree of circularity, characteristic of reduced adhesion to the ECM. Concomitantly, depleted ECs displayed significantly fewer lamellipodial protrusions and filopodial microspikes. Co-depletion of both NRP2 and α5 integrin was found to elicit the greatest deformations in circularity and microspike number (**Figure 3.8A, C-E**). SOAX software, a platform used for the analysis of complex 2D and 3D biopolymer networks, was subsequently employed to calculate radial actin fibre orientation and fibre length [216]. By labelling actin stress fibres by their azimuthal angle, we observed a reduced degree of fibre alignment in our depleted ECs compared to Ctrl ECs, and actin stress fibres were measured significantly shorter (**Figure 3.8F-G**).

Taken together, we can infer that whilst both NRP2 and α5 integrin support initial actin pattern development, they do so independently of each other. Stress fibre extension into dynamic lamellipodial protrusions and filopodial microspikes then becomes sequentially dependent upon the complex regulation of both NRP2 and α5 integrin, whereby their dual loss yields severe actin

remodelling defects. This finding supports previous published [225] and unpublished work performed in our laboratory, whereby if either receptor is lost individually, EC adhesion to FN is impaired.

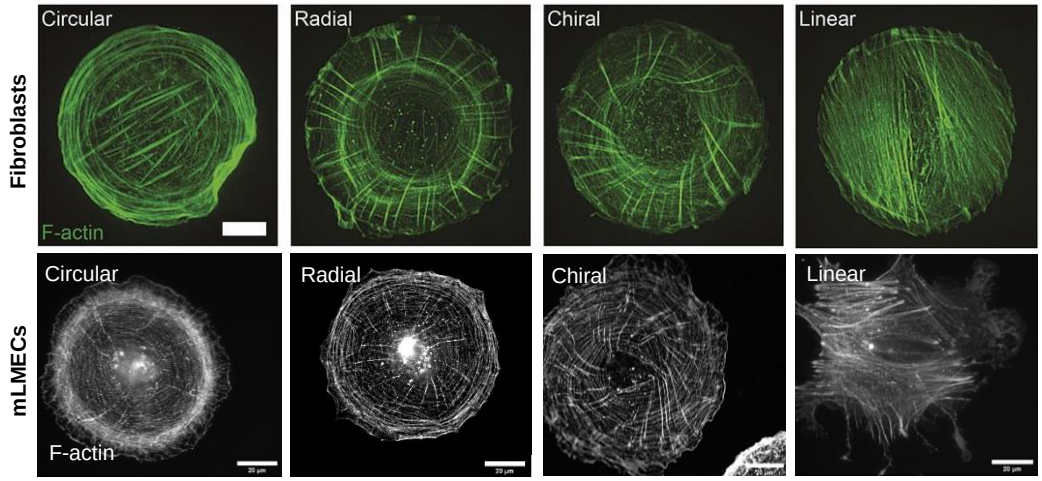

Figure 3.7 Evolution of actin pattern development during adhesion to FN. Representative images showing filamentous actin distribution in fibroblasts (top panels) and mLMECs (bottom panels) allowed to adhere to FN. Upon initial adhesion to FN, cells organise their actin cytoskeleton into peripheral circular rings consisting of circumferential actin bundles. As the cell continues to adhere, it transitions to a radial phenotype, during which there is radially symmetric growth of actin bundles inwards towards the cell body. Following this, radial actin bundles tilt anti-clockwise to form a chiral actin pattern. This persists until actin bundles eventually linearise to form long linear actin stress fibres (Figure adapted from [248]).

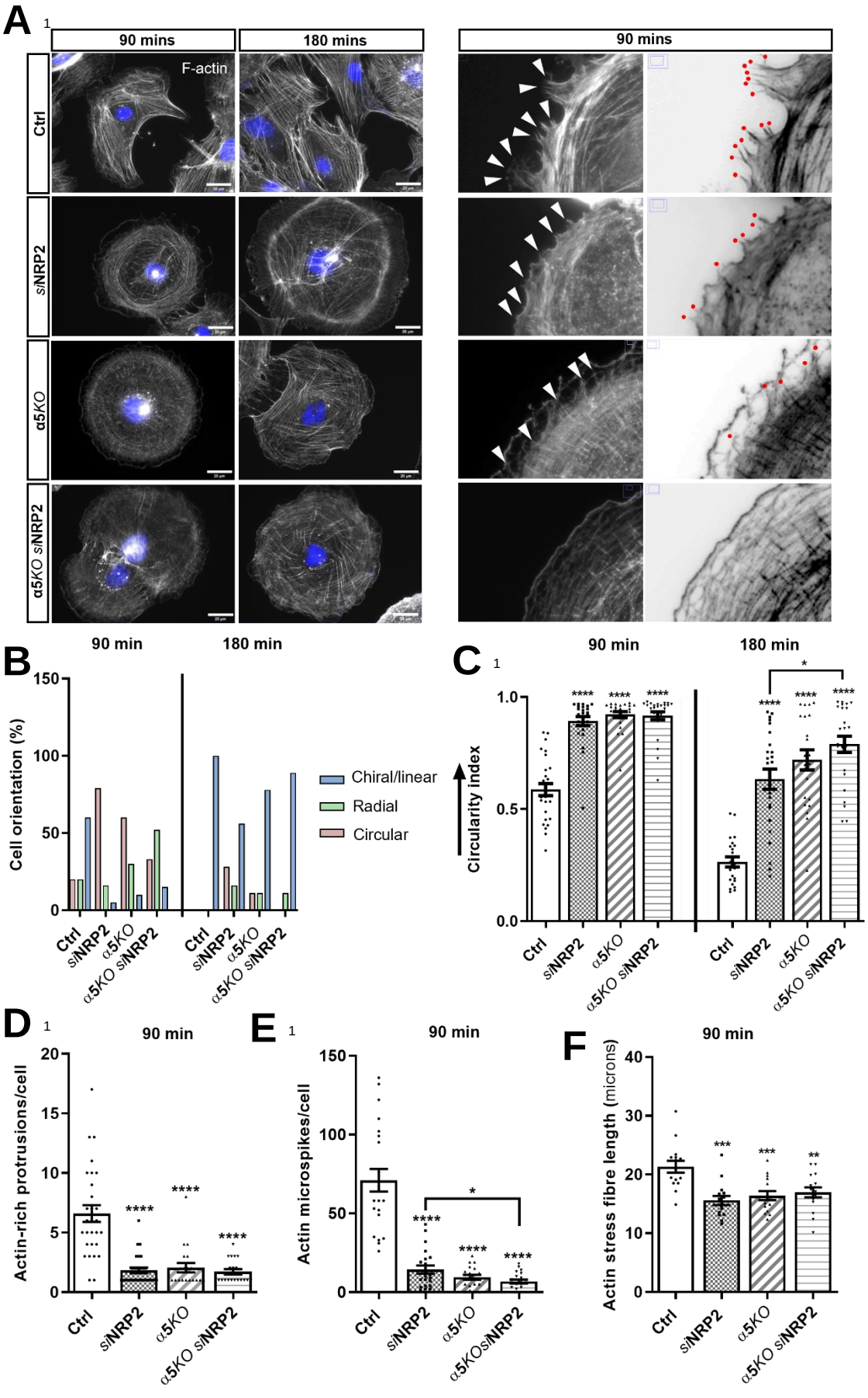
A
90 mins
180 mins
90 mins
F-actin
Ctrl
siNRP2
α5KO
α5KO siNRP2
B
90 min
180 min
Cell orientation (%)
Chiral/linear
Radial
Circular
C
90 min
180 min
Circularity index
D
90 min
Actin-rich protrusions/cell
E
90 min
Actin microspikes/cell
F
90 min
Actin stress fibre length (microns)

[1]Permission granted by FASEB Journal [230] to re-use figure panels.

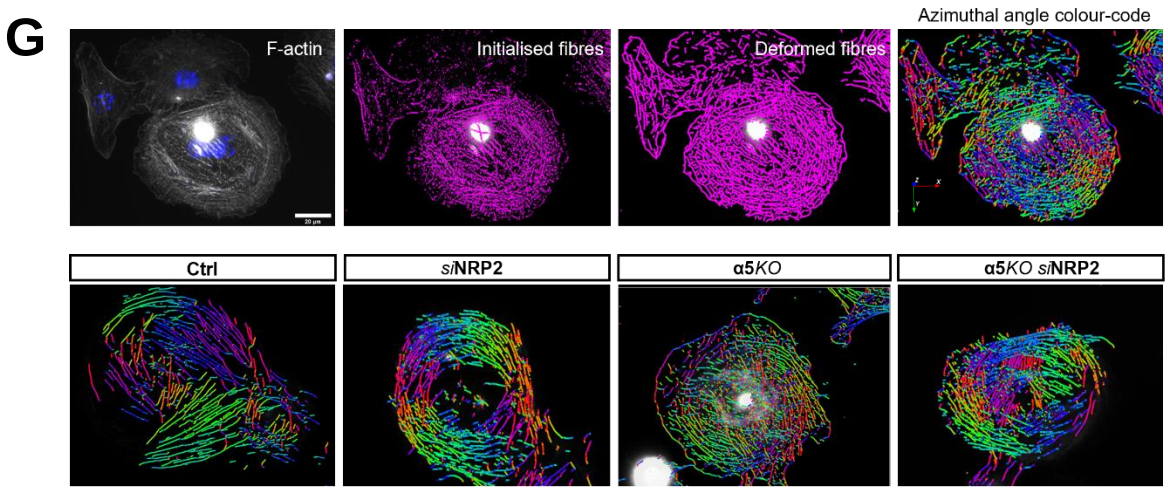

Figure 3.8 NRP2 and a5 integrin act cooperatively to promote dynamic actin pattern development and remodelling of stress fibres. 1x10^6 α5 Cre negative and positive ECs were nucleofected with either Ctrl siRNA or NRP2 siRNA and seeded on 10 cm dishes pre-coated with 10 µg/ml FN at 37°C in a CO_2 incubator for 48 hours. ECs were then trypsinised and seeded at a low density of 2.5 x 10^4 cells/well onto acid-washed, oven sterilised coverslips pre-coated with 10 µg/ml FN and incubated for either 90 or 180 minutes. Coverslips were fixed in 4% PFA, blocked and permeabilised. ECs were then incubated with phalloidin-568 at RT for 1 hour. Coverslips were mounted with Prolong Gold with DAPI. Scale bars show 20 µm. **A**) Representative images of siRNA-treated ECs at each timepoint. Right panels show enlarged representative images of actin microspikes. **B**) Cell orientation classification performed on images produced as shown in **A**). ECs were grouped according to actin orientation: circular, radial, chiral, linear; n≥25 ECs/group. **C**) EC circularity analysis calculated as 4*PiArea/Perimeter^2. Error bars show ± SEM; n≥25 ECs/group; ****=P<0.0001, unpaired students t-test (two-tailed with multiple comparisons). **D/E**) Accompanying actin protrusion and microspike quantification in control and depleted ECs, shown as mean protrusion/microspike number per cell ± SEM; n≥25 ECs/group at 90 minutes adhesion to FN, ****=P<0.0001, unpaired students t-test (two-tailed with multiple comparisons). **F**) Quantification of actin stress fibre length (µm) calculated using SOAX software. Error bars show mean ± SEM; n≥15 ECs/group at 90 minutes adhesion to FN; **=P<0.002, ***=P<0.0005, unpaired students t-test (two-tailed). **G**) Top panels show SOAX workflow, from original immunofluorescence image to fibre labelling and azimuthal angle colour-coding. Bottom panels show representative images of siRNA-treated ECs at 90 minutes adhesion to FN, with azimuthal angle colour-coding.

3.2.3 NRP2 regulates the propagation of core focal adhesion signalling networks

EC migration, driven by continuous remodelling of the actin cytoskeleton, is synchronised with the ability of ECs to propagate a complex network of signalling cascades following integrin engagement to the ECM [24], [136]. The assembly of FAs around these anchor points involves the recruitment of numerous signalling proteins, which not only enable the sequential activation of downstream effectors to mediate stress fibre dynamics, but also promote FA growth and maturation [24], [140], [145]–[147]. As we observed a delay in actin pattern development following both NRP2 and α5 integrin depletion, we first chose to consider whether VASP activation at its Ser^{157} residue would be reduced. When normalised against our loading control, VASP phosphorylation at Ser^{157} was significantly diminished in all our depleted ECs following 5 minutes of VEGF stimulation. Importantly, VASP phosphorylation in both *si*NRP2 and α5*KO si*NRP2 ECs was also significantly less robust than in our α5*KO* ECs, which matches the phenotypes observed from our actin pattern development analysis. This trend was also upheld when we normalised phosphorylated VASP levels with their respective total VASP band intensities (**Figure 3.9**).

Phosphorylation at Ser^{157} provides a signal for membrane or leading-edge localisation of VASP, enabling its interaction with FA-associated proteins such as FAK [247], [249]. When adhered to a laminin matrix, NRP2 expressed by breast tumour epithelial cells was found to localise preferentially to FAs expressing phosphorylated FAK. Furthermore, NRP2 has been demonstrated to regulate FAK signalling during branching morphogenesis in the developing mammary gland [208], [250]. Whether NRP2 influences FAK-mediated responses in lung microvascular ECs however remains unclear. Following VEGF stimulation, FAK undergoes autophosphorylation at its Tyr^{397} residue, which in turn, exposes binding sites for Src family kinases to potentiate the phosphorylation of FAK at additional sites such as Tyr^{407}. Both FAK Tyr^{397} and Tyr^{407} have been implicated in promoting EC migration and adhesion by propagating downstream signalling cascade responses, such as the activation of and translocation of Rac1 to assembling nascent adhesions [101], [162], [163]. To assess whether NRP2 regulates FAK phosphorylation at either Tyr^{397} or Tyr^{407}, we assessed the expression of total and phosphorylated FAK in mLMECs adhered to FN in a similar manner as described above for measuring VASP activation. Following 5 minutes stimulation with VEGF, only ECs depleted for NRP2 individually exhibited a significantly less robust pattern of FAK phosphorylation at both Tyr^{397} and Tyr^{407} residues compared to Ctrl ECs. When normalised to our loading control however, we also observed a significant reduction in FAK phosphorylation at Tyr^{407} in ECs co-depleted for both NRP2 and α5 integrin (**Figure 3.10A-B**). We did not observe any changes

EC survival signalling in any of our ECs, assessed by assaying both ERK and AKT phosphorylation following 5 or 15 minutes of VEGF stimulation (**Figure 3.10C**).

As both Rac1 and Cdc42 Rho GTPases were identified as candidate binding partners for NRP2 from our extended LFQ analysis, and given NRP2's modulatory role over FAK, we subsequently captured the relative abundance of active GTPase-GTP in our ECs stimulated for 180 minutes on FN using a recombinant PBD-domain protein (PAK-1) fused to glutathione-magnetic beads. Whilst we were unable to detect any GTP-bound Cdc42, we did reveal that compared to our Ctrl ECs, active Rac1 levels diminished significantly upon loss of NRP2 expression. We can infer from this that NRP2's ability to promote FAK phosphorylation directly potentiates Rac1 activation to facilitate actin branch nucleation and stress fibre remodelling. Interestingly, this impaired activation appeared not to be sensitised to the additional loss of α5 integrin, as we observed no significant alteration in Rac1 activation in either our α5*KO* or α5*KO si*NRP2 ECs (**Figure 3.11**).

Taken together, these results suggest that NRP2's modulatory role over FAK phosphorylation at residues Tyr^{397} or Tyr^{407}, and subsequent propagation of Rac1 activation, is dependent upon its ability to promote VASP-mediated actin remodelling. We can also infer that NRP2's ability to promote core focal adhesion signalling cascades to promote EC adhesion and migration largely functions independently of α5 integrin expression. Rather, it appears that any complex interactions existing between NRP2 and α5 integrin to potentiate such signals are mediated by the dominant actions of NRP2, not vice versa.

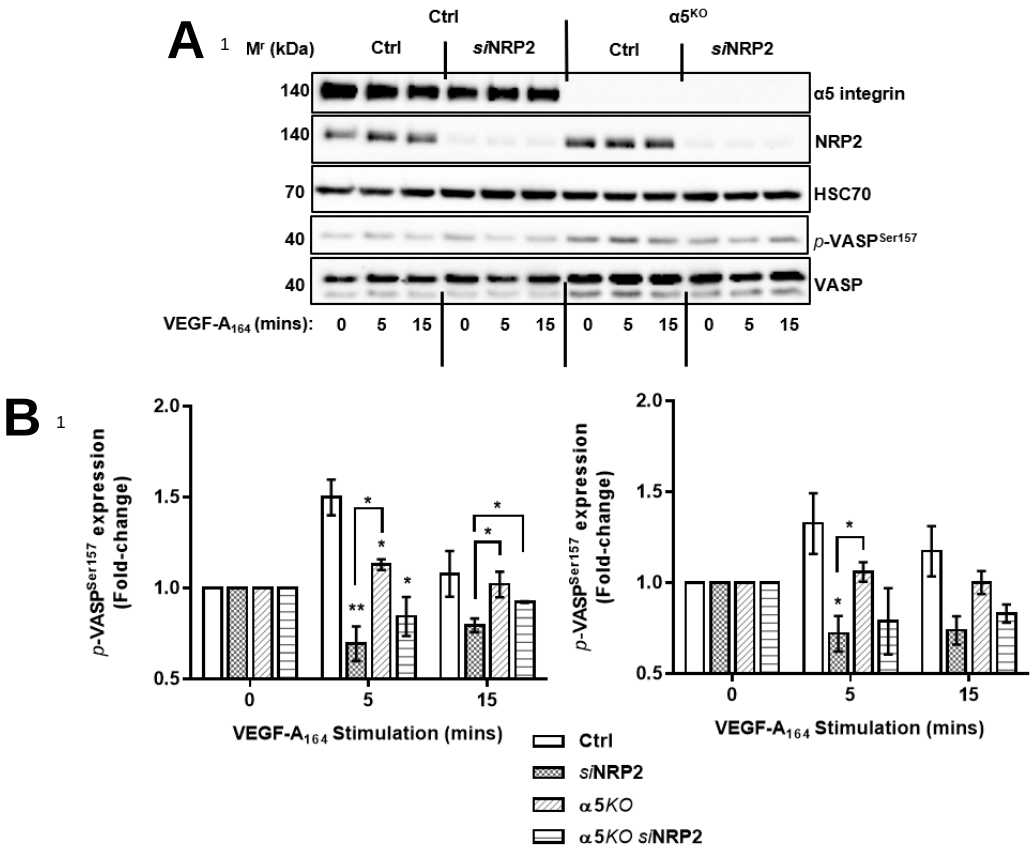

[1]Permission granted by FASEB Journal [230] to re-use figure panels.

Figure 3.9 VEGF induced phosphorylation of VASP is sensitive to the loss of NRP2 and α5 integrin. α5 Cre negative and positive ECs were nucleofected with either Ctrl siRNA or NRP2 siRNA and seeded into 6-well plates pre-coated with 10 µg/ml FN at a density of $3x10^5$ ECs per well, before being incubated at 37°C in a CO_2 incubator for 48 hours. Following two washes with PBS, the cells were starved in serum-free OptiMEM® for 3 hours. 30 ng/mL $VEGF_{164}$ was added to dishes being incubated for 5 and 15 minutes. Following incubation, all dishes, including those unstimulated, were immediately placed on ice. ECs were lysed in ESB and subjected to the DC protein assay before being analysed by Western blotting. HSC70 was used as a loading control. Bands were quantified using ImageJ™ densitometric analysis. **A**) Representative Western blot showing total VASP, phospho-VASP (Ser^{157}), NRP2 and α5 integrin expression in Ctrl and NRP2 siRNA treated ECs. **B**) Densitometric analysis of mean phospho-VASP (Ser^{157}) band intensities normalised against either HSC70 (left) or total VASP expression (right) and obtained using ImageJ™. Error bars show mean ± SEM; N=3; *=P<0.05, **=P<0.002, unpaired students t-test (two-tailed with multiple comparisons).

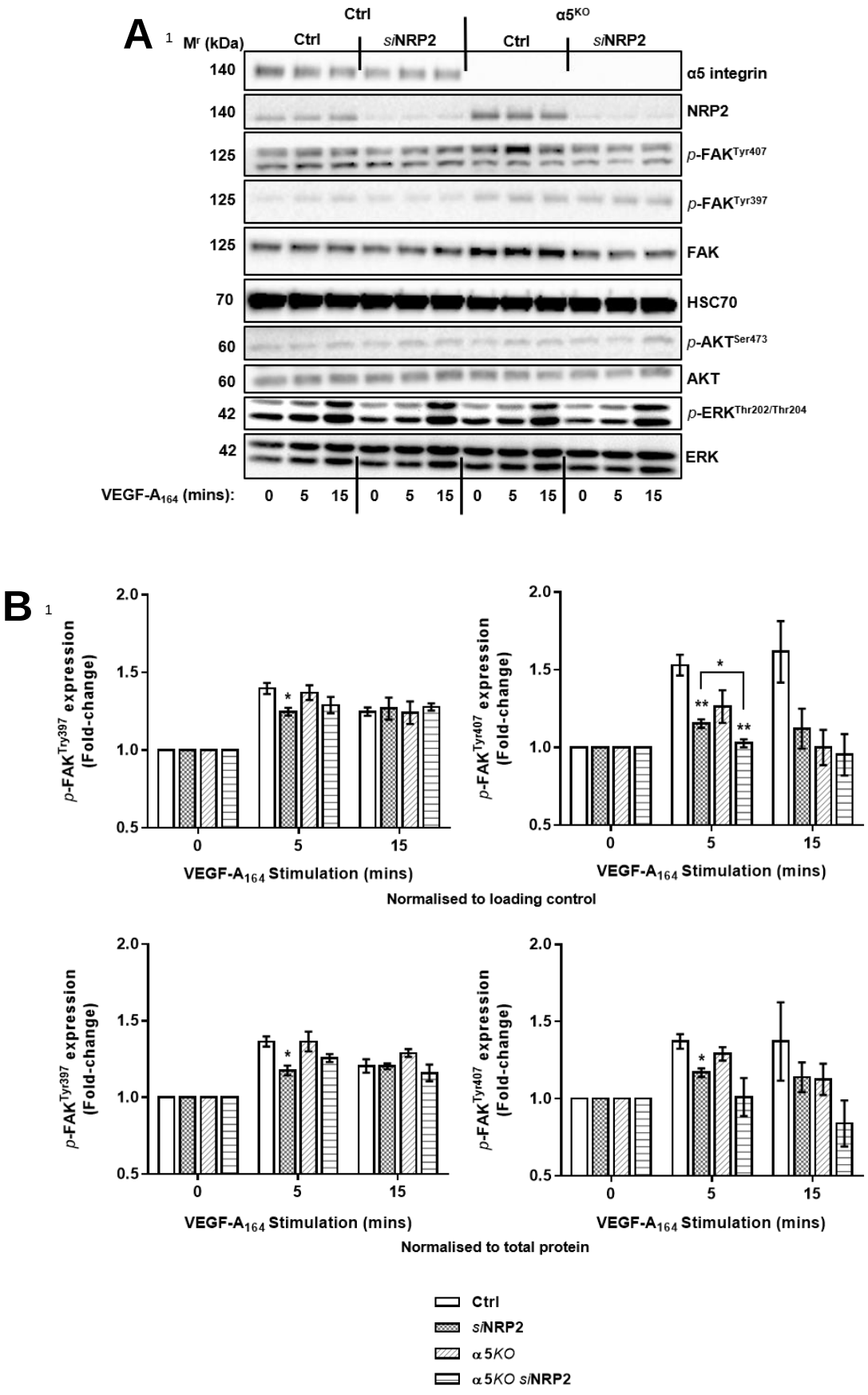
A
Ctrl
α5KO
Mr (kDa)
Ctrl
siNRP2
Ctrl
siNRP2
140
α5 integrin
140
NRP2
125
p-FAKTyr407
125
p-FAKTyr397
125
FAK
70
HSC70
60
p-AKTSer473
60
AKT
42
p-ERKThr202/Thr204
42
ERK
VEGF-A164 (mins): 0 5 15 0 5 15 0 5 15 0 5 15
B
p-FAKTry397 expression (Fold-change)
p-FAKTyr407 expression (Fold-change)
VEGF-A164 Stimulation (mins)
Normalised to loading control
Normalised to total protein
Ctrl
siNRP2
α5KO
α5KO siNRP2

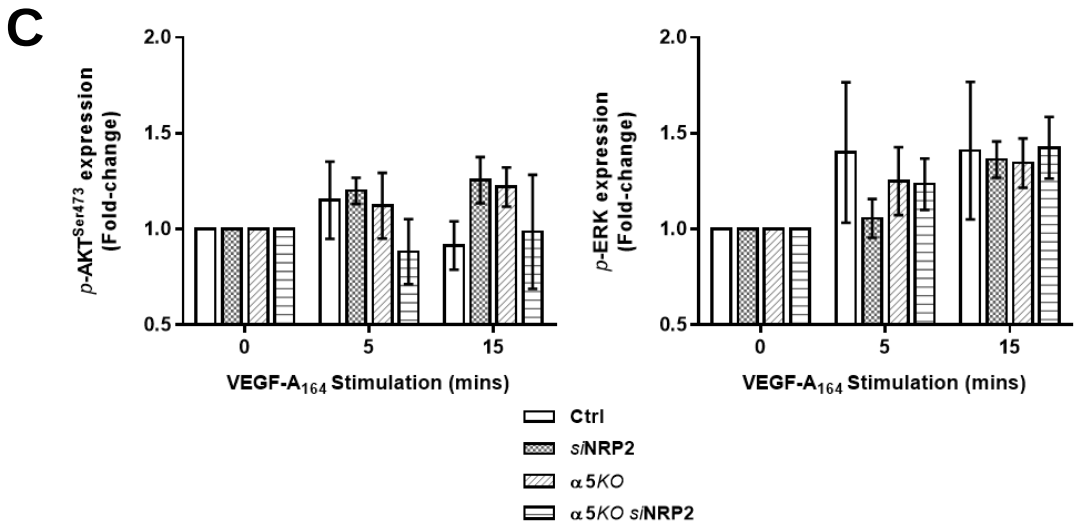

[1]Permission granted by FASEB Journal [230] to re-use figure panels.

Figure 3.10 NRP2 depletion dampens FAK phosphorylation at both Tyr^{397} and Tyr^{407}. α5 Cre negative and positive ECs were nucleofected with either Ctrl siRNA or NRP2 siRNA and seeded into 6-well plates pre-coated with 10 µg/ml FN at a density of 3x10^5 ECs per well, before being incubated at 37°C in a CO_2 incubator for 48 hours. Following two washes with PBS, the cells were starved in serum-free OptiMEM® for 3 hours. 30 ng/mL $VEGF_{164}$ was added to dishes being incubated for 5 and 15 minutes. Following incubation, all dishes, including those unstimulated, were immediately placed on ice. ECs were lysed in ESB and subjected to the DC protein assay before being analysed by Western blotting. HSC70 was used as a loading control. Bands were quantified using ImageJ™ densitometric analysis. **A**) Representative Western blot showing total FAK, phospho-FAK (Tyr^{397} and Tyr^{407}), NRP2, α5 integrin, total ERK, phospho-ERK, total AKT, phospho-AKT and HSC70 inn Ctrl and NRP2 siRNA treated ECs. **B**) Densitometric analysis of mean p-FAK (Tyr^{397} and Tyr^{407}) band intensities normalised against HSC70 (top) and total FAK (bottom) expression and obtained using ImageJ™. Error bars show mean ± SEM; N=3; *=P<0.05, **=P<0.002, unpaired students t-test (two-tailed with multiple comparisons). **C**) Densitometric analysis of mean p-AKT (Ser^{473}) and p-ERK band intensities normalised against total AKT and ERK expression respectively, and obtained using ImageJ™. Error bars show mean ± SEM; N=3.

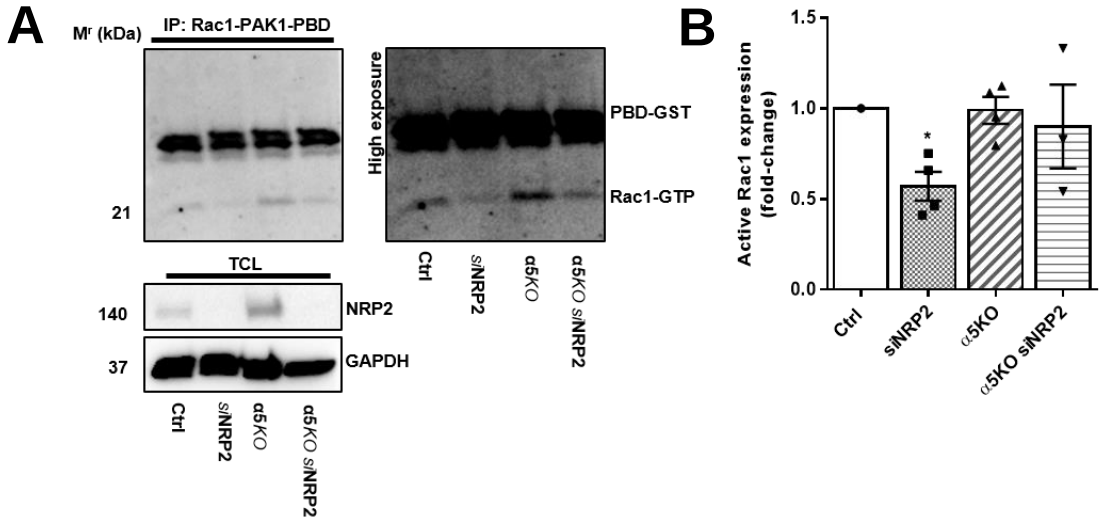

Figure 3.11 NRP2 depletion impairs Rac1 activation. siRNA-transfected ECs were seeded onto FN and incubated for 180 minutes at 37°C and 5% CO_2. EC extracts were immunoprecipitated by incubation with 10 µg Rac1 assay reagent (PAK-1 PBD magnetic beads) for 45 minutes at 4°C with gentle agitation. Immunoprecipitated complexes were subjected to Western blot analysis using antibodies against Rac1. **A**) Panels show low and high exposure images showing active Rac1 levels in Ctrl and NRP2 siRNA transfected lysate. NRP-2 depletion was confirmed by Western blot analysis using antibodies against NRP2 and GAPDH. **B**) Densitometric analysis of mean band intensities normalised against GAPDH and obtained using ImageJ™. Error bars show mean ± SEM; N=4; *=P<0.05, **=P<0.002, unpaired students t-test (two-tailed).

3.2.4 NRP2 is essential for normal focal adhesion development by regulating the recruitment of focal adhesion kinase

Upon binding to the ECM, integrins become stabilised, recruiting a plethora of signalling moieties, scaffolding proteins and cytoskeletal adaptors to their cytoplasmic tails to form FAs. These complex structures subsequently undergo stages of maturation as integrins cluster [24], [152]. FAK is a major signalling protein recruited in FA complexes, and is activated by binding to integrins directly or via the adaptors paxillin or talin through the autophosphorylation of its tyrosine residues. Phosphorylated FAK can then proceed to promote cell migration through its activation of the Rho family GTPases Rac1 and Cdc42, which are involved in mediating FA dynamics [162]–[164]. Principally, for cells to migrate over a matrix, FA complexes must rapidly undergo cycles of turnover, whereby nascent FA complexes assemble at the leading edge and those at the trailing edge disassemble [108], [225], [251]. Despite having no effect on the expression of total or phosphorylated paxillin, the Robinson laboratory has previously demonstrated NRP2 depletion to impair the rate of mature FA complex turnover [225]. Given that the loss of NRP2 individually also impaired FAK phosphorylation and Rac1 activation, we then thought it pertinent to examine whether FA development would also be affected in our mLMECs. This was achieved by immunolabelling for endogenous paxillin, a marker for FAs [176], [252], [253], in ECs allowed to adhere for either 90 or 180 minutes on FN.

At 90 minutes, all depleted ECs exhibited significantly fewer FAs than our Ctrl ECs. Whilst ECs depleted for either NRP2 or α5 integrin exhibited the greatest reduction in FA density, those depleted for both targets displayed a partial recovery, and exhibited significantly more FAs than siNRP2 or α5*KO* ECs. No obvious changes in the number of FAs between our *si*NRP2 and our α5*KO* ECs were observed (**Figure 3.12A-B**). This suggests that, in a similar manner to when NRP1 and α5 integrin are co-depleted, upon dual loss of both NRP2 and α5 integrin, a compensatory mechanism is triggered to ameliorate the effects elicited by the depletion of either receptor individually. An equivalent reduction in FA density was also observed when NRP2 was depleted using a second siRNA construct (**Figure 3.12E**). All apparent defects to FA density in our depleted ECs recovered to Ctrl levels following 180 minutes adhesion to FN (**Figure 3.12A-B**).

In addition to impairing the initial ability of cells to assemble FAs, individual depletion of NRP2 using multiple siRNA constructs also elicited a significant reduction in FA area following 90 minutes adhesion to FN. This defect was absent in both α5*KO* and α5*KO* *si*NRP2 ECs however, which displayed no differences to Ctrl siRNA-treated ECs (**Figure 3.12A, C, E**). Subsequent analysis

measuring the size distribution of all paxillin^{+} FAs expressed by our *si*NRP2 ECs compared to Ctrl ECs revealed proportionally fewer larger, mature FAs (**Figure 3.12A, D**), suggesting that not only does NRP2 regulate EC migration by promoting FA turnover, but also facilitates EC adhesion to FN by supporting the assembly and development of FAs themselves. In contrast, whilst α5 integrin appears to be essential for early FA assembly, it is dispensable for adhesion maturation. Rather, it is likely that the expression of another integrin, such as β3, is necessary for this transition. Our story becomes more complex when we consider the effects of our target depletion on FA area following 180 minutes adhesion to FN. FA size was observed to be significantly increased upon loss of NRP2, either individually or in combination with α5 integrin (**Figure 3.12A, C**). It is possible here that the extended depletion of NRP2 stimulates either the compensatory activation of β3 to promote an accelerated rate of FA development, or that the reduced rate of FA turnover elicited by NRP2 depletion forces FAs to mature artificially over time.

During nascent adhesion assembly, initial FAK recruitment and phosphorylation is dependent upon the active tethering of α5-integrin to its specific matrix ligand, FN. This subsequently enables adhesions to develop and mature into larger FA complexes [159], [254]. As *si*NRP2 ECs exhibited reduced FAK phosphorylation and impaired FA assembly, we sought to determine whether FAK recruitment to assembling α5 integrin adhesions was also diminished in ECs depleted for NRP2. NRP1 disseminates VEGF-mediated signalling via the phosphorylation of FAK at Tyr^{407} [101]. We therefore directed our efforts to examine whether interactions between α5-integrin and this residue specifically were impaired following NRP2 depletion by immunofluorescence confocal microscopy. To this end, we allowed Ctrl and NRP2 siRNA treated ECs to adhere to FN for 90 minutes before examining phosphorylated FAK^{Tyr407} (*p*-FAK^{Tyr407}) colocalisation with α5 integrin. Whilst we observed a strong colocalisation between α5 integrin and *p*-FAK^{Tyr407} close to the cell periphery of Ctrl ECs within characteristically large FAs, ECs depleted for NRP2 produced smaller, more punctate α5 integrin^{+} structures, and those present were less enriched in *p*-FAK^{Tyr407}. In conjunction, we observed an increased accumulation of *p*-FAK^{Tyr407} around the cell body of *si*NRP2 ECs (**Figure 3.13A-C**). To corroborate these findings, we assessed the physical interaction between α5 integrin and *p*-FAK^{Tyr407} in Ctrl and NRP2 siRNA-treated ECs biochemically by co-immunoprecipitation. Compared to lysate collected from Ctrl ECs, a far less robust interaction between α5 integrin and *p*-FAK^{Tyr407} was detected from NRP2 depleted lysate, confirming that NRP2 is likely required for the active recruitment and phosphorylation of FAK during the assembly of nascent α5 integrin containing adhesions (**Figure 3.13D**).

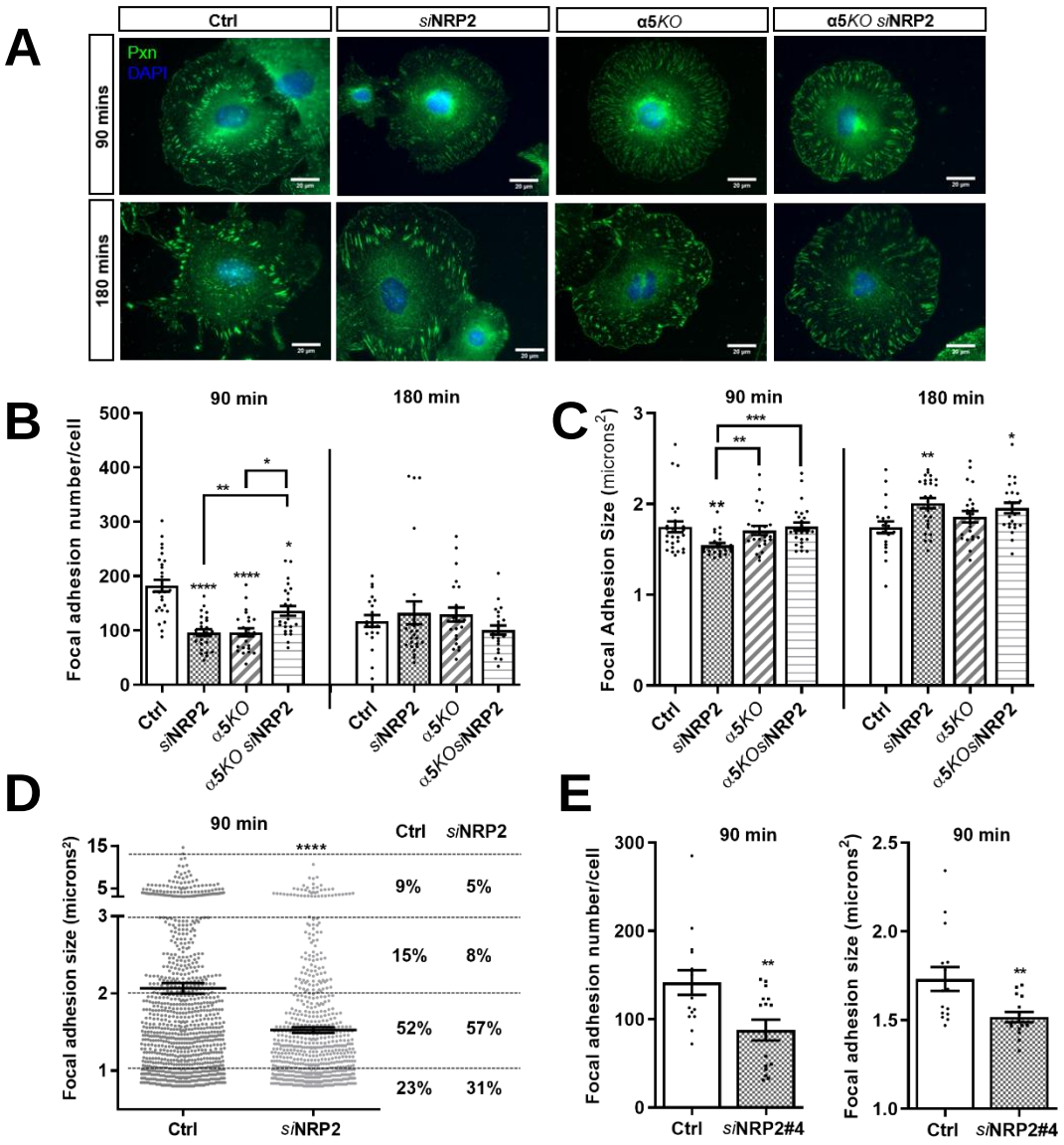

Figure 3.12 NRP2 depletion impairs EC FA assembly and maturation. 1x10^6 α5 Cre negative and positive ECs were nucleofected with either Ctrl siRNA or NRP2 siRNA and seeded on 10 cm dishes pre-coated with 10 µg/ml FN at 37°C in a CO_2 incubator for 48 hours. ECs were then trypsinised and seeded at a low density of 2.5 x 10^4 cells/well onto acid-washed, oven sterilised coverslips pre-coated with 10 µg/ml FN and incubated for either 90 or 180 minutes. Coverslips were fixed in 4% PFA, blocked and permeabilised. ECs were then incubated with anti-paxillin primary antibody overnight at 4°C. Following two washes to remove any unreacted primary antibody, ECs were incubated with donkey anti-rabbit Alexa 488 secondary antibody at RT for 1 hour. Coverslips were mounted with Prolong Gold with DAPI. Scale bars show 20 µm. **A**) Representative images of paxillin (Pxn) immunostained ECs at each timepoint. **B**) Quantification of the number of FAs/cell. **C**) Quantification of mean FA size (µm^2). Error bars show mean ± SEM; n≥25; *=P<0.05, **=P<0.002, ***=P<0.0005, ****=P<0.0001, unpaired students t-test (two-tailed with multiple comparisons). **D**) FA size distribution between Ctrl and siNRP2 ECs (µm^2) at 90 minutes adhesion. Error bars show mean ± SEM; n>700 adhesions; ****=P<0.0001, unpaired students t-test (two-tailed). **E**) Quantification of FA number and mean FA size in Ctrl and NRP2 siRNA (#04) transfected ECs at 90 minutes. Error bars show mean ± SEM; n≥15; **=P<0.002, unpaired students t-test (two-tailed).

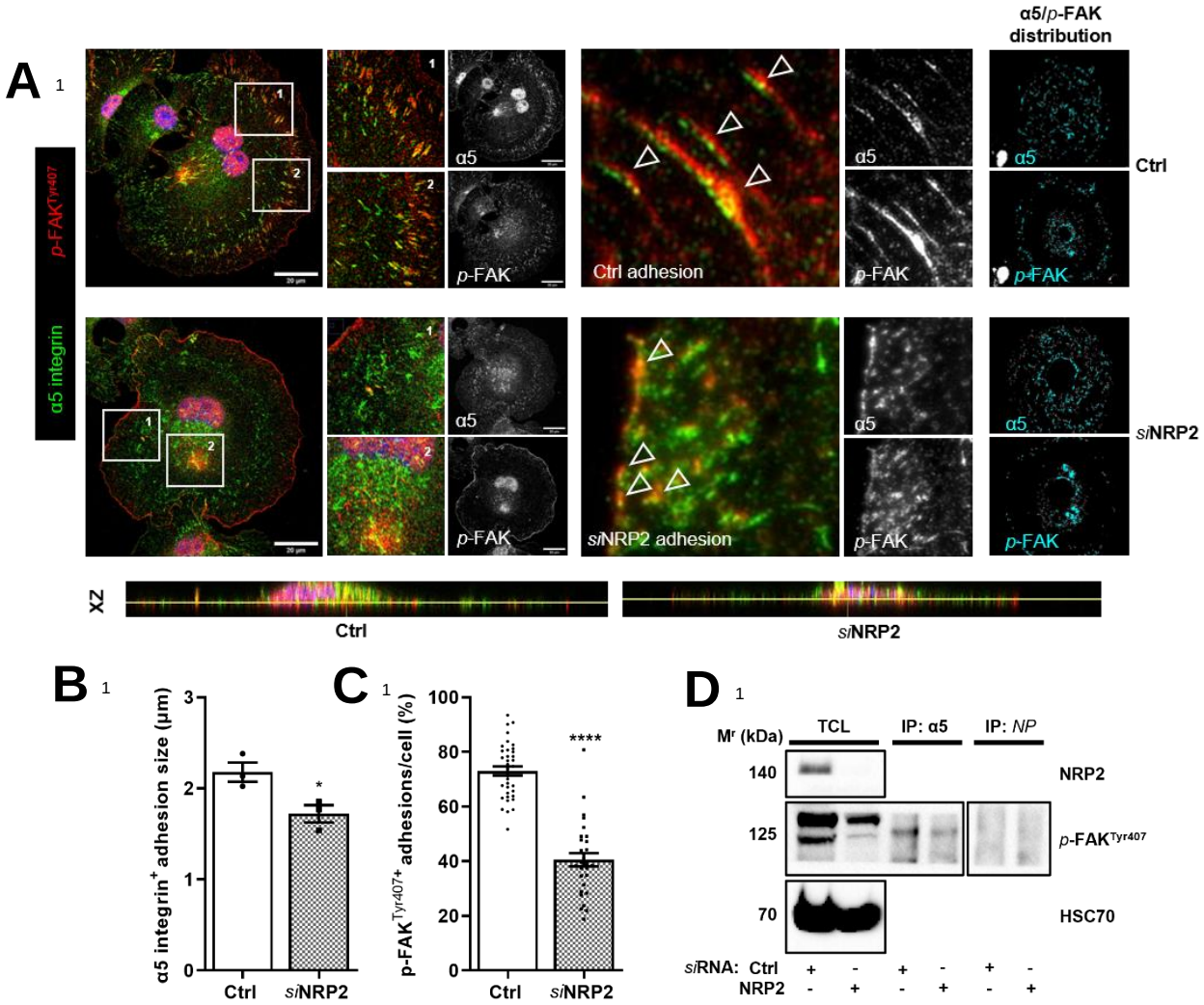

[1]Permission granted by FASEB Journal [230] to re-use figure panels.

Figure 3.13 NRP2 depletion disrupts p-FAK^{Tyr407} recruitment to α5 integrin containing adhesions. 1x10^6 ECs were nucleofected with either Ctrl siRNA or NRP2 siRNA and seeded on 10 cm dishes pre-coated with 10 µg/ml FN at 37°C in a CO_2 incubator for 48 hours. ECs were then trypsinised and seeded at a low density of 2.5 x 10^4 cells/well onto acid-washed, oven sterilised coverslips pre-coated with 10 µg/ml FN and incubated for 90 minutes. Coverslips were fixed in 4% PFA, blocked and permeabilised. ECs were then incubated with anti-α5 integrin and anti- *p*-FAK^{Tyr407} primary antibodies overnight at 4°C. Following two washes to remove any unreacted primary antibody, ECs were incubated with donkey anti-rabbit Alexa 546 and donkey anti-rat Alexa 488 secondary antibodies at RT for 1 hour. Coverslips were mounted with Prolong Gold with DAPI. Scale bars show 20 µm. **A**) Representative images of Ctrl and NRP2 siRNA treated ECs fixed at 90 minutes showing colocalisation between α5 integrin and *p*-FAK^{Tyr407}. Images were taken using a Zeiss LSM880 Airyscan Confocal microscope at 63X magnification. Arrowheads show co-localisation at peripheral adhesions. XZ plane images for each panel are also shown to display subcellular co-localisation. **B**) mean α5-integrin positive adhesion size (microns) between Ctrl siRNA and NRP2 siRNA-treated ECs. Error bars show ± SEM; N=3 (n≥180 adhesions); *=P<0.05, unpaired students t-test (two-tailed). **C**) Mean number of *p*-FAK^{Tyr407} positive adhesions/cell, error bars show mean ± SEM; n≥30; ****=P<0.0001, unpaired students t-test (two-tailed). **D**) ECs were transfected with either Ctrl or NRP2 siRNA and seeded onto 10 cm dishes pre-coated with 10 µg/ml FN and incubated for 48 hours at 37°C. EC extracts were immunoprecipitated by incubation with protein-G Dynabeads® coupled to antibodies against α5 integrin overnight at 4°C. Immunoprecipitated complexes were separated by SDS-PAGE and subjected to Western blot analysis using a primary antibody against p-FAK^{Tyr407}. Immunoprecipitated EC extracts were ran alongside total Ctrl siRNA and NRP2 siRNA cell lysates to confirm NRP2 depletion, and no primary (*NP*) immunoprecipitated control lysates.

3.2.5 Discussion

In this chapter, we have demonstrated that a complex regulatory interaction exists between NRP2 and α5 integrin to mediate microvascular EC anchorage to the ECM by promoting FA development. Prior investigations into the role of these receptors have revealed that both promote EC adhesion and migration on FN [108], [155], [186], [207], [208], [210], [225], however the precise mechanisms by which they interact to coordinate these functions remained unclear. The core events that drive angiogenesis; integrating and disseminating extracellular signals, enabling cells to adhere and migrate, are governed by a multitude of regulatory networks. A difficulty that therefore arises when attempting to decipher the diverging contributions of multiple target proteins, is that not all regulatory interactions exist for all cellular processes. In this case, we chose to consider EC adhesion to FN as a set of key sequential stages, making it possible to define how the influence of NRP2 and α5 integrin changes temporally. For example, we observed that both NRP2 and α5 integrin are crucial for the assembly of nascent adhesions, in comparison to when they are co-depleted, which elicits a partial amelioration effect. Initial tethering of α5 integrin to the FN matrix is paramount to early stage adhesion, and enables subsequent FA development and linkage to the actin cytoskeleton to mediate mechanical changes in the cell [159], [253], [254]. As *si*NRP2 and α5*KO* ECs were able to assemble far fewer nascent adhesions than either Ctrl or α5*KO si*NRP2 ECs, it tells us that both NRP2 and α5 integrin are both required for the initial interaction to be made between α5 integrin and FN. Furthermore, it suggests that in the absence of these receptors, another FN-binding integrin, such as αvβ3 integrin, intercedes to facilitate FA assembly.

FA assembly is required for the actin cytoskeleton to undergo remodelling into radial fibres that successively grow inwards. Anchored at FAs, these radial fibres can then transition into chiral and subsequently linear stress fibres to promote the extension of dynamic protrusions. This sequential actin pattern development is regulated by the actions of VASP and cofilin [248], proteins both identified by our LFQ analysis. Unlike during initial tethering to the FN matrix, which requires the expression of both NRP2 and α5 integrin, we found VASP phosphorylation and the transitioning to a linear actin phenotype to be a discernibly NRP2 dominant process. In addition to modulating VASP function, NRP2 has also been reported to regulate migration by upregulating cofilin activity, a key mediator of actin depolymerisation at slow growing filament ends [129]. Paired with its candidate interactions for numerous proteins known to stabilise and promote actin branch nucleation and stress fibre dynamics, notably cortactin and fascin, it is likely that NRP2 expression drives the turnover of F-actin at slow-growing filament ends to supply the demand for new actin monomers at assembling fast growing ends of extending filopodial protrusions.

Likewise, when we consider downstream FA-associated signalling, α5 integrin involvement becomes increasingly minimal. It is known that FAK phosphorylation is in part dependent upon the recruitment of VASP to the membrane. For example, VASP inhibition has been demonstrated to significantly dampen phosphorylation responses at Tyr^{925} in human chronic myeloid leukaemia (CML) cells, and reduce phosphorylation at Tyr^{397} during Xenopus somite development [255], [256]. As VASP is phosphorylated at its Ser^{157} residue following recruitment to assembling FAs [247], [249], we were unsurprised to observe a contemporaneous decrease in FAK phosphorylation at both Tyr^{397} and Tyr^{407} sites upon NRP2 depletion, residues known to promote canonical VEGF gradient-driven EC adhesion and migration [101], [162]. VEGF-induced FAK phosphorylation at Tyr^{407} during integrin-mediated adhesion and migration is also known to be NRP1 dependent [101]. Indeed, phenotypic defects in actin organisation have been reported in human ECs depleted for NRP1, which was later shown to arise from impaired Cdc42 and Rac1 activation [244]. Despite observing significant impairment in the ability of ECs depleted for either NRP2 or α5 integrin to form filopodial-like microspikes, we were unable to detect active Cdc42 expression in any of our ECs. Rac1 activation however, was revealed to be significantly attenuated upon the individual loss of NRP2. As previous studies have demonstrated an equivalent reduction in Rac1 or Cdc42 activation following NRP1 depletion [244], [257], it suggests that both NRPs are involved in promoting key Rho-GTPase activity to sustain mechanical changes in the cell as it migrates. We do find it interesting however that Rac1 activation is not sensitised to the loss of α5 integrin, in isolation or in combination with NRP2 depletion. Rac1 is typically activated via its translocation to α5 integrin containing nascent adhesions [163], [200]. It has since been shown that the loss of β3 integrin promotes the complex association between α5 integrin and Rac1, enhancing EC migration by altering microtubule stability [201]. We therefore speculate that in the absence of α5 integrin, the actions of β3 integrin supersede the preference for Rac1 to complex with α5 integrin, maintaining the ability for the cell to initiate its activation at a WT level.

By following the stages succeeding initial attachment to FN, we see that whilst NRP2 remains essential, the involvement of α5 integrin diminishes. This becomes evident from studying the effect of depleting our targets on the rate of migration, which can be considered our terminus, as only those depleted for NRP2 show any defect. Indeed, as the cell's principle FN-binding integrin, α5β1 is required for anchorage to the ECM and to stimulate nascent adhesion formation [24], [207]. However, we believe that redundancies in the specificities of different FN-binding integrins enable the cell to function over time, despite its loss. In contrast, the expression of NRP2 remains key for the cell to potentiate core FA signalling to mediate actin remodelling and subsequently polarised

EC migration. Confocal colocalisation microscopy revealed that NRP2 modulates the ability of the cell to activate these downstream signalling cascades by mediating the shuttling of FAK to α5 integrin containing adhesions. Whilst others have reported NRP2 to promote FAK-directed adhesion to laminin matrices in cancerous epithelial cells via α6β1 integrin [208], [250], we believe we are the first to reveal this delivery mechanism in microvascular ECs. Endogenous *p*-FAK^{Tyr407} staining in fixed ECs revealed that significantly less phosphorylated FAK is recruited to α5 integrin^{+} adhesion sites following silencing of NRP2, impairing FA assembly and development. Taking into account the previous work carried out by our laboratory and by others hypothesising that NRP2 exerts a mainly VEGF-independent role during EC adhesion and migration [129], [225], we propose a mechanism by which NRP2 instead promotes the auto-phosphorylation of FAK in response to initial α5 integrin engagement and clustering (**Figure 3.14**).

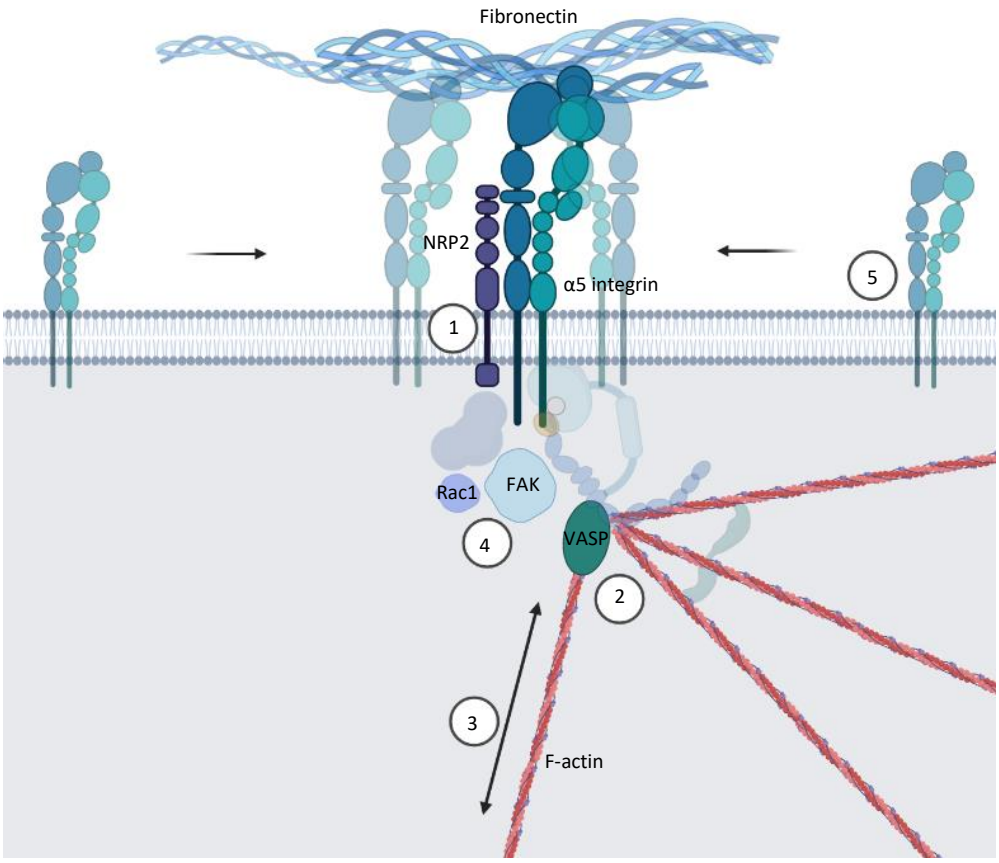

Figure 3.14 NRP2 and α5 integrin modulate EC adhesion and migration on FN summary schematic. Archetypal EC adhesion can be divided into a set of key sequential events. **1**: Initial binding between α5 integrin and the FN matrix, stimulating the assembly of nascent adhesion structures. α5 integrin binding to FN requires the expression of NRP2. **2/3**: VASP modulates the actin pattern development of the adhering cell, enabling the formation of dynamic linear stress fibres. Stress fibre remodelling subsequently drives the extension of lamellipodial and filopodial protrusions. VASP-mediated actin pattern development is regulated by the expression of both NRP2 and α5 integrin, however NRP2 plays a more dominant role. **4**: Phosphorylation of VASP at its Ser^{157} residue stimulates its subcellular translocation to the cell membrane where it facilitates the activation of FAK. FAK phosphorylation subsequently recruits Rac1 to the assembling α5 integrin-positive adhesion, potentiating its activation. Rac1 then mediates actin branch nucleation to support the extension of lamellipodia. FAK and Rac1 activation does not rely on the expression of α5 integrin, but rather requires the presence of NRP2 only. **5**: FAK recruitment to the assembling nascent adhesion faciliates integrin complex clustering to form larger FAs, amplifying downstream signalling cascades to promote EC migration. FA growth and EC migration are both dependent upon the expression of NRP2, whilst the expression of α5 integrin is dispensible. (Figure generated using Biorender).

3.3 NRP2 regulates the intracellular trafficking of α5 integrin to promote FA turnover

Dynamic membrane trafficking of integrins; the clathrin-dependent or independent endocytosis of active integrin heterodimers from disassembling FAs, and their subsequent recycling back to newly forming FAs at the leading edge of the cell via sorting endosomes, regulates FA turnover and cytoskeletal changes during migration [145], [168], [258]. In the previous chapter we saw that NRP2 mediates FA assembly and development by promoting FAK recruitment. Our laboratory has also already demonstrated that the loss of NRP2 impairs the rate of FA assembly and disassembly in mLMECs, which was subsequently found to result from a reduced rate of α5 integrin recycling [225].

Whilst intimating a role for NRP2 in regulating the intracellular trafficking of integrins is novel, this is not the case for NRP1. Studies by Valdembri *et al.*, demonstrated that binding of the endocytic adaptor GIPC1 to the cytoplasmic SEA domain of NRP1 selectively stimulates the direct and rapid endocytosis of active α5β1 integrin from fibrillar adhesions. This was shown to occur via myosin VI directed transport along F-actin microfilaments to early endosomes in a Rab5 dependent manner. By employing a photoactivatable α5-GFP construct, it was subsequently observed that α5β1 integrin recycles back to membrane adhesions in $NRP1^{+}$ vesicles [108]. In addition, studies have shown that NRP1, via its interactions with GIPC1, also mediates VEGFR2 recycling, deletion of the GIPC1-synectin binding motif of NRP1 preventing the transition of VEGFR2 through Rab11 associated recycling endosomes and attenuating signalling completely [86]–[88], [90].

Following review of our LFQ dataset, expanded to accommodate as many candidate interactions as possible, we identified 54 proteins whose function were related to cellular trafficking pathways. Of particular note were members of the clathrin and caveolin endocytosis pathways, such as both clathrin, caveolin-1 and -2, and EGFR substrate 15, a constitutive component of clathrin coated pits [258]–[261]. In addition, our analysis detected numerous proteins associated with intracellular recycling, including rab11Fip5, rab5c and scamp1/2 [108], [262]–[264], and members of the lysosomal degradation pathway; rab7 and vamp2/3 [90]. Taking this into account, and given the promising results of the preliminary investigations carried out by previous members of our laboratory prior to the start of my project, we subsequently chose to examine in further detail how NRP2 regulates α5 integrin traffic. This work would then go onto inform the hypotheses drawn from our previous chapter, examining how NRP2 and α5 integrin cooperate to modulate EC adhesion and migration.

3.3.1 NRP2 promotes the intracellular recycling of α5 integrin in endothelial cells

Studies have previously reported NRP1 to complex with α5 integrin in HUVECs [108] and NRP2 to complex with α5 integrin from co-cultures between HUVECs and renal cell carcinoma [210]. The Robinson laboratory has also previously demonstrated that a physical interaction exists by co-immunoprecipitating NRP2 and α5 integrin in both directions in mLMECs [225]. These co-immunoprecipitation studies confirmed that of the original LFQ analysis, which revealed both α5 and β1 integrin subunits as candidate binding partners of NRP2. In the previous chapter we showed that a complex regulatory interaction exists between NRP2 and α5 integrin to regulate FA dynamics and actin cytoskeleton remodelling. In addition, we demonstrated that NRP2 promotes FAK recruitment to α5 integrin^{+} adhesions to promote their development through FAK's modulatory effects on Rac1. To further understand this interaction, we therefore needed to examine where in our mLMECs NRP2 and α5 integrin colocalise.

A study published by Goel *et al*., previously described the use of a mouse-specific NRP2 antibody compatible with immunocytochemistry staining, and that showed no cross-reactivity with NRP1, to examine NRP2's regulation of α6β1 integrin during FA signalling [208]. Using this same antibody, we co-immunolocalised NRP2 with α5 integrin in ECs allowed to adhere on FN. Staining revealed that NRP2 does indeed co-localise with α5 integrin at a number of different sites within ECs, including at the perinuclear region, (i/ii), within intracellular vesicles (iii), and at the cell membrane (iv), providing weight to the preliminary co-immunoprecipitation studies previously performed. Surprisingly, and in conflict to what we have supposed thus far, NRP2 was observed to only very weakly colocalise with α5 integrin at FA sites, suggesting that NRP2 does not mediate interactions between α5 integrin and FN directly, but rather regulates α5 integrin activity by modulating its transport to and from FAs (**Figure 3.15A-B**). To assess whether NRP2 and α5 integrin are transported as a complex within internalised endosomal compartments, we next utilised the receptor recycling inhibitor primaquine (PMQ), which has been shown to preserve endosomal integrin complexes in the cell [108], [175]. We therefore immunoprecipitated α5 integrin or NRP2 from ECs following a 10 minute pre-treatment with PMQ, and probed for the presence of an endosomal complex by Western blotting. PMQ incubation greatly increased the stoichiometry of their interaction in both directions, indicating that NRP2/α5 integrin complexes exist more stably within endosomes than at the plasma membrane (**Figure 3.15C**).

Previous members of the Robinson laboratory have demonstrated that silencing NRP2 expression in ECs impairs the rate FA turnover [225]. Given NRP1's role in regulating α5β1 integrin traffic in ECs [108], we hypothesised that NRP2 also plays a concomitant role in regulating the subcellular trafficking of α5 integrin to and from FAs. Next, we therefore chose to quantitatively assess the effects of depleting NRP2 on intracellular α5 integrin trafficking by performing internalisation and recycling cell surface biotinylation assays. These have previously been used with success by Remacle *et al*., and by members of the Robinson laboratory [107], [215], [219], [225]. In these assays, cell surface proteins are labelled with biotin, before being incubated for increasing timepoints at 37°C to allow proteins to internalise. Any remaining biotin is then stripped using a membrane-impermeable reducing agent, in this case Mesna, before cell lysates are subjected to immunoprecipitation for biotin. To measure recycling, a biotinylation assay was performed in the same manner to our internalisation assay, however biotin-labelled cell surface proteins were re-incubated to allowed for recycling. The level of biotinylated α5 integrin was then compared to a stripped control at each timepoint. Pilot biotinylation data previously collected in the Robinson Laboratory by Dr Abdullah Alghamdi, quantifying the rate of internalisation and recycling of total α5 integrin in Ctrl and NRP2 siRNA-treated ECs had signposted NRP2 as playing no role in regulating integrin internalisation. In contrast, two independent recycling experiments had revealed NRP2 silencing to impair the rate of total α5 integrin recycling back to the plasma membrane [225]. To confirm these results, and to allow for robust statistical analysis, we performed a third and final biotinylation assay to assess the effect of NRP2 depletion on total α5 integrin internalisation and recycling. Whilst we did not achieve complete stripping in our *si*NRP2 control at 0 minutes, once pooled with our pilot data (graphs shown as pooled datasets) we observed no difference in the rate of total α5 integrin internalisation following NRP2 knockdown. A significant reduction in the rate of total α5 integrin recycling upon NRP2 depletion was found however, confirming the results of Dr Abdullah Alghamdi (**Figure 3.16**).

Unfortunately, we are unable to comment on the effect of NRP2 depletion on trafficking of active α5β1 integrin in our murine cells, as at the time of writing, no commercially available antibody detected mouse active α5β1 integrin. Indeed, Valdembri *et al*., only observed defects in the rate of endocytosis when probing for active α5β1 integrin, rather than total levels, in ECs depleted for NRP1 [108]. It is therefore possible that, were we to assess the rate of active α5β1 integrin internalisation in our mLMECs following NRP2 depletion, we would also find a similar impairment.

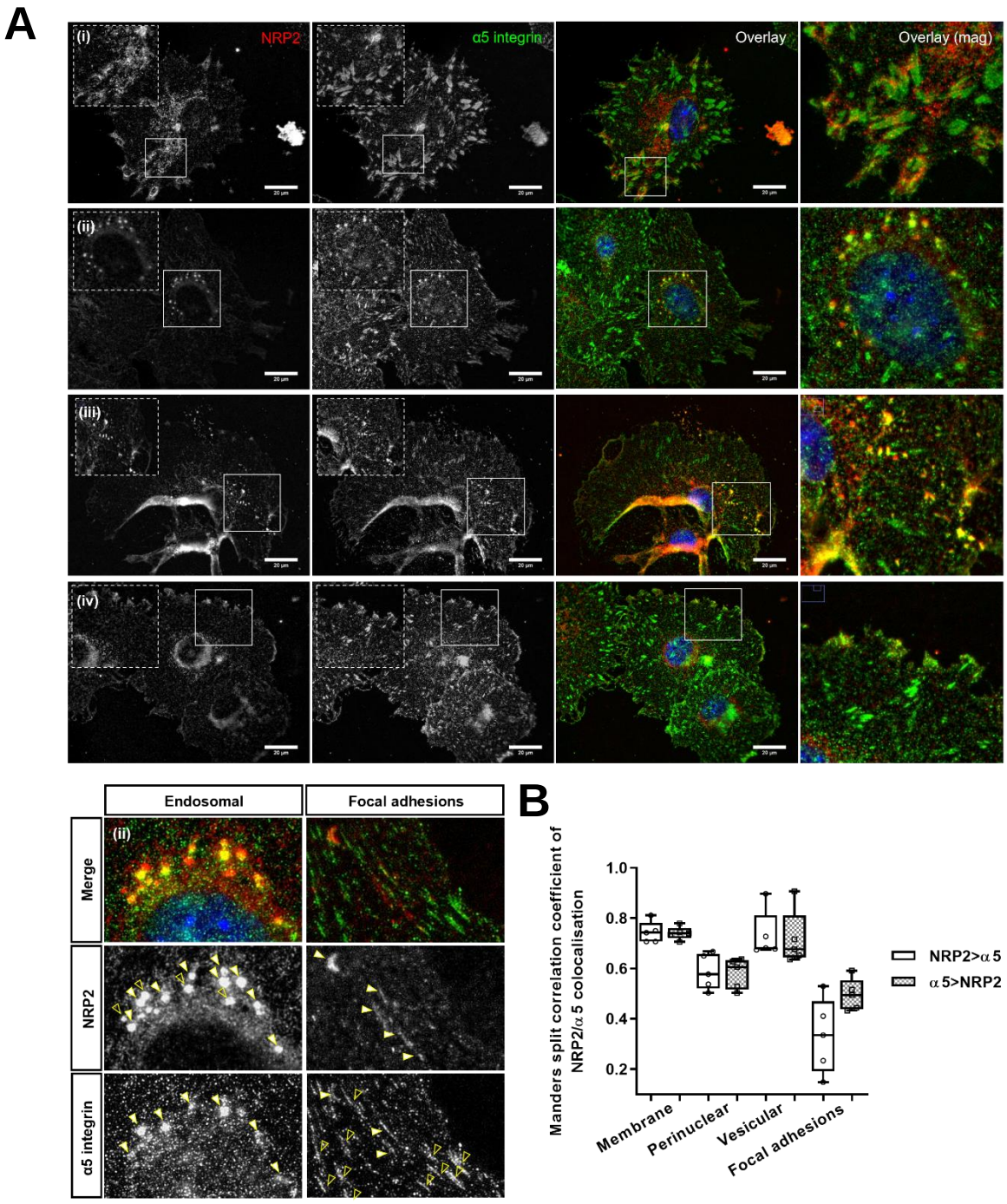
A
(i)
NRP2
α5 integrin
Overlay
Overlay (mag)
(ii)
(iii)
(iv)
Endosomal
Focal adhesions
Merge
NRP2
α5 integrin
B
Manders split correlation coefficient of NRP2/α5 colocalisation
1.0
0.8
0.6
0.4
0.2
Membrane
Perinuclear
Vesicular
Focal adhesions
NRP2>α5
α5>NRP2
C
- PMQ
+ PMQ
Lyse, IP: NRP2/α5
37°C
37°C
IP:
NRP2
NP
PMQ
- + +
Mr (kDa)
140
α5
IP:
α5
NP
- + +
NRP2

Figure 3.15 NRP2 colocalises with a5 integrin at the cell surface and in trafficking vesicles from the PNRC. $1x10^6$ ECs were nucleofected with Ctrl siRNA and seeded on 10 cm dishes pre-coated with 10 µg/ml FN at 37°C in a CO_2 incubator for 24 hours. ECs were then trypsinised and seeded at a low density of 2.5×10^4 cells/well onto acid-washed, oven sterilised coverslips pre-coated with 10 µg/ml FN and incubated for 90 minutes. Coverslips were fixed in 4% PFA, blocked and permeabilised. ECs were then incubated with anti-α5 integrin and anti-NRP2 primary antibody overnight at 4°C. Following two washes to remove any unreacted primary antibody, ECs were incubated with donkey anti-rabbit Alexa 488 and anti-mouse Alexa-546 secondary antibodies at RT for 1 hour. Coverslips were mounted with Prolong Gold with DAPI. Scale bars show 20 µm. **A**) Representative images of NRP2 colocalising with α5 integrin at the perinuclear region (i/ii), within trafficking vesicles (iii) and at the membrane (iv). Bottom panel set shows highlighted region shown in (ii). Empty arrows show locations of negative colocalisation, filled arrows show locations of positive colocalisation. **B**) Quantitative colocalisation determined using thresholded Mander's split colocalisation coefficients. Colocalisation thresholds set by the Costes Auto Threshold method coefficients. Error bars show mean ± SEM; (n≥5, 5 RIOs/cell). **C**) Immunoprecipitation of endogenous NRP2 and α5 integrin from ECs pre-incubated for 10 minutes in the absence or presence of 0.3 mM primaquine (PMQ). Ctrl siRNA transfected ECs were seeded onto 10 cm dishes pre-coated with 10 µg/ml FN and incubated for 48 hours at 37°C. Following PMQ incubation, EC extracts were immunoprecipitated by incubation with protein-G Dynabeads® coupled to antibodies against either α5 integrin or NRP2 overnight at 4°C. Immunoprecipitated complexes were separated by SDS-PAGE and subjected to Western blot analysis using primary antibodies against NRP2 or α5 integrin respectively. Immunoprecipitated EC extracts were ran alongside no primary (*NP*) immunoprecipitated control lysates. Left panel shows assay schematic, right panel shows Western blot images.

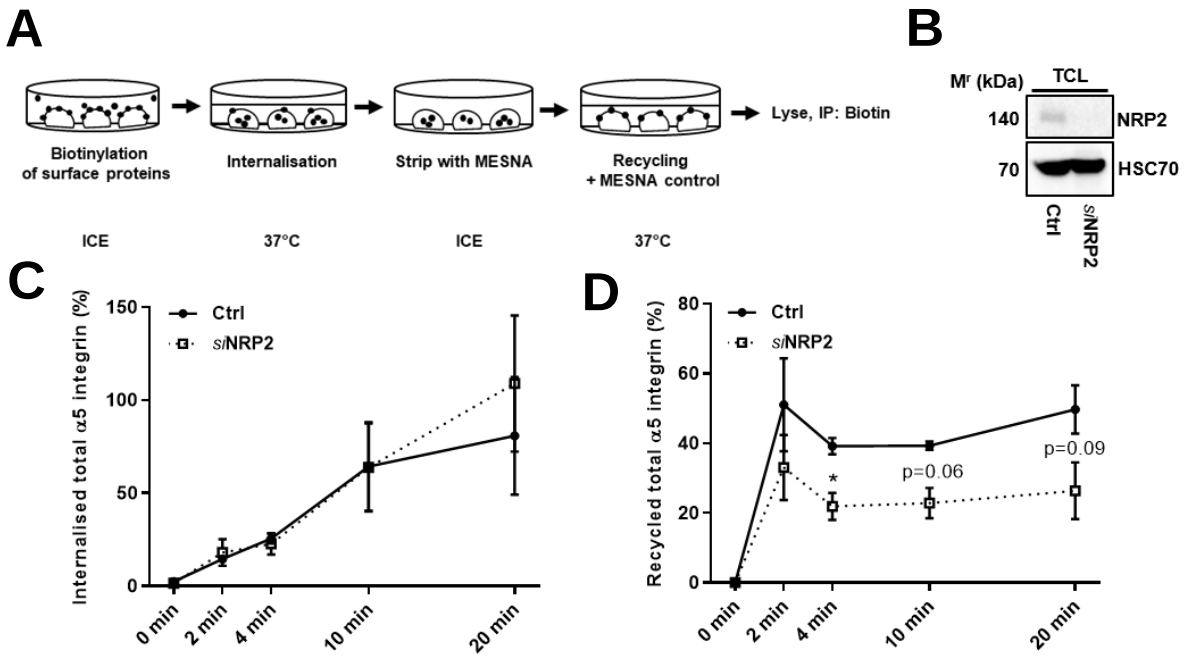

Figure 3.16 NRP2 depletion slows the rate of total α5 integrin recycling. ECs were transfected with either Ctrl or NRP2 siRNA and seeded onto 10 cm dishes pre-coated with 10 µg/ml FN and incubated for 48 hours at 37°C. ECs were subsequently starved in serum-free media, before being placed on ice. EC cell surface proteins were labelled with 0.3 mg/ml biotin. After biotin surface labelling, ECs were incubated in serum free media for 20 minutes at 37°C to allow for internalisation. A sample of ECs were maintained at 4°C for use as positive/negative controls. The remaining ECs were then placed on ice, and any un-internalised biotin-labelled proteins stripped off using 100 mM Mesna. The internalised protein fraction was then allowed to recycle by incubating the ECs for the indicated timepoints at 37°C. ECs were then returned to ice and incubated in 100 mM Mesna. No Mesna treatment dishes at each timepoint were used as controls. EC lysates were then immunoprecipitated with protein-G Dynabeads® coupled to an anti-biotin antibody overnight at 4°C. Immunoprecipitated biotin-labelled proteins were separated by SDS-PAGE and subjected to Western blot analysis. The level of internalised and recycled total α5 integrin at each time of incubation was normalised to the (- Mesna) control. **A**) Biotinylation assay schematic. **B**) Western blot showing confirmation of NRP2 silencing. **C**) Mean densitometric analysis obtained using ImageJ™ pooled with two independent preliminary experiments measuring total α5 integrin internalisation totalling N=3. **D**) Mean densitometric analysis obtained using ImageJ™ pooled with two independent preliminary experiments measuring total α5 integrin recycling totalling N=3. Error bars show mean ± SEM; N=3; *=P<0.05, unpaired students t-test (two-tailed). N=2 data generated by Dr Abdullah Alghamdi.

3.3.2 Dynamin-2 recruitment to α5 integrin containing adhesions is sensitive to NRP2 depletion

Whilst the inability to measure active levels of α5 integrin trafficking highlighted a fundamental caveat to our investigations, we can provide superficial evidence that NRP2 also regulates α5 integrin internalisation. Our LFQ analysis identified numerous candidate interactions with proteins essential for clathrin and caveolin-mediated integrin endocytosis (**Figure 3.17A**). Moreover, in an attempt to corroborate these candidate interactions, we successfully co-immunoprecipitated NRP2 with both clathrin heavy-chain A, and caveolin-1, and revealed a strong co-localisation between NRP2 and clathrin at cell protrusions by immunofluorescence (**Figure 3.17B-C**). In addition, past members of the Robinson laboratory have illustrated that NRP2 silencing significantly impairs the rate of FA disassembly from the membrane, which fundamentally relies on integrin endocytosis. As we lacked the tools to biochemically measure the kinetics of active integrin trafficking however, we chose to rely on alternative approaches to quantify any impediment to the ability for α5 integrin to internalise.

It is well known that the recruitment of dynamin-2 (dyn-2) GTPase is essential for clathrin-dependent integrin endocytosis. Targeted to clathrin coated pits following FAK phosphorylation, dyn-2 forms a helical polymer around the vesicle neck, mediating vesicle release by GTP hydrolysis-dependent constriction [265], [266]. Studies have since ratified its importance during FA disassembly by demonstrating that its loss results in increased FA size and integrin surface level expression in MLECs [267]. We have, thus far, demonstrated a primary role for NRP2 in the activation and localisation of FAK to α5 integrin^{+} FAs. Dyn-2 was also identified in our LFQ data. We therefore sought to confirm whether NRP2 mediates dyn-2 targeting in our ECs, and should this arise to be the case, to apply it as a rudimentary measure of α5 integrin's ability to internalise.

To achieve this, fixed ECs were co-immunolabelled with antibodies against α5 integrin and dyn-2, and imaged using confocal microscopy. Compared to Ctrl siRNA treated ECs, where dyn-2 robustly colocalised with α5 integrin^{+} sites around the cell periphery, dyn-2 targeting was reduced by approximately half following depletion of NRP2 at 90 minutes (**Figure 3.17D-E**). An increased physical interaction between dyn-2 and *p*-FAK^{Tyr407} was also detected in NRP2 knockdown lysates by co-immunoprecipitation (**Figure 3.17F-G**). As we found NRP2 depletion to attenuate FAK phosphorylation, it is possible that as a consequence, dyn-2's ability to effectively target α5 integrin^{+} FAs to stimulate endocytosis is also impaired. As a result, dyn-2 may remain in close proximity to FAK, increasing their stoichiometric interaction.

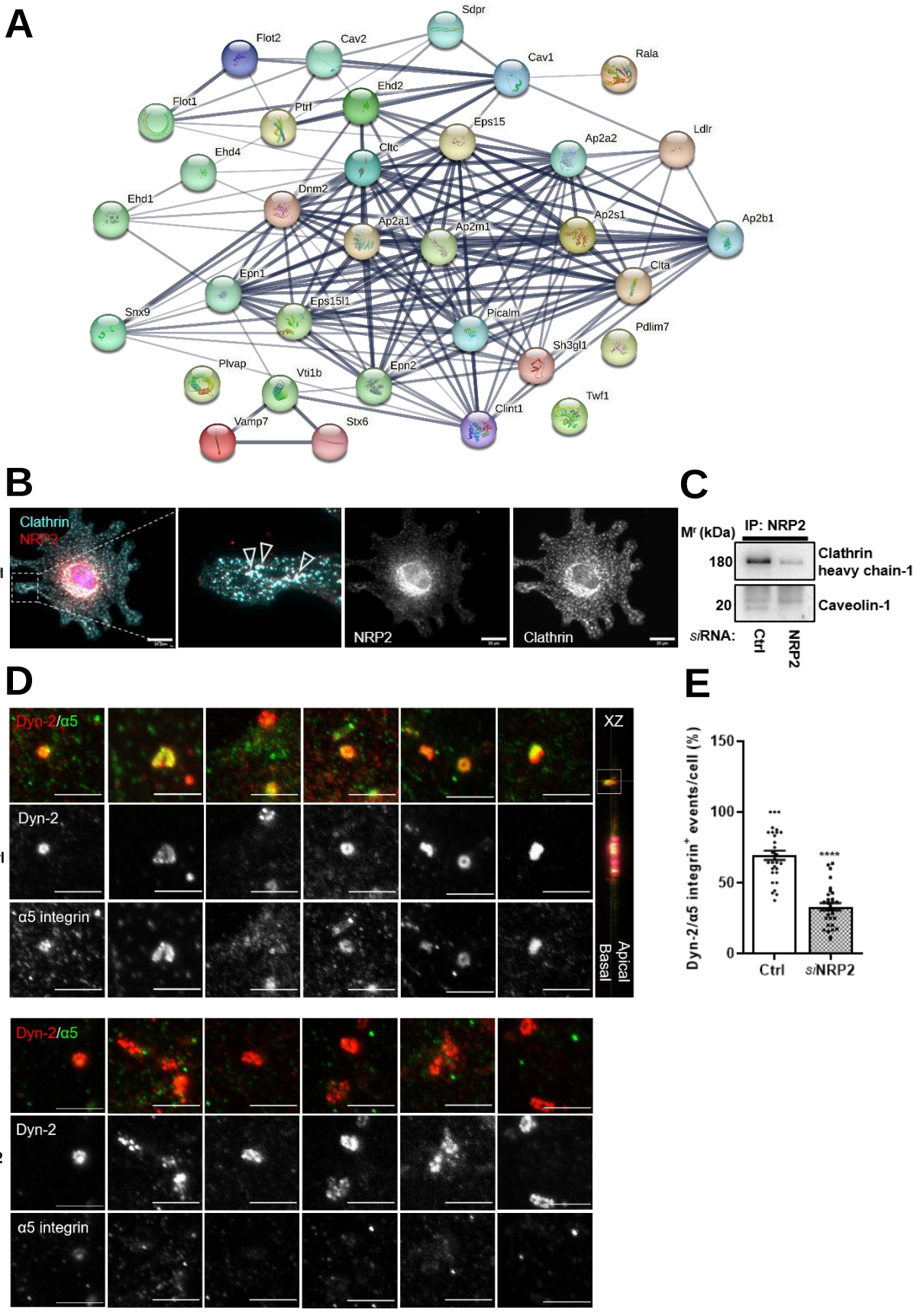
A
Sdpr
Flot2
Cav2
Cav1
Rala
Flot1
Ehd2
Ptrf
Eps15
Ldlr
Ap2a2
Ehd4
Cltc
Dnm2
Ehd1
Ap2a1
Ap2m1
Ap2s1
Ap2b1
Epn1
Clta
Eps15l1
Snx9
Picalm
Pdlim7
Sh3gl1
Plvap
Vti1b
Epn2
Twf1
Clint1
Vamp7
Stx6
B
Ctrl
Clathrin
NRP2
NRP2
Clathrin
C
Mr (kDa)
IP: NRP2
180
Clathrin heavy chain-1
20
Caveolin-1
siRNA:
Ctrl
NRP2
D
Dyn-2/α5
XZ
Ctrl
Dyn-2
α5 integrin
Apical
Basal
siNRP2
Dyn-2/α5
Dyn-2
α5 integrin
E
Dyn-2/α5 integrin+ events/cell (%)
150
100
50
0
****
Ctrl
siNRP2

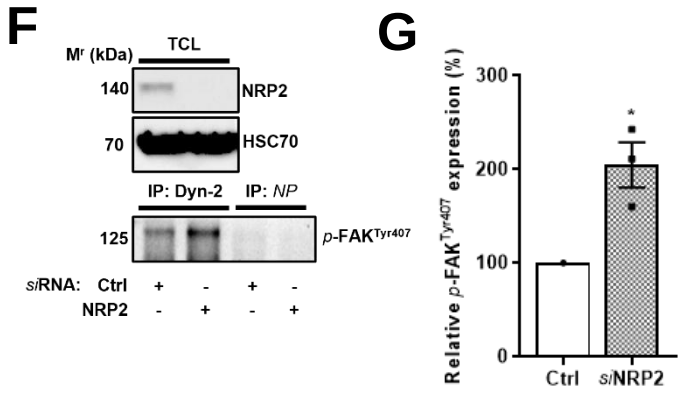

Figure 3.17 Dynamin-2 recruitment to α5 integrin containing adhesions is sensitive to NRP2 depletion. A) Internalisation-associated LFQ mass spectrometry hits identified as proteins immunoprecipitating with NRP2 at a significantly increased fold change compared to proteins analysed from NRP2 knockdown cell lysates. Line width correlates with interaction confidence, measured according to the STRING mouse database. Diagrams generated using STRING built-in online tool set to default parameters. (Data generated by Dr Abdullah Alghamdi). **B**) ECs were transfected with either Ctrl or NRP2 siRNA and seeded onto 10 cm dishes pre-coated with 10 µg/ml FN and incubated for 24 hours at 37°C. ECs were then trypsinised and seeded at a low density of 2.5 x 10^4 cells/well onto acid-washed, oven sterilised coverslips pre-coated with 10 µg/ml FN and incubated for 90 minutes. Coverslips were fixed in 4% PFA, blocked and permeabilised. ECs were then incubated with anti-NRP2 and anti-clathrin primary antibody overnight at 4°C. Following two washes to remove any unreacted primary antibody, ECs were incubated with donkey anti-rabbit Alexa 488 and anti-mouse Alexa-546 secondary antibodies at RT for 1 hour. Coverslips were mounted with Prolong Gold with DAPI. Scale bars show 20 µm. Arrows indicate co-localisation. **C**) ECs were transfected with either Ctrl or NRP2 siRNA and seeded onto 10 cm dishes pre-coated with 10 µg/ml FN and incubated for 48 hours at 37°C. EC extracts were immunoprecipitated by incubation with protein-G Dynabeads® coupled to a NRP2 antibody overnight at 4°C. Immunoprecipitated complexes were separated by SDS-PAGE and subjected to Western blot analysis using primary antibodies against clathrin heavy chain-1 and caveolin-1. **D**) ECs were prepared as described in **B**), using primary antibodies against dyn-2 and α5 integrin. Panels show representative images taken from multiple cells. Scale bars show 10 µm. Top right panel shows XZ plane colocalisation between dyn-2 and α5 integrin in Ctrl ECs. **E**) Relative number of dyn-2 and α5 integrin$^+$ events/cell (%), error bars show mean ± SEM; n≥30; ****=P<0.0001, unpaired students t-test (two-tailed). **F**) ECs were prepared as described in **C**), with the exception that EC extracts were immunoprecipitated with protein-G Dynabeads® coupled to a dyn-2 antibody. Immunoprecipitated complexes were separated by SDS-PAGE and subjected to Western blot analysis using a primary antibody against *p*-FAK^{Tyr407}. TCLs were assayed to confirm NRP2 depletion. **G**) Accompanying densitometric analysis. Error bar shows mean ± SEM; N=3; *=P<0.05, one sample t-test (two-tailed).

3.3.3 NRP2 regulates an α5 integrin-*p*-FAK-Rab11 trafficking axis to promote focal adhesion assembly and turnover

Whilst it is possible that NRP2 coordinates α5 integrin internalisation by regulating dyn-2 recruitment, without the means to fully substantiate our findings biochemically, we chose to instead focus our efforts on delineating the mechanisms by which NRP2 promotes α5 integrin recycling. Following endocytosis, integrins are sorted to specific subdomains of the early endosome, before being either rapidly recycled back to the plasma membrane via Rab4 or Rab5 GTPase, or passed to the PNRC and recycled via a long-loop recycling pathway. This long-loop recycling mechanism is under the control of Rab11 GTPase [155], [175]–[177], [181]. α5β1 integrin is known to accumulate at the PNRC in $Rab11^+$ vesicles before being transported to the cell surface at dynamic cell protrusions via the actin cytoskeleton. More importantly, disruption to recycling via the Rab11 compartment has also been shown to compromise α5β1 integrin-dependent cell spreading and migration [181], [268]. Studies have subsequently demonstrated $Rab11^+$ vesicles to be trafficked using the myosin Vb motor via Rab11Fip adaptor proteins, which are known to regulate various temporally and spatially distinct stages of Rab11-mediated recycling [269]. In addition to being recycled via this long-loop pathway, α5β1 integrin has also been shown to be recycled back to assembling FAs via $Rab5^+$ vesicles in a NRP1 dependent manner [108].

With this in mind, we began by examining whether NRP2 shares a physical association with either Rab11, Rab5 or Rab4 by co-immunoprecipitation. Whilst no direct interaction was observed between NRP2 and either Rab5 or Rab4, NRP2 did positively co-immunoprecipitate with Rab11 (**Figure 3.18A**). Further co-immunoprecipitation studies assessing this interaction in both directions confirmed this (**Figure 3.18B**), and also revealed that total Rab11 expression decreases significantly upon siRNA-mediated depletion of NRP2 (**Figure 3.18C-D**). Despite Rab11Fip5 being identified by our LFQ analysis as a candidate binding protein of NRP2, previously reported to regulate α6β1 integrin recycling [262], we observed no direct interactions with NRP2 by co-immunoprecipitation (data not shown) nor did we observe any changes in its total expression (**Figure 3.18C-D**) or spatial localisation in *si*NRP2 ECs (data not shown). Furthermore, whilst we detected a co-association between Rab11 and Rab11Fip5, no difference in band intensity was observed between Ctrl and NRP2 depleted Rab11 IP lysates, suggesting that their interaction is not mediated by NRP2 (**Figure 3.18E**). After confirming a direct physical interaction between NRP2 and Rab11 in our ECs, we co-immunostained both to ascertain their spatial colocalisation. NRP2 colocalised with Rab11 at both the perinuclear region of the cell and within trafficking vesicles, confirming our co-

immunoprecipitation studies and suggesting that NRP2 regulates Rab11-directed recycling, perhaps by modulating Rab11 expression (**Figure 3.18F**).

Studies have revealed that the retention of *p*-FAK within integrin complexes actively undergoing endocytosis sustains the active integrin conformation during their subsequent Rab11-associated recycling, thereby enabling an enhanced polarised reassembly of nascent adhesive structures at the leading edge of the cell [165]. Kao *et al.,* also recently implemented live imaging microscopy to demonstrate that *p*-FAK is transported in Rab11 vesicles to promote the directional migration of fibrosarcoma cells [270]. As the recruitment and phosphorylation of FAK to α5 integrin adhesion sites was found to be disrupted following the loss of NRP2, we next sought to determine whether NRP2 promotes an α5 integrin-*p*-FAK-Rab11 recycling axis to promote nascent adhesion assembly and maturation. In order to visualise the functional consequences of NRP2 silencing on Rab11-associated recycling, we co-immunolabelled Rab11 with endogenous *p*-FAK^{Tyr407} and/or α5 integrin in siRNA-treated ECs adhered to FN for 90 minutes. As observed previously, NRP2 depletion resulted in a significant accumulation of *p*-FAK^{Tyr407} arresting around the perinuclear region, positively colocalising with Rab11. *si*NRP2 ECs were also found to display a weaker co-localisation with fewer peripheral Rab11^{+} vesicles likely undergoing recycling back to assembling adhesion sites (**Figure 3.19A-B**). This was subsequently confirmed first by XZ-plane confocal imaging, and then by measuring the relative intensity of endogenous *p*-FAK^{Tyr407} staining across the cell diameter. This enabled us to generate mean intensity maps from pools of both Ctrl and NRP2-siRNA treated EC, and substantiated our prior findings that NRP2 depletion causes the accumulation of *p*-FAK^{Tyr407} at the perinuclear region (**Figure 3.19C**). Furthermore, we observed NRP2 depleted ECs to display a dramatic un-coupling between α5 integrin and Rab11^{+} vesicles at both the perinuclear region and at the membrane (**Figure 3.20**), suggestive that NRP2 regulates Rab11-facilitated transport of both α5 integrin and *p*-FAK^{Tyr407} in ECs. Upon NRP2 silencing, assembling nascent adhesions are less developed, arising as a consequence of a reduced rate of α5 integrin recycling and *p*-FAK^{Tyr407} recruitment, concomitant with the accumulation of both α5 integrin and *p*-FAK^{Tyr407} at the perinuclear region. These co-localisation studies are shown as a set of sequential figures for ease of inspection, ending with **Figure 3.21**, which shows the triple co-localisation between Rab11, *p*-FAK^{Tyr407} and α5 integrin in Ctrl and *si*NRP2 ECs.

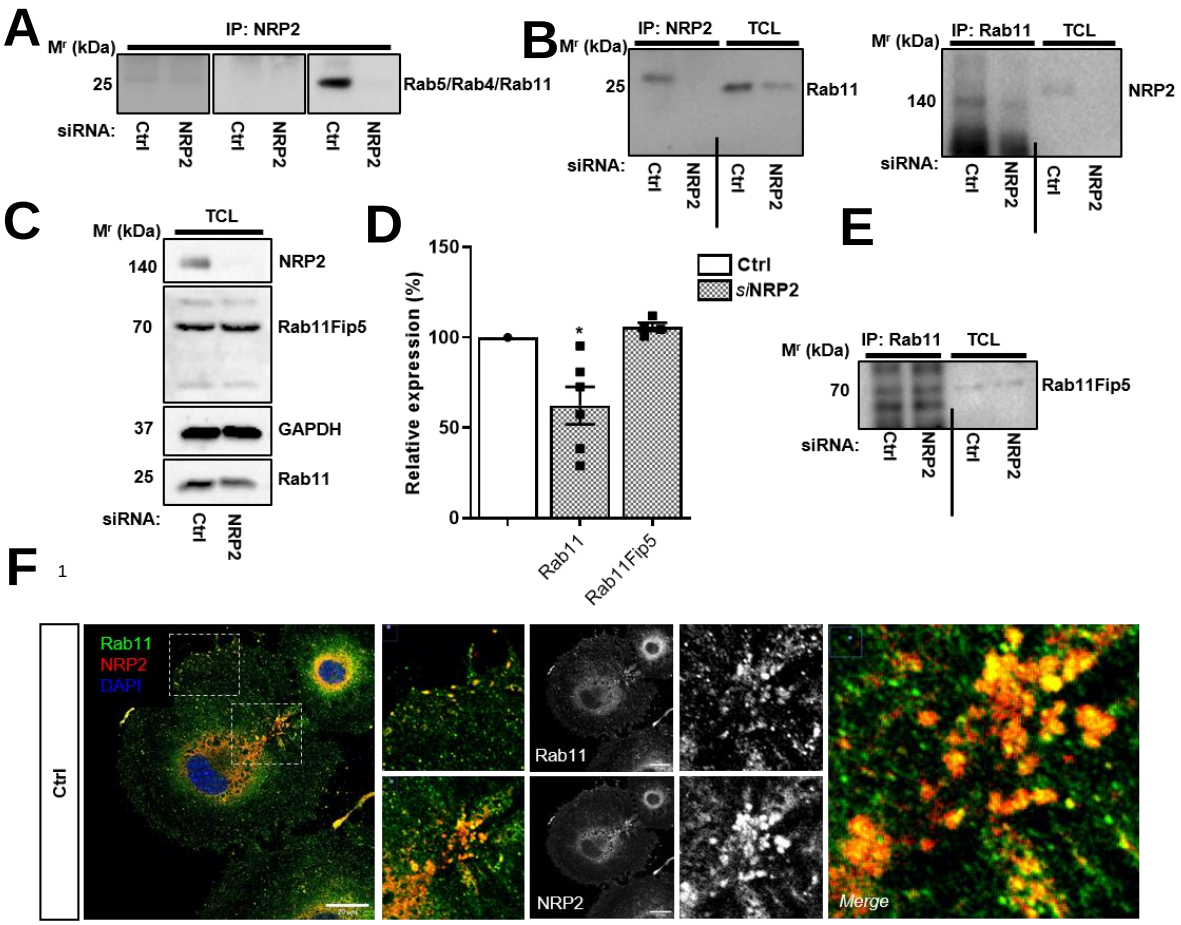

[1]Permission granted by FASEB Journal [230] to re-use figure panels.

Figure 3.18 NRP2 regulates Rab11-mediated recycling of α5 integrin. ECs were transfected with either Ctrl or NRP2 siRNA and seeded onto 10 cm dishes pre-coated with 10 µg/ml FN and incubated for 48 hours at 37°C. EC extracts were immunoprecipitated by incubation with protein-G Dynabeads® coupled to antibodies against NRP2 overnight at 4°C. Immunoprecipitated complexes were separated by SDS-PAGE and subjected to Western blot analysis using a primary antibody against Rab5, Rab4 or Rab11 respectively. **B**) siRNA-transfected ECs were seeded onto 10 cm dishes precoated with 10 µg/ml FN and incubated for 48 hours at 37°C. EC extracts were immunoprecipitated in the same manner as described in **A**) either with protein-G Dynabeads® coupled to antibodies against NRP2 or Rab11 overnight at 4°C. Immunoprecipitated EC extracts were run alongside total Ctrl siRNA and NRP2 siRNA cell lysates. **C**) siRNA-transfected ECs were seeded onto 10 cm dishes pre-coated with 10 µg/ml FN and incubated for 48 hours at 37°C. ECs were lysed in ESB and subjected to the DC protein assay before being analysed by Western blotting using primary antibodies against NRP2, Rab11Fip5 and Rab11. GAPDH was used as a loading control. Bands were quantified using ImageJ™ densitometric analysis. **D/E**) Accompanying densitometric analysis. Error bar shows mean ± SEM; (N=6/4 respectively); *=P<0.05, one sample t-test (two-tailed). **F**) 1x10^6 ECs were seeded on 10 cm dishes pre-coated with 10 µg/ml FN at 37°C in a CO_2 incubator for 48 hours. ECs were re-seeded onto coverslips pre-coated with 10 µg/ml FN at 37°C in a CO_2 incubator for 90 minutes. Coverslips were fixed in 4% PFA, blocked and permeabilised. ECs were incubated with Rab11Fip5 primary antibody overnight at 4°C. Following two washes to remove any unreacted primary antibody, ECs were incubated with donkey anti-rabbit Alexa 488 secondary antibody at RT for 1 hour. Coverslips were mounted with Prolong Gold with DAPI. Scale bars show 20 µm. **G**) ECs were prepared as described in **B**) with protein-G Dynabeads® coupled to a primary antibody against Rab11 overnight at 4°C. Immunoprecipitated EC extracts were run alongside total Ctrl siRNA and NRP2 siRNA cell lysates, and used to probe for Rab11Fip5 expression. **H**) As described in **F**), with the exception that ECs were incubated with anti-NRP2 and Rab11 primary antibodies overnight at 4°C. Scale bars show 20 µm.

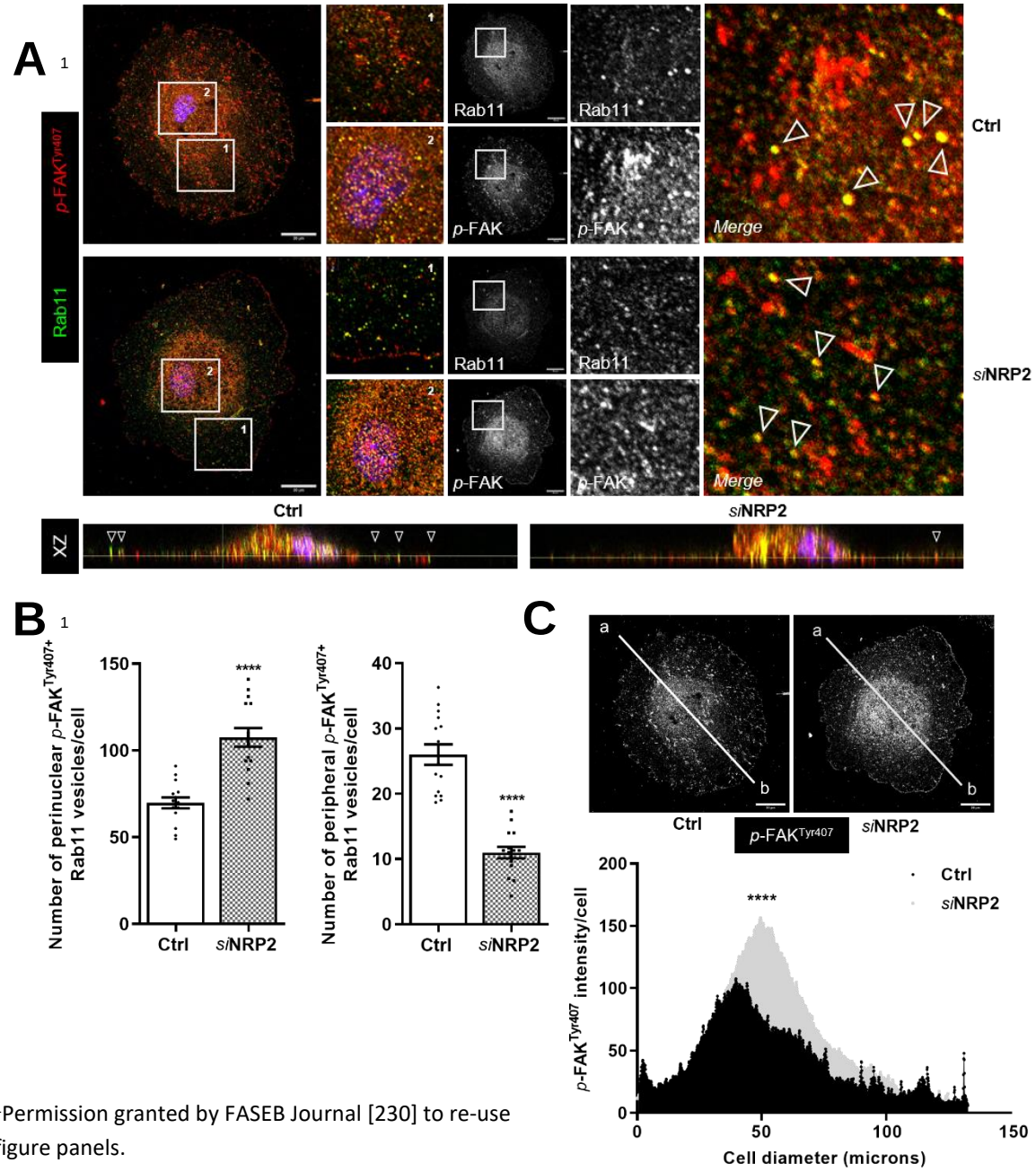

[1]Permission granted by FASEB Journal [230] to re-use figure panels.

Figure 3.19 NRP2 depletion disrupts Rab11 mediated traffic of p-FAK^{Tyr407} to adhesion sites. 1x10^6 ECs were nucleofected with either Ctrl siRNA or NRP2 siRNA and seeded on 10 cm dishes pre-coated with 10 µg/ml FN at 37°C in a CO_2 incubator for 24 hours. ECs were then trypsinised and seeded at a low density of 2.5x10^4 cells/well onto acid-washed, oven sterilised coverslips pre-coated with 10 µg/ml FN and incubated for 90 minutes. Coverslips were fixed in 4% PFA, blocked and permeabilised. ECs were then incubated with anti-Rab11 and anti-*p*-FAK^{Tyr407} primary antibodies overnight at 4°C. Following two washes to remove any unreacted primary antibody, ECs were incubated in anti-rabbit Alexa 488 and anti-rat Alexa 555 secondary antibodies at RT for 1 hour. Coverslips were mounted with Prolong Gold with DAPI. Scale bars show 20 µm. **A**) Representative images of Ctrl and NRP2 siRNA treated ECs fixed at 90 minutes showing colocalisation between Rab11 and *p*-FAK^{Tyr407} at the perinuclear region and at the cell periphery. Bottom panels show confocal XZ sectioning microscopy analysis of Rab11 colocalisation with *p*-FAK^{Tyr407} **B**) Left panel: number of perinuclear *p*-FAK^{Tyr407} positive Rab11 vesicles positive adhesions/ 20 x 20 µm ROI. Right panel: number of cell periphery *p*-FAK^{Tyr407} positive Rab11 vesicles positive adhesions/ 20 x 20 µm ROI. 3x 20 x 20 µm ROIs taken per cell. Error bars show mean ± SEM; n≥15; ****=P<0.0001, unpaired students t-test (two-tailed). **C**) Mean

p-FAK^{Tyr407} intensity distribution profile from ≥20 ECs treated with either Ctrl or NRP2 siRNA; ****=P<0.0001, Kolmogorov-Smirnov test.

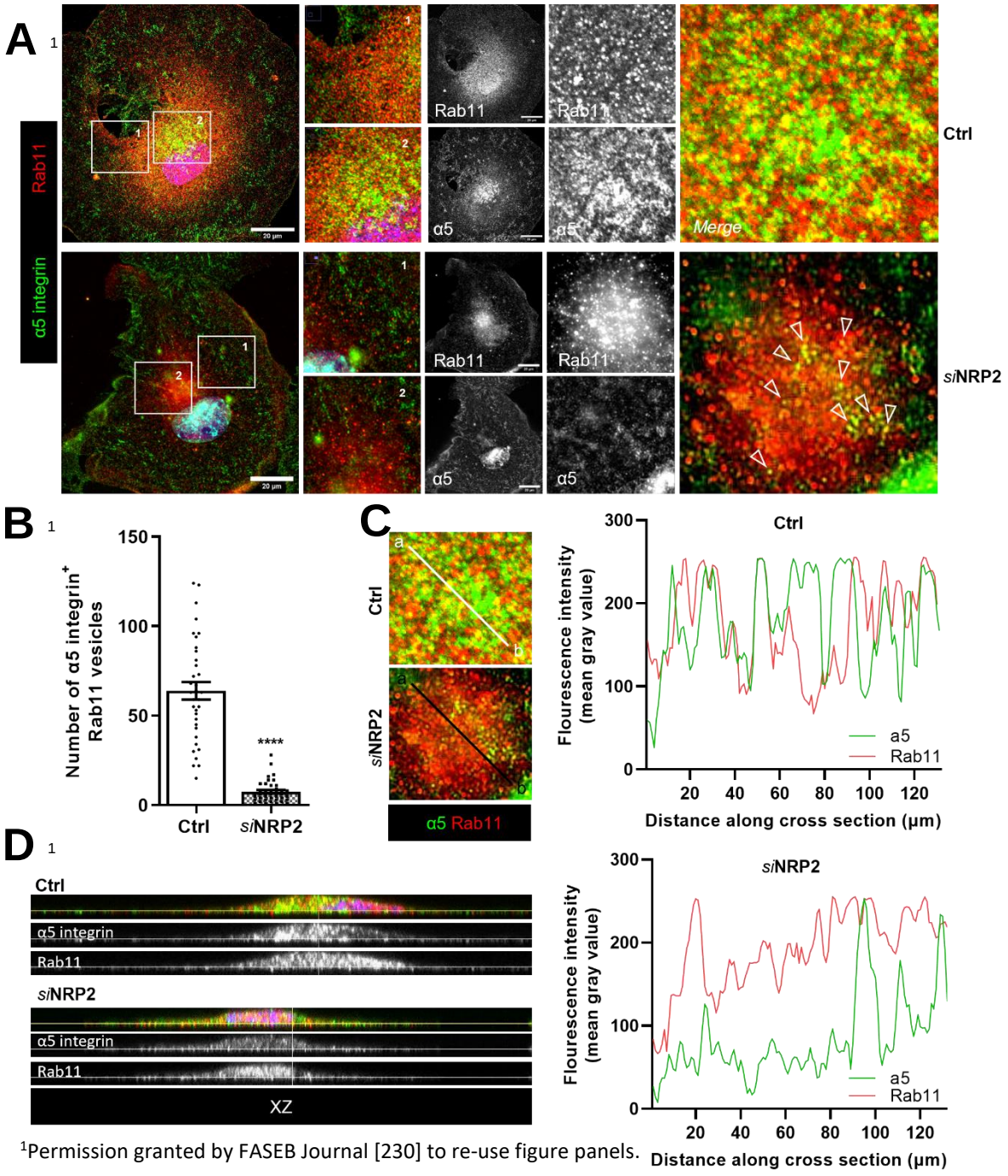

[1]Permission granted by FASEB Journal [230] to re-use figure panels.

Figure 3.20 NRP2 depletion disrupts Rab11 mediated traffic of α5 integrin. 1x10^6 ECs were nucleofected with either Ctrl siRNA or NRP2 siRNA and seeded on 10 cm dishes pre-coated with 10 μg/ml FN at 37°C in a CO_2 incubator for 48 hours. ECs were re-seeded onto coverslips pre-coated with 10 μg/ml FN at 37°C in a CO_2 incubator for 90 minutes. Coverslips were fixed in 4% PFA, blocked and permeabilised. ECs were incubated with anti-α5 integrin and Rab11 primary antibodies overnight at 4°C. Following two washes to remove any unreacted primary antibody, ECs were incubated with donkey anti-rabbit Alexa 546 and donkey anti-rat Alexa 488 secondary antibodies at RT for 1 hour. Coverslips were mounted with Prolong Gold with DAPI. Scale bars show 20 μm. **A**) Panels show representative images of Ctrl and NRP2 siRNA treated ECs fixed at 90 minutes showing colocalisation between α5 integrin and Rab11. **B**) Number of α5 integrin positive Rab11 vesicles/cell. Error bars show mean ± SEM; n≥30; ****=P<0.0001, unpaired students t-test (two-tailed). **C**) Mean fluorescence intensity distribution showing colocalisation between α5 integrin and Rab11 in Ctrl and *si*NRP2

ECs shown in **A**). **D**) Confocal XZ sectioning microscopy analysis of Rab11 colocalisation with α5 integrin in Ctrl and *si*NRP2 ECs.

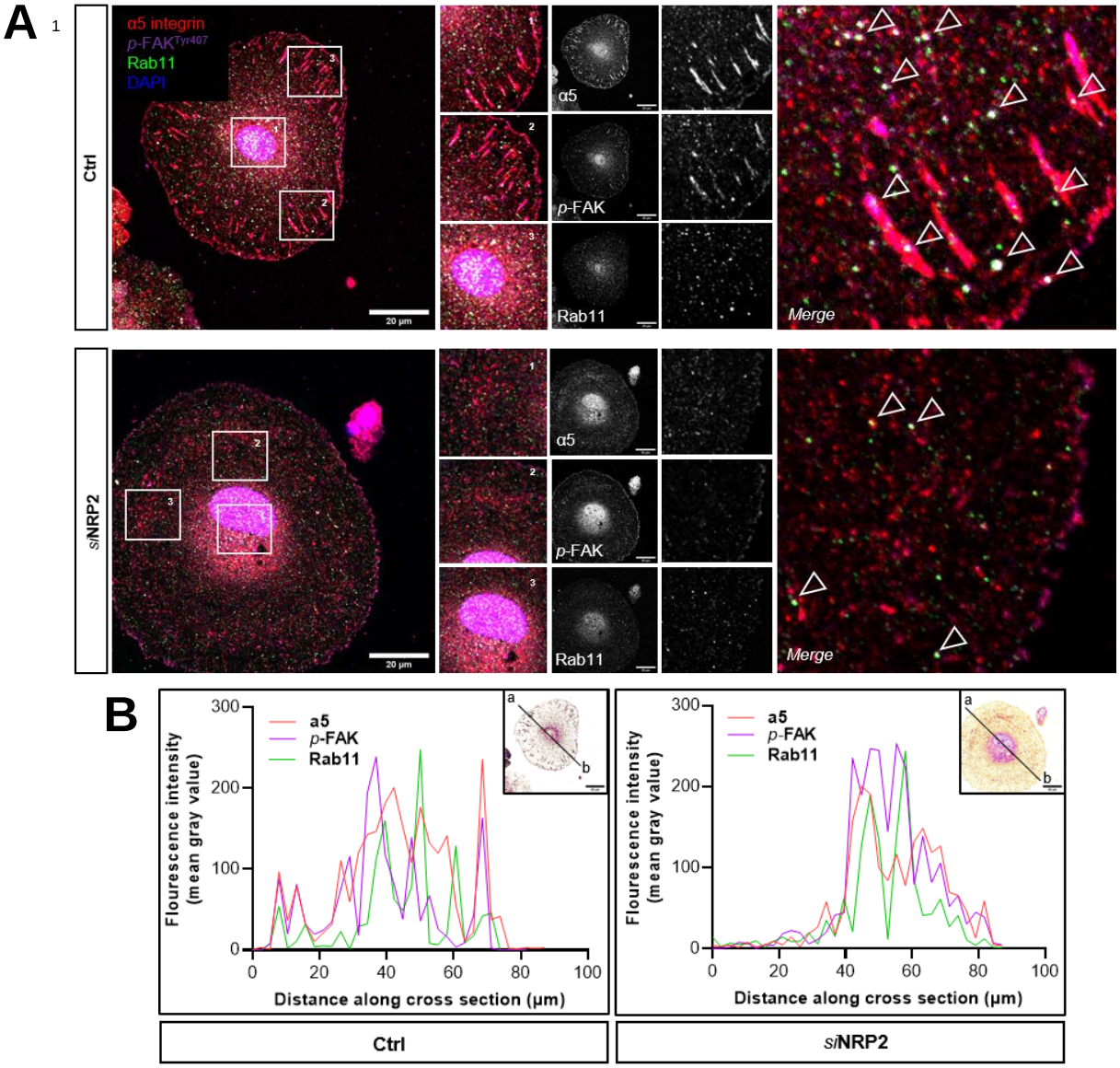

[1]Permission granted by FASEB Journal [230] to re-use figure panels.

Figure 3.21 NRP2 depletion disrupts Rab11 mediated traffic of *p*-FAK^{Tyr407} and α5 integrin to assembling adhesion sites. 1x10^6 ECs were nucleofected with either Ctrl siRNA or NRP2 siRNA and seeded on 10 cm dishes pre-coated with 10 µg/ml FN at 37°C in a CO_2 incubator for 48 hours. ECs were re-seeded onto coverslips pre-coated with 10 µg/ml FN at 37°C in a CO_2 incubator for 90 minutes. Coverslips were fixed in 4% PFA, blocked and permeabilised. ECs were then incubated with anti-Rab11 primary antibody for 6 hours at 4°C. Following two washes to remove any unreacted primary antibody, ECs were incubated in anti-rabbit Alexa 488 secondary antibody at RT for 1 hour. Following a further two washes, ECs were blocked for 30 minutes and then incubated with anti-*p*-FAK^{Tyr407} and α5 integrin primary antibodies overnight at 4°C. Coverslips were washed twice to remove any unreacted primary antibody and then incubated in anti-rabbit Alexa 555 and anti-Rat 647 secondary antibodies at RT for 1 hour. Coverslips were mounted with Prolong Gold with DAPI. Scale bars show 20 µm. **A**) Panels show representative images of Ctrl and NRP2 siRNA treated ECs fixed at 90 minutes showing triple colocalisation between Rab11, *p*-FAK^{Tyr407} and α5 integrin. **B**) Mean fluorescence intensity distribution showing colocalisation between α5 integrin, *p*-FAK^{Tyr407} and Rab11 in Ctrl and siNRP2 ECs shown in **A**).

3.3.4 α5 integrin accumulates in early endosomes in response to reduced Rab11-directed recycling

Since α5 integrin was found to longer reside within a $Rab11^+$ compartment, but remained localised around the perinuclear region, we next considered whether it would positively colocalise with another endosomal marker such as lysosomal-associated membrane protein-1 (LAMP1) or early endosome antigen-1 (EEA1). If either was found to be the case, it would greatly inform our understanding of which trafficking routes are regulated by NRP2. For example, should α5 integrin accumulate within $LAMP1^+$ late endosomes in NRP2 depleted ECs, it would suggest that it becomes rapidly targeted for degradation rather than undergoing recycling, explicating the reduced rate of transport back to the membrane. Equally, if α5 integrin accumulated in $EEA1^+$ early endosomes, then NRP2 likely mediates its transport to the PNRC via Rab21 and p120RasGAP, [176]–[178] in addition to Rab11-dependent recycling. Indeed, NRP2 regulating endocytosis and endosomal delivery is not novel; NRP2 silencing in human prostate cancer cells was previously shown to result in the inhibition of early to late endosome maturation, increasing the diameter of $EEA1^+$ punctae [271].

To investigate this in our mLMECs, we allowed Ctrl and NRP2 siRNA treated ECs to adhere to FN for 90 minutes followed by additional treatment with PMQ. ECs were then fixed and α5 integrin co-immunolabelled with either LAMP1 or EEA1. In both cases, incubation with PMQ successfully preserved α5 integrin expression within endosomal compartments to a greater extent than when compared to untreated ECs. Whilst the negligible fraction of internalised α5 integrin colocalising with $LAMP^+$ late endosomes was not affected by NRP2 silencing (**Figure 3.22A**), fluorescence confocal microscopy analyses of perinuclear punctae revealed that NRP2 depleted ECs exhibited significantly more $EEA1^+$ early endosomes positive for α5 integrin regardless of PMQ pre-treatment (**Figure 3.22B-C**). Given we are now aware that NRP2 regulates Rab11-directed recycling, it follows that disruptions to this trafficking route would result in the accumulation of α5 integrin within early endosomes. It is also possible that NRP2 also regulates the Rab21-dependent delivery of α5 integrin from the early endosome to the PNRC, however this would require further investigation. We observed no gross changes in $EEA1^+$ endosome diameter between our Ctrl and NRP2 depleted ECs (**Figure 3.22D**).

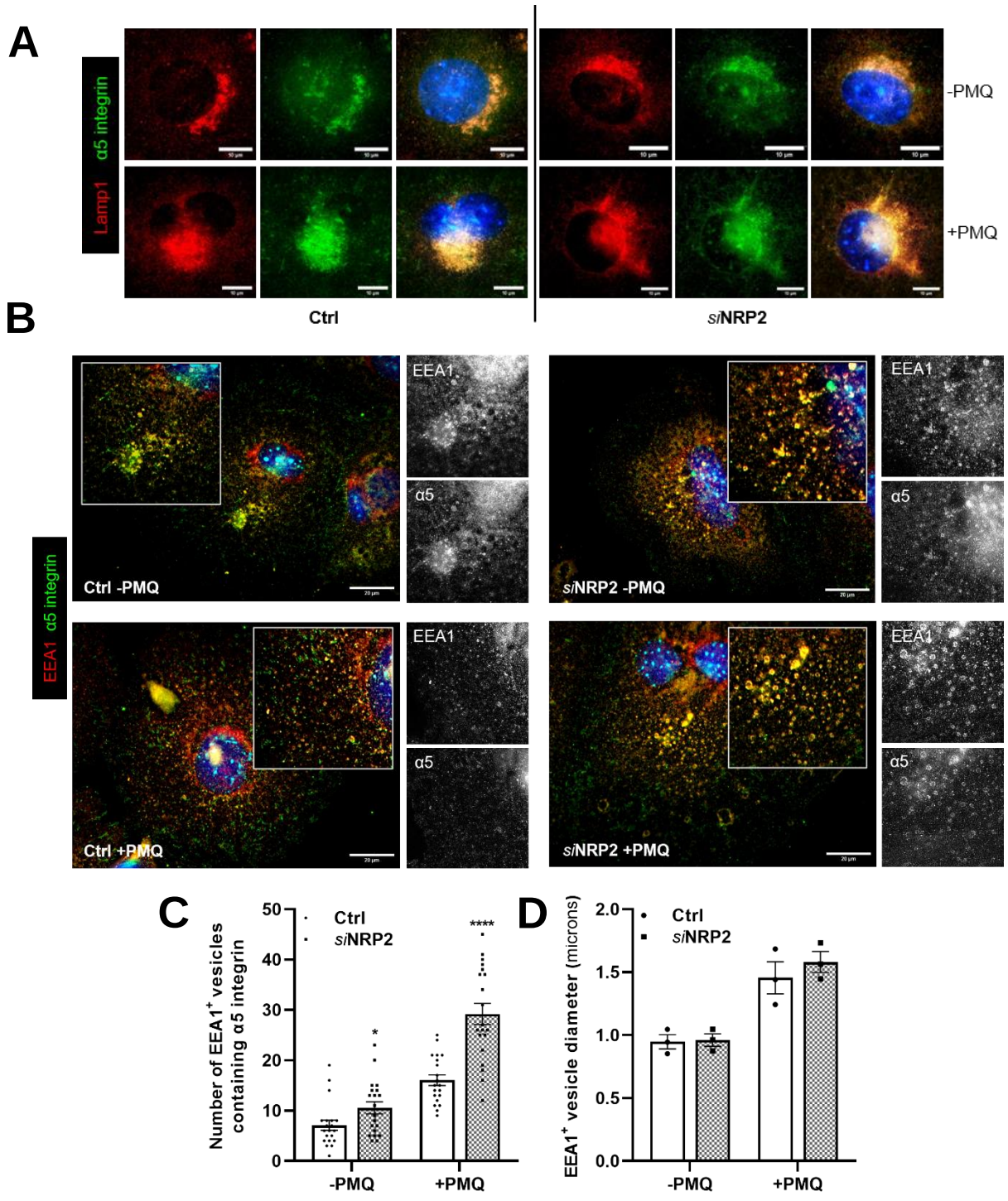
A
α5 integrin
Lamp1
-PMQ
+PMQ
Ctrl
siNRP2
B
EEA1 α5 integrin
Ctrl -PMQ
siNRP2 -PMQ
Ctrl +PMQ
siNRP2 +PMQ
EEA1
α5
C
Number of EEA1+ vesicles containing α5 integrin
Ctrl
siNRP2
****
*
-PMQ
+PMQ
D
EEA1+ vesicle diameter (microns)
Ctrl
siNRP2
-PMQ
+PMQ

Figure 3.22 α5 integrin accumulates in early endosomes in response to reduced Rab11-directed recycling. $1x10^6$ ECs were nucleofected with either Ctrl siRNA or NRP2 siRNA and seeded on 10 cm dishes pre-coated with 10 µg/ml FN at 37°C in a CO_2 incubator for 48 hours. ECs were re-seeded onto coverslips pre-coated with 10 µg/ml FN at 37°C in a CO_2 incubator for 90 minutes. Following PMQ incubation, ECs were fixed in 4% PFA, blocked and permeabilised. ECs were incubated with anti-α5 integrin and either anti-Lamp1 or anti-EEA1 primary antibodies overnight at 4°C. Following two washes to remove any unreacted primary antibody, ECs were incubated with donkey anti-rat Alexa 488 and donkey anti-rabbit Alexa 546 secondary antibodies at RT for 1 hour. Coverslips were mounted with Prolong Gold with DAPI. **A**) Panels show representative images of Ctrl and NRP2 siRNA treated ECs fixed at 90 minutes showing colocalisation between α5 integrin and Lamp1 with or without PMQ pre-treatment. Scale bars show 10 µm. **B**) Panels show representative images of Ctrl and NRP2 siRNA treated ECs fixed at 90 minutes showing colocalisation between α5 integrin and EEA1 with or without PMQ pre-treatment. Scale bars show 20 µm. **C**) Quantification of the number of $EEA1^+$ vesicles containing α5 integrin/cell. Error bars show mean ± SEM; n≥25; *=P<0.05, ****=P<0.0001, unpaired students t-test (two-tailed). **D**) Quantification of EEA1+ vesicle diameter. Error bars show mean ± SEM; N=3 (n≥50) vesicles.

3.3.5 Sustained impairment to FA turnover rate, elicited by NRP2 depletion, accelerates fibrillar adhesions formation

As FAs mature and become increasingly influenced by actomyosin-driven forces, their composition shifts; highly tyrosine phosphorylated focal contacts becoming large macromolecular assemblies [153], [154]. Whilst immature focal contacts are rapidly turned over to promote cell migration, and can undergo polarised translocation by extending centripetally and contracting peripherally, larger, more mature FA complexes anchor to the actin cytoskeleton to mediate more stable mechanical changes within the cell. Approximately 24 to 48 hours after initial adhesion, stress-fibre-associated FAs can then undergo a final transition into what are known as fibrillar adhesions, during which engaged α5β1-integrin is translocated along actin cables centripetally towards the cell body. As they extend from the medial ends of the stationary FA, it actively recruits the actin-binding protein tensin-1, which stabilises its growth [152], [155].

As NRP2 silencing was observed to impair initial FA assembly by reducing the rate of Rab11-mediated recycling of α5 integrin and *p*-FAK^{Tyr407}, we considered whether its protracted depletion would continue to disrupt FA maturation over time. Unexpectedly however, NRP2 siRNA-treated ECs adhered to FN for 180 minutes and 16 hours were found to exhibit significantly larger α5 integrin^{+} adhesions than their Ctrl siRNA-treated counterparts (**Figure 3.23A-C**). Whilst Ctrl siRNA-treated ECs fixed at 16 hours exhibited mature, punctate α5 integrin adhesions at the cell periphery, NRP2 depleted ECs displayed a high density of hyperextended fibril structures colocalised along actin filaments (**Figure 3.23D**). To exclude any chance of this fibrillar phenotype arising from any off-target effects, we repeated these co-localisation studies using our second NRP2-specific siRNA (#04). Furthermore, a 16 hour period of NRP2 depletion was also found to elicit the same accelerated formation of fibrillar adhesions in primary ECs (**Figure 3.23E-F**).

Further colocalisation studies using a tensin-1 specific antibody confirmed the identity of these α5 integrin-containing structures as fibrillar adhesions. This was reaffirmed by employing confocal XZ plane imaging, which revealed that compared to Ctrl ECs, where tensin-1 exclusively colocalised with endogenous α5 integrin at peripheral punctae, those depleted for NRP2 exhibited a strong co-localisation around the cell body (**Figure 3.24A**). Subsequent Western blot analysis revealed that this apparent accelerated transition from FAs to fibrillar adhesions was not due to any changes in total tensin-1 expression that this 16 hour timepoint, however *si*NRP2 ECs were found to express significantly more tensin-1 at 90 minutes than their Ctrl counterparts (**Figure 3.24B**). It is possible that this increased tensin-1 expression facilitates the premature development of fibrillar adhesions

following the loss of NRP2. Alternatively, the reduced rate of FA turnover, elicited by impaired Rab11-driven trafficking of α5 integrin-*p*-FAK^{Tyr407} complexes to assembling nascent adhesions, influences developing FAs to mature artificially rather than disassemble.

Indeed, by transfecting ECs with siRNAs specific to Rab11's known isoforms, individually, or in combination, we observed a significant increase in the development of fibrillar adhesions after 16 hours adhesion to FN. Co-depletion of both Rab11a and b, yielded the highest density of fibrillar adhesions compared to Ctrl ECs, equalling the fibrillar adhesion density of ECs depleted for NRP2 at 16 hours. ECs depleted for Rab11b also exhibited significantly more fibrillar adhesions than ECs depleted for Rab11a (**Figure 3.25A-C**). At 90 minutes adhesion to FN, where, following the depletion of NRP2, we had previously revealed an impaired ability of *p*-FAK^{Tyr407} to target α5 integrin^{+} adhesion sites, we also observed a similar perturbation following the depletion of both Rab11a and b isoforms, ECs exhibiting significantly fewer *p*-FAK^{Tyr407}-enriched α5 integrin FAs despite exhibiting no reduction in total *p*-FAK^{Tyr407} expression (**Figure 3.25A, D-E**). In polarised epithelial cells, Rab11a and Rab11b reside in distinct vesicular compartments, Rab11a, and not Rab11b mediating the apical delivery of post-Golgi cargoes. Rather, Mana *et al*., have reported that in primary arterial ECs, Rab11b alone drives the basolateral recycling of active α5 integrin and the subsequent deposition of FN fibrils [155], [272]. As a dense fibrillar distribution at 16 hours, and a reduced targeting of *p*-FAK^{Tyr407} to α5 integrin containing adhesions at 90 minutes were only observed following the co-depletion of both Rab11a and Rab11b, we can infer that NRP2 likely coordinates integrin traffic through both Rab11 isoforms in our mLMECs, and therefore perhaps both apical and basolateral transport to the membrane.

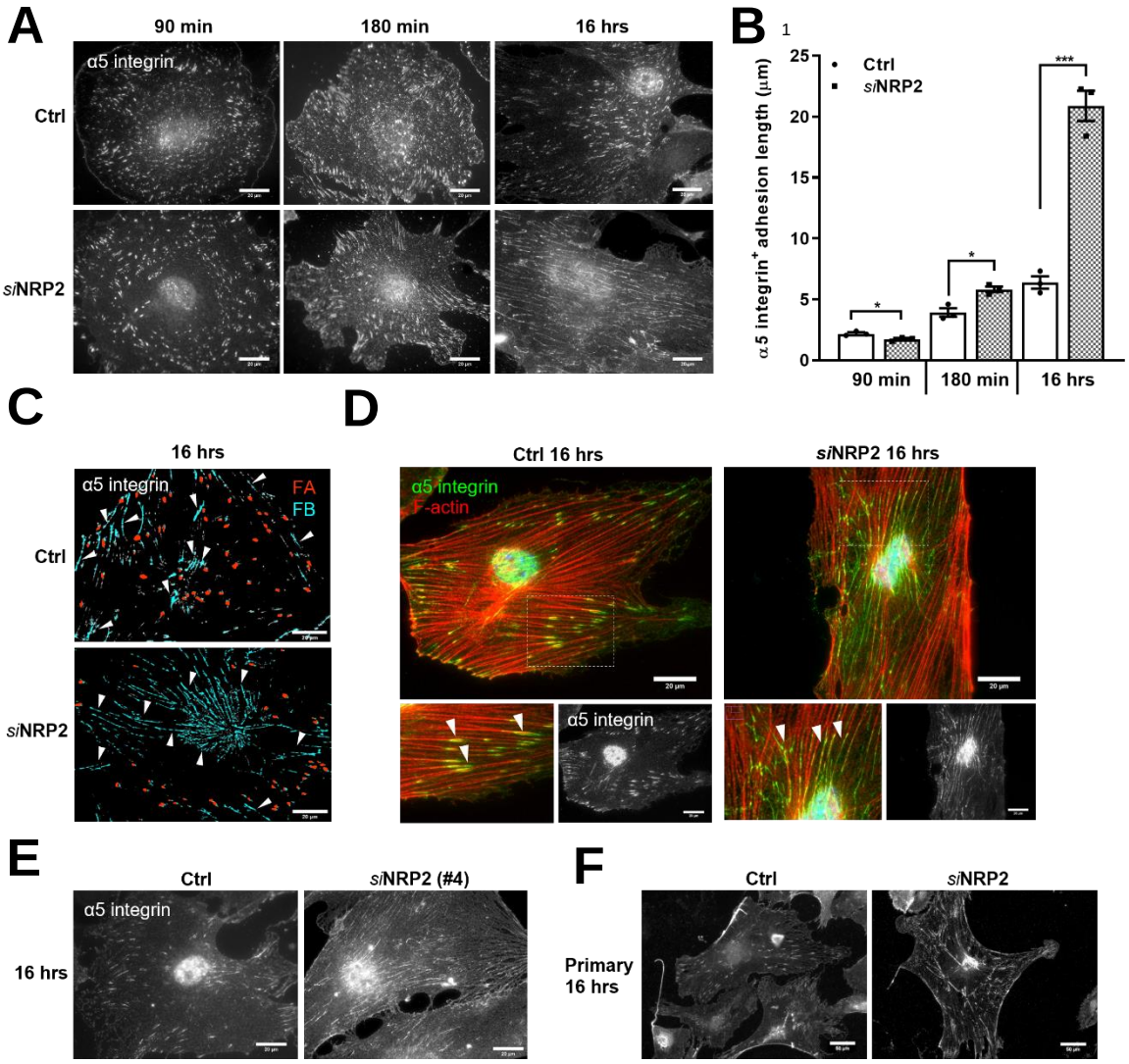

[1]Permission granted by FASEB Journal [230] to re-use figure panels.

Figure 3.23 NRP2 depletion accelerates the development of fibrillar adhesions over time. $1x10^6$ ECs were nucleofected with either Ctrl siRNA or NRP2 siRNA and seeded on 10 cm dishes pre-coated with 10 µg/ml FN at 37°C in a CO_2 incubator for 48 hours. ECs were then re-seeded onto acid-washed, oven sterilised coverslips pre-coated with 10 µg/ml FN and incubated for either 90 minutes, 180 minutes or 16 hours. Coverslips were fixed in 4% PFA, blocked and permeabilised. ECs were then incubated with anti-α5 integrin primary antibody overnight at 4°C. Following two washes to remove any unreacted primary antibody, ECs were incubated with donkey anti-rabbit Alexa 488 secondary antibody at RT for 1 hour. Coverslips were mounted with Prolong Gold. Scale bars show 20 µm. **A**) Representative images of each condition at each timepoint. **B**) Mean length of α5 integrin adhesions (µm), error bars show mean ± SEM; N=3 (n≥150 adhesions/timepoint/condition); *=P>0.05, ***=P>0.0002, unpaired students t-test (two-tailed). **C**) Representative images of fixed Ctrl and NRP2 siRNA treated ECs manually labelled to show differences in the distribution of focal adhesions (0.2-6 μm^2) (orange) and fibrillar adhesions (>6 μm^2) (blue). **D**) siRNA-transfected ECs were prepared as described in **A**) with the exception that ECs were subsequently incubated with phalloidin-568 at RT for 1 hour during secondary antibody incubation. Arrows show colocalisation, scale bars show 20 µm. **E**) siRNA-transfected ECs were prepared as described in **A**); however, ECs were transfected with either with Ctrl siRNA or NRP2 siRNA (#04). **F**) Lungs from 10 WT C57 mice were digested in 0.1% collagenase solution for 1 hour at 37°C before being passed through a 19G needle 3 times, and subsequently a 21G needle into a 70 µm strainer. The resulting solution was then centrifuged, and the pellet resuspended in fresh media, before being seeded into 2x T75 pre-coated with 0.1% gelatin, 10 µg/ml FN and 10 µg/ml collagen type 1 and incubated at 37°C overnight. Two successive primary EC sorts were then performed using rat primary antibody against endomucin and anti-rat IgC coated magnetic Dynabeads to positively select for ECs. Primary ECs were then transfected with either Ctrl siRNA or NRP2 siRNA and prepared for immunostaining as described in **A**). Scale bars show 50 µm.

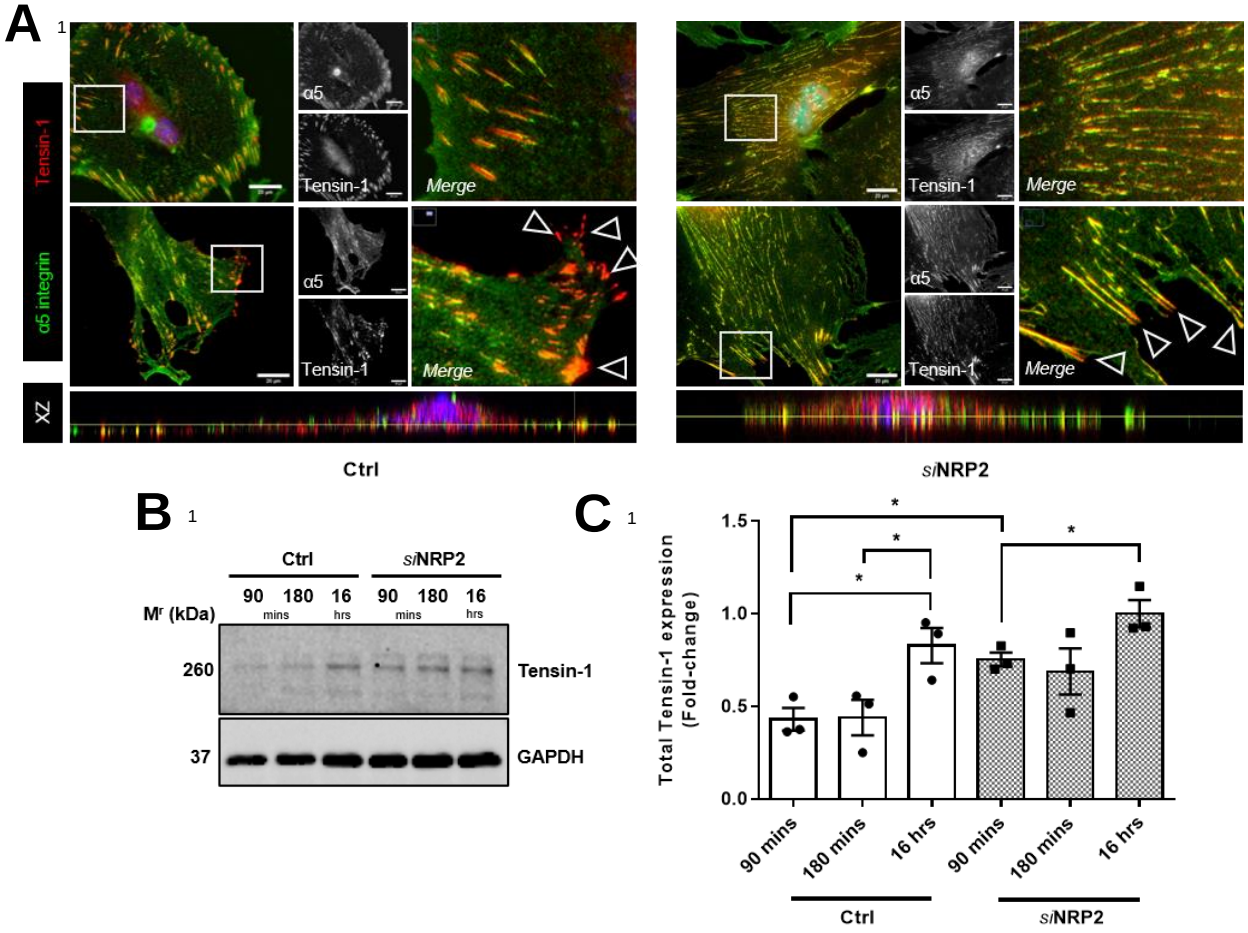

[1]Permission granted by FASEB Journal [230] to re-use figure panels.

Figure 3.24 NRP2 depletion promotes tensin-1 expression early during initial adhesion to FN. 1x10^6 ECs were nucleofected with either Ctrl siRNA or NRP2 siRNA and seeded on 10 cm dishes pre-coated with 10 µg/ml FN at 37°C in a CO_2 incubator for 48 hours. ECs were then re-seeded at a low density onto acid-washed, oven sterilised coverslips pre-coated with 10 µg/ml FN and incubated for 16 hours. Coverslips were fixed in 4% PFA, blocked and permeabilised. ECs were then incubated with anti-α5 integrin and anti-tensin-1 primary antibodies overnight at 4°C. Following two washes to remove any unreacted primary antibody, ECs were incubated with donkey anti-rat Alexa 488 and donkey anti-rabbit Alexa 555 secondary antibodies at RT for 1 hour. Coverslips were mounted with Prolong Gold. Arrows show colocalisation, scale bars show 20 µm. **A**) Representative images of Ctrl and NRP2 siRNA treated ECs showing colocalisation between tensin-1 and α5 integrin either in punctate FAs or within fibrillar adhesions. Bottom panels show confocal XZ plane images showing α5 integrin colocalisation with tensin-1 in Ctrl and NRP2 siRNA-treated ECs adhered to FN for 16 hours. **B**) siRNA-transfected ECs were seeded onto 6 cm dishes pre-coated with 10 µg/ml FN and incubated for either 90 minutes, 180 minutes or 16 hours at 37°C. ECs were lysed in ESB and subjected to the DC protein assay before being analysed by Western blotting using primary antibodies against tensin-1. GAPDH was used as a loading control. Representative Western blot image. **C**) Quantification of tensin-1 expression measured by densitometric analysis. Bands were quantified using ImageJ™. Error bar shows mean ± SEM; N=3; *=P<0.05, unpaired students t-test (two-tailed with multiple comparisons).

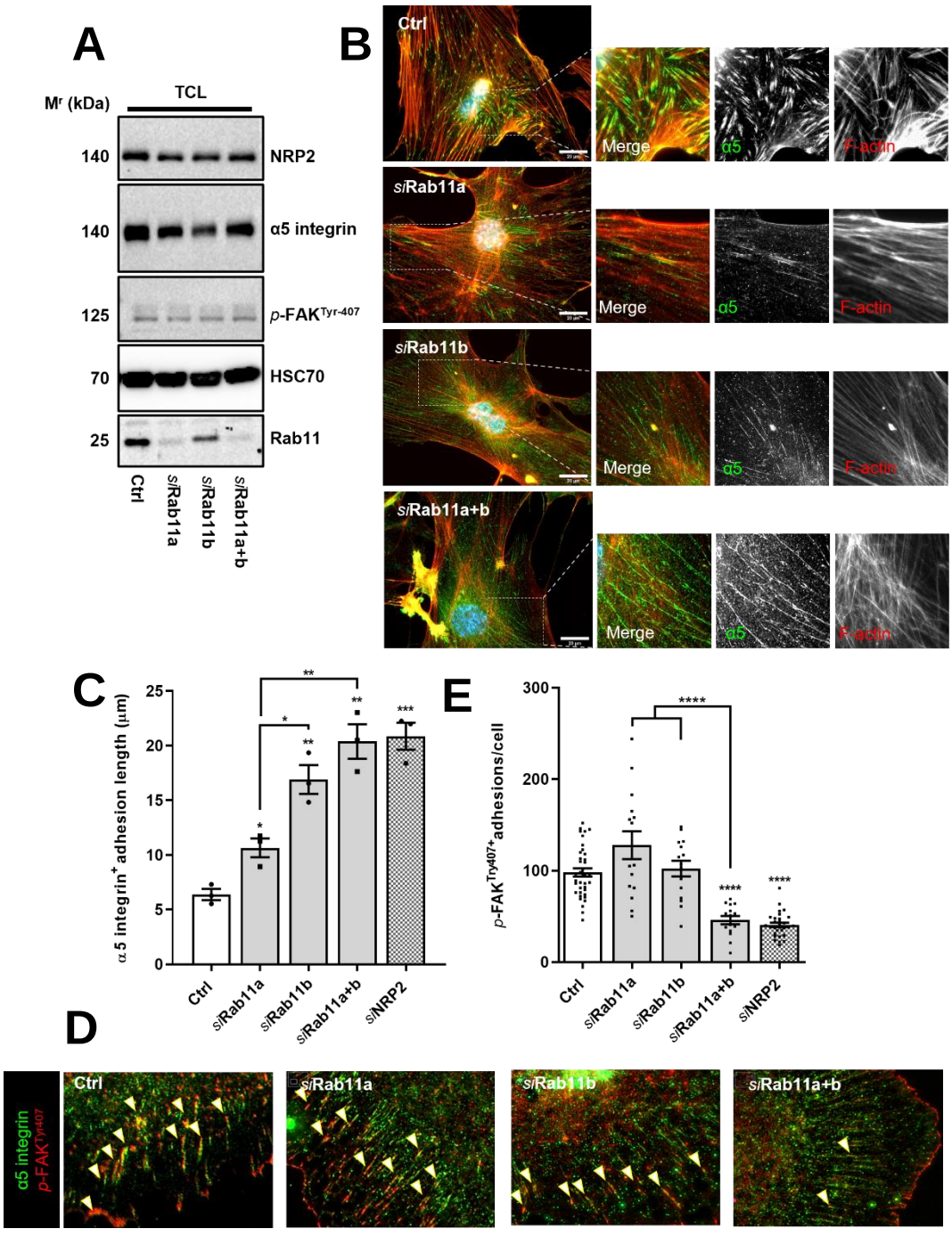
A
Mr (kDa)
TCL
140
NRP2
140
α5 integrin
125
p-FAKTyr-407
70
HSC70
25
Rab11
Ctrl
siRab11a
siRab11b
siRab11a+b
B
Ctrl
Merge
α5
F-actin
siRab11a
siRab11b
siRab11a+b
C
α5 integrin+ adhesion length (μm)
siNRP2
D
α5 integrin
p-FAKTyr407
E
p-FAKTry407+ adhesions/cell

Figure 3.25 NRP2 mediates α5 integrin recycling via both Rab11a and Rab11b. A) $1x10^6$ ECs were nucleofected with either Ctrl siRNA, Rab11a, Rab11b or Rab11a and Rab11b siRNA, and seeded on 10 cm dishes pre-coated with fibronectin for 48 hours at 37°C in a CO_2 incubator. ECs were lysed in ESB and subjected to the DC protein assay before being analysed by Western blotting to confirm depletion of Rab11. HSC70 was used as a loading control. NRP2, α5 integrin and p-FAK^{Tyr407} expression is also shown for completeness. **B**) $1x10^6$ ECs were nucleofected with either Ctrl siRNA or Rab11 a, b, or a+b siRNA and seeded on 10 cm dishes pre-coated with 10 µg/ml FN at 37°C in a CO_2 incubator for 48 hours. ECs were then re-seeded at a low density onto acid-washed, oven sterilised coverslips pre-coated with 10 µg/ml FN and incubated for 16 hours. Coverslips were fixed in 4% PFA, blocked and permeabilised. ECs were then incubated with anti-α5 integrin primary antibody overnight at 4°C. Following two washes to remove any unreacted primary antibody, ECs were incubated with donkey anti-rat Alexa 488 and phalloidin-568 at RT for 1 hour. Coverslips were mounted with Prolong Gold. Scale bars show 20 µm. Panels show representative images of Ctrl and siRab11 treated ECs showing localisation of α5 integrin either in punctate FAs (Ctrl) or within fibrillar adhesions (siRab11). **C**) Mean length of α5 integrin adhesions (µm) observed in siRNA-treated ECs allowed to adhere for 16 hours on FN. *si*NRP2 bar shown for comparison purposes. Error bars show mean ± SEM; N=3 (n≥120 adhesions/group); *=P>0.05, **=P>0.002, ***=P>0.0005, unpaired students t-test (two-tailed with multiple comparisons). **D**) ECs were prepared as described in **B**), with the exception that ECs were adhered to FN for 90 minutes, and immuno-stained for both α5 integrin and *p*-FAK^{Tyr407}. Arrows indicate colocalisation. **E**) Mean number of *p*-FAK^{Tyr407} positive α5 integrin adhesions per cell observed following 90 minutes adhesion to FN. *si*NRP2 bar shown for comparison purposes. Error bars show mean ± SEM; n≥15; *=P<0.05, ****=P>0.0001, unpaired students t-test (two-tailed with multiple comparisons).

3.3.6 NRP2 deficiency transiently enables premature fibronectin secretion and matrix assembly

The primary function of fibrillar adhesions is to funnel the necessary actomyosin tension required to unfold and integrate secreted FN dimers into an extracellular fibrillar network. Fibrillar adhesion formation is therefore commonly associated with a reduced motility and an increased contractility as cells anchor themselves to the enriched matrix layer [152], [155], [272]. Since an extended period of NRP2 depletion was found to accelerate the transition to fibrillar adhesions in our ECs, we asked whether this would also influence the polymerisation and incorporation of secreted FN into their ECM.

To answer this question, we first immunolabelled siRNA-treated ECs fixed at 16 hours with α5 integrin and extra domain-A (EDA)-containing cellular FN (EDA FN), a spliced isoform of endothelial FN which has previously been employed to examine cell secreted FN specifically [155], [272]. Confocal microscopy revealed that NRP2 silencing significantly increased EDA-FN secretion from the cell body and from the medial ends of fibrillar adhesions (**Figure 3.26A-B**). To ratify this, we subsequently assessed the relative quantity of EDA-FN in lysates collected from both Ctrl and NRP2 siRNA treated ECs biochemically by employing the deoxycholate fractionation assay as described previously [155], [272], and found that NRP2 depleted ECs exhibited significantly increased levels of both soluble and insoluble polymerised EDA-FN at this 16 hour timepoint (**Figure 3.26A, C-D**). (For the purpose of clarification, 'soluble' EDA-FN can be described as FN dimers that have been secreted but have not yet been incorporated into an insoluble matrix, compared to 'insoluble' EDA-FN, which describes FN that has been both secreted and subsequently incorporated). Taken together, these data indicate that the initial impairment in α5 integrin trafficking and FA turnover rate elicited by loss of NRP2 compels FAs to develop early into mature fibrillar adhesions. This is then accompanied by a concomitant surge in FN fibrillogenesis. Since NRP2 siRNA treated ECs exhibited increased levels of both soluble and insoluble EDA-FN equally, we can also infer that NRP2 knockdown does not impair the ability for secreted soluble FN to be incorporated into the insoluble fibrillar ECM. No differences in fibrillar α5 integrin and EDA-FN secretion between Ctrl and NRP2 depleted ECs were observed following an adhesion period of 48 hours however, suggesting that any aberrations elicited by NRP2 silencing becomes compensated for by this later timepoint (**Figure 3.26A-D**).

Quantitative analysis of apico-basal mean intensity ratios by confocal XZ sectioning on ECs adhered for 16 hours revealed no differences in the distribution of EDA-FN between Ctrl ECs and ECs

depleted for NRP2, its expression localising to both the basolateral and apical surfaces (**Figure 3.26E-G**).

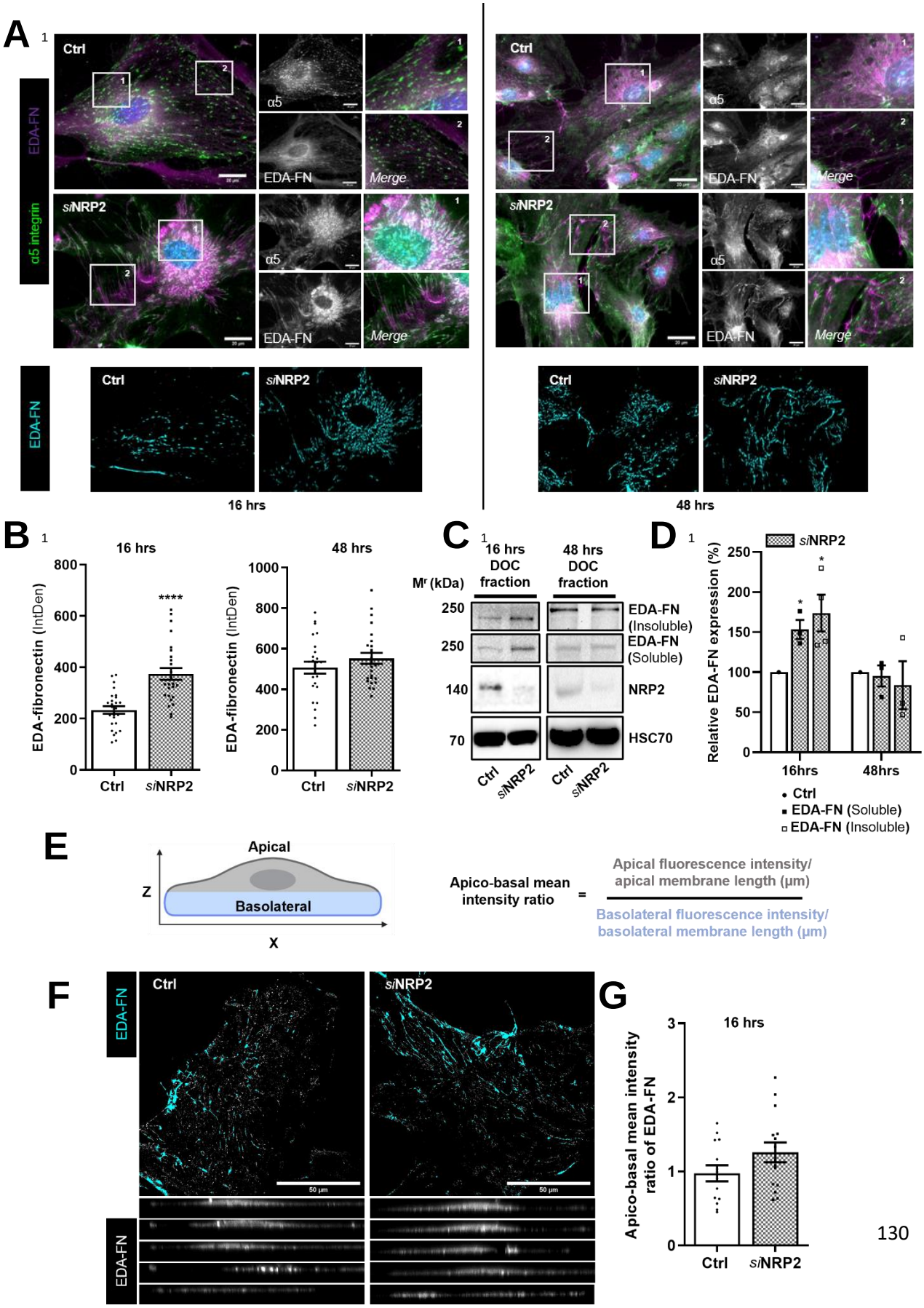

[1]Permission granted by FASEB Journal [230] to re-use figure panels.

Figure 3.26 NRP2 depletion promotes FN fibrillogenesis. 1x10^6 ECs were nucleofected with either Ctrl siRNA or NRP2 siRNA and seeded on 10 cm dishes pre-coated with 10 µg/ml FN at 37°C in a CO_2 incubator for 48 hours. ECs were then trypsinised and re-seeded onto acid-washed, oven sterilised coverslips pre-coated with 10 µg/ml FN and incubated for either 16 hours (left panel) or 48 hours (right panel). Coverslips were fixed in 4% PFA, blocked and permeabilised. ECs were then incubated with anti-α5 integrin and anti-EDA-FN primary antibodies overnight at 4°C. Following two washes to remove any unreacted primary antibody, ECs were incubated with donkey anti-rabbit Alexa 488 and donkey anti-mouse Alexa 555 secondary antibodies at RT for 1 hour. Coverslips were mounted with Prolong Gold. Scale bars show 20 µm. Panels show representative images of each condition at either 16 hours or 48 hours adhesion to FN. **B**) EDA-FN density/cell of each condition at either 16 hours or 48 hours adhesion to FN. Error bars show mean ± SEM; n≥25 ECs/group, ****=P<0.0001, unpaired students t-test (two-tailed). **C**) 3x10^5 ECs were nucleofected with either Ctrl siRNA or NRP2 siRNA and seeded into 6-well plates pre-coated with 10 µg/ml FN at 37°C in a CO_2 incubator for either 16 hours for 48 hours. ECs were then PBS washed on ice and lysed. Lysates were cleared by centrifugation at 21000*G for 30 minutes at 4 °C, allowing for the isolation of soluble and insoluble fractions. Soluble and insoluble fractions were separated by SDS-PAGE and subjected to Western blot analysis. Membranes were incubated in anti-EDA-FN primary antibody to assess quantities of soluble and insoluble cell secreted FN, anti-NRP2 primary antibody to confirm NRP2 depletion, and anti-HSC70 antibody as a loading control. **D**) % EDA-FN quantified from soluble and insoluble fractions at indicated timepoints. Mean densitometric analysis obtained using ImageJ™. Error bars show mean ± SEM; N≥3; *=P<0.05, unpaired students t-test (two-tailed). **E**) Schematic representation of the quantification of apico-basal mean intensity ratio of surface EDA-FN. **F**) Representative images of EDA-FN localisation in Ctrl and NRP2 siRNA treated ECs. Bottom panels show confocal XZ sections of Ctrl and NRP2 siRNA treated ECs depicting EDA-FN distribution on both apical and basolateral surfaces. **G**) Apico-basal mean intensity ratio of EDA-FN in ECs adhered for 16 hours. Error bars show mean ± SEM; n≥15 ECs/group.

3.3.7 NRP co-depletion severely impairs EC migration by limiting directional traffic of α5 integrin

NRP1, through its cytoplasmic SEA motif, is known to selectively stimulate the rapid internalisation of active α5β1 integrin heterodimers from fibrillar adhesions, before promoting integrin recycling back to assembling nascent adhesions via a Rab5 dependent short-loop pathway [108]. Thus far, we have intimated a novel role for NRP2 in regulating the traffic of α5 integrin-*p*-FAK^{Tyr407} complexes back to assembling adhesions via a Rab11 dependent long-loop pathway. The causative reduction in FA turnover subsequently places the cell into a contractile state, whereby fibrillar adhesion formation and FN fibrillogenesis is promoted. We therefore proceeded to consider the impact of simulating the loss of both NRP receptors simultaneously on α5 integrin transport in ECs. Global knockout *in vivo* studies have previously demonstrated that NRP1/NRP2-null mice exhibit more severe vascular defects than NRP1-null mice, exhibiting a largely avascular phenotype resembling VEGF and VEGFR-2 knockout models [114]. Despite this, no in depth *in vitro*-based investigations have described the behaviour of NRP1/NRP2 depleted ECs in culture.

To examine this, we employed siRNA-mediated depletion of NRP2 in NRP1$^{fl/fl}$ Cre-negative and Cre-positive isolated ECs to artificially generate lines depleted for either NRP individually or in combination. First we examined the distribution of endogenous α5 integrin in fixed ECs adhered to FN for 16 hours. NRP1 depletion resulted in a high density of fibrillar α5 integrin, similar to that which was observed in *si*NRP2 ECs, rather than α5 integrin appearing in peripheral punctae as in Ctrl ECs. This suggests that, in a similar manner to when NRP2 is depleted, the rate of FA maturation is also augmented when NRP1 is lost. In ECs depleted for both NRP1 and NRP2 however, α5 integrin was found to become localised to the membranous edge; we observed minimal α5 integrin staining within adhesive structures, either fibrillar or punctate.

Further staining in non-permeabilised ECs to visualise surface α5 integrin only, revealed that transport to dynamic cell protrusions was lost following the co-depletion of both NRP1 and NRP2. Rather, α5 integrin appeared to arrest in and around the cell body, failing to track to cell protrusions. Upon further inspection, only in our Ctrl ECs did α5 integrin appear in mature adhesion structures at dynamic cell edges. In contrast, whilst α5 integrin successfully localised to cell protrusions in ECs depleted for either NRP1 or NRP2, it did so within small singular vesicular structures rather than mature adhesions. (**Figure 3.27A-B**).

To substantiate these findings, we biochemically measured the relative expression of α5 integrin present at the cell surface in each of our EC lines by biotin-labelling. To our surprise, surface

expression of α5 integrin in ECs depleted for both NRP1 and NRP2 remained unchanged compared to Ctrl ECs (**Figure 3.27C-D**). It is possible here that in the absence of both NRPs, α5 integrin is neither endocytosed, nor recycled, and therefore despite its surface level expression remaining intact, its directional transport to and from assembling adhesion sites at cell protrusions is lost. In comparison, surface expression of α5 integrin was significantly elevated following individual depletion of either NRP (**Figure 3.27C-D**). If NRP2 does indeed promote α5 integrin internalisation via its modulatory role over dyn-2, as NRP1 does so via GIPC-1, this elevated surface α5 integrin expression can be attributed to an impaired rate of endocytosis. Alternatively, the elevation in α5 integrin surface expression may simply correlate with the concomitant increase in fibrillar adhesion development in ECs depleted for either NRP1 or NRP2. Further studies assessing the migration rate of ECs co-depleted for both NRPs revealed a dramatic reduction in migratory capacity over FN compared to both our Ctrl ECs and ECs depleted for either NRP individually (**Figure 3.27E**).

Taken together, these data indicate that whilst the loss of NRP2 disrupts total α5 integrin recycling back to the membrane, the involvement of NRP1 is sufficient to maintain the transport of an active α5 integrin pool to and from the leading edge of the cell. Similarly, if NRP1 is lost, NRP2 preserves a degree of α5 integrin traffic. Importantly however, the individual actions of either NRP are insufficient to preserve a WT-level of α5 integrin traffic. Without an antibody to detect mouse active α5β1 integrin in our murine cells however, we cannot comment further on whether NRP2 regulates inactive or active integrin pools within the cell. Finally, if both NRP1 and NRP2 are lost in combination, transport of α5 integrin to dynamic cell projections is ablated, severely impairing migration over FN. These data support evidence that both NRPs are major angiogenic players, functioning not only as co-receptors but also to regulate efficient trafficking of integrin receptors to promote cellular migration.

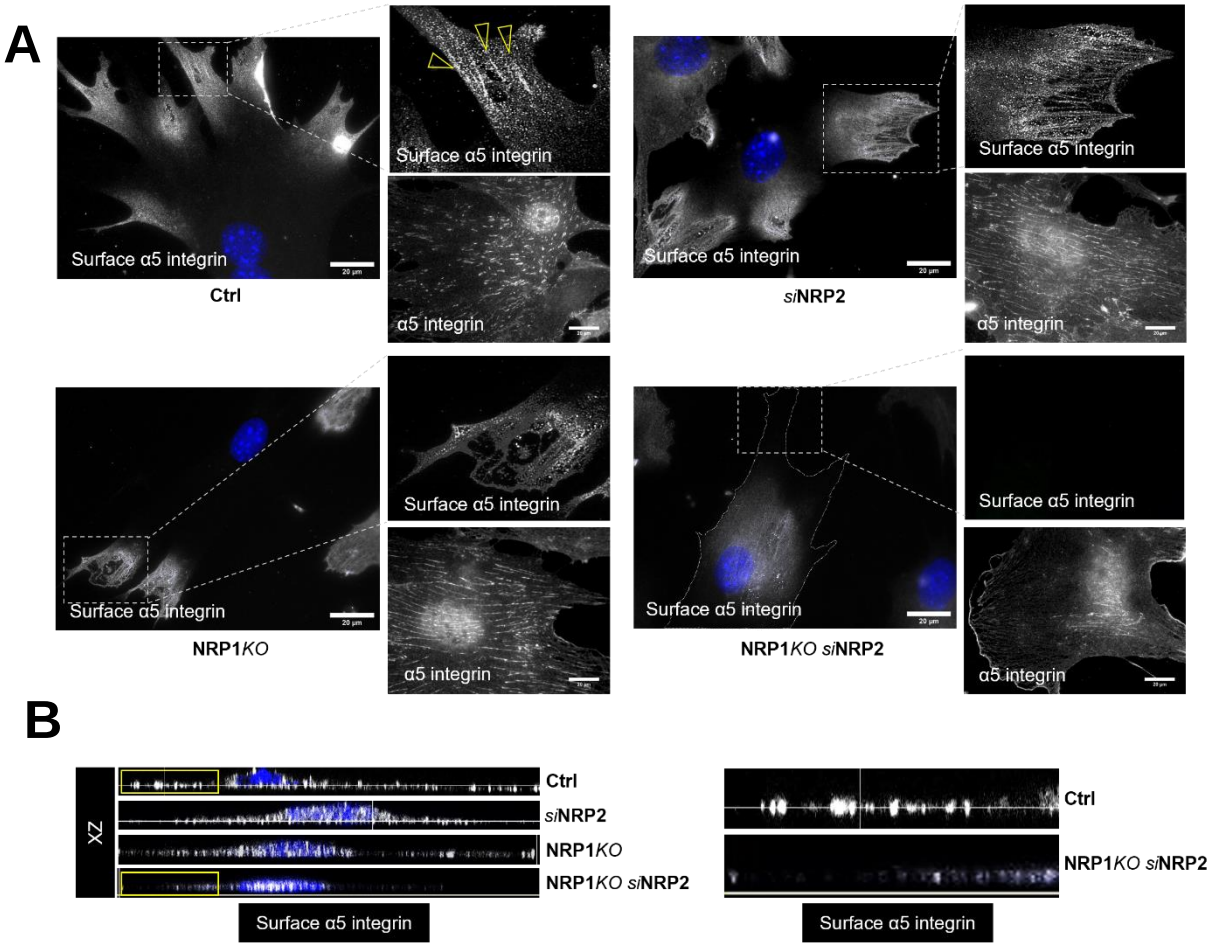
A
Surface α5 integrin
α5 integrin
Ctrl
siNRP2
NRP1KO
NRP1KO siNRP2
B
XZ
Ctrl
siNRP2
NRP1KO
NRP1KO siNRP2
Surface α5 integrin
C
IP: Biotin
MESNA:
Mr (kDa)
140
Surface α5 integrin
TCL
α5 integrin
NRP2
37
GAPDH
Ctrl
siNRP2
NRP1KO
NRP1KO siNRP2
D
Relative surface α5 integrin expression
2.0
1.5
1.0
0.5
0.0
E
Random migration speed (microns/sec)
0.015
0.010
0.005
0.000

Figure 3.27 NRP co-depletion severely impairs EC migration by limiting directional traffic of α5 integrin. A) NRP1 Cre negative and positive ECs were nucleofected with either Ctrl siRNA or NRP2 siRNA and seeded on 10 cm dishes pre-coated with 10 μg/ml FN at 37°C in a CO2 incubator for 24 hours. ECs were then re-seeded at a low density onto acid-washed, oven sterilised coverslips pre-coated with 10 μg/ml FN and incubated for 16 hours. Coverslips were fixed in 4% PFA and either blocked and permeabilised or blocked only. ECs were then incubated with anti-α5 integrin primary antibody overnight at 4°C. Following two washes to remove any unreacted primary antibody, ECs were incubated with donkey anti-rabbit Alexa 488 secondary antibody at RT for 1 hour. Coverslips were mounted with Prolong Gold with DAPI. Scale bars show 20 μm. Panels show representative images of each condition. Arrows point to mature surface adhesions. **B**) Left panels show confocal XZ plane images of surface α5 integrin in Ctrl, *si*NRP2, NRP1*KO* and NRP1*KO si*NRP2 ECs adhered to FN for 16 hours. Right panels show highlighted regions of Ctrl and NRP1*KO si*NRP2 XZ plane images. **C**) NRP1 Cre negative and positive ECs were transfected with either Ctrl or NRP2 siRNA and seeded onto 10 cm dishes pre-coated with 10 μg/ml FN and incubated for 48 hours at 37°C. ECs were subsequently starved in serum-free media, before being placed on ice. EC cell surface proteins were labelled with 0.3 mg/ml biotin. Any unreacted biotin was subsequently quenched with 100 mM glycine. ECs were then either lysed or incubated with 100 mM MESNA to strip off any biotin-labelled surface proteins for use as a negative control sample. Following incubation, any excess MESNA was quenched using 100 mM iodoacetamide. EC lysates were immunoprecipitated with Dynabeads® coupled to an anti-biotin antibody overnight at 4°C. Immunoprecipitated biotin-labelled proteins were separated by SDS-PAGE and subjected to Western blot analysis. Western blot shows α5 integrin surface levels, successful stripping by MESNA, and confirmation of NRP2 silencing. **D**) Mean densitometric analysis obtained using ImageJ™ measuring α5 integrin surface levels. Error bars show mean ± SEM; N=2/4; *=P<0.05, unpaired students t-test (two-tailed). **E**) $1x10^6$ NRP1 Cre negative and positive ECs were nucleofected with either Ctrl siRNA or NRP2 siRNA and seeded on 10 cm dishes pre-coated with 10 μg/ml FN at 37°C in a CO_2 incubator for 24 hours. ECs were then re-seeded onto 10 μg/ml FN, and incubated for 180 minutes at 37°C to allow ECs to adhere. EC migration was captured by timelapse microscopy: fixed images of multiple field/well of each condition were taken every 20 minutes for 16 hours at 37°C and 5% CO_2 using an inverted Axiovert (Zeiss) microscope in one phase contrast. Individual cell migration was manually tracked using the ImageJ™ MTrackJ plugin. Left panel shows quantification of random migration speed of individual cells was calculated in μm/sec. Error bars show mean ± SEM; N=3 (n≥60); *=P<0.05, **=P<0.002, **=P<0.0005, unpaired students t-test (two-tailed with multiple comparisons). Right panel shows Ctrl and NRP1*KO si*NRP2 phase contrast images.

3.3.8 Discussion

Accumulating evidence supports a model whereby integrins and their respective ligands display a high traffic-dependent turnover within adhesion sites [155]. Small GTPases Rab5 and Rab21 are known to control the early endocytosis of β1 integrin heterodimers, following which they are principally recycled within $Rab11^{+}$ vesicles back to the cell surface from the PNRC [108], [155], [178], [181]. In this chapter we describe a novel role for NRP2 in directly regulating the Rab11-dependent recycling of α5 integrin-*p*-FAK^{Tyr407} complexes back to nascent adhesions. Considered alongside our findings outlined in chapter 3.2, it is likely that NRP2 is capable of potentiating FAK-induced signalling cascades by regulating the pool of available α5β1 integrin capable of binding the FN matrix. In support of this hypothesis, it has been elucidated that endocytosing α5 integrin is preserved in an active, unliganded conformation with active FAK, before undergoing Rab11-mediated recycling. As a result, more efficient integrin engagement-mediated reassembly of polarised FAs can occur to promote directional migration [165]. As the colocalisation between *p*-FAK^{Tyr407} and α5 integrin within $Rab11^{+}$ vesicles was lost in *si*NRP2 ECs, we can infer that NRP2 is involved in maintaining the interactions between active FAK and α5 integrin during Rab11-driven "long-loop" vesicular transport.

Valdembri *et al*., have previously described a mechanism whereby NRP1 mediates the transport of active α5β1 integrin along the actin cytoskeleton from disassembling FAs, and its subsequent Rab5-dependent recycling back to nascent adhesions at the leading cell edge [108]. We therefore believe that both NRPs differentially regulate the subcellular traffic of α5β1 integrin. Unfortunately, we are limited to commenting on the effects of NRP2 depletion on total subunit trafficking, as there is no commercially available antibody to detect mouse active α5β1 integrin. Whilst this highlights a caveat to these studies, it is pertinent to note that we do not rule out the possibility that NRP2 also regulates active α5β1 internalisation (and recycling) in our murine cells. For example, previous members of our laboratory have demonstrated that the rate of FA disassembly is sensitive to the loss of NRP2 [225]. In addition, both clathrin and caveolin, key mediators of integrin endocytosis [259], were observed to co-immunoprecipitate with NRP2, and dyn-2 targeting to α5 integrin adhesions was impaired following NRP2 depletion. In further support of this, Valdembri *et al*., revealed that loss of endothelial NRP1 only impaired active α5β1 integrin internalisation and not total α5β1 internalisation in HUVECs, postulating that inactive and active integrin pools are trafficked separately [108]. Arjonen *et al*., subsequently established this to be the case in cancer cells, examining the endocytic trafficking of active and inactive β1 integrins. Whilst both were endocytosed in a clathrin-dependent manner, the net rate of internalisation for active β1 integrin

was found to be greater. The far slower rate of inactive β1 endocytosis is instead compensated for by rapid actin-dependent recycling through Rab4$^+$ vesicles. Owing to these distinct trafficking routes, active and inactive receptor pools were observed to exhibit divergent subcellular localisation, active β1 integrin predominantly localising intracellularly, whilst inactive β1 integrin localising to the cell surface membrane at dynamic cell protrusions [273].

Contrary to our predictions, protracted siRNA-mediated depletion of NRP2 accelerated the centripetal translocation of α5 integrin into large tensin-1$^+$ fibrillar adhesions. One explanation behind this may be that such fibrillar adhesions arise as an artefact of aberrations in FA turnover rate, during which FAs are forced to mature prematurely rather than be dynamically endocytosed and subsequently recycled. To confirm this model, we proceeded to examine the effect of NRP2 silencing on the assembly and exocytosis of fibrillar FN, whose secretion relies on the actomyosin tension accrued from α5β1 integrin translocation into fibrillar adhesions and is essential for vessel outgrowth and stabilisation [152], [155]. It was unsurprising therefore that contemporaneous to the accelerated development of fibrillar adhesions in our NRP2 depleted ECs fixed at 16 hours, we observed a corresponding surge in secreted EDA-FN originating from α5 integrin containing fibrillar adhesions. In support of these findings, Mana *et al*., demonstrated that Rab11-mediated recycling of active α5β1 integrin orchestrates the cyclic renewal of polarised FN fibrils being secreted from the basolateral surface of ECs to renew the fibrillar ECM, a process vital for vascular remodelling *in vivo*. These studies however proceeded to reveal that while Ctrl and Rab11a siRNA-treated ECs polymerised EDA-FN into insoluble fibrils, *si*Rab11b ECs instead accumulated both FN and active α5β1 integrin within their perinuclear compartments. Rab11b silencing was subsequently shown to preferentially impair the basolaterally polarised secretion and incorporation of cell-secreted FN [155]. These results directly contradict those we present in this report, whereby the silencing of Rab11b, re-capitulating the effects imposed by silencing NRP2, promoted fibrillar adhesion development and therefore likely EDA-FN polymerisation. Indeed, numerous studies have demonstrated that FN fibrillogenesis requires both the internalisation and recycling of active α5β1 integrin. To this end, Valdembri *et al*., demonstrated that the depletion of NRP1, known to disrupt active α5β1 integrin traffic in ECs, impaired their ability to incorporate soluble FN into a dense fibrillar network [108]. Further evidence for this was provided by Sundararaman *et al*., who revealed that the silencing of the small GTPase RhoJ, a major carrier of active α5β1 integrin to the TGN46$^+$ recycling compartment, was shown to suppress both α5β1 internalisation and FN fibrillogenesis [272]. It is possible here that the hypotheses drawn from our data apply exclusively to mouse microvascular ECs. Alternatively, we can speculate that during initial nascent adhesion

assembly, NRP2 promotes the recycling of active α5 integrin, complexed with *p*-FAK^{Tyr407} via both Rab11a and Rab11b. This can be evidenced from the fact we only observed significantly fewer *p*-FAK^{+} α5 integrin adhesions upon co-depletion of both Rab11 isoforms. As FAs mature however, NRP2's role promoting α5 integrin recycling is superseded by its ability to actively inhibit active α5 integrin translocation into fibrillar adhesions. It is also possible that the accelerated transition from mature FAs to fibrillar adhesions, concomitant with an increase in basolateral FN secretion, arises purely as an artefact of the reduced rate of FA turnover elicited by NRP2 silencing. Regardless, it appears that a major role of NRP2 is to promote EC motility through mediating dynamic α5 integrin traffic. When considered alongside other knockout studies, this hypothesis also supports a growing field of evidence in multiple cell types that NRP2 deficiency can promote cell contractility and sedentariness [274].

Though via distinct mechanisms, it is evident that both NRP1 and NRP2 regulate α5 integrin transport in ECs. In addition, both NRPs have been shown to promote EC adhesion to FN through their interactions with both Rac1 and FAK [101], [108], [225], [244]. To examine whether the expression of at least one NRP receptor is required to sustain a level of α5 integrin traffic, both from disassembling FAs and to assembling nascent adhesions, we performed a series of pilot studies in ECs depleted for both NRP1 and NRP2. These revealed that α5 integrin fails to reach cell-surface protrusions, severely impairing the ability for cells to migrate over FN. In contrast, in ECs depleted for either NRP receptor individually, the expression of the remaining NRP receptor was sufficient to direct the transport of α5 integrin to dynamic cell projections. Whilst this reaffirms our hypothesis that NRP1 and NRP2 regulate distinct trafficking pathways, it also suggests that targeting both simultaneously to ablate α5 integrin trafficking in ECs may provide an alternative approach to modulating pathologies defined by enhanced vessel growth.

3.4 Investigating the interplay between NRP1, NRP2 and α5 integrin during pathological and developmental angiogenesis *in vivo*

Unlike NRP2, the contributions of NRP1 during both developmental and pathological angiogenesis have been well documented [93], [95]–[99], [103], [275]. Whilst global depletion of NRP1 causes extensive cardiac abnormalities and diminished vessel sprouting, resulting in embryonic lethality by E14.5 [97], [98], endothelial-specific inducible depletion post embryogenesis has demonstrated its essential role in tip cell selection during postnatal development [102], [103], [244], [276]. NRP1 has also been implicated in contributing to the vascularisation and progression of growing tumours in a number of cancer types, its expression positively correlating with an increased risk of cancer metastasis [277], [278].

α5β1 integrin is also known to be upregulated on neovasculature. However, despite its global depletion conferring an embryonic lethal phenotype, its endothelial-specific depletion was found not to produce any developmental defects during embryogenesis, nor to reduce tumour angiogenesis or growth [184], [207], [279]. Whilst subsequent studies have shown minor reductions in neovascular formation during postnatal development of the retinal superficial vascular plexus, mice are born viable, without any major developmental defects [33], [186].

Like NRP1, the upregulation of NRP2 expression is known to promote tumorigenicity and metastasis in a multitude of cancers, labelling it as a candidate diagnostic or prognostic biomarker and therapeutic target for inhibiting primary tumour growth [280]. Despite this, few investigations have attempted to annotate its endothelial-specific contributions during physiological development. In previous chapters, we elucidated that NRP2, alongside NRP1, acts as a major regulator of α5 integrin dynamics. We had yet to implement our genetically modified animal models to explore the roles of our three receptors *in vivo.* Whilst the angiogenic contributions of NRP1 and α5 integrin have been widely explored, NRP2's role in integrating and disseminating ECM and growth factor signals to coordinate EC responses during angiogenesis was unclear.

In this section, we proceeded to examine the effects of inducing endothelial-specific depletion of NRP2 individually, and in combination with either NRP1 or α5 integrin. Previous work performed in our laboratory has demonstrated that redundancies in the angiogenic cascade often compensate for the loss of a single angiogenic receptor. Only by targeting a combination of angiogenic receptors were these redundancies incapable of restoring deleterious effects over time. In a similar manner,

we hoped to assess whether core angiogenic cascades become sensitised to a combinatory loss of our receptors during developmental and pathological angiogenesis.

By employing multiple experimental mouse breeders for each knockout model, we were aware that a degree of experimental variance may naturally arise however. Whilst we would attempt to minimise this variance by normalising our results against Cre-negative littermate controls for each discrete experiment, we also thought it pertinent to show all subsequent data as 'Super-plots'. By superimposing summary statistics from experimental repeats against all biological replicates, these graphs capably identify experimental reproducibility in addition to biological variance [281]. For example, as shown in **Figure 3.28**, different colours (turquoise, blue, red etc) are used to distinguish between different experimental and biological replicates.

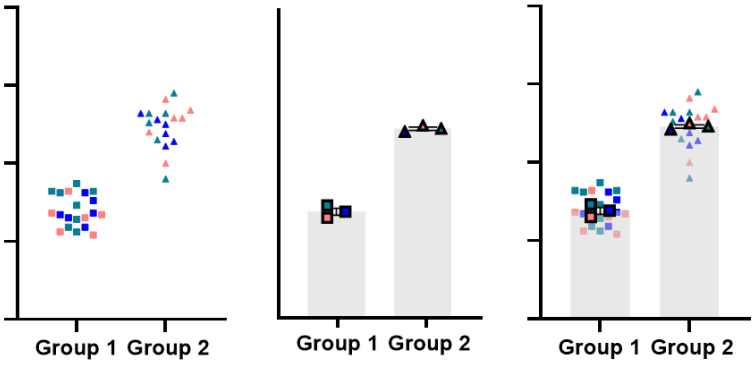

Figure 3.28 Generating Super-plots. Left panel: Individual biological replicates are graphed using different colours to distinguish between experiments. Different shapes are used to define experimental groups. Middle panel: Experimental replicates are graphed separately using corresponding colours and shapes to differentiate between experiments and experimental groups respectively. Right panel: Both graphs are superimposed to produce a 'Super-plot', enabling easier visualisation of experimental reproducibility and biological variance.

3.4.1 Endothelial NRP2 expression drives primary tumour growth by promoting tumour angiogenesis

Angiogenesis is a key hallmark of cancer, for without the ability to form the necessary neovascular network to support the development of a solid tumour, growth cannot occur beyond 1 – 2 mm^3. As a result, the race to identify appropriate anti-angiogenic therapies against a combination of pro-angiogenic targets to ablate neovascular formation specifically has become a major focus in the struggle against cancer [20], [282]. Unlike normal physiological vasculature, which is established via the coordination of numerous strictly regulated cascades, tumours can establish their own blood-supply by several means. In addition to inducing the formation of neovasculature from the pre-existing microvasculature, tumour-derived cells have the ability to grow around an existing vessel to propagate tumour development; this process is mediated by circulating angioblast precursors from the bone marrow [283]. Despite tumour-induced vasculature acting as an effective conduit for the delivery of metabolites, vessels develop abnormally, reflecting the pathological nature of the cancerous growth. For instance, the ultrastructure of tumorigenic microvessels is highly tortuous, many lacking functional overlaying pericytes. As a result, vessels become dilated and develop numerous fenestrae and transcellular holes. The absence of a functional BM also contributes to an exceptionally permeant vascular network [31], [284].

We have shown that NRP2 promotes FAK phosphorylation and recruitment to treadmilling FAs, events that, in a pathological environment, play a crucial role in FA turnover and actin cytoskeletal remodelling to promote cancer cell metastasis [251]. Indeed, upregulations in FAK activity giving rise to aggressive tumour phenotypes has been well substantiated [285]–[288]. Enhanced expression of FAK in tumour angiogenic vessels has also been reported [289]. Similarly, the pathological overexpression of NRP2 is also understood to accelerate tumorigenicity and extravasation in various cancer subtypes, and as such, represents a promising diagnostic or prognostic biomarker and therapeutic target for inhibiting primary tumour growth [280]. Despite this, it remains unclear as to whether endothelial NRP2 promotes tumour vascularisation. To isolate the role of NRP2 during tumour angiogenesis, we performed an endothelial-specific depletion of NRP2 and examined its effect on subcutaneous allograft tumour growth using CMT19T lung carcinoma cells [107]. In a similar manner, we also examined the consequences of depleting NRP2 in combination with α5 integrin or NRP1, both previously implicated in promoting tumour angiogenesis [277], [278], [290]. CMT19T cells were allowed to grow for a period of 18 days in conjunction with thrice weekly injections of tamoxifen, a regimen previously employed by our laboratory, and one that has been confirmed to effectively activate Cre-recombinase to deplete our

targets within the tumour vasculature specifically. In doing so, we aimed to avoid the complications of interpreting NRP2 function using global knockout models. By commencing our tamoxifen regime 4 days prior to tumour cell injection, we hoped to achieve efficient silencing of our target receptors throughout the growth of the tumour, even from the day of implantation (**Figure 3.29A**). Furthermore, by tracking changes in tumour volume from day 10 post implantation using calliper measurements, we were able to observe any temporal limitations to depleting our target receptors in this manner.

Previous unpublished work performed in our laboratory by Dr Robert Johnson has shown that the singular depletion of either α5 integrin or NRP1 from the endothelium does not significantly perturb tumour growth. Only when these pro-angiogenic receptors were lost in combination did CMT19T cell-derived tumours grow significantly smaller than their Cre-negative counterparts. From day 10 post implantation however, we observed tumours grown in mice deficient in endothelial NRP2 to develop significantly smaller compared to those grown in control littermates. A downwards trend in tumour weight was also observed, whilst gross animal weight remained stable throughout the duration of the regime. The dual loss of both NRP2 and α5 integrin also significantly inhibited tumour growth by day 18 to a comparable degree, without affecting animal weight. Inducing endothelial-specific deletion of both NRP1 and NRP2 however, resulted in the most severe perturbation in tumour growth, with tumours grown in Cre-positive animals only developing to approximately 20% the size of tumours grown in Cre-negative littermate control animals (**Figure 3.29B-F**, **Suppl. Figure 5.1, Suppl. Figure 5.2**).

To directly assess the effects of specifically depleting NRP2 individually, or in combination with α5 integrin or NRP1 within the endothelium on tumour angiogenesis, we performed immuno-fluorescence analysis on all tumours harvested from Cre-negative and Cre-positive mice. After confirming endothelial specific depletion of our targets within endomucin-positive blood vessels in Cre-positive tumour sections (**Figure 3.30A-C**), we found that compared to tumours from Cre-negative animals, those deficient in endothelial NRP2 displayed significantly less vasculature (**Figure 3.31**). NRP2 depleted vasculature also exhibited a reduced colocalisation with *p*-FAK^{Tyr407} (**Figure 3.32**). Likewise, tumours deficient in both NRP2 and α5 integrin, or indeed deficient in both NRPs, were significantly less vascularised (**Figure 3.31**), indicating that the supressed tumour growth and reduced tumour angiogenesis we observe in Cre-positive mice likely results from EC-intrinsic defects elicited by the targeted depletion of our angiogenic receptors. Tumours depleted for both NRP1 and NRP2 exhibited significantly less vasculature than tumours depleted for either NRP2 individually, or those depleted for NRP2 and α5 integrin however. Whilst this is somewhat

unsurprising considering their dramatically reduced size, it does confirm that in this model, angiogenesis cannot proceed upon the simultaneous loss of both NRPs within the endothelium. As the endothelial depletion of NRP1 individually was shown not to affect tumour growth significantly, we can also infer from our results that NRP2, and not NRP1, functions in a dominant fashion during tumorigenesis.

To ratify these findings, we performed two subsequent 'intervention' allograft tumour studies in our NRP1/NRP2 floxed animals only. In these studies, we delayed tamoxifen administration until 7 days after implantation of either CMT19T cells (**Figure 3.33A**) or luminal B PyMT-BO1 breast cancer cells [291] (**Figure 3.33F**). By doing so, we aimed to provide a far more clinically relevant study design during which tumour growth is targeted only after the cancer has become vascularised. Following this regimen, we observed a comparably severe impediment to tumour growth (**Figure 3.33A-D, F-I**) and tumour angiogenesis (**Figure 3.33E, J**) following the combinatory loss of both endothelial NRP1 and NRP2 in both cancer models.

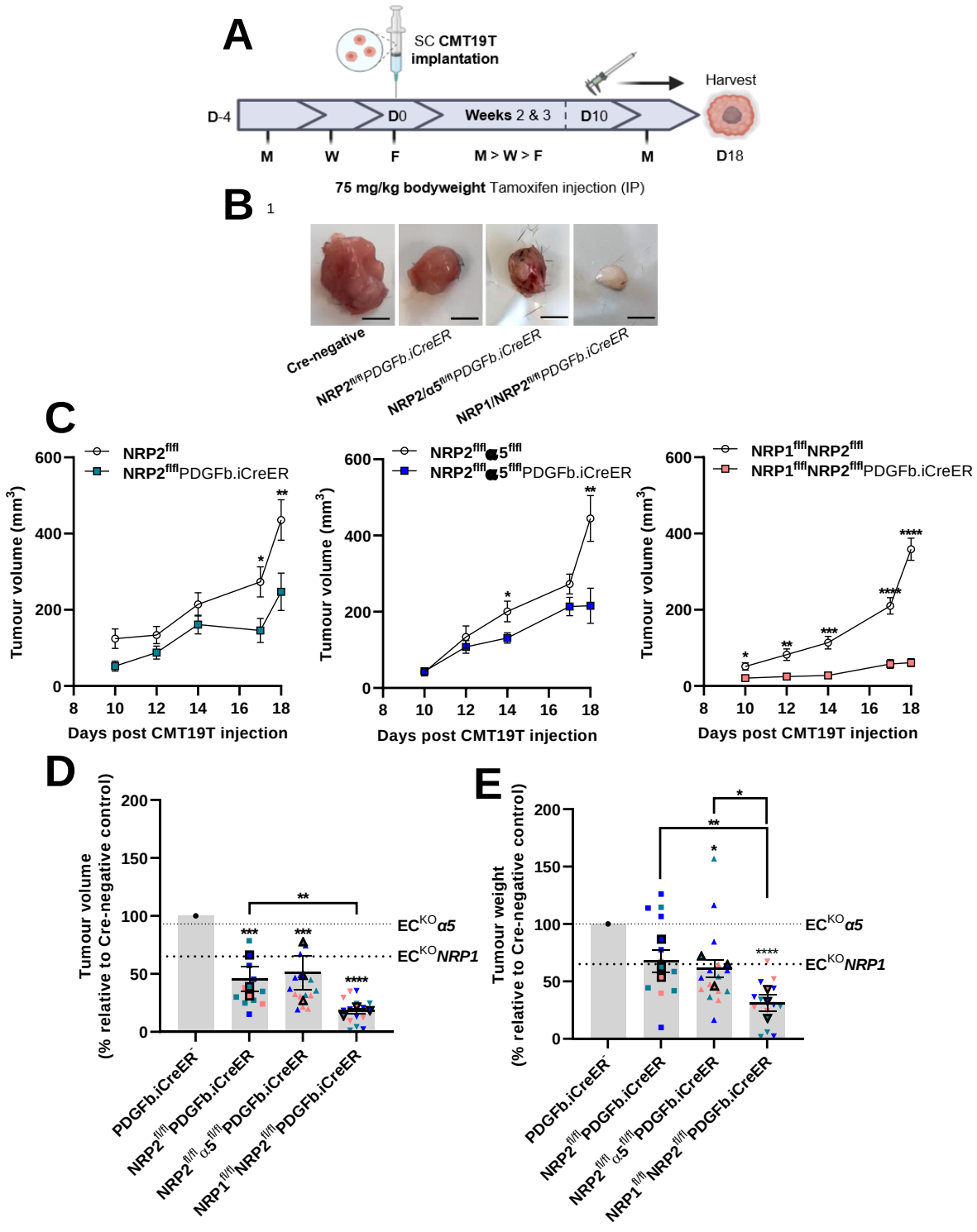

[1]Permission granted by FASEB Journal [230] to re-use figure panels.

Figure 3.29 Deletion of endothelial NRP2 impairs tumour angiogenesis. Inducible, endothelial specific deletion of NRP2, either individually, or in combination with α5 integrin or NRP1, was achieved by crossing mice expressing the PDGFb.iCreER promoter of Cre-recombinase to those floxed for NRP2, NRP2/ α5 integrin, or NRP1/NRP2. **A**) Experimental schematic: tamoxifen-induced activation of Cre-recombinase and thus deletion of our targets was employed via the following regime in order to study its role during tumorigenesis. Cre-positive and Cre-negative littermate control mice received intraperitoneal (IP) injections of tamoxifen (75 mg/kg bodyweight, 2mg/ml stock) thrice weekly (Monday, Wednesday, Friday) for the duration of the experiment from D-4 to D17 to induce Cre-recombinase activity. CMT19T lung carcinoma cells ($1x10^6$) were implanted subcutaneously (SC) into the flank of mice at D0 and allowed to grow until D18. **B**) Representative images of CMT19T tumours harvested on D18 removed from Cre-negative and positive mice. Scale bar shows 5 mm. **C**) Raw tumour volume kinetics (mm^3) measured from tumour bearing mice measured between D10 and D18 post CMT19T injection. Tumour volume calculated using the formula: length x $width^2$ x 0.52. Error bars show mean ± SEM; N=3 (n≥12), *=P<0.05, **=P<0.002, ***=P<0.0005, ****=P<0.0001, unpaired students t-test (two-tailed). **D**) Quantification of tumour volume measured on D18. Data presented as percentages of the average tumour volume observed in respective littermate controls. Error bars show mean ± SEM; N=3 (n≥12), **=P<0.002, ***=P<0.0005, ****=P<0.0001, unpaired students t-test (two-tailed)/ one-way ANOVA. **E**) Quantification of tumour weight (g) measured on D18. Data presented as percentages of the average tumour weight (g) observed in respective littermate controls. Error bars show mean ± SEM; N=3 (n≥12), *=P<0.05 **=P<0.002, ****=P<0.0001, unpaired students t-test (two-tailed)/ one-way ANOVA. Data from $NRP1^{flfl}$PDGFb.iCreER and $\alpha5^{flfl}$PDGFb.iCreER mice, collected by Dr Robert Johnson prior to commencing this thesis, is also shown when applicable as horizonal dashed lines, for comparison purposes only.

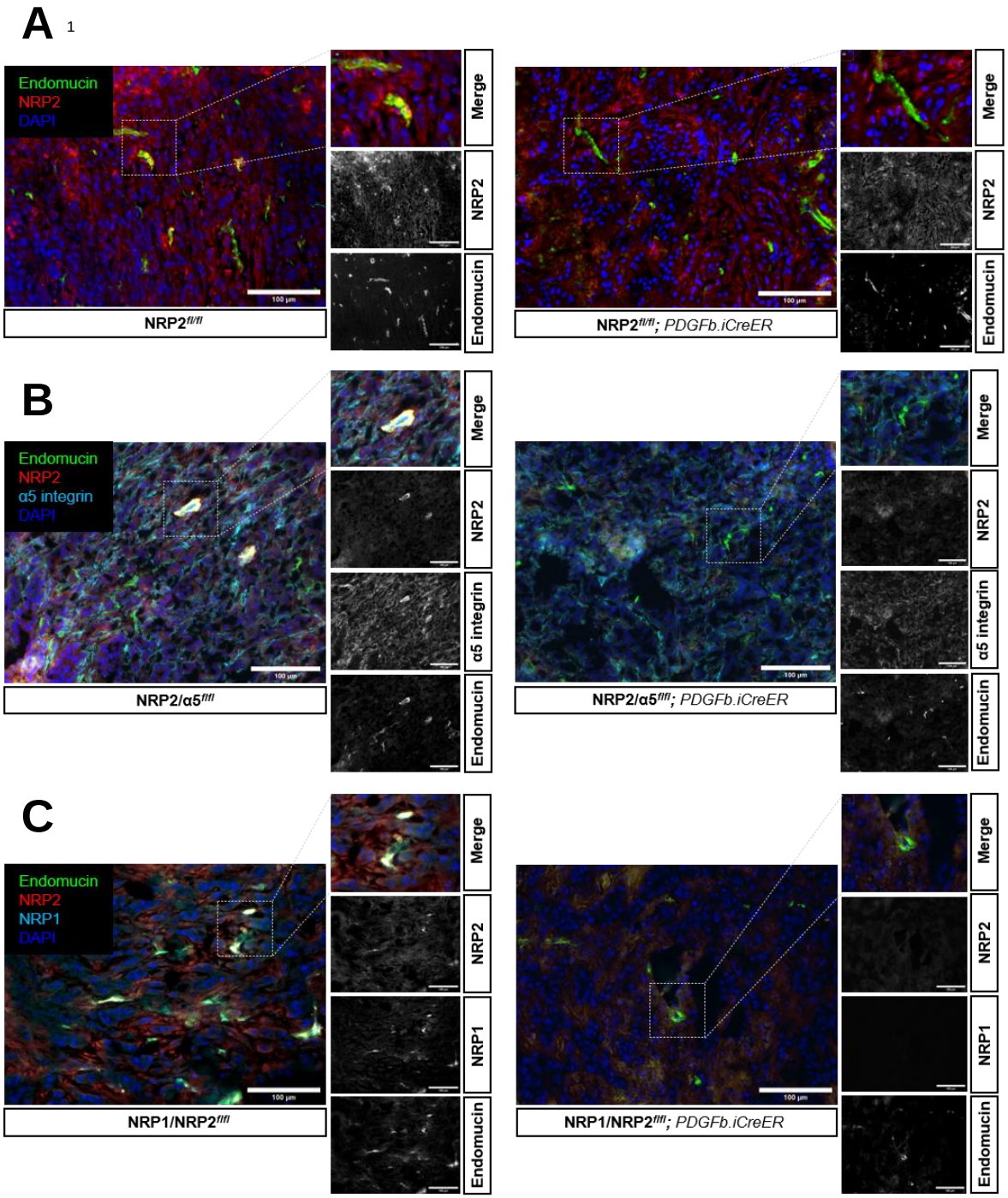

[1]Permission granted by FASEB Journal [230] to re-use figure panels.

Figure 3.30 Confirming target deletion following administration of tamoxifen. Inducible, endothelial specific deletion of NRP2, individually, or in combination with either α5 integrin or NRP1, was achieved by crossing mice expressing the PDGFb.iCreER promoter of Cre-recombinase to those floxed for NRP2, NRP2/α5 integrin, or NRP1/NRP2. **A**) Tamoxifen-induced NRP2 deletion in CMT19T tumours was confirmed by co-staining NRP2 with BS1-lectin. Scale bar = 100 µm. **B**) Tamoxifen-induced NRP2 and α5 integrin co-depletion in CMT19T tumours was confirmed by co-staining NRP2 and α5 integrin with BS1-lectin. Scale bar = 100 µm. **C**) Tamoxifen-induced NRP co-depletion in CMT19T tumours was confirmed by co-staining NRP1 and NRP2 with BS1-lectin. Scale bar = 100 µm. CMT19T tumours were harvested from all animals on D18.

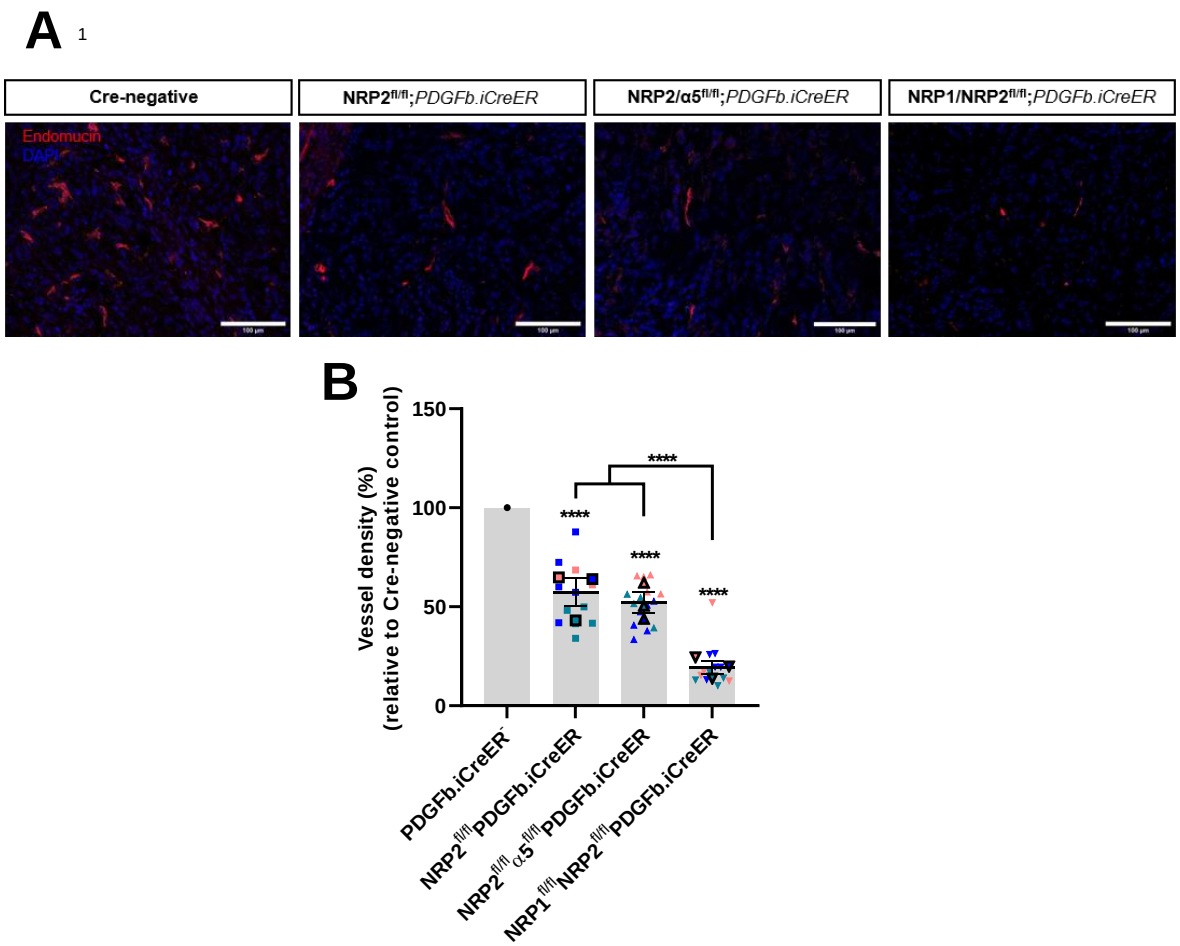

[1]Permission granted by FASEB Journal [230] to re-use figure panels.

Figure 3.31 Endothelial depletion of NRP2 impairs tumour vascularisation. Representative tumour sections from Cre-negative and Cre-positive tumours showing endomucin-positive blood vessels. Scale bar = 100 µm. **B**) Quantification of % blood vessel density per mm^2. Mean quantification performed on 3x ROIs per tumour section, from 3x sections per tumour. Data presented as a percentage of the average % vessel density observed in their Cre-negative littermate controls. Error bars show mean ± SEM; N=3 (n≥12), ****=P<0.0001, unpaired students t-test (two-tailed)/ one-way ANOVA.

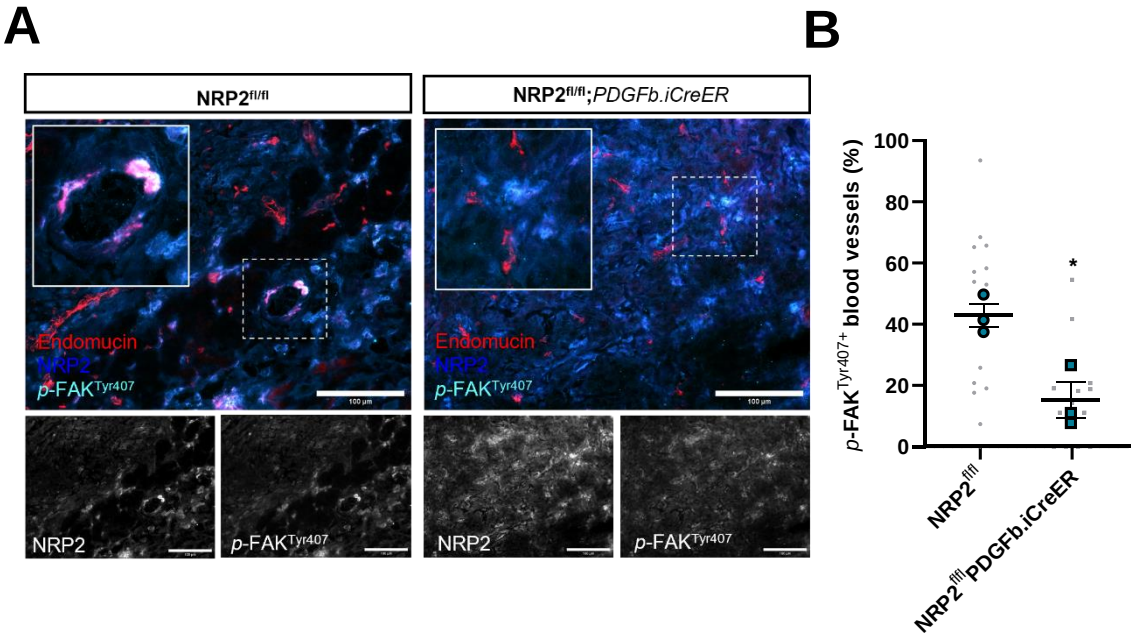

Figure 3.32 Endothelial depletion of NRP2 impairs *p*-FAK^{Tyr407} recruitment to tumour vasculature. A) Representative tumour sections from Cre-negative and Cre-positive tumours showing colocalisation between endomucin positive blood vessels, NRP2, and *p*-FAK^{Tyr407}. Scale bar = 100 µm. **B**) Quantification of % *p*-FAK^{Tyr407} positive blood vessels per field. Error bars show mean ± SEM; n≥3 tumours/group, (5 sections/tumour), *=P<0.05, unpaired students t-test (two-tailed).

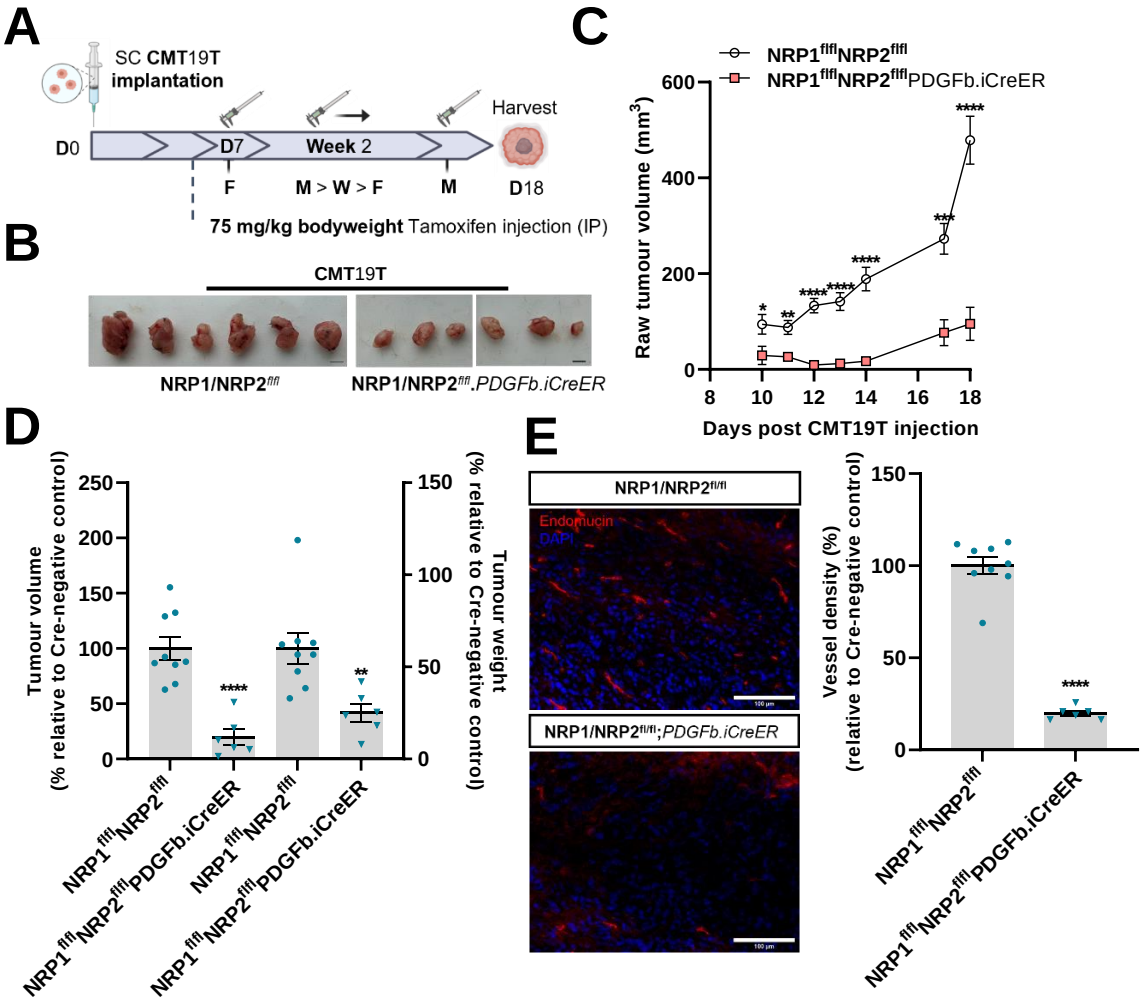
A
SC CMT19T implantation
D0
D7
Week 2
Harvest
D18
F
M > W > F
M
75 mg/kg bodyweight Tamoxifen injection (IP)
B
CMT19T
NRP1/NRP2fl/fl
NRP1/NRP2fl/fl.PDGFb.iCreER
C
NRP1fl/flNRP2fl/fl
NRP1fl/flNRP2fl/flPDGFb.iCreER
Raw tumour volume (mm3)
Days post CMT19T injection
D
Tumour volume (% relative to Cre-negative control)
Tumour weight (% relative to Cre-negative control)
NRP1fl/flNRP2fl/fl
NRP1fl/flNRP2fl/flPDGFb.iCreER
E
NRP1/NRP2fl/fl
Endomucin
DAPI
NRP1/NRP2fl/fl;PDGFb.iCreER
Vessel density (% (relative to Cre-negative control)

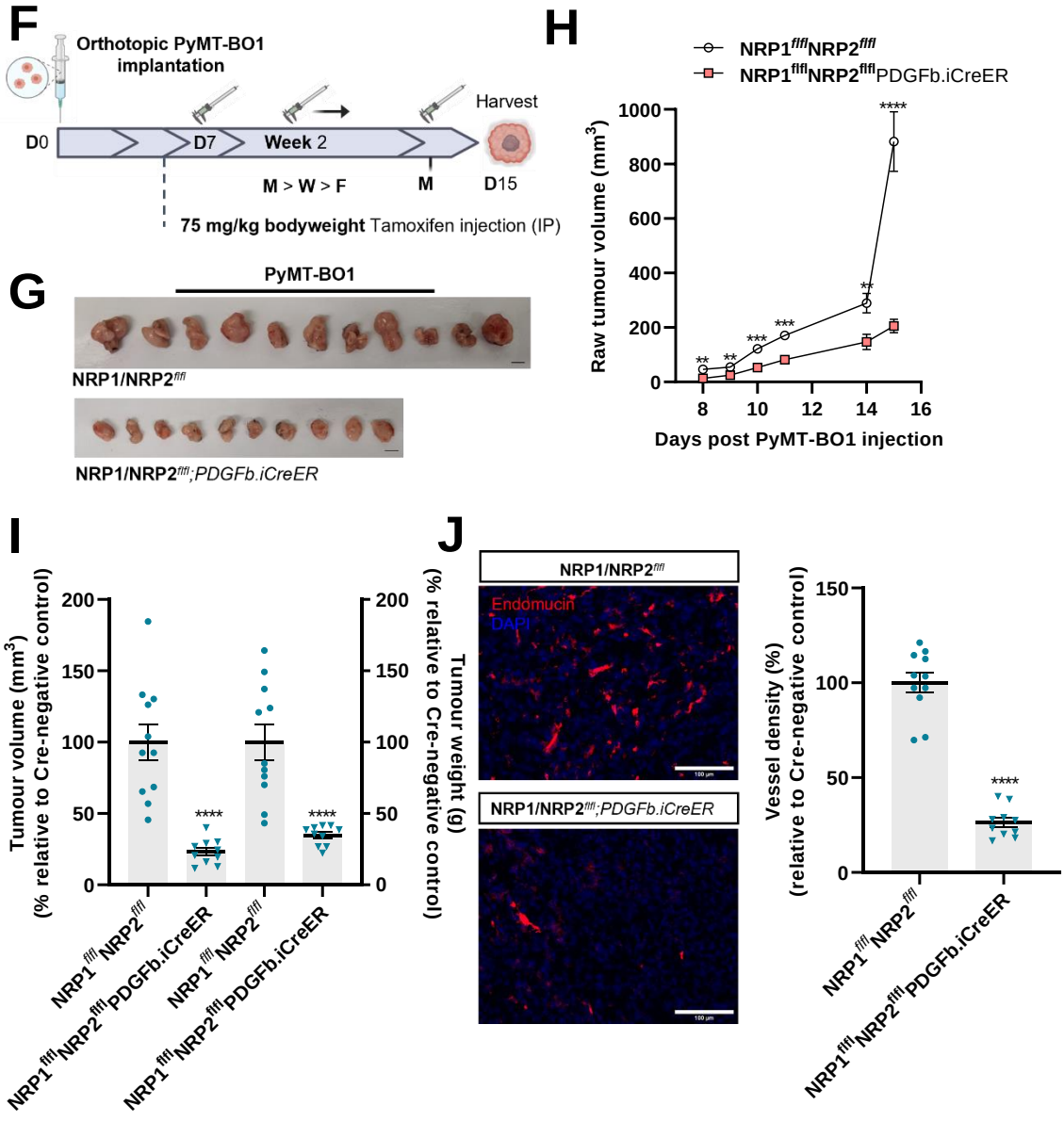
F
Orthotopic PyMT-BO1 implantation
D0
D7
Week 2
Harvest
D15
M > W > F
M
75 mg/kg bodyweight Tamoxifen injection (IP)
G
PyMT-BO1
NRP1/NRP2fl/fl
NRP1/NRP2fl/fl;PDGFb.iCreER
H
NRP1fl/flNRP2fl/fl
NRP1fl/flNRP2fl/flPDGFb.iCreER
Raw tumour volume (mm3)
Days post PyMT-BO1 injection
I
Tumour volume (mm3) (% relative to Cre-negative control)
Tumour weight (g) (% relative to Cre-negative control)
NRP1fl/flNRP2fl/fl
NRP1fl/flNRP2fl/flPDGFb.iCreER
J
NRP1/NRP2fl/fl
Endomucin
DAPI
NRP1/NRP2fl/fl;PDGFb.iCreER
Vessel density (%) (relative to Cre-negative control)

Figure 3.33 Delayed inducible deletion of NRP1 and NRP2 impairs tumour development and angiogenesis. Inducible, endothelial specific deletion of NRP1 and NRP2 was achieved by crossing mice expressing the PDGFb.iCreER promoter of Cre-recombinase to those floxed for NRP1/NRP2. **A**) Experimental schematic: tamoxifen-induced activation of Cre-recombinase and thus target deletion was employed via the following regime. Cre-positive and Cre-negative littermate control mice received intraperitoneal (IP) injections of tamoxifen (75 mg/kg bodyweight, 2mg/ml stock) thrice weekly (Monday, Wednesday, Friday) for the duration of the experiment from D7 to D17 to induce Cre-recombinase activity. CMT19T lung carcinoma cells ($1x10^6$) were implanted subcutaneously (SC) into the flank of mice at D0 and allowed to grow until D18. **B**) Representative images of CMT19T tumours harvested on D18 removed from Cre-negative and positive mice. Scale bar shows 5 mm. **C**) Raw tumour volume kinetics (mm^3) measured from tumour bearing mice measured between D10 and D18 post CMT19T injection. Tumour volume calculated using the formula: length x $width^2$ x 0.52. Error bars show mean ± SEM; N=1 (n≥6), *=P<0.05, **=P<0.002, ***=P<0.0005, ****=P<0.0001, unpaired students t-test (two-tailed). **D**) Quantification of tumour volume (left axis) and tumour weight (g) (right axis) measured on D18. Data presented as percentages of the average tumour volume/ tumour weight observed in respective littermate control animals. Error bars show mean ± SEM; N=1 (n≥6), **=P<0.002, ****=P<0.0001, unpaired students t-test (two-tailed). **E**) (Left panels): Representative tumour sections from Cre-negative and Cre-positive tumours showing endomucin-positive blood vessels. Scale bar = 100 µm. (Right panel): Quantification of % blood vessel density per mm^2. Mean quantification performed on 3x ROIs per tumour section, from 3x sections per tumour. Data presented as a percentage of the average % vessel density observed in their Cre-negative littermate controls. Error bars show mean ± SEM; N=1 (n≥6), ****=P<0.0001, unpaired students t-test (two-tailed). **F**) Experimental schematic: Cre-positive and Cre-negative littermate control mice received intraperitoneal (IP) injections of tamoxifen thrice weekly for the duration of the experiment from D7 to D14 to induce Cre-recombinase activity. PyMT-BO1 breast cells ($1x10^5$) were orthotopically implanted into the fourth inguinal mammary gland of mice at D0 and allowed to grow until D15. **G**) Representative images of PyMT-BO1 tumours harvested on D15 removed from Cre-negative and positive mice. Scale bar shows 5 mm. **H**) Raw tumour volume kinetics (mm^3) measured from tumour bearing mice measured between D10 and D15 post PyMT-BO1 injection. Error bars show mean ± SEM; N=1 (n≥10), **=P<0.002, ***=P<0.0005, ****=P<0.0001, unpaired students t-test (two-tailed). **I**) Quantification of tumour volume (left axis) and tumour weight (g) (right axis) measured on D15. Data presented as percentages of the average tumour volume/ tumour weight observed in respective littermate control animals. Error bars show mean ± SEM; N=1 (n≥10), ****=P<0.0001, unpaired students t-test (two-tailed). **J**) (Left panels): Representative tumour sections from Cre-negative and Cre-positive tumours showing endomucin-positive blood vessels. Scale bar = 100 µm. (Right panel): Quantification of % blood vessel density per mm^2. Data presented as a percentage of the average % vessel density observed in their Cre-negative littermate controls. Error bars show mean ± SEM; N=1 (n≥10), ****=P<0.0001, unpaired students t-test (two-tailed).

3.4.2 Developmental angiogenesis in the postnatal mouse retina model is sensitive to complex interactions between NRP2 and both α5 integrin and NRP1

Whilst many of the same processes and stimuli drive both pathological and physiological angiogenesis, tumour vasculature is very much distinct from vasculature that forms under physiological homeostasis [292], [293]. To obtain any mechanistic insight into NRP2's function during developmental angiogenesis, it was therefore necessary to study the effects of its depletion in a model of physiological vascularisation. By assessing the effects of depleting NRP2 in combination with either α5 integrin or NRP1, we also aimed to shed further light on their complex interactions. As others have employed previously with great success, we utilised the postnatal mouse retina to examine the effects of depleting our targets specifically within the endothelium. A highly characterised and hierarchical model of physiological developmental angiogenesis, the postnatal mouse retina develops following a series of sequential checkpoints, each defined by a set of distinct angiogenic processes [294]. Establishing which combination of angiogenic receptors are required to progress each discrete stage and its corresponding mechanism of action would therefore provide a fundamental understanding of how these targets interact to promote angiogenesis.

When mice are born, their retinas are avascular. During the first three weeks of postnatal (P) development, the retina becomes vascularised, starting from the optic nerve. From postnatal day 0 (P0) to P7, sprouting vessels radially extend outwards to the vascular periphery to form the superficial vascular plexus (SP). Once the SP is formed, sprouting vessels descend to vascularise the deep vascular plexus (DP), which is completed by P12. By P21, a third vascular bed, the intermediate vascular plexus (IP) develops between the SP and the DP (**Figure 3.34**). This tri-laminar network subsequently undergoes widespread remodelling until around P42, pruning unnecessary or defective vessels to ensure maximum efficiency of the organ [295]–[297].

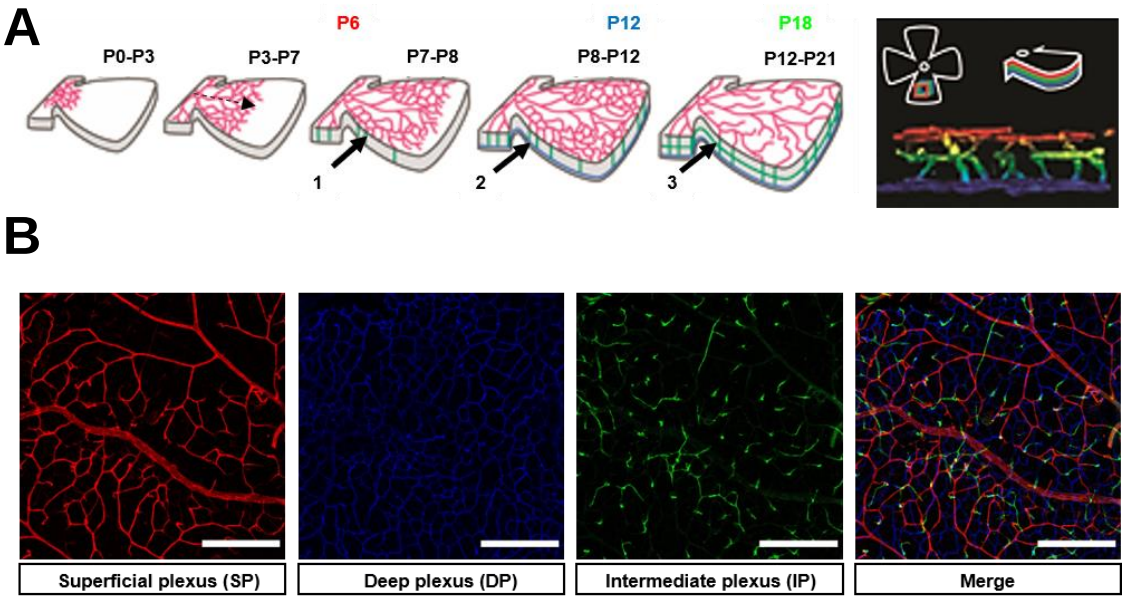

Figure 3.34 The hierarchical vascularisation of the developing murine retina. A) Schematic depicting the sequential multi-plexus vascularisation of the murine retina from P0 to P21. From P0-P7, the SP (red) expands radially outwards from the optic nerve towards the periphery. From P8-P12, vascular sprouts descend to form the deep plexus (blue). From P13-P21, an intermediate plexus (green) is formed between the superficial and deep layers. (Panels adapted from [298]). **B**) Corresponding images showing superficial, deep and intermediate layers labelled in red, blue and green respectively. Scale bars show 150 µm.

3.4.2.1 Assessing the expression profile of NRP2 in the developing mouse retina

The expression of NRP2 is largely considered to be more venous than arterial within the endothelium [275], [299]. It is also known that NRP2 expression in the postnatal mouse retina is normal in mice lacking the cytoplasmic domain, and therefore the SEA motif, of NRP1 (NRP1cytoΔ/Δ) [94]. That being said, surprisingly little investigation into its expression within the disseminating microvasculature has been made.

Prior to examining the effects of its depletion on retinal vascularisation therefore, we co-immunolabelled NRP2 with BS-1 lectin, an EC marker, and assessed its patterns of expression within the SP and the DP of Cre-negative animals. At P6, whilst NRP2 was found to be expressed within the disseminating microvasculature of the SP, its expression was enriched at the vascular front and within sprouting tip cells (**Figure 3.35A**). We also observed a robust level of expression localising to the abluminal surface in veins of the SP, confirmed by co-immunolabelling with α-smooth muscle actin (α-SMA), a marker of smooth muscle cells that are known to primarily ensheathe arteries [300]. In contrast, subsequent multi-plexus analysis from retinas harvested at P12 revealed minimal levels NRP2 expression within the vasculature of the DP. Rather, it was found to be enriched at the apical ends of vessels descending downwards in a corkscrew-like motion towards the DP (**Figure 3.35B-D**). Based solely on its localisation, we can therefore postulate that NRP2 plays a prominent role during vessel sprouting and tip cell anchorage to the underlying FN-dense retinal matrix.

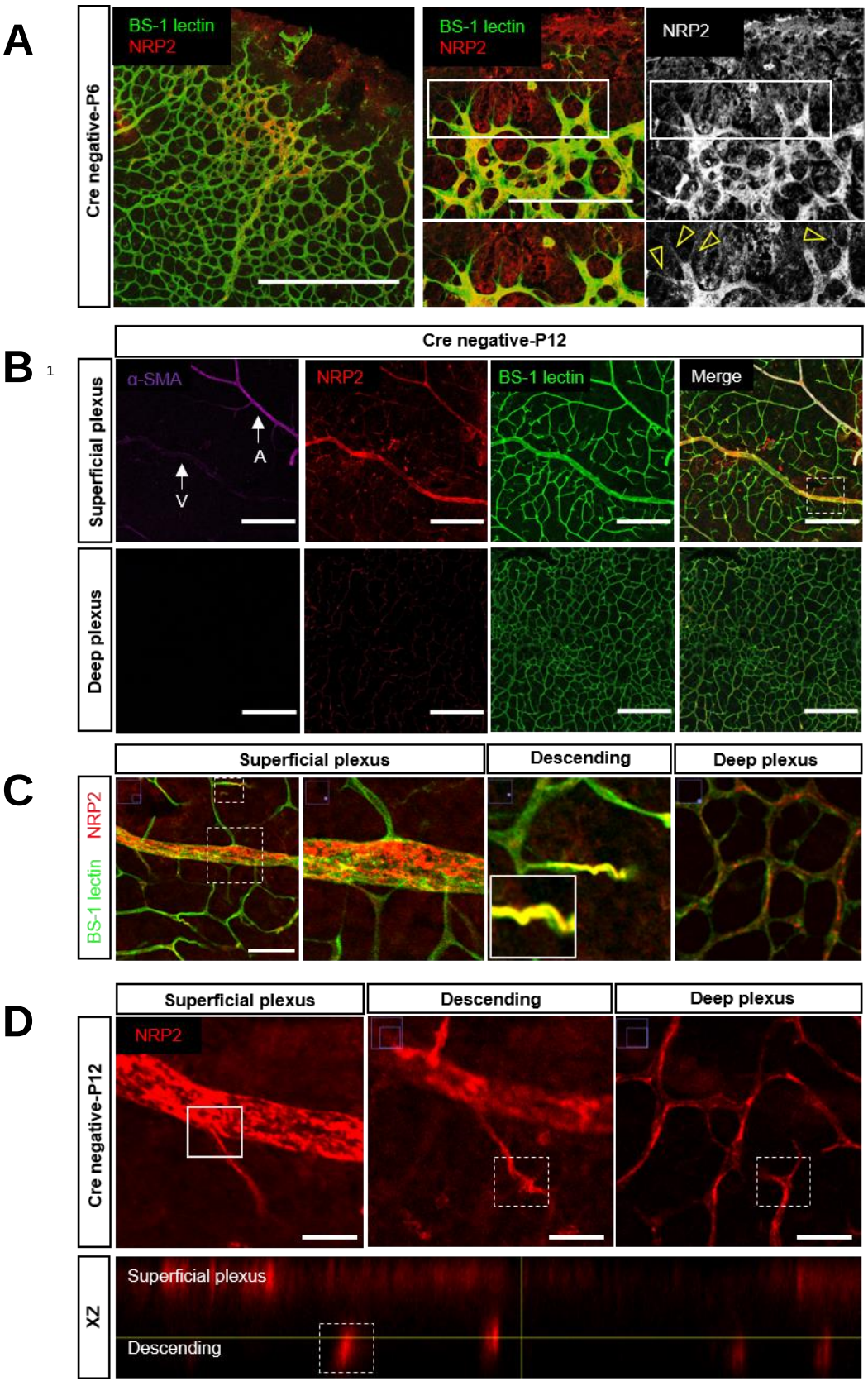

[1]Permission granted by FASEB Journal [230] to re-use figure panels.

Figure 3.35 NRP2 is preferentially expressed within sprouting vessels of the postnatal mouse retina. A) Endothelial NRP2 is preferentially expressed at the vascular front of the superficial plexus at P6. Panels show co-staining between BS-1 lectin and NRP2 in Cre-negative retinas. Arrows show NRP2 localisation within sprouting tip cells. Scale bar = 150 μm. **B**) NRP2 is expressed in both superficial and deep plexus layers at P12. The arterial/venous identity of NRP2 was confirmed by co-staining with α-smooth-muscle-actin (α-SMA) to label arteries. Scale bar = 150 μm. **C/D**) Magnified images from highlighted area selected in **B**) showing prominent NRP2 expression in major vessels of the superficial plexus, and moderate expression in descending vessels and the deep plexus layer. Scale bar = 50 μm. **D**) XZ orthogonal plane images show NRP2 expression in descending vessels.

3.4.2.2 Tamoxifen-induced activation of Cre-recombinase effectively induces target depletion

Whilst many have modelled developmental angiogenesis using the postnatal mouse retina, the tamoxifen regime by which they induce Cre-recombinase expression and therefore target depletion varies between research groups. Our laboratory follows the tamoxifen induction regime previously published by Raimondi *et al*., whereby pups receive consecutive 100 µg injections between P2 and P5 [102]. The developing retina is subsequently harvested at P6 (**Figure 3.36A**), allowing us to observe the effects of any angiogenic defect, elicited by target depletion, on SP formation. Past members of our laboratory have previously followed this regime to study the effects of depleting angiogenic receptors on DP formation also, injecting tamoxifen between P2 and P5, before harvesting the retinas on P12. Due to the hierarchical nature of retina development however, were SP to develop abnormally, arising as a consequence of target depletion, it is likely that vascularisation of the DP would also be perturbed. Isolating the contributions of specific target receptors during its formation exclusively, therefore becomes difficult. As such, we opted for an alternative injection regime whereby tamoxifen administration was delayed until between P7 and P10 (**Figure 3.36B**), thereby enabling the SP to develop normally, before harvesting the retina on P12.

Following these two tamoxifen administration regimens, we first confirmed successful depletion of NRP2, individually, and in combination with either α5 integrin or NRP1, by co-immunolabelling with BS-1 lectin in retinas harvested from Cre-negative and Cre-positive mice at both P6 (**Figure 3.36C, E, G**) and P12 (**Figure 3.36D, F, H**). By doing so, we also reaffirmed the localisation of α5 integrin [301] and NRP1 [98], [102], [103], [275] within the postnatal retina as reported previously. Whilst α5 integrin expression was found to be almost exclusively localised to the angiogenic front at P6, enriched along filopodial protrusions and at the base of sprouting tip cells (**Figure 3.36E**), NRP1 expression was more ubiquitously expressed throughout the superficial vascular bed (**Figure 3.36G**). We observed no changes in overall animal weight following either tamoxifen regimes in any of our GEMMs (**Suppl. Figure 5.3**).

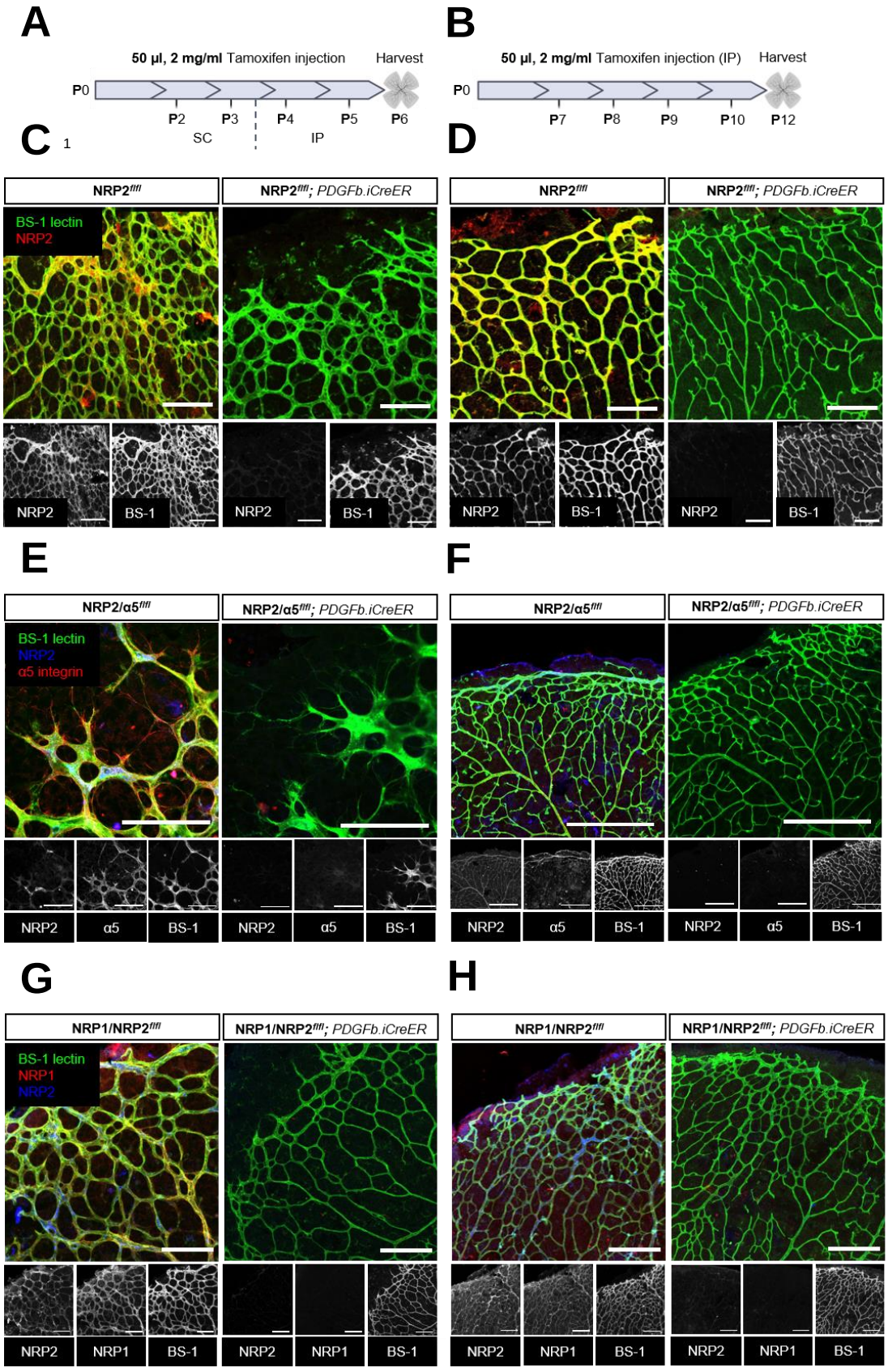

[1]Permission granted by FASEB Journal [230] to re-use figure panels.

Figure 3.36 Tamoxifen-induced Cre-recombinase activity provides effective target depletion in the postnatal mouse retina. A/B) Tamoxifen-induced activation of Cre-recombinase was achieved via two regimens. To study the development of the SP, Cre-positive and Cre-negative littermate control mice received subcutaneous (SC) injections of tamoxifen (50 µl, 2mg/ml stock) on P2 and P3, followed by intraperitoneal (IP) injections of the same dose on P4 and 5. Retinas were then harvested at P6 (**A**). To study the development of the DP, Cre-positive and Cre-negative mice received IP injections of tamoxifen (50 µl, 2mg/ml stock) between P7 and P10. Retinas were then harvested at P12 (**B**). **C-H**) Target depletion was confirmed at both P6 (**C, E, G**) and P12 (**D, F, H**) by co-immunolabelling NRP1, NRP2 and α5 integrin with BS-1 lectin. Scale bars = 50 µm.

3.4.2.3 Development of the superficial vascular plexus is NRP dependent

With the knowledge that our tamoxifen regimens were sufficient to induce the expression of Cre-recombinase, and therefore produce an efficient depletion of our angiogenic target receptors, we were able to pursue their roles during the sequential vascularisation of both the SP and the DP as a paradigm for developmental angiogenesis. Throughout our investigations, our Cre-positive animals were compared against their corresponding Cre-negative control littermates. This enabled us to effectively remove any significant bias arising from differences in genetic background or exact age.

Loss of endothelial NRP1 is known to significantly impair the radial extension of the SP, tip cell sprouting, and the EC density of the vascular network by P6 [6], [98], [102], [244]. In mice expressing the $^{Y297A/Y297A}$ mutation, abrogating NRP1 - VEGF binding, NRP1 was also shown to promote arterial differentiation and patterning [103]. These findings have since been confirmed in our laboratory, vascular extension from the optic nerve, EC density and arterial maturation all found to be significantly impaired following the endothelial-specific depletion of NRP1. Whilst far less is known about α5 integrin's involvement during retinal vascularisation, it has been shown that its endothelial-specific depletion results in an increased number of misaligned filopodia, and a marginal reduction in vascular outgrowth from the optic nerve. This phenotype was also observed in mice expressing a heterozygous mutation for the inactive RGE motif, impairing RGD-mediated integrin binding to FN, elucidating a role for integrin-FN interactions during filopodial alignment and stabilisation [301]. Given NRP2's prominent expression at the vascular front of the SP, alongside its regulatory interplay with both α5 integrin and NRP1, we sought to examine its angiogenic contributions during the vascularisation of the SP. We subsequently considered whether its role would be influenced by the additional loss of either α5 integrin or NRP1.

Compared to Cre-negative control littermates, in Cre-positive, NRP2 depleted mice, vascular extension from the optic nerve outwards to the retinal periphery was marginally but significantly reduced. An equivalent impairment to vascular extension was also observed following the co-depletion of both NRP2 and α5 integrin, implying that NRP2's involvement during angiogenic cascade initiation is upstream of that of α5 integrin. Upon review of unpublished data accrued by past members of our laboratory, the impaired radial outgrowth observed in either NRP2 or NRP2/ α5 integrin co-depleted retinas was not however, found to be as severe as when NRP1 is lost within the endothelium. We can therefore infer that whilst NRP2 promotes vascular outgrowth, overall, the process is NRP1 dependent. Indeed, when we depleted both NRPs in combination, the radial expansion of the SP was no different to when NRP1 is lost individually (**Figure 3.37A-B**).

This supposition holds true when analysis of the vascular density directly behind the proliferative vascular front is considered. Whilst measuring vascular extension provides an impression of the endothelium's ability to adhere, migrate, and proliferate over the retinal ECM, vascular density provides us with a summary of the angiogenic mechanisms that provide the structural integrity to support vessel sprouting at the vascular front of the SP; vessel bifurcation and junction formation, and vessel regression. Whilst it has been established that depletion of NRP1 within the endothelium significantly reduces the vascular density of the SP, our laboratory has demonstrated that this is not the case following the depletion of α5 integrin. Likewise, we observed no perturbations in vascular density, vessel branching, or ERG^{+} endothelial nuclei when NRP2 was depleted alone. Only when both NRP2 and α5 integrin were co-depleted did these parameters become significantly impaired, suggesting that whilst functional redundancies in the expression of other pro-angiogenic receptors are sufficient to compensate the loss of either NRP2 or α5 integrin individually, they fail to entirely rescue the effects of losing both receptors simultaneously. This impairment was still found to be less than when both NRP receptors were lost in tandem however, the vascular density of the SP reaching only approximately 60% of that exhibited by Cre-negative littermate controls. That being said, and in a similar manner to vascular extension, the vascular density and frequency of ERG^{+} endothelial nuclei were found to be no different than in NRP1 depleted P6 retinas. We can therefore assume once again, that the dominant actions of NRP1 drive the development of the SP (**Figure 3.37C-F**).

As the SP becomes vascularised, the network of microvessels directly behind the proliferative front undergoes maturation and remodelling. Branches that do not become perfused during vascular loop formation are pruned, undergoing regression to remove any redundant vasculature. This process leaves behind empty collagen IV^{+} basement membrane sleeves, which can subsequently be analysed as a rudimentary measure of the functionality of the vascular network [302]. With this in mind, in addition to demonstrating that our angiogenic receptors interact to regulate the formation of neovasculature, we next chose to consider how their depletion would affect the functionality of disseminating vasculature. To this end, we proceeded to assess the frequency of vessel regression, in addition to the diameter of microvessels directly behind the highly proliferative vascular front. Whilst we were aware that the process of flat-mounting retinas prior to imaging would invariability distort the vasculature's 3D morphology, we had no access to an alternative imaging system, such as light-sheet fluorescence microscopy (LSFM), to resolve vascular structures in their native conformation [303]. A greater degree of sample variation when analysing microvessel diameter was therefore to be expected. Taking this into account, whilst all of our depleted lines exhibited

reductions in microvessel diameter, perturbations were found to be greatest upon co-depletion of both NRPs. Likewise, we observed a concomitant increase in vessel regression in our depleted lines compared to their respective Cre-negative controls. In addition to exhibiting the greatest degree of vessel regression, retinas depleted for both NRPs were also found to display a high number of regressed tip cells at the vascular front (**Figure 3.37G-J**). Unlike regressed vessels identified directly behind the proliferative zone however, likely pruned as a result of impaired microvascular perfusion, the immediate regression of sprouting tip cells as the SP develops is suggestive of a profound inability to form connections to the retinal ECM. Without sufficient anchorage to the matrix, migratory sprouts subsequently regress, severely impeding vascular outgrowth. At the time of writing, additional studies examining vascular leakage had commenced by immunolabeling red blood cells in the disseminating retinal vasculature using the Ter119 antibody. This analysis would be greatly informative as to the functionality of a vascular bed depleted for our target receptors, and would aim to complement the results shown in this thesis.

The radial expansion of the SP relies on the ability of sprouting ECs to sense, integrate and disseminate physiological angiogenic stimuli as they adhere and migrate outwards towards the vascular periphery. As the depletion of our receptors, in any combination, significantly impaired vascular extension, we next considered whether this defect arose from an impaired ability to form functional tip cells. Compared to Cre-negative control littermates, P6 retinas harvested from Cre-positive NRP2 or NRP1/NRP2 depleted mice exhibited significantly fewer sprouting ECs at the vascular front of the SP. This was found to match a concomitant reduction in the number of filopodial extensions per sprout. To our surprise, the combinatory loss of both NRP2 and α5 integrin ameliorated these perturbations, tip cell and filopodial numbers returning to normal physiological levels (**Figure 3.37K-M**). Despite this, many of the filopodial extensions presented by NRP2/ α5 integrin deficient ECs were found to be highly tortuous (**Figure 3.37N**), reminiscent of the misaligned filopodia in α5 integrin deficient mice as reported by Stenzel *et al*., [301]. This finding suggests that whilst the expression of α5 integrin is essential for filopodial alignment and stabilisation through its interactions with the retinal ECM, the production of sprouting tip cells and their filopodial extensions is NRP2 dependent. We can also infer that in this instance, α5 integrin functions in an anti-angiogenic manner, acting as an angiogenic break to prevent the hypervascularisation of the SP. When α5 integrin is depleted in combination with NRP2, this inhibition is lost, and tip cell sprouting increases. We observed only minimal fluctuations in filopodial length between Cre-negative control mice and their respective depleted counterparts (**Suppl. Figure 5.4**).

Whilst the physical existence of FA structures and their turnover in sprouting retinal ECs is disputed, it has been demonstrated that FA-associated signalling cascades do exist in the postnatal retina to promote tip cell migration [102], [304]. In an attempt to corroborate our *in vitro* findings, and those discussed above, we next sought to assess the pattern of differential FAK phosphorylation in retinas harvested during SP vascularisation. Confocal microscopy of Cre-negative control retinas revealed that *p*-FAK^{Tyr407} expression preferentially localised to the vascular front at P6, and was enriched at the apical ends of sprouting tip cells. *p*-FAK^{Tyr407} was also detected along the length of extending filopodial projections, and colocalised with NRP2 expression. In comparison, retinas harvested from Cre-positive NRP2 depleted mice exhibited a significantly reduced relative intensity of *p*-FAK^{Tyr407} staining in sprouting tip cells and in the directly adjoining disseminating vasculature (**Figure 3.38A-C**). We can therefore infer that the reduced vascular extension we observe following NRP2 depletion, in addition to the impaired production of tip cells and increased vessel regression, likely arises from a reduced capacity for NRP2-deficient ECs to form stable cell-matrix interactions.

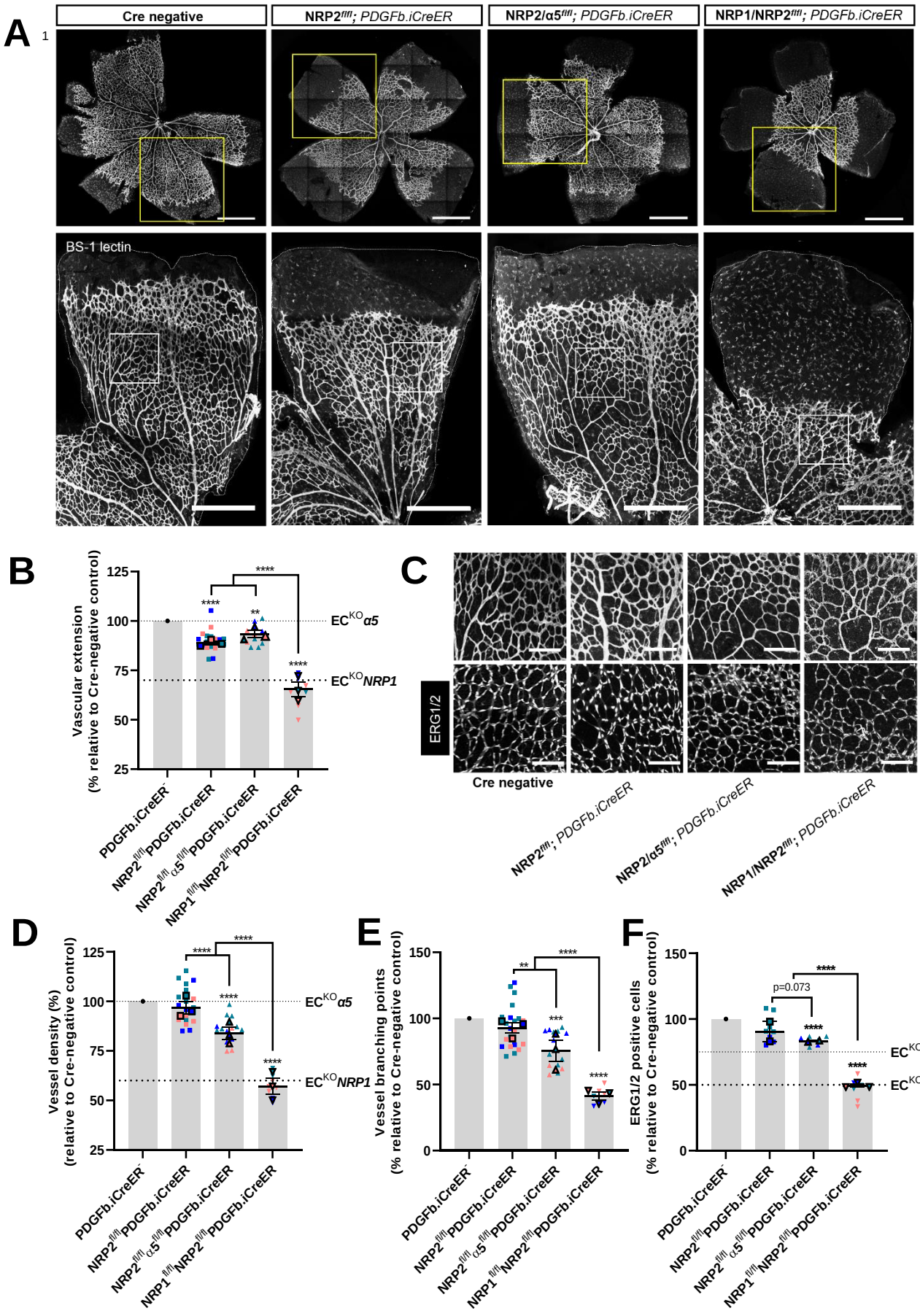
A
Cre negative
NRP2fl/fl; PDGFb.iCreER
NRP2/α5fl/fl; PDGFb.iCreER
NRP1/NRP2fl/fl; PDGFb.iCreER
BS-1 lectin
B
Vascular extension (% relative to Cre-negative control)
125
100
75
50
25
****
**
****
****
ECKOα5
ECKONRP1
PDGFb.iCreER
NRP2fl/flPDGFb.iCreER
NRP2fl/flα5fl/flPDGFb.iCreER
NRP1fl/flNRP2fl/flPDGFb.iCreER
C
ERG1/2
Cre negative
NRP2fl/fl; PDGFb.iCreER
NRP2/α5fl/fl; PDGFb.iCreER
NRP1/NRP2fl/fl; PDGFb.iCreER
D
Vessel density (%) (relative to Cre-negative control)
125
100
75
50
25
****
****
****
ECKOα5
ECKONRP1
PDGFb.iCreER
NRP2fl/flPDGFb.iCreER
NRP2fl/flα5fl/flPDGFb.iCreER
NRP1fl/flNRP2fl/flPDGFb.iCreER
E
Vessel branching points (% relative to Cre-negative control)
150
100
50
0
**
****
***
****
PDGFb.iCreER
NRP2fl/flPDGFb.iCreER
NRP2fl/flα5fl/flPDGFb.iCreER
NRP1fl/flNRP2fl/flPDGFb.iCreER
F
ERG1/2 positive cells (% relative to Cre-negative control)
150
100
50
0
p=0.073
****
****
****
ECKOα5
ECKONRP1
PDGFb.iCreER
NRP2fl/flPDGFb.iCreER
NRP2fl/flα5fl/flPDGFb.iCreER
NRP1fl/flNRP2fl/flPDGFb.iCreER

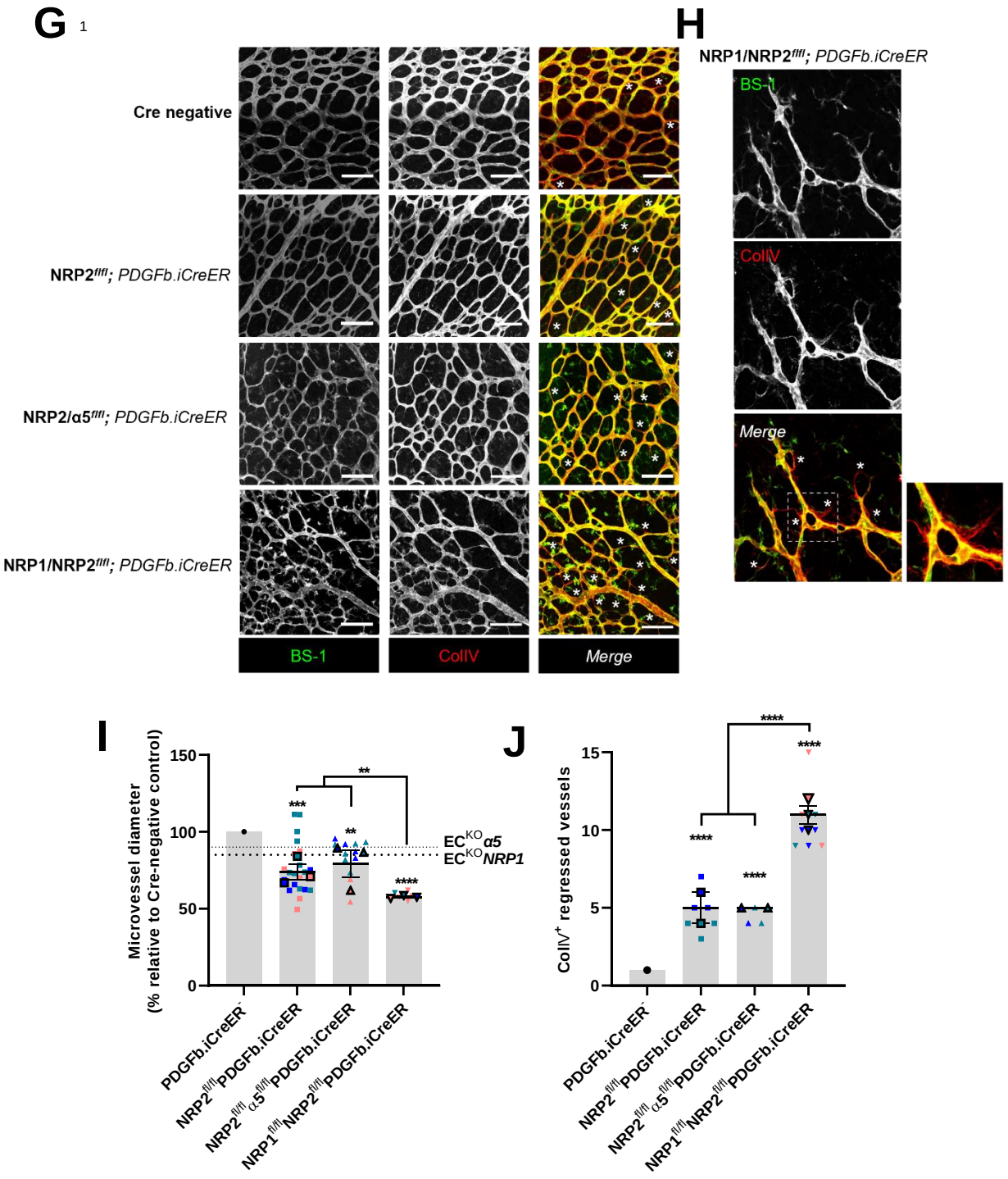
G
Cre negative
NRP2fl/fl; PDGFb.iCreER
NRP2/α5fl/fl; PDGFb.iCreER
NRP1/NRP2fl/fl; PDGFb.iCreER
BS-1
CollV
Merge
H
NRP1/NRP2fl/fl; PDGFb.iCreER
BS-1
CollV
Merge
I
Microvessel diameter (% relative to Cre-negative control)
150
100
50
0
**
***
**
****
EC^KO α5
EC^KO NRP1
PDGFb.iCreER
NRP2fl/flPDGFb.iCreER
NRP2fl/fl α5fl/flPDGFb.iCreER
NRP1fl/flNRP2fl/flPDGFb.iCreER
J
CollV+ regressed vessels
15
10
5
0
****
****
****
****
PDGFb.iCreER
NRP2fl/flPDGFb.iCreER
NRP2fl/fl α5fl/flPDGFb.iCreER
NRP1fl/flNRP2fl/flPDGFb.iCreER

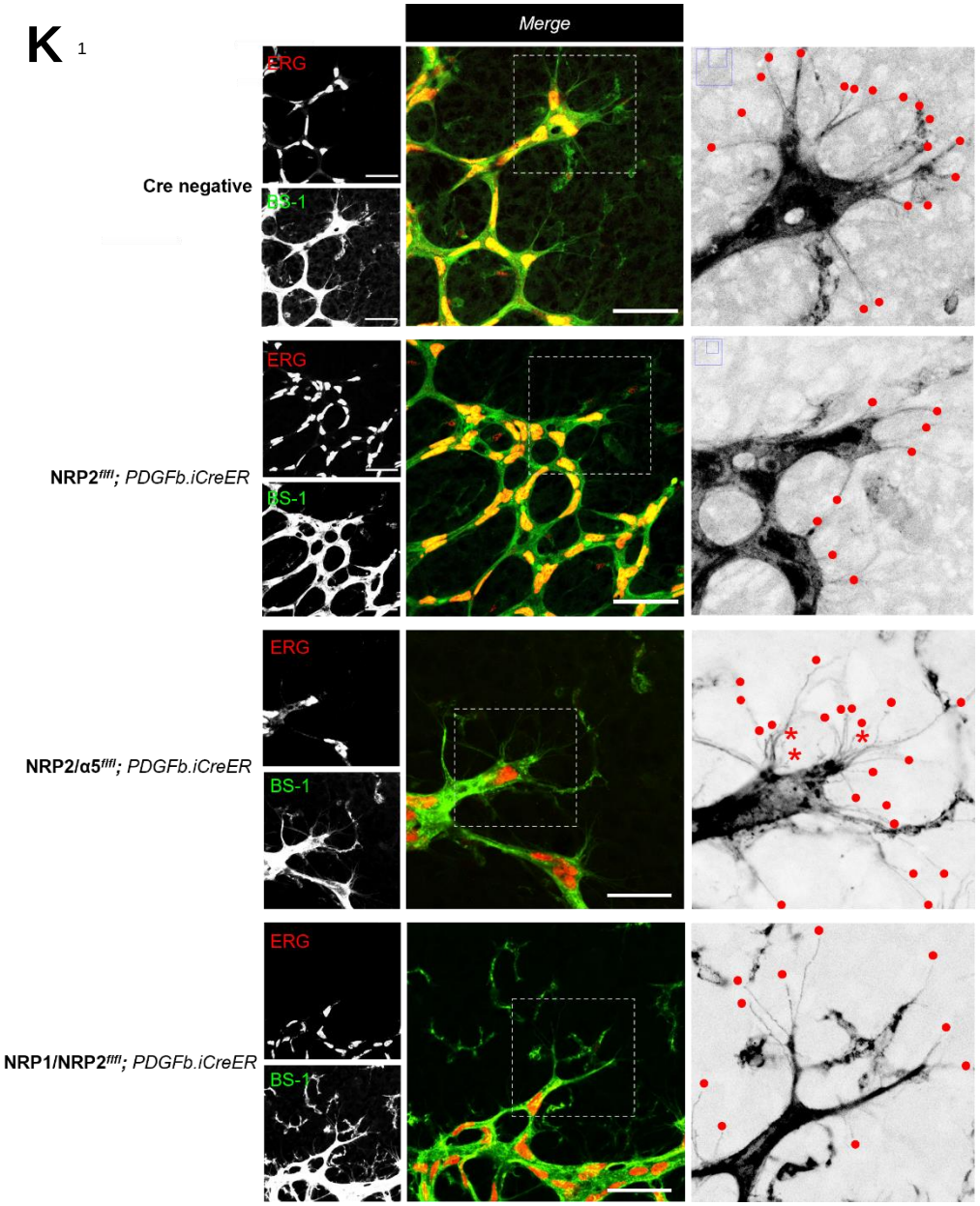
K 1
Merge
ERG
BS-1
Cre negative
NRP2fl/fl; PDGFb.iCreER
NRP2/α5fl/fl; PDGFb.iCreER
NRP1/NRP2fl/fl; PDGFb.iCreER

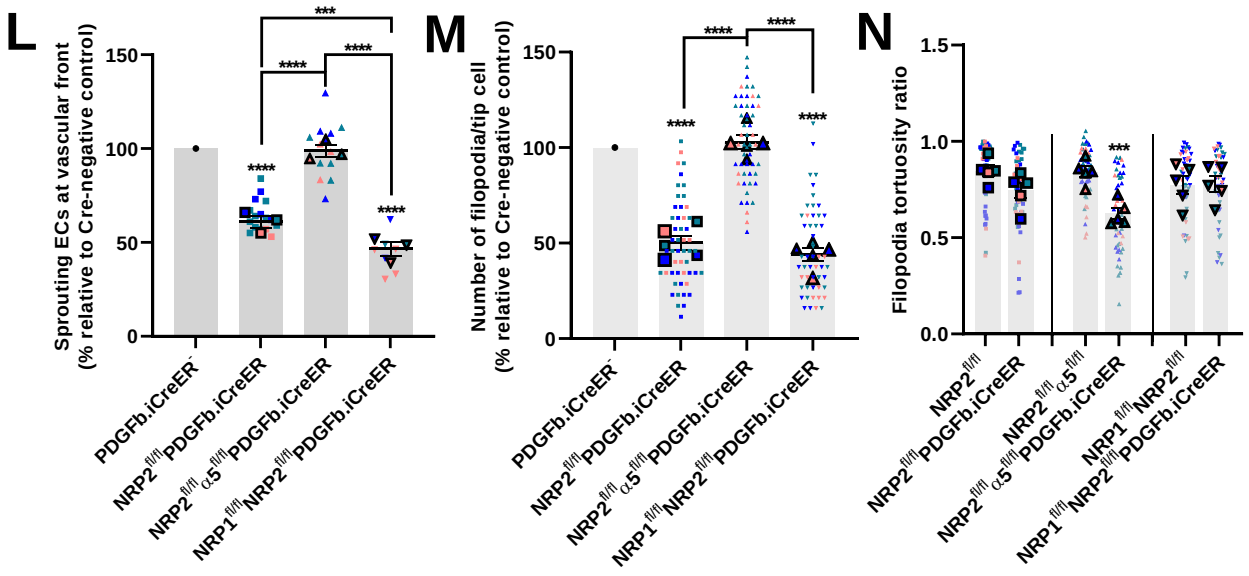

[1]Permission granted by FASEB Journal [230] to re-use figure panels.

Figure 3.37 Endothelial NRP2 promotes developmental angiogenesis in the murine retina at P6. A) Representative images of BS-1 lectin labelled retinal vasculature from Cre-negative and Cre-positive mice. Scale bar = 500 µm. **B**) Quantification of vascular extension from the optic nerve observed at P6, presented as a percentage of the average extension observed in Cre-negative littermate controls. Error bars show mean ± SEM; N=3 (n≥8), **=P<0.002, ****=P<0.0001, unpaired students t-test (two-tailed)/ one-way ANOVA. **C**) Representative images of ERG1/2 labelled EC nuclei from Cre-negative and Cre-positive mice. Scale bar = 150 µm. **D-F**) Quantification of vessel density, branching points and ERG^{+} endothelial nuclei respectively observed at P6, presented as a percentage of the average values observed in Cre-negative littermate controls. Error bars show mean ± SEM; N=3 (n≥6), **=P<0.002, ***=P<0.0005, ****=P<0.0001, unpaired students t-test (two-tailed)/ one-way ANOVA. **G**) Representative images of collagen IV^{+} labelled vessel sleeves. Bottom panels show overlays with BS-1 lectin to identify collagen IV^{+}, BS-1 lectin negative sleeves. Arrows show regressed vessels. Scale bar = 150 µm. **H**) Representative images of collagen IV^{+} labelled vessel sleeves observed at the vascular front of P6 retinas harvested from NRP1/NRP2 co-depleted mice. Asterixis show regressed tip cells. Scale bar = 50 µm. **I**) Quantification of microvascular diameter observed at P6, presented as a percentage of the average diameter observed in Cre-negative littermate controls. Error bars show mean ± SEM; N=3 (n≥8), **=P<0.002, ***=P<0.0005, ****=P<0.0001, unpaired students t-test (two-tailed)/ one-way ANOVA. **J**) Quantification of vessel regression observed at P6, presented as raw values. Error bars show mean ± SEM; N≥2 (n≥5), ****=P<0.0001, unpaired students t-test (two-tailed)/ one-way ANOVA. **K**) Representative images of BS-1 labelled vascular sprouts at the retinal vascular front, co-labelled with ERG to show endothelial nuclei. Scale bar = 50 µm. Bottom panels show inverted magnified images of highlighted areas. Red circles label filopodia. Asterixis show misaligned filopodia. **L**) Quantification of the number of sprouting ECs/retina observed at P6, presented as percentages of the average values observed in Cre-negative littermate controls. Error bars show mean ± SEM; N=3 (n≥8), ***=P<0.0005, ****=P<0.0001, unpaired students t-test (two-tailed)/ one-way ANOVA. **M**) Quantification of the number of filopodia per sprouting EC observed at P6, presented as percentages of the average values observed in Cre-negative littermate controls. Error bars show mean ± SEM; N=3 (n≥5; 50 filopodia/genotype), ****=P<0.0001, unpaired students t-test (two-tailed)/ one-way ANOVA. **N**) Quantification of filopodia tortuosity between Cre-negative and positive retinas. Error bars show mean ± SEM; N=3 (n≥5; 50 filopodia/genotype), ***=P<0.0005, unpaired students t-test (two-tailed). Data from NRP1$^{fl/fl}$PDGFb.iCreER and α5$^{fl/fl}$PDGFb.iCreER mice, collected by Dr Robert Johnson prior to commencing this thesis, is also shown when applicable as horizonal dashed lines, for comparison purposes only.

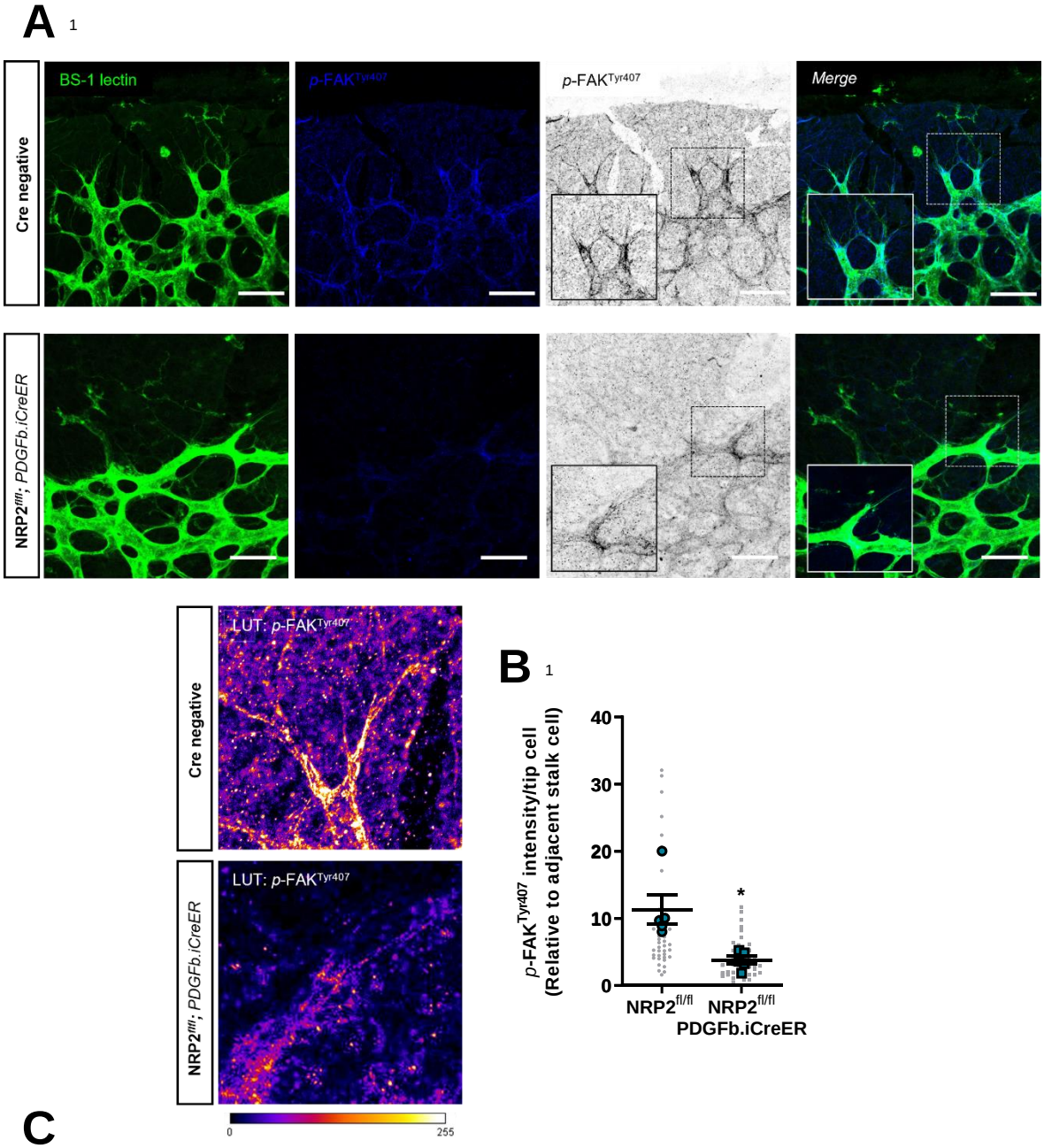

[1]Permission granted by FASEB Journal [230] to re-use figure panels.

Figure 3.38 Endothelial NRP2 promotes FAK phosphorylation in sprouting tip cells. A) Representative images of *p*-FAK^{Tyr407} labelled retinal vasculature co-labelled with BS-1 lectin from Cre-negative and NRP2^{flfl};PDGFb.iCreER mice at P6. Bottom panels show LUT images of highlighted areas. Scale bar = 50 μm. **B**) Quantification of *p*-FAK^{Tyr407} intensity within sprouting tip cells made relative to adjacent stalk cell intensities. Error bars show mean ± SEM; n=5 retinas/genotype (>50 tip cells); *=P<0.05, unpaired students t-test (two-tailed). **C**) Representative images of *p*-FAK^{Tyr407} labelled retinal vasculature co-labelled with BS-1 lectin and NRP2 from a Cre-negative retina at P6. Scale bar = 50 μm. Far right panel shows colocalisation at sprouting tip cells.

3.4.2.4 Development of the deep vascular plexus is NRP2 independent

The development of the DP occurs as ECs of the SP sprout vertically downwards from the ganglion cell layer to the inner nuclear layer of the eye. This vertical branching into the deep retinal layer is orchestrated by the spatiotemporal regulation of VEGF-A by neuronal VEGFR-2 [295], [298], [305]. The expression of NRP1 is also known to regulate DP formation, its depletion from the endothelium by P12 resulting in the failure of the DP to vascularise properly [306], [307]. As, by this timepoint, the vascular impairment observed in the SP of NRP1-depleted retinas has yet to fully recover, it has been previously conjectured that the vertical sprouting required to establish the DP cannot proceed until the vascularisation of the SP has been completed. With this in mind, we delayed our tamoxifen regime to enable the SP to vascularise normally, before proceeding to examine the effects of losing our targets on DP development specifically.

In retinas harvested from mice depleted for NRP2 individually, we observed complete vascularisation of the SP, and no defects in DP vessel density compared to their respective Cre-negative littermate controls. Interestingly however, both the SP and the DP were found to be significantly hypervascularised upon co-depletion with α5 integrin (**Figure 3.39A-B, D-G**). By depleting the expression of our target receptors from P7, and thereby allowing the SP to develop normally, we can infer that this hypervascularisation arises as an artefact of an impaired ability for vessels to regress and remodel overtime. As the retinal vasculature undergoes extensive remodelling and pruning until approximately P42 [295]–[297], an impaired ability for vessels to regress within both SP and DP layers would result in a denser, albeit less functional, vascular network. In comparison, the vascular perturbations observed in retinas depleted for both NRP1 and NRP2 were phenotypically identical to those observed by previous and current members of our laboratory in retinas harvested from NRP1 depleted mice. Whilst we found the SP to be comparatively hypervascularised to retinas co-depleted for both NRP2 and α5 integrin, the deep retinal layer exhibited minimal vessel coverage. In addition, compared to their respective Cre-negative controls, mice depleted for both NRPs displayed fewer vertical sprouts descending from the SP despite its hypervascularisation (**Figure 3.39A-B, D-G**). Upon further inspection, of these descending sprouts, many had developed into large vascular tuft malformations, resembling those previously reported in mouse hindbrains and retinas when NRP1 is lost within the endothelium (**Figure 3.39C**). As NRP1 is known not to drive EC proliferation, but is instead essential for directional migration over FN, the development of these vascular tufts at vessel termini has been speculated to arise as a result of abnormal EC sprouting [103], [244], [303].

In an attempt to pursue this finding, we considered whether the impaired ability for vessel sprouts to interact with, and penetrate through the retinal ECM to establish the deeper plexi, as observed following the endothelial co-depletion of both NRPs, might arise as a result of disruptions to FN remodelling and distribution. In the retina, the FN matrix is laid by astrocytes, and provides an essential scaffold to support the migration of sprouting ECs towards the retinal periphery [308]. FN has also been reported to be expressed in the deep plexus by Corliss *et al*., suggestive that its deposition is also necessary for deep plexus vascularisation [309]. As FN fibrillogenesis has been shown to be sensitive to the loss of either NRP1 [108] or NRP2 *in vitro*, and given that we hypothesise that both NRPs are central regulators of α5 integrin (the principle FN-binding integrin) localisation, we next sought to examine the distribution of the FN matrix in retinas harvested from mice co-depleted for both NRPs. Unfortunately, in our hands, all attempts to visualise the FN network by immunostaining were unsuccessful. Any conclusions drawn from our findings at this time are therefore limited to evidencing that deep plexus development is not sensitive to the depletion of NRP2, but rather is likely regulated by the ability for NRP1 to act as a coreceptor for VEGF-A and thereby promote neuronal VEGFR-2 induced vertical vessel branching.

A 1

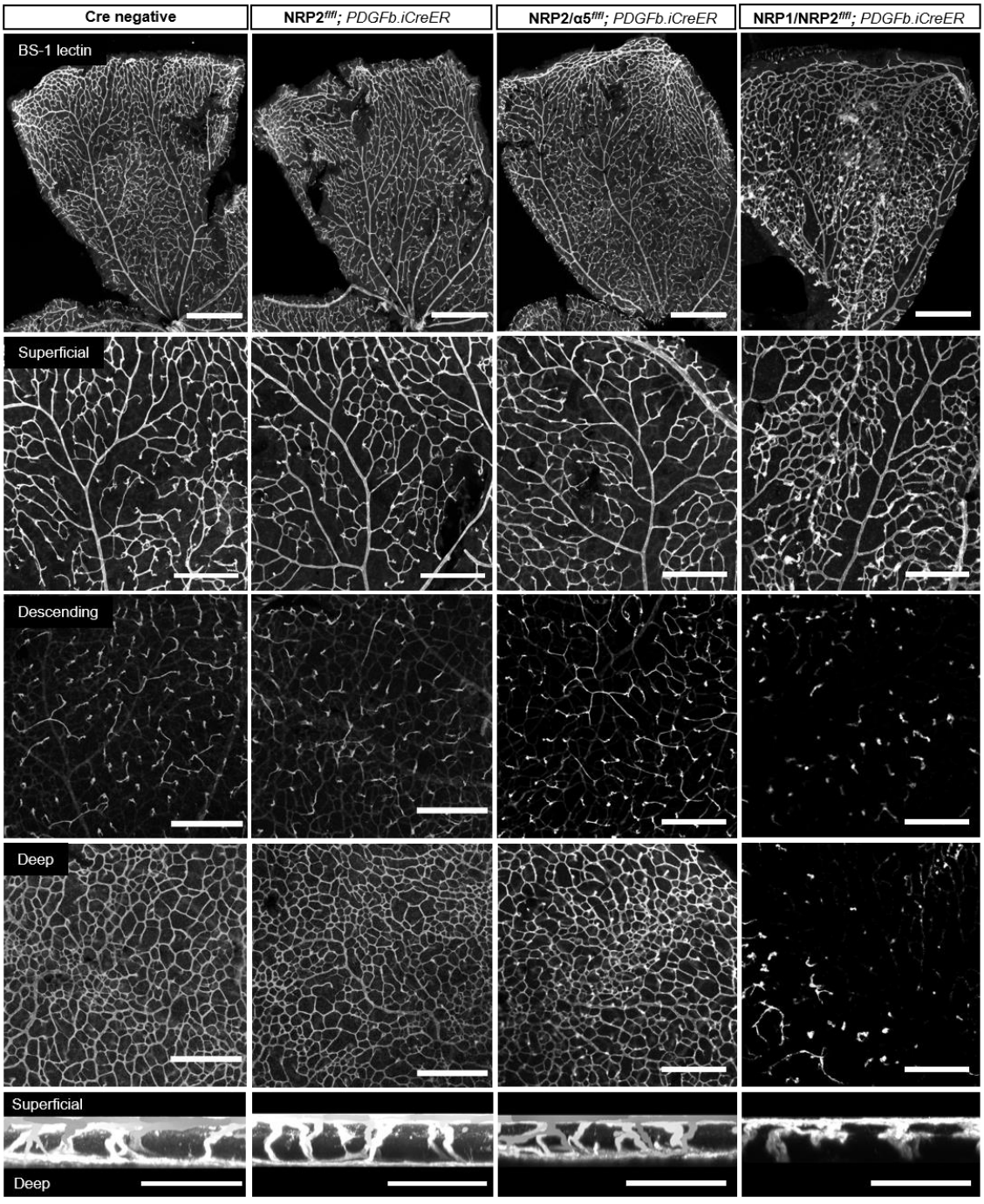
Cre negative
NRP2fl/fl; PDGFb.iCreER
NRP2/α5fl/fl; PDGFb.iCreER
NRP1/NRP2fl/fl; PDGFb.iCreER
BS-1 lectin
Superficial
Descending
Deep
Superficial
Deep

B

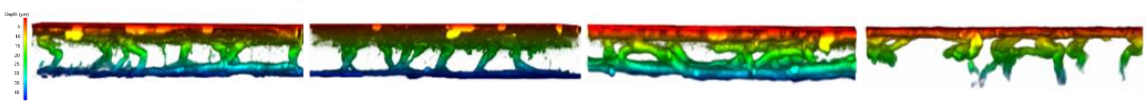

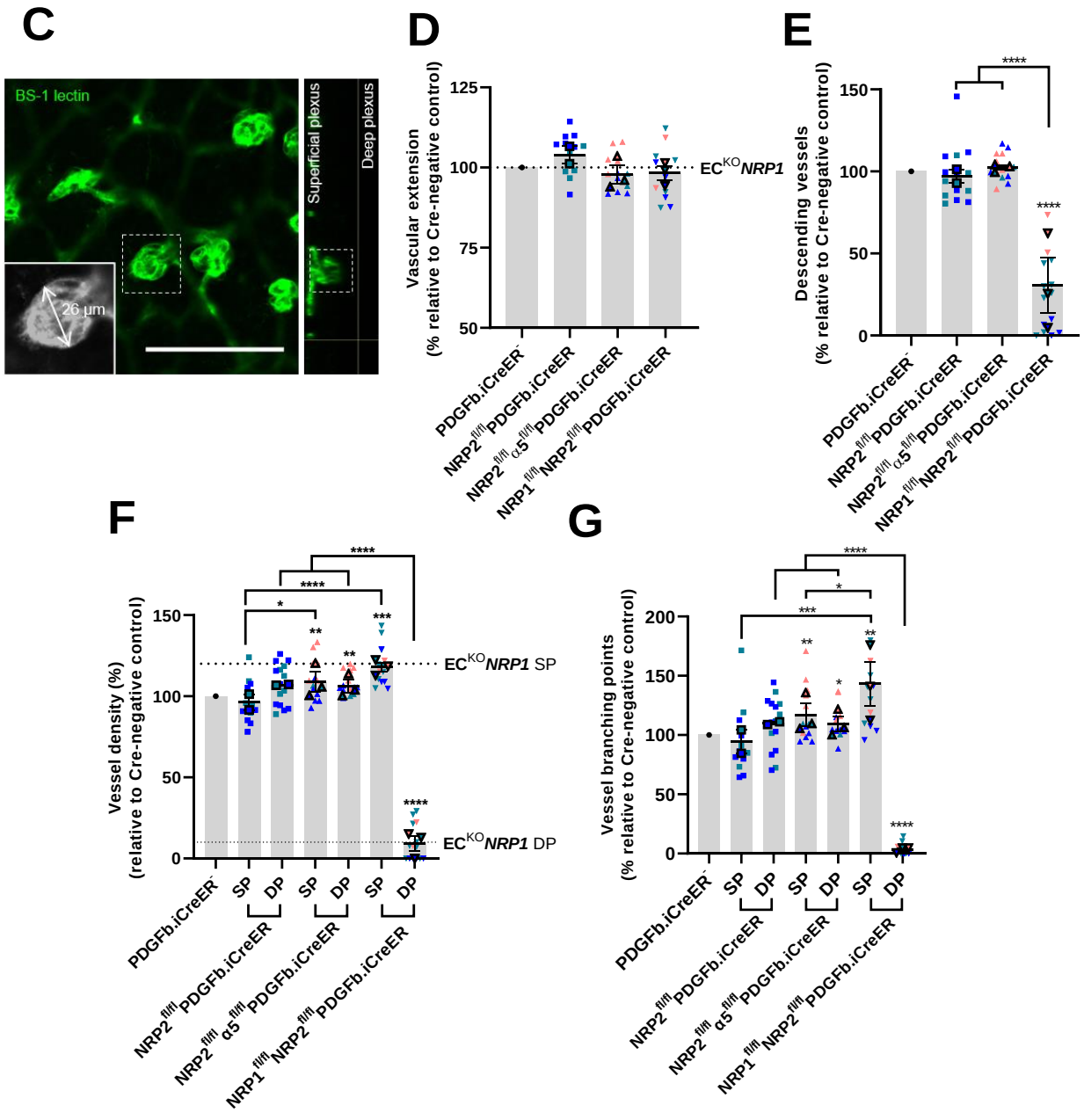

[1]Permission granted by FASEB Journal [230] to re-use figure panels.

Figure 3.39 Development of the deep vascular plexus is NRP2 independent. A) Representative images of BS-1 lectin labelled P12 retinas from Cre-negative and Cre-positive mice showing full vascularisation of the superficial plexus, comparable vessel density of both superficial and deep plexus layers, descending vessels and XZ plane stack images to show all plexus layers. **B**) Colour depth-coded XZ plane stack images. **C**) High magnification image showing enlarged EC tufts observed in NRP1/NRP2 depleted retinas. Right panel shows tuft descension downwards from the SP towards the DP. Scale bar = 50 μm. **D**) Quantification of vascular extension from the optic nerve, presented as a percentage of the average extension observed in Cre-negative littermate controls. Error bars show mean ± SEM; N=3 (n≥12). **E**) Quantification of number of descending vessels, presented as a percentage of the average number of descending vessels observed in Cre-negative littermate controls. Error bars show mean ± SEM, N=3 (n≥12); ****=P<0.0001, unpaired students t-test (two-tailed)/ one-way ANOVA. **F-G**) Quantification of vessel density and number of branching points observed at P12, presented as a percentage of the average values observed in Cre-negative littermate controls. Error bars show mean ± SEM; N=3 (n≥12), *=P<0.05, **=P<0.002, ***=P<0.0005, ****=P<0.0001, unpaired students t-test (two-tailed)/ one-way ANOVA. Data from $NRP1^{flfl}$PDGFb.iCreER and $\alpha5^{flfl}$PDGFb.iCreER mice, collected by Dr Robert Johnson prior to commencing this thesis, is also shown when applicable as horizonal dashed lines, for comparison purposes only.

3.4.3 Discussion

In an effort to emphasise the biological and clinical relevance of specifically depleting endothelial NRP2, we modelled the effects during both pathological and physiological angiogenesis *in vivo*. Whilst many have contributed evidence to suggest that upregulations in NRP2 expression promote a more aggressive cancer phenotype [280], our results clearly demonstrate that the expansion of tumour vasculature to support primary tumour growth is dependent upon endothelial NRP2 activity. We can therefore infer that, in this context, NRP2 acts pro-angiogenically. Mice depleted for both NRP2 and α5 integrin also developed tumours of comparable sizes with the same degree of vascularisation. When considered alongside unpublished data produced by the Robinson laboratory, demonstrating that the loss of endothelial α5 integrin is insufficient to significantly impede tumour growth, we can also infer that NRP2 drives tumorigenesis independently of α5 integrin involvement. Whilst it was also previously demonstrated that the loss of NRP1 was insufficient to inhibit tumour growth, we observed a significantly more severe perturbation in tumorigenesis following the loss of both endothelial NRP1 and NRP2 than when NRP2 was lost individually or in combination with α5 integrin. In addition to substantiating the findings of Takashima *et al*., who demonstrated that NRP1/NRP2 mice exhibit more severe vascular defects than NRP1-null mice [114], this finding supports our hypothesis that NRP1 and NRP2 function cooperatively in ECs to traffic α5 integrin. When either is lost individually, the functional redundancy that exists between the two receptors rescues any critical angiogenic impairment. When both are lost simultaneously however, neovascularisation of the tumour is prohibited completely, and cancerous growth is prevented.

Our understanding of how NRP2 regulates neovascularisation during physiological angiogenesis was subsequently refined by employing the postnatal retina model. As before, we were also able to complement our assessments with a set of preliminary data showing the consequences of depleting either NRP1 or α5 integrin specifically within the endothelium. Generated by a previous member of our laboratory, Dr Robert Johnson, this dataset had been acquired using largely the same methods of analysis as shown in this report, and therefore provided us with the means to dissect the plethora of mechanism-specific interactions taking place between our three receptors during retinal angiogenesis. Indeed, whilst we discovered that NRP2 promotes SP neo-vascularisation, its roles are made somewhat redundant by the dominant actions of NRP1; we observed no differences in vascular outgrowth or vascular density between retinas depleted for NRP1 individually and retinas co-depleted for both NRP1 and NRP2. This supports the findings of Fantin *et al*., who elucidated that whilst the cytoplasmic domain of NRP1 is required for

developmental angiogenesis, specifically arterio-venous patterning, its loss is not compensated for by the actions of NRP2 [275].

We did however, reveal that NRP2 depletion gives rise to a significant reduction in tip cell numbers at the vascular front of the SP, either when lost individually, or in combination with NRP1. It has recently been alluded to that NRP2 expression is associated with promoting a tip cell phenotype in hMVECs, Dallinga et al., observing a significant elevation in NRP2 mRNA levels in $CD34^{+}$ tip cells compared to $CD34^{-}$ control cells [310]. In support of this, NRP2 expression was found to be localised to the vascular front of Cre-negative control P6 retinas within sprouting tip cells. In a similar manner to Raimondi *et al*., who established that the loss of NRP1 impaired paxillin phosphorylation at the apical ends of sprouting tip cells [102], we subsequently demonstrated that FAK phosphorylation at the vascular front was significantly perturbed upon loss of NRP2. When considered alongside our *in vitro* findings, we can infer that NRP2 promotes vessel sprouting by facilitating EC interactions with the retinal ECM. Indeed, the analyses from our NRP2 depleted P6 retinas appear to phenocopy those reported for FAK^{ECKO} retinas by Tavora et al., showing a mild impairment to vascular extension, and blunted tip cell formation [311].

Further evidence to suggest NRP2 regulates tip cell behaviour was found following review of our LFQ mass spectrometry data, which revealed that NRP2 formed candidate interactions with Notch-1, Presenilin-1 and Nicastrin. During tip cell selection, Presenilin-1 and Nicastrin have been implicated in proteolytically processing Notch-1, allowing for the activation of Jagged-1 in stalk cells [312]. Jagged-1 is then known to moderate Notch-1 activity in tip cells, removing the inhibition of NRP1 and VEGFR-2 and promoting their expression to drive tip cell migration [35], [36]. It would be appropriate therefore to examine the expression of NRP2 in retinas depleted for endothelial Jagged-1 during SP vascularisation. If NRP2 expression was found to be impaired, then it would provide strong evidence to suggest that its activity in tip cells is Notch-1 dependent.

Whilst far less is understood regarding the mechanisms coordinating DP development, vertical branching from the SP downwards to initiate deep layer neovascularisation is known to be orchestrated by the spatiotemporal availability of VEGF-A by neuronal VEGFR-2 [295], [298], [305]. DP formation has also been shown to be strictly dependent upon NRP1 expression within the endothelium. Dissimilar to NRP1, NRP2 has been reported not to influence VEGFR-2 mediated signalling in ECs [225], which may explain why we observed no impediment to vertical branching or DP vascularisation upon its individual depletion. This was not found to be the case following the additional co-depletion of α5 integrin however, both the SP and the DP exhibiting similar degrees

of hypervascularisation when compared to retinas harvested from respective Cre-negative control mice. Given that comparable vascular perturbations (and recovery phenotypes) also arose during SP development at P6 upon co-depletion of both NRP2 and α5 integrin, we believe that there exists a degree of cooperation between the two receptors during developmental angiogenesis. As we observed no additional impairment to vertical branching or DP vascularisation upon depletion of both NRP1 and NRP2 compared to when NRP1 is lost individually however, it remains clear that its development is largely a NRP1 dependent process.

4 Final discussion and future directions

The expansion of the vascular network occurs allometrically with tissue growth and development. Accordingly, angiogenesis drives pathological disorders defined by uninhibited neovascularisation [19]. To this end, researchers have, in the past, focussed on attempting to perturb angiogenesis by modulating the expression of core angiogenic receptors known to regulate its progression. Efforts to control pathological angiogenesis by depleting such receptors individually however, have been frustrated by an evolved myriad of compensatory and competing regulatory networks that enable the recovery of vascular defects over time [313]. Only by targeting the expression of multiple receptors simultaneously within the endothelium, have previous members of our laboratory managed to consistently moderate pathological vascular expansion [107].

Historically, the Robinson laboratory has investigated three angiogenic receptors known to regulate the angiogenic cascade, NRP1, α5 integrin, and β3 integrin. During tumorigenesis, the inhibition of NRP1 was only found to impair neovascular development when either or both integrins were also depleted. Co-depleting these receptors, and thereby sensitising pathological angiogenesis to NRP1 disruption, was therefore postulated to provide an effective anti-angiogenic therapeutic strategy [107]. NRP2, the closest structural relative to NRP1, is also known to promote an aggressive cancer phenotype [280], and to interact with α5 integrin [210], [225], however detailed investigations into its mechanistic contributions during the core mechanisms that drive angiogenesis (VEGF-A-driven signalling, adhesion and migration) had been lacking in the field. Despite this, and based on its close structural homology with NRP1, we hypothesised that NRP2, like its ortholog, would function pro-angiogenically to promote vessel growth through its regulatory interactions with α5 integrin. To test this hypothesis, we utilised siRNA mediated depletion of NRP2 in immortalised mLMEC lines depleted for either α5 integrin or NRP1 to elucidate mechanisms by which these three receptors regulate each other's angiogenic involvement. Employing the Cre-loxP system to generate three genetically engineered mouse models in which we would induce endothelial-specific target depletion of NRP2 individually, or in combination with α5 integrin or NRP1, subsequently enabled us to describe a role for NRP2 in models simulating both developmental angiogenesis, and pathological tumorigenesis. Going forward, it would be pertinent to explore NRP2's interactions with other endothelial integrins, such as β3 integrin, in addition to confirming its angiogenic function during other pathological disorders defined by an augmented vascular growth, such as oxygen-induced retinopathy (OIR), a model system which is now a priority to employ in our laboratory going forward.

Various steps in this study were informed by a descriptive set of preliminary data produced by Dr Abdullah Alghamdi, a past member the Robinson laboratory. NRP2 was shown to directly interact with α5 integrin, facilitating FA turnover and EC migration. *In vitro*, we expanded upon these findings, providing us with cellular mechanisms with which we were better able to interpret the results from our animal studies. Not only was NRP2 confirmed to promote the recycling of α5 integrin in mLMECs, but it was also found to do so in a distinct manner to NRP1, utilising a Rab11-directed mechanism of intracellular trafficking to promote initial FA development. Furthermore, NRP2 was found to facilitate core FA signalling cascades by coordinating the complex recruitment of *p*-FAK^{Tyr407} during the transport of α5 integrin. One such signalling cascade that was found to be perturbed following the depletion of NRP2 was the activation of Rac1, a member of the Rho GTPase family with central roles during actin remodelling and nucleation [163]. Indeed, we found that NRP2 promotes stress fibre development in cultured ECs, filopodial extension, and the development of dynamic protrusions *in vivo*. Given the actin cytoskeleton's emerging utility as a highway for endocytic and intracellular traffic [108], it is probable that polarised α5 integrin transport and FA development is directly expedited by NRP2's ability to promote stress fibre remodelling in the cell. Comparing the behaviour of ECs depleted for NRP2 individually to those depleted for both NRP2 and α5 integrin, also enabled us to identify likely points of compensation and temporal regulation between the two receptors. For example, by following the stages succeeding initial attachment to the FN matrix, we see that whilst NRP2 expression remains essential, the requirement for α5 integrin diminishes rapidly. It would therefore be pertinent to explore whether the transition to a more β3 integrin enriched adhesome during FA maturation is also NRP2 dependent. Indeed, evidence of a NRP-β3 integrin signalling axis has been elucidated previously; β3$^{HET\ (fl/wt)}$ ECs exhibit enhanced expression of both NRP1 and NRP2, which, at least in the case of NRP1, promotes its ability for NRP1 to facilitate EC migration over FN matrices [107], [201], [225].

Our *in vitro* investigations subsequently led us to examine the consequences of depleting both NRPs in tandem. NRP1 has previously been reported to promote actin-mediated α5 integrin transport via a Rab5 trafficking route [108], directing us to hypothesise that the combined loss of both NRP receptors would severely impair the ability of ECs to regulate α5 integrin localisation to assembling FAs. This was subsequently found to be the case, α5 integrin failing to reach dynamic cell protrusions along the migratory front of cells, resulting in their failure to migrate over a FN substrate. To complement this, it is important that biotinylation experiments quantifying α5 integrin internalisation and recycling in ECs depleted for both NRP1 and NRP2 are performed, alongside immunocytochemistry studies to assess the spatial localisation of α5 integrin with Rab5

and Rab11 when both NRPs are lost. Assessing the localisation of other Rab GTPases such as Rab21 may also identify points of convergence between NRP1 and NRP2-directed transport of α5 integrin. Substantiating our random migration studies with those assaying GM130^{+} Golgi orientation would further aid in our ability to comment on how NRPs crosstalk to promote polarised migration.

By utilising two tumour progression models, we revealed that endothelial NRP2 directly facilitates a more aggressive cancer phenotype by promoting the growth of pathological neovasculature. When compared against unpublished data produced by the Robinson laboratory, demonstrating that the individual loss of either α5 integrin or NRP1 is insufficient to significantly impair tumorigenesis, we can infer that NRP2 plays a dominant role during pathological angiogenesis. Whilst depleting α5 integrin alongside NRP2 yielded a similar phenotype to our NRP2 single knockout model, loss of both NRPs together severely impeded tumour development and tumour vascularisation, substantiating our *in vitro* findings. We hypothesise here that the functional redundancies between NRP1 and NRP2 enable either one to support the intracellular traffic of α5 integrin individually. Conversely, if both receptors are targeted simultaneously, the processes required to support vessel growth collapse without the functional localisation of α5 integrin in ECs. At the time of writing, additional experiments employing a number of different cancer cell lines to model NRP2's involvement during tumorigenesis are underway to confirm these findings. Likewise, assessing the expression of *p*-FAK^{Tyr407} within NRP2/ α5 integrin, and NRP1/ NRP2 depleted tumour vasculature would provide further insight into the tumour's dependency on FAK activation during NRP-driven angiogenesis.

Assessing the impact of targeting NRP1 and NRP2 in the context of the immune system would also be appropriate moving forward. Increasing evidence suggests that NRP1 can accelerate tumour progression by stabilising regulatory T cell function and survival, in addition to modulating tumour-associated macrophages from infiltrating into the normoxic tumour microenvironment [314], [315]. NRP2-expressing macrophages have also been demonstrated to enhance tumour growth by promoting an immune suppressive response [316]. Considering the impact of depleting the expression of NRP1 and NRP2 within the tumour endothelium, an organ that has an active role in the recruitment and stimulation of leukocytes, in addition to serving as an interface for regulatory T cells trafficking into tissues [317], is vital when attempting to understand the impact of targeting our receptors in a clinical setting.

We have, nevertheless, revealed a novel therapeutic approach whereby co-targeting both endothelial NRP1 and NRP2 expression provides a more effective inhibition of tumour growth than

when either are targeted individually. On account of cancers evolving a range of adaptive escape mechanisms, the identification of original combinations of angiogenic targets to enhance the therapeutic index of anti-VEGF/VEGFR-2 strategies still remains a focus for oncology research. We therefore believe that further investigation into the mechanisms that regulate this novel NRP1/NRP2 axis is required.

Developmental angiogenesis, modelled using the postnatal mouse retina, did not show the same dependency on NRP2 expression as our tumour progression studies however. Rather, the vascularisation of the SP at P6, and indeed the DP at P12, was found to be coordinated by the dominant actions of NRP1; our NRP1/NRP2 depleted line exhibited no additional angiogenic impairment than when NRP1 was depleted individually. Despite observing no defects in SP vascular density at P6, loss of endothelial NRP2 expression was found to impair radial outgrowth. This finding substantiates the loss of directional migration seen in *si*NRP2 ECs *in vitro*, and suggests that NRP2 promotes radial outgrowth by potentiating polarised *p*-FAK-mediated filopodial extension. Assessing Golgi orientation in NRP2 depleted tip cells at P6 would further ratify this hypothesis, in addition to providing further evidence of a degree of functional redundancy between NRP1 and NRP2 during sprouting angiogenesis. Vascular density was found to be perturbed when NRP2 was co-depleted with either α5 integrin or NRP1. It could be inferred here that the various redundancies that exist within the angiogenic cascade to avoid pathology begin to collapse following the targeted loss of multiple pro-angiogenic receptors. This supposition does not hold true when EC sprouting and filopodial extension is considered however. Whilst both are significantly impaired following the individual depletion of NRP2, or when NRP2 is depleted alongside NRP1, upon additional loss of either α5 integrin, tip cell and filopodial numbers return to normal physiological levels. Previous work performed in the Robinson laboratory has intimated that α5 integrin functions to modulate neovascular formation by limiting the pro-angiogenic contributions of β3 integrin. By doing so, it acts to provide an angiogenic break to prevent the hypervascularisation of the SP. It is possible therefore that the co-depletion of both NRP2 and α5 integrin removes this angiogenic inhibition, restoring normal levels of EC sprouting at the vascular front. Nevertheless, we provide strong evidence that NRP2 promotes polarised vascular sprouting and ECM anchorage by regulating FAK phosphorylation. Given that NRP1 regulates paxillin phosphorylation in the same manner [102], further investigation is required to isolate the differential contributions of the NRPs during tip cell activation. As we revealed a marked absence of α5 integrin at dynamic protrusions in cultured ECs depleted for both NRP1 and NRP2, we would also hypothesise that a similar reduction in α5 integrin

at the sprouting angiogenic front of NRP1/NRP2 depleted P6 retinas would be observed should it be examined.

To conclude, it is clear that a complex regulatory network exists within the endothelium between the NRPs and α5 integrin. We elucidate that endothelial NRP1 and NRP2 differentially coordinate developmental and pathological angiogenesis, NRP2 playing an essential role in tumorigenesis, but largely dispensable during physiological vascularisation of the postnatal retina. That being said, we have revealed a promising line of evidence that a dual-combative NRP1/NRP2 targeting approach offers a clinically beneficial method of inhibiting tumorigenesis. Various small-molecule inhibitors directed solely against NRP1, or against its interactions with VEGF-A, are under development [100], [318], however with the exception of one novel inhibitor designed to target its interactions with VEGF-C, none exist to target NRP2 [319], [320]. Based on the results presented in this thesis, we believe that investigations into the design, synthesis and evaluation of small-molecule inhibitors against both endothelial NRPs is warranted. As both NRPs are expressed on the surface of multiple cell types however, the incorporation of the RGD peptide into such inhibitors to specifically target cancer cells on which cell membrane integrins are upregulated, would be essential to moderate any off-target effects that often arise as a result of implementing such antagonists.

Indeed, given more time this thesis would aim to perform a number of repeat allograft tumour studies under an intervention-based regime, using various different cancer cell lines to substantiate our current findings. Utilising the B16F10 murine melanoma cell line would be of particular interest as it is also known to preferentially metastasise to the lung following intravenous injection [321]. As the co-depletion of endothelial NRP1 and NRP2 provided efficient inhibition against primary tumour growth, we would strongly suggest that investigations be carried out to assess the potential benefits of targeting these receptors on metastatic burden and secondary site angiogenesis using this model. Combining our endothelial-specific depletion of NRP1 and NRP2 with a relevant chemotherapeutic may also provide an even more robust degree of tumorigenic inhibition. For example, the clinical benefits of targeting known pro-angiogenic signalling cascades against tumour development have previously remained modest, only minimal increases in progression-free survival rates for various tumour types, including lung, breast, kidney and colon cancers, having been reported following treatment [322]. Only when combined with chemotherapy have such therapies become recognised as an effective strategy against cancer growth, anti-angiogenics acting to selectively prune leaky, and immature tumour-associated vessels to facilitate more efficient delivery of chemotherapeutic agents [323]–[325]. By implementing a similar strategy, it may be possible to induce complete tumour regression.

5 Supplementary information

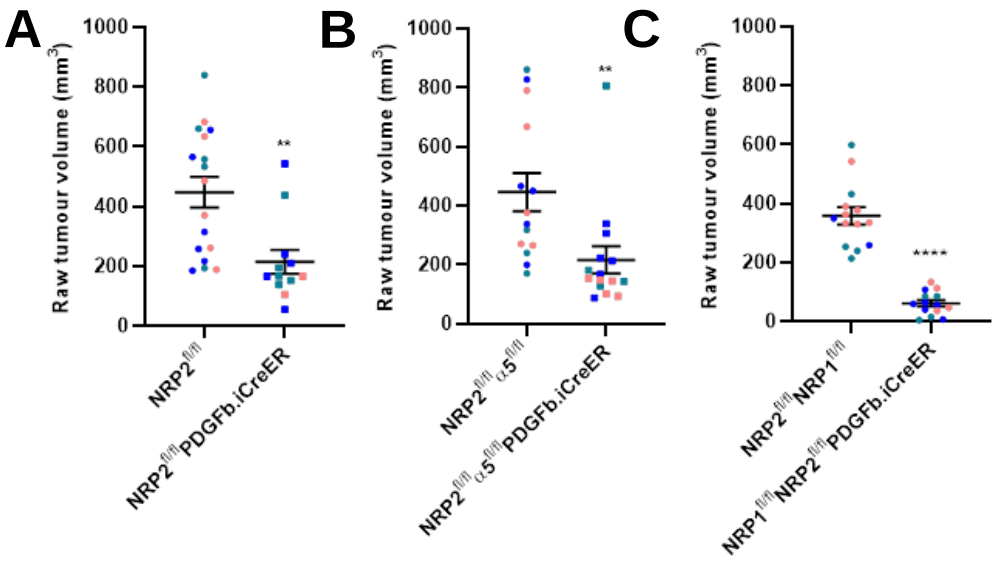

Figure 5.1 Raw tumour volumes. Quantification of raw tumour volumes measured on D18 from NRP2^{flfl} Cre-negative and NRP2^{flfl}PDGFb.iCreER Cre-positive mice. **B**) Quantification of raw tumour volumes measured on D18 from NRP2^{flfl}α5^{flfl} Cre-negative and NRP2^{flfl}α5^{flfl}PDGFb.iCreER Cre-positive mice. **C**) Quantification of raw tumour volumes measured on D18 from NRP1^{flfl}NRP2^{flfl} Cre-negative and NRP1^{flfl}NRP2^{flfl}PDGFb.iCreER Cre-positive mice. Error bars show mean ± SEM; N=3 (n>12); **=P<0.002, ****=P<0.0001, unpaired students t-test (two-tailed).

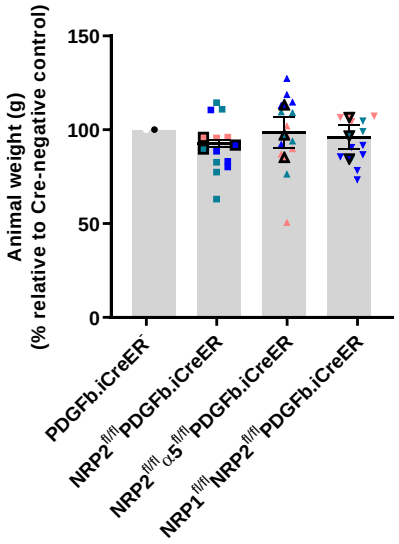

Figure 5.2 Tumour bearing animal weights. Quantification of animal weight (g) measured on D18. Data presented as percentages of the average animal weight (g) observed in respective littermate controls. Error bars show mean ± SEM; N=3 (n≥12).

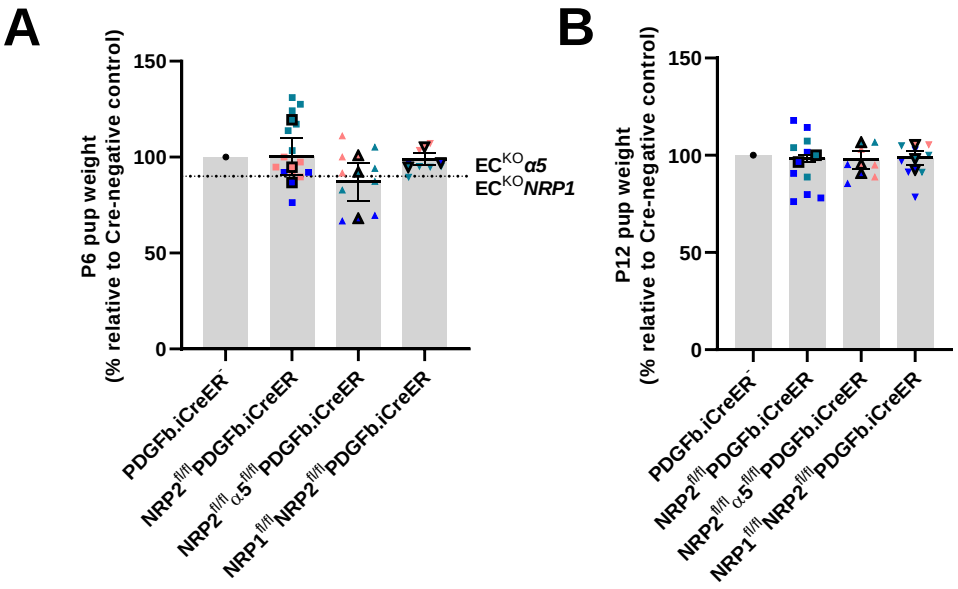

Figure 5.3 P6 and P12 animal weights. Quantification of animal weights measured at P6 (A) and P12 (B) from Cre-negative and Cre-positive mice, presented as a percentage of the average weight observed in respective Cre-negative littermate controls. Error bars show mean ± SEM; N=3 (n>7). Data from NRP1$^{fl/fl}$PDGFb.iCreER and α5$^{fl/fl}$PDGFb.iCreER mice, collected by Dr Robert Johnson prior to commencing this thesis, is also shown when applicable as horizonal dashed lines, for comparison purposes only.

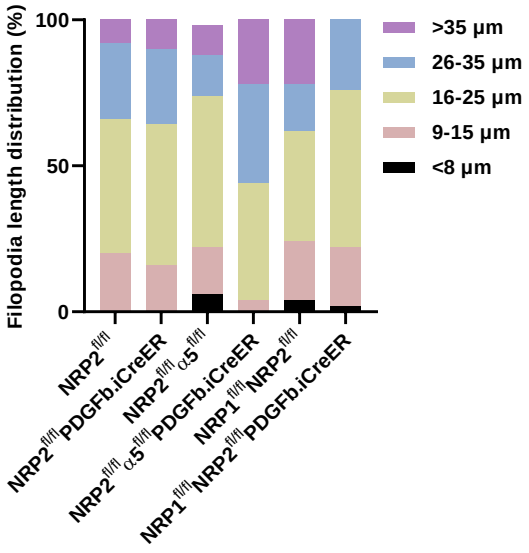

Figure 5.4 Filopodia length distributions. Quantification of filopodial length distribution, presented as percentages between Cre-negative and positive retinas. N=3 (n≥5; 50 filopodia/genotype).

6 Publications

A.A Alghamdi[1] & C. J. Benwell[1], S. J. Atkinson, J. Lambert, R. T. Johnson, and S. D. Robinson, "NRP2 as an Emerging Angiogenic Player; Promoting Endothelial Cell Adhesion and Migration by Regulating Recycling of α5 Integrin," *Front. Cell Dev. Biol.*, vol. 8, no.395, pp. 1–16, 2020, doi: 10.3389/fcell.2020.00395.

C. J. Benwell, J. A. G. E. Taylor, S. D. Robinson, "Endothelial Neuropilin-2 Influences Angiogenesis by Regulating Actin Pattern Development and α5 integrin-*p*-FAK Complex Recruitment to Assembling Adhesion Sites," *FASEB J.*, vol. 35 no.8 pp. 1-19 2021, doi: 10.1096/fj.202100286R.

J. A. G. E Taylor[1], C. J. Benwell[1], S. D. Robinson, "Using immortalised endothelial cells to study the roles of adhesion molecules in VEGF-induced signalling", *Methods Molecular Biology*, 2022

C. J. Benwell, R. T. Johnson, J. A. G. E Taylor, C. A. Price, S. D. Robinson, "Endothelial Neuropilin-1 and Neuropilin-2 are Essential for Tumour Angiogenesis," Cancer Research Communications, 2022

[1] *Joint first authorship*

7 Abbreviations

αSMA: α-smooth muscle actin

Ab: Antibody

ADAMs: A dis-integrin and metalloproteinases

ANG1: Angiopoietein-1

ANG2: Angiopoietein-2

FGF: Fibroblast growth factor

Bp: Base pair

BSA: Bovine serum albumin

Cdc42: Cell division control protein 42

ColIV: Collagen IV

DAPI: 4'6-diamidino-2-phenylindole

dH2O: Distilled water

DLL-4: Delta-like ligand-4

DMEM: Dulbecco's modified eagle medium

DP: Deep vascular plexus

Dyn-2: Dynamin-2

ECs: Endothelial cells

ECM: Extracellular matrix

ECL: Enhanced chemiluminescence

EDTA: Ethylenediaminetetraacetic acid

EE: Early endosome

EEA1: Early endosome antigen-1

EDA-FN: Fibronectin containing extra domain-A

EDB-FN: Fibronectin containing extra domain-B

EGFR: Epidermal growth factor receptor

ERG: ETS related gene

ERK: Extracellular regulated kinase

EtOH: Ethanol

ESB: Electrophoresis sample buffer

F12: Ham's F12 nutrient mixture

FA: Focal Adhesion

FAK: Focal adhesion kinase

FBS: Fetal bovine serum

FGF: Fibroblast growth factor

Fl/fl: Floxed (flanked by loxP sites)

FRET: Fluorescence resonance energy transfer

GAPDH: Glyceraldehyde 3-phosphate dehydrogenase

GEMM: Genetically engineered mouse model

GIPC1: GAIP interacting protein C terminus, member 1

GSK-3: Glycogen synthase kinase-3

HCl: Hydrochloric acid

HEPES: (4-(2-hydroxyethyl)-1-piperazineethanesufonic acid

HET: Heterozygous

HIFs: Hypoxia inducible factors

HRP: Horse-radish peroxidase

HSCs: Hematopoietic stem cells

HSC70: Heat shock cognate 71 kDa

HUAEC: Human umbilical artery endothelial cells

HUVEC: Human umbilical vein endothelial cells

ICAM-2: Intracellular adhesion molecule-2

IF: Immunofluorescence

IMMLEC: Immortalised mouse lung endothelial cell

IP: Intraperitoneal

KO: Knockout

Lamp-1: Lysosome-associated membrane glycoprotein-1

M^r: Molecular weight

MACS: Magnetic activated cell sorting

MAM – (meprin, A-5, mu)

MAPK: Mitogen activated protein kinase

MeOH: Methanol

MLEC: Mouse lung endothelial cell

MMPs: Matrix-metalloproteases

Myo6: Myosin VI

NRP: Neuropilin

NRP1: Neuropilin-1

NRP2: Neuropilin-2

P: Postnatal day

p38MAPK: p38 mitogen activated protein kinase

p130Cas: p130 CRK-associated substrate

PAGE: Polyacrylamide gel electrophoresis

PBS: Phosphate buffered saline

PBST: PBS supplemented with 0.1% Tween-20

PCR: Polymerase chain reaction

PDGF: Platelet Derived Growth Factor

PDZ: PSD-95/Dlg/ZO-1 domain

PFA: Paraformaldehyde

PI3K: Phosphoinositide 3-kinase

PKB: Protein kinase B/AKT

PKC: Protein kinase C

PLC: Phospholipase C

PXN: Paxillin

PyMT: Polyoma-middle-T-antigen

P120RasGAP:

Rac1: Ras-related C3 botulinum toxin substrate 1

RGD: Arginine-Glycine-Asparagine184

ROI: Region of interest

SDS: Sodium dodecyl sulfate

SEA: Serine-Glutamic Acid-Alanine motif

SEM: Standard error of the mean

Sema3A: Semaphorin 3A

SH2: SRC homology 2

Src: Proto-oncogene tyrosine protein kinase

SP: Superficial vascular plexus

TE: Tris-HCl- EDTA

TGF: Transforming growth factor

TGF-β: Transforming growth factor-β

TGN- Trans-Golgi network

Tie2: Tyrosine protein kinase receptor-2

TIMPs: Tissue inhibitors of matrix-metalloproteinases

Tyr: Tyrosine

VASP: Vasodilator-stimulated phosphoprotein

VEGF: Vascular endothelial growth factor

VEGFR: Vascular endothelial growth factor receptor

VEGFR1: VEGF Receptor 1

VEGFR2: VEGF Receptor 2

VEGFR3: VEGF Receptor 3

VSMC: Vascular smooth muscle cells

WB: Western blotting

WT: Wild-type

8 References

[1] R. Werner and I. Flamme, “Vasculogenesis,” *Annu. Rev. Cell. Dev.*, vol. 11, pp. 73–91, 1995.

[2] B. Berridge, J. Van Vleet, and E. Herman, *Cardiovascular system*. Elsivier, 2018.

[3] R. Touyz, A. Montezano, and C. Rosendorff, *Vascular function in health and disease*. Elsivier, 2014.

[4] M. Pugsley and R. Tabrizchi, “The vascular system: an overview od structure and function,” *J. Pharmacol. Toxicol. Methods*, vol. 44, pp. 333–340, 2000.

[5] O. Cleaver and D. A. Melton, “Endothelial signaling during development,” *Nat. Med.*, vol. 9, no. 6, pp. 661–668, 2003, doi: 10.1038/nm0603-661.

[6] A. Plein, A. Fantin, and C. Ruhrberg, “Neuropilin regulation of angiogenesis, arteriogenesis, and vascular permeability,” *Microcirculation*, vol. 21, no. 4, pp. 315–323, 2014, doi: 10.1111/micc.12124.

[7] M. I. Setyawati, C. Y. Tay, D. Docter, R. H. Stauber, and D. T. Leong, “Understanding and exploiting nanoparticles’ intimacy with the blood vessel and blood,” *Chem. Soc. Rev.*, vol. 44, no. 22, pp. 8174–8199, 2015, doi: 10.1039/c5cs00499c.

[8] R. Marcu *et al.*, “Human Organ-Specific Endothelial Cell Heterogeneity,” *iScience*, vol. 4, pp. 20–35, 2018, doi: 10.1016/j.isci.2018.05.003.

[9] E. Iivanainen, V. M. Kähäri, J. Heino, and K. Elenius, “Endothelial cell-matrix interactions,” *Microsc. Res. Tech.*, vol. 60, no. 1, pp. 13–22, 2003, doi: 10.1002/jemt.10238.

[10] A. D. Theocharis, S. S. Skandalis, C. Gialeli, and N. K. Karamanos, “Extracellular matrix structure,” *Adv. Drug Deliv. Rev.*, vol. 97, pp. 4–27, 2016, doi: 10.1016/j.addr.2015.11.001.

[11] P. Singh, C. Carraher, and J. E. Schwarzbauer, “Assembly of fibronectin extracellular matrix,” *Annu. Rev. Cell Dev. Biol.*, vol. 26, pp. 397–419, 2010, doi: 10.1146/annurev-cellbio-100109-104020.

[12] W. S. To and K. S. Midwood, “Plasma and cellular fibronectin: Distinct and independent functions during tissue repair,” *Fibrogenes. Tissue Repair*, vol. 4, no. 1, pp. 1–17, 2011, doi: 10.1186/1755-1536-4-21.

[13] A. K. Chauhan, A. Iaconcig, F. E. Baralle, and A. F. Muro, “Alternative splicing of fibronectin: A mouse model demonstrates the identity of in vitro and in vivo systems and the processing autonomy of regulated exons in adult mice,” *Gene*, vol. 324, no. 1–2, pp. 55–63, 2004, doi: 10.1016/j.gene.2003.09.026.

[14] J. W. Tamkun and R. O. Hynes, “Plasma fibronectin is synthesized and secreted by hepatocytes,” *J. Biol. Chem.*, vol. 258, no. 7, pp. 4641–4647, 1983, doi: 10.1016/s0021-9258(18)32672-3.

[15] L. Xiang, G. Xie, J. Ou, X. Wei, F. Pan, and H. Liang, “The extra domain a of fibronectin increases VEGF-C expression in colorectal carcinoma involving the PI3K/AKT signaling pathway,” *PLoS One*, vol. 7, no. 4, pp. 1–10, 2012, doi: 10.1371/journal.pone.0035378.

[16] P. E. Saw *et al.*, “Extra-domain B of fibronectin as an alternative target for drug delivery and a cancer diagnostic and prognostic biomarker for malignant glioma,” *Theranostics*, vol. 11, no. 2, pp. 941–957, 2020, doi: 10.7150/thno.44948.

[17] J. E. Ferguson, R. W. Kelley, and C. Patterson, “Mechanisms of endothelial differentiation in embryonic vasculogenesis,” *Arterioscler. Thromb. Vasc. Biol.*, vol. 25, no. 11, pp. 2246–2254, 2005, doi: 10.1161/01.ATV.0000183609.55154.44.

[18] K. Krah, V. Mironov, W. Risau, and I. Flamme, “Induction of Vasculogenesis in Quail Blastodisc-Derived Embryoid Bodies,” *Dev. Biol.*, vol. 164, no. 1, pp. 123–132, 1994.

[19] H. S. Baldwin, “Early embryonic vascular development,” *Cardiovasc. Res.*, vol. 31, no. Extra Issue, pp. 34–45, 1996, doi: 10.1016/0008-6363(95)00215-4.

[20] J. Folkman, “What is the evidence that tumors are angiogenesis dependent?,” *J. Natl. Cancer Inst.*, vol. 82, no. 1, pp. 4–7, 1990, doi: 10.1093/jnci/82.1.4.

[21] A. F. Karamysheva, “Mechanisms of angiogenesis,” *Biochem.*, vol. 73, no. 7, pp. 751–762, 1997, doi: 10.1134/S0006297908070031.

[22] Z. K. Otrock, R. A. R. Mahfouz, J. A. Makarem, and A. I. Shamseddine, “Understanding the biology of angiogenesis: Review of the most important molecular mechanisms,” *Blood Cells, Mol. Dis.*, vol. 39, no. 2, pp. 212–220, 2007, doi: 10.1016/j.bcmd.2007.04.001.

[23] D. Noden, “Embryonic Origins and Assembly of Blood Vessels,” *Am. Rev. Respir. Dis.*, vol. 140, no. 4, pp. 1097–1103, 1989.

[24] R. Hynes, “Integrins: Bidirectional Allosteric Signaling Machines,” *Cell*, vol. 110, pp. 673–687, 2002.

[25] U. Fiedler and H. G. Augustin, “Angiopoietins: a link between angiogenesis and inflammation,” *Trends Immunol.*, vol. 27, no. 12, 2006.

[26] A. N. Stratman *et al.*, “Interactions between mural cells and endothelial cells stabilize the developing zebrafish dorsal aorta,” *Dev.*, vol. 144, no. 1, pp. 115–127, 2017, doi: 10.1242/dev.143131.

[27] L. Evensen *et al.*, “Mural cell associated VEGF is required for organotypic vessel formation,” *PLoS One*, vol. 4, no. 6, 2009, doi: 10.1371/journal.pone.0005798.

[28] P. Carmeliet, “Mechanisms of angiogenesis and arteriogenesis,” *Nat. Med.*, vol. 6, 2000.

[29] P. Carmeliet and R. K. Jain, “Molecular mechanisms and clinical applications of angiogenesis,” *Nature*, vol. 473, no. 7347, pp. 298–307, 2011, doi: 10.1038/nature10144.

[30] T. L. Haas *et al.*, “Matrix metalloproteinase activity is required for activity-induced angiogenesis in rat skeletal muscle,” *Am. J. Physiol. - Hear. Circ. Physiol.*, vol. 279, no. 4 48-4, pp. 1540–1547, 2000, doi: 10.1152/ajpheart.2000.279.4.h1540.

[31] M. Papetti and I. M. Herman, “Mechanisms of normal and tumor-derived angiogenesis,” *Am. J. Physiol. - Cell Physiol.*, vol. 282, no. 5 51-5, 2002, doi: 10.1152/ajpcell.00389.2001.

[32] H. Gerhardt *et al.*, “VEGF guides angiogenic sprouting utilizing endothelial tip cell filopodia,” *J. Cell Biol.*, vol. 161, no. 6, pp. 1163–1177, 2003, doi: 10.1083/jcb.200302047.

[33] D. Stenzel *et al.*, “Endothelial basement membrane limits tip cell formation by inducing Dll4/Notch signalling in vivo,” *EMBO Rep.*, vol. 12, no. 11, pp. 1135–1143, 2011, doi: 10.1038/embor.2011.194.

[34] S. Herbert and D. Stainier, “Molecular control of endothelial cell behaviour during blood vessel morphogenesis,” *Nat. Rev Mol Cell Biol*, vol. 12, pp. 551–564, 2011.

[35] L. Jakobsson *et al.*, “Endothelial cells dynamically compete for the tip cell position during angiogenic sprouting,” *Nat. Cell Biol.*, vol. 12, no. 10, pp. 943–953, 2010, doi: 10.1038/ncb2103.

[36] R. Benedito *et al.*, “The Notch Ligands Dll4 and Jagged1 Have Opposing Effects on Angiogenesis,” *Cell*, vol. 137, no. 6, pp. 1124–1135, 2009, doi: 10.1016/j.cell.2009.03.025.

[37] A. Fantin *et al.*, “Tissue macrophages act as cellular chaperones for vascular anastomosis downstream of VEGF-mediated endothelial tip cell induction,” *Blood*, vol. 116, no. 5, pp. 829–840, 2010, doi: 10.1182/blood-2009-12-257832.

[38] G. Bergers and S. Song, “The role of pericytes in blood-vessel formation and maintenance,” *Neuro. Oncol.*, vol. 7, no. 4, pp. 452–464, 2005, doi: 10.1215/s1152851705000232.

[39] W. Auerbach and R. Auerbach, “Angiogenesis inhibition: A review,” *Pharmacol. Ther.*, vol. 63, no. 3, pp. 265–311, 1994, doi: 10.1016/0163-7258(94)90027-2.

[40] R. H. Adams *et al.*, “Roles of ephrinB ligands and EphB receptors in cardiovascular development: Demarcation of arterial/venous domains, vascular morphogenesis, and sprouting angiogenesis,” *Genes Dev.*, vol. 13, no. 3, pp. 295–306, 1999, doi: 10.1101/gad.13.3.295.

[41] R. H. Adams, “Molecular control of arterial-venous blood vessel identity,” *J. Anat.*, vol. 202, no. 1, pp. 105–112, 2003, doi: 10.1046/j.1469-7580.2003.00137.x.

[42] F. le Noble *et al.*, “Flow regulates arterial-venous differentiation in the chick embryo yolk sac,” *Development*, vol. 131, no. 2, pp. 361–375, 2004, doi: 10.1242/dev.00929.

[43] M. Simons, “An inside view: VEGF receptor trafficking and signaling,” *Physiology*, vol. 27, no. 4, pp. 213–222, 2012, doi: 10.1152/physiol.00016.2012.

[44] W. Leung, D, G. Cachianes, J. Kuang, W, V. Goeddel, D, and N. Ferrara, “Vascular endothelial growth factor is a secreted angiogenic mitogen,” *Science (80-.).*, vol. 246, no. 4935, pp. 1306–1309, 1989, doi: 10.1126/science.2479986.

[45] L. Miquerol, B. L. Langille, and A. Nagy, “Embryonic development is disrupted by modest increases in vascular endothelial growth factor gene expression,” *Development*, vol. 127, no. 18, pp. 3941–3946, 2000.

[46] A. Hoeben, B. Landuyt, M. Highley, H. Wildiers, A. Van Oosterom, and E. De Bruijn, “Vascular Endothelial Growth Factor and Angiogenesis,” *Phamacological Rev.*, vol. 56, no. 4, pp. 549–580, 2004, doi: https://doi.org/10.1124/pr.56.4.3.

[47] H. Dvorak, “Vascular Permeability Factor/Vascular Endothelial Growth Factor: A Critical Cytokine in Tumor Angiogenesis and a Potential Target for Diagnosis and Therapy,” *J. Clin. Oncol.*, vol. 20, no. 21, pp. 4368–4380, 2002, doi: https://doi.org/10.1200/JCO.2002.10.088.

[48] M. Simons, E. Gordon, and L. Claesson-Welsh, “Mechanisms and regulation of endothelial VEGF receptor signalling,” *Nat. Rev.*, vol. 17, pp. 611–625, 2016.

[49] L. Jakeman, M. Armanini, H. Phillips, and N. Ferrara, “Developmental expression of binding sites and messenger ribonucleic acid for vascular endothelial growth factor suggests a role for this protein in vasculogenesis and angiogenesis,” *Endocrinology*, vol. 133, no. 2, pp. 848–859, 1993, doi: https://doi.org/10.1210/en.133.2.848.

[50] P. Carmeliet *et al.*, “Abnormal blood vessel development and lethality in embryos lacking a

single VEGF allele," *Nature*, vol. 380, pp. 435–439, 1996.

[51] N. Ferrara *et al.*, "Heterozygous embryonic lethality induced by targeted inactivation of the VEGF gene," *Nature*, vol. 380, pp. 439–442, 1996.

[52] J. J. Haigh, H. P. Gerber, N. Ferrara, and E. F. Wagner, "Conditional inactivation of VEGF-A in areas of collagen2a1 expression results in embryonic lethality in the heterozygous state," *Development*, vol. 127, no. 7, pp. 1445–1453, 2000.

[53] X. Ren *et al.*, "FOXF1 transcription factor is required for formation of embryonic vasculature by regulating VEGF signaling in endothelial cells," *Circ. Res.*, vol. 115, no. 8, pp. 709–720, 2014, doi: 10.1161/CIRCRESAHA.115.304382.

[54] M. J. Cross, J. Dixelius, T. Matsumoto, and L. Claesson-Welsh, "VEGF-receptor signal transduction," *Trends Biochem. Sci.*, vol. 28, no. 9, pp. 488–494, 2003, doi: 10.1016/S0968-0004(03)00193-2.

[55] N. Ferrara, H. P. Gerber, and J. LeCouter, "The biology of VEGF and its receptors," *Nat. Med.*, vol. 9, no. 6, pp. 669–676, 2003, doi: 10.1038/nm0603-669.

[56] S. Koch, S. Tugues, X. Li, L. Dualandi, and L. Claesson-Welsh, "Signal transduction by vascular endothelial growth factor receptors," *Biochem. J.*, vol. 437, no. 2, pp. 169–183, 2011.

[57] N. Ferrara, "Vascular endothelial growth factor: Basic science and clinical progress," *Endocr. Rev.*, vol. 25, no. 4, pp. 581–611, 2004, doi: 10.1210/er.2003-0027.

[58] H. Takahashi and M. Shibuya, "The vascular endothelial growth factor (VEGF)/VEGF receptor system and its role under physiological and pathological conditions," *Clin. Sci.*, vol. 109, no. 3, pp. 227–241, 2005, doi: https://doi.org/10.1042/CS20040370.

[59] M. Shibuya, "Vascular Endothelial Growth Factor (VEGF) and Its Receptor (VEGFR) Signaling in Angiogenesis: A Crucial Target for Anti- and Pro-Angiogenic Therapies," *Genes and Cancer*, vol. 2, no. 12, pp. 1097–1105, 2011, doi: 10.1177/1947601911423031.

[60] S. Masoumi Moghaddam, A. Amini, D. L. Morris, and M. H. Pourgholami, "Significance of vascular endothelial growth factor in growth and peritoneal dissemination of ovarian cancer," *Cancer Metastasis Rev.*, vol. 31, no. 1–2, pp. 143–162, 2012, doi: 10.1007/s10555-011-9337-5.

[61] G. Fong, J. Rossant, M. Gertsenstein, and L. Breitman, M, "Role of the Flt-1 receptor tyrosine kinase in regulating the assembly of vascular endothelium," *Nature*, vol. 376, pp. 66–70, 1995.

[62] G. Zarkada, K. Heinolainen, T. Makinen, Y. Kubota, and K. Alitalo, "VEGFR3 does not sustain retinal angiogenesis without VEGFR2," vol. 112, no. 3, 2015, doi: 10.1073/pnas.1423278112.

[63] A. Alvarez-Aznar, L. Muhl, and K. Gaengel, "VEGF Receptor Tyrosine Kinases: Key Regulators of Vascular Function," *Curr. Top. Dev. Biol.*, vol. 123, pp. 433–482, 2017, doi: https://doi.org/10.1016/bs.ctdb.2016.10.001.

[64] S. Soker, S. Takashima, H. Q. Miao, G. Neufeld, and M. Klagsbrun, "Neuropilin-1 is expressed by endothelial and tumor cells as an isoform- specific receptor for vascular endothelial growth factor," *Cell*, vol. 92, no. 6, pp. 735–745, 1998, doi: 10.1016/S0092-8674(00)81402-6.

[65] I. Zachary, "Neuropilins: Role in Signalling, Angiogenesis and Disease," *Chem Immunol*

Allergy, vol. 99, pp. 37–70, 2014.

[66] A. Sharma, J. Verhaagen, and A. R. Harvey, "Receptor complexes for each of the class 3 Semaphorins," *Front. Cell. Neurosci.*, vol. 6, no. JUNE 2012, pp. 1–13, 2012, doi: 10.3389/fncel.2012.00028.

[67] S. Takagi, T. Tsuji, T. Amagai, T. Takamatsu, and H. Fujisawa, "Specific cell surface labels in the visual centers of Xenopus laevis tadpole identified using monoclonal antibodies," *Dev. Biol.*, vol. 122, no. 1, pp. 90–100, 1987, doi: 10.1016/0012-1606(87)90335-6.

[68] M. Klagsbrun and A. Shimizu, "Semaphorin 3E , an exception to the rule Find the latest version : Semaphorin 3E , an exception to the rule," *J. Clin. Invest.*, vol. 120, no. 8, pp. 2658–2660, 2010, doi: 10.1172/JCI44110.2658.

[69] G. J. Prud'homme and Y. Glinka, "Neuropilins are multifunctional coreceptors involved in tumor initiation, growth, metastasis and immunity," *Oncotarget*, vol. 3, no. 9, pp. 921–939, 2012, doi: 10.18632/oncotarget.626.

[70] R. E. Bachelder *et al.*, "Competing autocrine pathways involving alternative neuropilin-1 ligands regulate chemotaxis of carcinoma cells," *Cancer Res.*, vol. 63, no. 17, pp. 5230–5233, 2003.

[71] S. Moretti *et al.*, "Semaphorin3A signaling controls Fas (CD95)-mediated apoptosis by promoting Fas translocation into lipid rafts," *Blood*, vol. 111, no. 4, pp. 2290–2299, 2008, doi: 10.1182/blood-2007-06-096529.

[72] A. Vacca *et al.*, "Loss of inhibitory semaphorin 3A (SEMA3A) autocrine loops in bone marrow endothelial cells of patients with multiple myeloma," *Blood*, vol. 108, no. 5, pp. 1661–1667, 2006, doi: 10.1182/blood-2006-04-014563.

[73] D. R. Bielenberg, A. Shimizu, and M. Klagsbrun, "Chapter 15 Semaphorin-Induced Cytoskeletal Collapse and Repulsion of Endothelial Cells," *Methods Enzymol.*, vol. 443, no. 08, pp. 299–314, 2008, doi: 10.1016/S0076-6879(08)02015-6.

[74] A. Sakurai, C. Doci, and J. S. Gutkind, "Semaphorin signaling in angiogenesis, lymphangiogenesis and cancer," *Cell Res.*, vol. 22, no. 1, pp. 23–32, 2012, doi: 10.1038/cr.2011.198.

[75] G. B. Whitaker, B. J. Limberg, and J. S. Rosenbaum, "Vascular Endothelial Growth Factor Receptor-2 and Neuropilin-1 Form a Receptor Complex that is Responsible for the Differential Signaling Potency of VEGF165 and VEGF121," *J. Biol. Chem.*, vol. 276, no. 27, pp. 25520–25531, 2001, doi: 10.1074/jbc.M102315200.

[76] G. Neufeld, T. Cohen, N. Shraga, T. Lange, O. Kessler, and Y. Herzog, "The neuropilins: Multifunctional semaphorin and VEGF receptors that modulate axon guidance and angiogenesis," *Trends Cardiovasc. Med.*, vol. 12, no. 1, pp. 13–19, 2002, doi: 10.1016/S1050-1738(01)00140-2.

[77] S. Soker, H. Miao, M. Nomi, S. Takashima, and M. Klagsbrun, "VEGF 165 Mediates Formation of Complexes Containing VEGFR-2 and Neuropilin-1 That Enhance VEGF 165 -Receptor Binding," *J. Cell. Biochem.*, vol. 85, pp. 357–368, 2002.

[78] H. Fujisawa, T. Kitsukawa, A. Kawakami, S. Takagi, M. Shimizu, and T. Hirata, "Roles of a neuronal cell-surface molecule, neuropilin, in nerve fiber fasciculation and guidance," *Cell Tissue Res.*, vol. 290, pp. 465–470, 1997.

[79] Z. He and M. Tessier-Lavigne, “Neuropilin is a receptor for the axonal chemorepellent semaphorin III,” *Cell*, vol. 90, no. 4, pp. 739–751, 1997, doi: 10.1016/S0092-8674(00)80534-6.

[80] M. Klagsbrun, S. Takashima, and R. Mamluk, *The Role of Neuropilin in Vascular and Tumour Biology*. Springer, Boston, MA, 2002.

[81] P. Gaur *et al.*, “Role of class 3 semaphorins and their receptors in tumor growth and angiogenesis,” *Clin. Cancer Res.*, vol. 15, no. 22, pp. 6763–6770, 2009, doi: 10.1158/1078-0432.CCR-09-1810.

[82] R. Mamluk, Z. Gechtman, M. E. Kutcher, N. Gasiunas, J. Gallagher, and M. Klagsbrun, “Neuropilin-1 binds vascular endothelial growth factor 165, placenta growth factor-2, and heparin via its b1b2 domain,” *J. Biol. Chem.*, vol. 277, no. 27, pp. 24818–24825, 2002, doi: 10.1074/jbc.M200730200.

[83] H. Fujisawa, *From the Discovery of Neuropilin to the Determination of its Adhesion Sites*. Springer, Boston, MA, 2002.

[84] Q. Schwarz and C. Ruhrberg, “Neuropilin, you gotta let me know: Should I stay or should I go?,” *Cell Adhes. Migr.*, vol. 4, no. 1, pp. 61–66, 2010, doi: 10.4161/cam.4.1.10207.

[85] L. M. Ellis, “The role of neuropilins in cancer,” *Mol. Cancer Ther.*, vol. 5, no. 5, pp. 1099–1107, 2006, doi: 10.1158/1535-7163.MCT-05-0538.

[86] C. Prahst *et al.*, “Neuropilin-1-VEGFR-2 complexing requires the PDZ-binding domain of neuropilin-1,” *J. Biol. Chem.*, vol. 283, no. 37, pp. 25110–25114, 2008, doi: 10.1074/jbc.C800137200.

[87] G. Zhang *et al.*, “Neuropilin-1 (NRP-1)/GIPC1 pathway mediates glioma progression,” *Tumour Biol.*, vol. 37, pp. 13777–13788, 2016.

[88] H. Cai and R. R. Reed, “Cloning and characterization of neuropilin-1-interacting protein: A PSD- 95/Dlg/ZO-1 domain-containing protein that interacts with the cytoplasmic domain of neuropilin-1,” *J. Neurosci.*, vol. 19, no. 15, pp. 6519–6527, 1999, doi: 10.1523/jneurosci.19-15-06519.1999.

[89] Y. Gao, M. Li, W. Chen, and M. Simons, “Synectin, syndecan-4 cytoplasmic domain binding PDZ protein, inhibits cell migration,” *J. Cell. Physiol.*, vol. 184, no. 3, pp. 373–379, 2000, doi: 10.1002/1097-4652(200009)184:3<373::AID-JCP12>3.0.CO;2-I.

[90] K. Ballmer-Hofer, A. E. Andersson, L. E. Ratcliffe, and P. Berger, “Neuropilin-1 promotes VEGFR-2 trafficking through Rab11 vesicles thereby specifying signal output,” *Blood*, vol. 118, no. 3, pp. 816–826, 2011, doi: 10.1182/blood-2011-01-328773.

[91] A. Lanahan *et al.*, “The Neuropilin 1 Cytoplasmic Domain Is Required for VEGF-A-Dependent Arteriogenesis,” *Dev. Cell*, vol. 25, no. 2, pp. 156–168, 2013, doi: 10.1016/j.devcel.2013.03.019.

[92] A. Salikhova *et al.*, “Vascular endothelial growth factor and semaphorin induce neuropilin-1 endocytosis via separate pathways,” *Circ. Res.*, vol. 103, no. 6, pp. 71–79, 2008, doi: 10.1161/CIRCRESAHA.108.183327.

[93] T. Kawasaki *et al.*, “A requirement for neuropilin-1 in embryonic vessel formation,” *Development*, vol. 126, no. 21, pp. 4895–4902, 1999.

[94] A. Fantin, Q. Schwarz, K. Davidson, E. M. Normando, L. Denti, and C. Ruhrberg, “The cytoplasmic domain of neuropilin 1 is dispensable for angiogenesis, but promotes the spatial separation of retinal arteries and veins,” *Development*, vol. 138, no. 19, pp. 4185–4191, 2011, doi: 10.1242/dev.070037.

[95] A. Fantin, A. Plein, and C. Ruhrberg, “Neuropilin signalling in vascular development and pathology,” *Curr. Angiogenes.*, vol. 1, no. 2, pp. 125–138, 2012.

[96] T. Kitsukawa, A. Shimono, A. Kawakami, H. Kondoh, and H. Fujisawa, “Overexpression of a membrane protein, neuropilin, in chimeric mice causes anomalies in the cardiovascular system, nervous system and limbs,” *Development*, vol. 121, no. 12, pp. 4309–4318, 1995.

[97] H. Gerhardt, C. Ruhrberg, A. Abramsson, H. Fujisawa, D. Shima, and C. Betsholtz, “Neuropilin-1 is required for endothelial tip cell guidance in the developing central nervous system,” *Dev. Dyn.*, vol. 231, no. 3, pp. 503–509, 2004, doi: 10.1002/dvdy.20148.

[98] A. Fantin *et al.*, “NRP1 acts cell autonomously in endothelium to promote tip cell function during sprouting angiogenesis,” *Blood*, vol. 121, no. 12, pp. 2352–2362, 2013, doi: https://doi.org/10.1182/blood-2012-05-424713.

[99] P. Fernández-Robredo, S. Selvam, M. B. Powner, D. A. Sim, and M. Fruttiger, “Neuropilin 1 involvement in choroidal and retinal neovascularisation,” *PLoS One*, vol. 12, no. 1, pp. 1–11, 2017, doi: 10.1371/journal.pone.0169865.

[100] A. Jarvis *et al.*, “Small molecule inhibitors of the neuropilin-1 vascular endothelial growth factor A (VEGF-A) interaction,” *J. Med. Chem.*, vol. 53, no. 5, pp. 2215–2226, 2010, doi: 10.1021/jm901755g.

[101] B. Herzog, C. Pellet-Many, G. Britton, B. Hartzoulakis, and I. C. Zachary, “VEGF binding to NRP1 is essential for VEGF stimulation of endothelial cell migration, complex formation between NRP1 and VEGFR2, and signaling via FAK Tyr407 phosphorylation,” *Mol. Biol. Cell*, vol. 22, no. 15, pp. 2766–2776, 2011, doi: 10.1091/mbc.E09-12-1061.

[102] C. Raimondi, A. Fantin, A. Lampropoulou, L. Denti, A. Chikh, and C. Ruhrberg, “Imatinib inhibits VEGF-independent angiogenesis by targeting neuropilin 1- dependent ABL1 activation in endothelial cells,” *J. Exp. Med.*, vol. 211, no. 6, pp. 1167–1183, 2014, doi: 10.1084/jem.20132330.

[103] A. Fantin *et al.*, “Neuropilin 1 (NRP1) hypomorphism combined with defective VEGF-A binding reveals novel roles for NRP1 in developmental and pathological angiogenesis,” *Dev.*, vol. 141, no. 3, pp. 556–562, 2014, doi: 10.1242/dev.103028.

[104] C. Pellet-Many, P. Frankel, H. Jia, and I. Zachary, “Neuropilins: Structure, function and role in disease,” *Biochem. J.*, vol. 411, no. 2, pp. 211–226, 2008, doi: 10.1042/BJ20071639.

[105] D. R. Bielenberg, Y. Hida, A. Shimizu, A. Kaipainen, C. C. Kreuter, MKim, and M. Klagsbrun, “Semaphorin 3F , a chemorepulsant for endothelial cells , induces a ...,” *J Clin Invest*, vol. 114, no. 9, pp. 1260–1271, 2004, doi: 10.1172/JCI200421378.1260.

[106] M. Fukasawa, A. Matsushita, and M. Korc, “Neuropilin-1 interacts with integrin β1 and modulates pancreatic cancer cell growth, survival and invasion,” *Cancer Biol. Ther.*, vol. 6, no. 8, pp. 1184–1191, 2007, doi: 10.4161/cbt.6.8.4363.

[107] T. S. Ellison *et al.*, “Suppression of β3-integrin in mice triggers a neuropilin-1- dependent change in focal adhesion remodelling that can be targeted to block pathological

angiogenesis," *DMM Dis. Model. Mech.*, vol. 8, no. 9, pp. 1105–1119, 2015, doi: 10.1242/dmm.019927.

[108] D. Valdembri *et al.*, "Neuropilin-1/GIPC1 signaling regulates α5β1 integrin traffic and function in endothelial cells," *PLoS Biol.*, vol. 7, no. 1, 2009, doi: 10.1371/journal.pbio.1000025.

[109] L. Yuan *et al.*, "Abnormal lymphatic vessel development in neuropilin 2 mutant mice," *Development*, vol. 129, no. 20, pp. 4797–4806, 2002.

[110] Y. Herzog, C. Kalcheim, N. Kahane, R. Reshef, and G. Neufeld, "Differential expression of neuropilin-1 and neuropilin-2 in arteries and veins," *Mech. Dev.*, vol. 109, no. 1, pp. 115–119, 2001, doi: 10.1016/S0925-4773(01)00518-4.

[111] K. Bouvrée *et al.*, "Semaphorin3A, Neuropilin-1, and PlexinA1 are required for lymphatic valve formation," *Circ. Res.*, vol. 111, no. 4, pp. 437–445, 2012, doi: 10.1161/CIRCRESAHA.112.269316.

[112] G. Jurisic *et al.*, "An unexpected role of semaphorin3A-neuropilin-1 signaling in lymphatic vessel maturation and valve formation," *Circ. Res.*, vol. 111, no. 4, pp. 426–436, 2012, doi: 10.1161/CIRCRESAHA.112.269399.

[113] P. Mucka *et al.*, "Inflammation and Lymphedema Are Exacerbated and Prolonged by Neuropilin 2 Deficiency," *Am. J. Pathol.*, vol. 186, no. 11, pp. 2803–2812, 2016, doi: 10.1016/j.ajpath.2016.07.022.

[114] S. Takashima *et al.*, "Targeting of both mouse neuropilin-1 and neuropilin-2 genes severely impairs developmental yolk sac and embryonic angiogenesis," *Proc. Natl. Acad. Sci. U. S. A.*, vol. 99, no. 6, pp. 3657–3662, 2002, doi: 10.1073/pnas.022017899.

[115] B. Favier *et al.*, "Neuropilin-2 interacts with VEGFR-2 and VEGFR-3 and promotes human endothelial cell survival and migration," *Blood*, vol. 108, no. 4, pp. 1243–1250, 2006, doi: 10.1182/blood-2005-11-4447.

[116] M. W. Parker, P. Xu, X. Li, and C. W. Vander Kooi, "Structural Basis for Selective Vascular Endothelial Growth," vol. 287, no. 14, pp. 11082–11089, 2012, doi: 10.1074/jbc.M111.331140.

[117] T. Karpanen *et al.*, "Functional interaction of VEGF-C and VEGF-D with neuropilin receptors," *FASEB J.*, vol. 20, no. 9, pp. 1462–1472, 2006, doi: 10.1096/fj.05-5646com.

[118] J. Shen *et al.*, "Deficiency of neuropilin 2 suppresses VEGF-induced retinal neovascularization," *Mol. Med.*, vol. 10, no. 1–6, pp. 12–18, 2004, doi: 10.2119/2004-00017.Campochiaro.

[119] M. Fakhari *et al.*, "Selective upregulation of vascular endothelial growth factor receptors neuropilin-1 and -2 in human neuroblastoma," *Cancer*, vol. 94, no. 1, pp. 258–263, 2002, doi: 10.1002/cncr.10177.

[120] T. Kawakami *et al.*, "Neuropilin 1 and neuropilin 2 co-expression is significantly correlated with increased vascularity and poor prognosis in nonsmall cell lung carcinoma," *Cancer*, vol. 95, no. 10, pp. 2196–2201, 2002, doi: 10.1002/cncr.10936.

[121] Y. Tomizawa *et al.*, "Inhibition of lung cancer cell growth and induction of apoptosis after reexpression of 3p21.3 candidate tumor suppressor gene SEMA3B," *Proc. Natl. Acad. Sci. U.*

S. A., vol. 98, no. 24, pp. 13954–13959, 2001, doi: 10.1073/pnas.231490898.

[122] S. Lantuéjoul, B. Constantin, H. Drabkin, C. Brambilla, J. Roche, and E. Brambilla, "Expression of VEGF, semaphorin SEMA3F, and their common receptors neuropilins NP1 and NP2 in preinvasive bronchial lesions, lung tumours, and cell lines," *J. Pathol.*, vol. 200, no. 3, pp. 336–347, 2003, doi: 10.1002/path.1367.

[123] A. Vales *et al.*, "Myeloid leukemias express a broad spectrum of VEGF receptors including neuropilin-1 (NRP-1) and NRP-2," *Leuk. Lymphoma*, vol. 48, no. 10, pp. 1997–2007, 2007, doi: 10.1080/10428190701534424.

[124] R. E. Bachelder, G. Robinson, J. Chung, M. A. Wendt, L. M. Shaw, and A. M. Mercurio, "Vascular endothelial growth factor is an autocrine survival factor for neuropilin-expressing breast carcinoma cells," *Cancer Res.*, vol. 61, no. 15, pp. 5736–5740, 2001.

[125] K. Fukahi, M. Fukasawa, G. Neufeld, J. Itakura, and M. Korc, "Aberrant Expression of Neuropilin-1 and -2 in Human Pancreatic Cancer Cells," *Clin. Cancer Res.*, vol. 10, no. 2, pp. 581–590, 2004, doi: 10.1158/1078-0432.CCR-0930-03.

[126] M. J. Gray *et al.*, "Therapeutic targeting of neuropilin-2 on colorectal carcinoma cells implanted in the murine liver," *J. Natl. Cancer Inst.*, vol. 100, no. 2, pp. 109–120, 2008, doi: 10.1093/jnci/djm279.

[127] N. A. Dallas *et al.*, "Neuropilin-2-mediated tumor growth and angiogenesis in pancreatic adenocarcinoma," *Clin. Cancer Res.*, vol. 14, no. 24, pp. 8052–8060, 2008, doi: 10.1158/1078-0432.CCR-08-1520.

[128] H. S. Ong *et al.*, "Cytoplasmic neuropilin 2 is associated with metastasis and a poor prognosis in early tongue cancer patients," *Int. J. Oral Maxillofac. Surg.*, vol. 46, no. 10, pp. 1205–1219, 2017, doi: 10.1016/j.ijom.2017.03.035.

[129] X. Luo *et al.*, "Vascular NRP2 triggers PNET angiogenesis by activating the SSH1-cofilin axis," *Cell Biosci.*, vol. 10, no. 1, pp. 1–16, 2020, doi: 10.1186/s13578-020-00472-6.

[130] C. Grandclement *et al.*, "Neuropilin-2 expression promotes TGF-β1-Mediated epithelial to mesenchymal transition in colorectal cancer cells," *PLoS One*, vol. 6, no. 7, 2011, doi: 10.1371/journal.pone.0020444.

[131] A. Sodhi *et al.*, "Angiopoietin-like 4 binds neuropilins and cooperates with VEGF to induce diabetic macular edema," *J. Clin. Invest.*, vol. 129, no. 11, pp. 4593–4608, 2019, doi: 10.1172/JCI120879.

[132] J. L. Harman, J. Sayers, C. Chapman, and C. Pellet-Many, "Emerging roles for neuropilin-2 in cardiovascular disease," *Int. J. Mol. Sci.*, vol. 21, no. 14, pp. 1–18, 2020, doi: 10.3390/ijms21145154.

[133] D. E. Ingber, "Fibronectin controls capillary endothelial cell growth by modulating cell shape," *Proc. Natl. Acad. Sci. U. S. A.*, vol. 87, no. 9, pp. 3579–3583, 1990, doi: 10.1073/pnas.87.9.3579.

[134] R. A. F. Clark, P. DellaPelle, E. Manseau, J. M. Lanigan, H. F. Dvorak, and R. B. Colvin, "Blood vessel fibronectin increases in conjunction with endothelial cell proliferation and capillary ingrowth during wound healing," *J. Invest. Dermatol.*, vol. 79, no. 5, pp. 269–276, 1982, doi: 10.1111/1523-1747.ep12500076.

[135] R. Hynes, “Integrins: A Family of Cell Surface Receptors,” *Cell*, vol. 48, no. 4, pp. 549–554, 1987.

[136] C. Bökel and N. H. Brown, “Integrins in development: Moving on, responding to, and sticking to the extracellular matrix,” *Dev. Cell*, vol. 3, no. 3, pp. 311–321, 2002, doi: 10.1016/S1534-5807(02)00265-4.

[137] M. Srichai and R. Zent, *Integrin Structure and Function: Cell-Extracellular Matrix Interactions in Cancer*. Springer, Boston, MA, 2010.

[138] I. Campbell and M. Humphries, *Integrin Structure, Activation and Interactions*. Cold Spring Harbor Perspectives in Biology, 2011.

[139] L. Pan, Y. Zhao, Z. Yuan, and G. Qin, “Research advances on structure and biological functions of integrins,” *Springerplus*, vol. 5, no. 1, 2016, doi: 10.1186/s40064-016-2502-0.

[140] E. F. Plow, J. Meller, and T. V. Byzova, “Integrin function in vascular biology,” *Curr. Opin. Hematol.*, vol. 21, no. 3, pp. 241–247, 2014, doi: 10.1097/moh.0000000000000042.

[141] P. J. Sims, M. H. Ginsberg, E. F. Plow, and S. J. Shattil, “Effect of platelet activation on the conformation of the plasma membrane glycoprotein IIb-IIIa complex,” *J. Biol. Chem.*, vol. 266, no. 12, pp. 7345–7352, 1991.

[142] D. Woodside, S. Liu, and M. Ginsberg, “Integrin activation,” *Thromb Haemost*, vol. 86, pp. 316–323, 2001.

[143] D. A. Calderwood, “Integrin activation,” *J. Cell Sci.*, vol. 117, no. 5, pp. 657–666, 2004, doi: 10.1242/jcs.01014.

[144] P. Hu and B. H. Luo, “Integrin bi-directional signaling across the plasma membrane,” *J. Cell. Physiol.*, vol. 228, no. 2, pp. 306–312, 2013, doi: 10.1002/jcp.24154.

[145] N. R. Paul, G. Jacquemet, and P. T. Caswell, “Endocytic Trafficking of Integrins in Cell Migration,” *Curr. Biol.*, vol. 25, no. 22, pp. R1092–R1105, 2015, doi: 10.1016/j.cub.2015.09.049.

[146] C. De Pascalis and S. Etienne-Manneville, “Single and collective cell migration: The mechanics of adhesions,” *Mol. Biol. Cell*, vol. 28, no. 14, pp. 1833–1846, 2017, doi: 10.1091/mbc.E17-03-0134.

[147] J. D. Humphries, A. Byron, and M. J. Humphries, “Integrin ligands at a glance,” *J. Cell Sci.*, vol. 119, no. 19, pp. 3901–3903, 2006, doi: 10.1242/jcs.03098.

[148] A. B. C. Buskermolen, N. A. Kurniawan, and C. V. C. Bouten, “An automated quantitative analysis of cell, nucleus and focal adhesion morphology,” *PLoS One*, vol. 13, no. 3, pp. 1–16, 2018, doi: 10.1371/journal.pone.0195201.

[149] A. R. Gingras *et al.*, “Rap1 binding and a lipid-dependent helix in talin F1 domain promote integrin activation in tandem,” *J. Cell Biol.*, vol. 218, no. 6, pp. 1799–1809, 2019, doi: 10.1083/JCB.201810061.

[150] H. Sun, F. Lagarrigue, and M. H. Ginsberg, “The Connection Between Rap1 and Talin1 in the Activation of Integrins in Blood Cells,” *Front. Cell Dev. Biol.*, vol. 10, no. June, pp. 1–8, 2022, doi: 10.3389/fcell.2022.908622.

[151] S. Tadokoro *et al.*, “Talin binding to integrin β tails: A final common step in integrin

activation," *Science (80-.).*, vol. 302, no. 5642, pp. 103–106, 2003, doi: 10.1126/science.1086652.

[152] E. Zamir *et al.*, "Dynamics and segregation of cell-matrix adhesions in cultured fibroblasts," *Nat. Cell Biol.*, vol. 2, no. 4, pp. 191–196, 2000, doi: 10.1038/35008607.

[153] J. N. Ajeian *et al.*, "Proteomic analysis of integrin-associated complexes from mesenchymal stem cells," *Proteomics - Clin. Appl.*, vol. 10, no. 1, pp. 51–57, 2016, doi: 10.1002/prca.201500033.

[154] O. Rossier *et al.*, "Integrins β 1 and β 3 exhibit distinct dynamic nanoscale organizations inside focal adhesions," *Nat. Cell Biol.*, vol. 14, no. 10, pp. 1057–1067, 2012, doi: 10.1038/ncb2588.

[155] G. Mana *et al.*, "PPFIA1 drives active α5β1 integrin recycling and controls fibronectin fibrillogenesis and vascular morphogenesis," *Nat. Commun.*, vol. 7, no. November, 2016, doi: 10.1038/ncomms13546.

[156] E. Cukierman, R. Pankov, R. Stevens, D, and M. Yamada, K, "Taking cell-matrix adhesions to the third dimension," *Science (80-.).*, vol. 294, no. 5547, pp. 1708–1712, 2001, doi: 10.1126/science.1064829.

[157] S. I. Fraley, Y. Feng, D. Wirtz, and G. D. Longmore, "Reply: Reducing background fluorescence reveals adhesions in 3D matrices," *Nat. Cell Biol.*, vol. 13, no. 1, pp. 5–7, 2011, doi: 10.1038/ncb0111-5.

[158] S. Harunaga, J and M. Yamada, K, "Cell-Matrix Adhesions in 3D," *Matrix Biol.*, vol. 30, no. 7–8, pp. 363–368, 2011, doi: 10.1016/j.matbio.2011.06.001.

[159] M. D. Schaller, "Cellular functions of FAK kinases: Insight into molecular mechanisms and novel functions," *J. Cell Sci.*, vol. 123, no. 7, pp. 1007–1013, 2010, doi: 10.1242/jcs.045112.

[160] S. Mitra, D. Hanson, and D. Schlaepfer, "Focal adhesion kinase: in command and control of cell motility," *Nat. Rev. Mol. Cell Biol.*, vol. 6, pp. 56–68, 2005.

[161] T. R. Polte and S. K. Hanks, "Interaction between focal adhesion kinase and Crk-associated tyrosine kinase substrate p130Cas," *Proc. Natl. Acad. Sci. U. S. A.*, vol. 92, no. 23, pp. 10678–10682, 1995, doi: 10.1073/pnas.92.23.10678.

[162] X. Zhao and J. L. Guan, "Focal adhesion kinase and its signaling pathways in cell migration and angiogenesis," *Adv. Drug Deliv. Rev.*, vol. 63, no. 8, pp. 610–615, 2011, doi: 10.1016/j.addr.2010.11.001.

[163] F. Chang, C. Lemmon, D. Park, and L. Romer, "FAK Potentiates Rac1 Activation and Localization to Matrix Adhesion Sites: A Role for Beta-PIX," *Mol. Biol. Cell*, vol. 18, pp. 253–264, 2007.

[164] A. Sadok and C. J. Marshall, "Rho gtpases masters of cell migration," *Small GTPases*, vol. 5, no. 4, 2014, doi: 10.4161/sgtp.29710.

[165] G. P. F. Nader, E. J. Ezratty, and G. G. Gundersen, "FAK, talin and PIPKI 3 regulate endocytosed integrin activation to polarize focal adhesion assembly," *Nat. Cell Biol.*, vol. 18, no. 5, pp. 491–503, 2016, doi: 10.1038/ncb3333.

[166] J. Alanko, A. Mai, G. Jacquemet, K. Schauer, and R. Kaukonen, "Integrin endosomal signalling suppresses anoikis," vol. 17, no. 11, pp. 1412–1421, 2015, doi: 10.1038/ncb3250.Integrin.

[167] T. M. E. Scales and M. Parsons, “Spatial and temporal regulation of integrin signalling during cell migration,” *Curr. Opin. Cell Biol.*, vol. 23, no. 5, pp. 562–568, 2011, doi: 10.1016/j.ceb.2011.05.008.

[168] D. Valdembri and G. Serini, “Regulation of adhesion site dynamics by integrin traffic,” *Curr. Opin. Cell Biol.*, vol. 24, no. 5, pp. 582–591, 2012, doi: 10.1016/j.ceb.2012.08.004.

[169] G. Mana, D. Valdembri, and G. Serini, “Conformationally active integrin endocytosis and traffic: Why, where, when and how?,” *Biochem. Soc. Trans.*, vol. 48, no. 1, pp. 83–93, 2020, doi: 10.1042/BST20190309.

[170] A. C. Zovein *et al.*, “β1 Integrin Establishes Endothelial Cell Polarity and Arteriolar Lumen Formation via a Par3-Dependent Mechanism,” *Dev. Cell*, vol. 18, no. 1, pp. 39–51, 2010, doi: 10.1016/j.devcel.2009.12.006.

[171] E. J. Ezratty, C. Bertaux, E. E. Marcantonio, and G. G. Gundersen, “Clathrin mediates integrin endocytosis for focal adhesion disassembly in migrating cells,” *J. Cell Biol.*, vol. 187, no. 5, pp. 733–747, 2009, doi: 10.1083/jcb.200904054.

[172] M. Mettlen, P. Chen, S. Srinivasan, G. Danuser, and L. Schmid, S, “Regulation of Clathrin mediated endocytosis,” *Annu Rev Biochem*, vol. 87, pp. 871–896, 2018, doi: 10.1146/annurev-biochem-062917-012644.

[173] P. Atherton, F. Lausecker, A. Harrison, and C. Ballestrem, “Low-intensity pulsed ultrasound promotes cell motility through vinculin-controlled Rac1 GTPase activity,” *J. Cell Sci.*, vol. 130, no. 14, pp. 2277–2291, 2017, doi: 10.1242/jcs.192781.

[174] M. S. Roberts, A. J. Woods, T. C. Dale, P. van der Sluijs, and J. C. Norman, “Protein Kinase B/Akt Acts via Glycogen Synthase Kinase 3 To Regulate Recycling of αvβ3 and α5β1 Integrins,” *Mol. Cell. Biol.*, vol. 24, no. 4, pp. 1505–1515, 2004, doi: 10.1128/mcb.24.4.1505-1515.2004.

[175] A. J. Woods, D. P. White, P. T. Caswell, and J. C. Norman, “PKD1/PKCμ promotes αvβ3 integrin recycling and delivery to nascent focal adhesions,” *EMBO J.*, vol. 23, no. 13, pp. 2531–2543, 2004, doi: 10.1038/sj.emboj.7600267.

[176] C. M. Laukaitis, D. J. Webb, K. Donais, and A. F. Horwitz, “Differential dynamics of α5 integrin, paxillin, and α-actinin during formation and disassembly of adhesions in migrating cells,” *J. Cell Biol.*, vol. 153, no. 7, pp. 1427–1440, 2001, doi: 10.1083/jcb.153.7.1427.

[177] P. T. Caswell *et al.*, “Rab25 Associates with α5β1 Integrin to Promote Invasive Migration in 3D Microenvironments,” *Dev. Cell*, vol. 13, no. 4, pp. 496–510, 2007, doi: 10.1016/j.devcel.2007.08.012.

[178] A. Mai *et al.*, “Competitive binding of Rab21 and p120RasGAP to integrins regulates receptor traffic and migration,” *J. Cell Biol.*, vol. 194, no. 2, pp. 291–306, 2011, doi: 10.1083/jcb.201012126.

[179] L. M. Machesky, “Rab11FIP proteins link endocytic recycling vesicles for cytoskeletal transport and tethering,” *Biosci. Rep.*, vol. 39, no. 1, pp. 1–5, 2019, doi: 10.1042/BSR20182219.

[180] D. P. White, P. T. Caswell, and J. C. Norman, “αvβ3 and α5β1 integrin recycling pathways dictate downstream Rho kinase signaling to regulate persistent cell migration,” *J. Cell Biol.*, vol. 177, no. 3, pp. 515–525, 2007, doi: 10.1083/jcb.200609004.

[181] P. T. Caswell and J. C. Norman, “Integrin trafficking and the control of cell migration,” *Traffic*, vol. 7, no. 1, pp. 14–21, 2006, doi: 10.1111/j.1600-0854.2005.00362.x.

[182] G. Serini, D. Valdembri, and F. Bussolino, “Integrins and angiogenesis: A sticky business,” *Exp. Cell Res.*, vol. 312, no. 5, pp. 651–658, 2006, doi: 10.1016/j.yexcr.2005.10.020.

[183] C. Ruegg and A. Mariotti, “Vascular integrins: pleiotropic adhesion and signaling molecules in vascular homeostasis and angiogenesis,” *Cell. Mol. Life Sci.*, vol. 60, pp. 1135–1157, 2003.

[184] K. Hodivala-Dilke, A. Reynolds, and L. Reynolds, “Integrins in angiogenesis: multitalented molecules in a balancing act,” *Cell Tissue Res.*, vol. 314, pp. 131–144, 2003.

[185] P. Somanath, N. Malinin, and T. Byzova, “Cooperation between integrin αvβ3 and VEGFR2 in angiogenesis,” *Angiogenesis*, vol. 12, pp. 177–185, 2009.

[186] A. Van Der Flier *et al.*, “Endothelial α5 and αv integrins cooperate in remodeling of the vasculature during development,” *Development*, vol. 137, no. 14, pp. 2439–2449, 2010, doi: 10.1242/dev.049551.

[187] P. C. Brooks, R. A. F. Clark, and D. A. Cheresh, “Requirement of vascular integrin αvβ3 for angiogenesis,” *Science (80-.).*, vol. 264, no. 5158, pp. 569–571, 1994, doi: 10.1126/science.7512751.

[188] F. Schaffner, A. M. Ray, and M. Dontenwill, “Integrin α5β1, the fibronectin receptor, as a pertinent therapeutic target in solid tumors,” *Cancers (Basel).*, vol. 5, no. 1, pp. 27–47, 2013, doi: 10.3390/cancers5010027.

[189] S. D. Robinson *et al.*, “Avβ3 Integrin Limits the Contribution of Neuropilin-1 To Vascular Endothelial Growth Factor-Induced Angiogenesis,” *J. Biol. Chem.*, vol. 284, no. 49, pp. 33966–33981, 2009, doi: 10.1074/jbc.M109.030700.

[190] L. Reynolds *et al.*, “Enhanced pathological angiogenesis in mice lacking Beta-3 integrin or Beta-3 and Beta-5 integrins,” *Nat. Med.*, vol. 8, no. 1, pp. 27–34, 2002.

[191] R. Soldi, S. Mitola, M. Strasly, P. Defilippi, G. Tarone, and F. Bussolino, “Role of α(v)β3 integrin in the activation of vascular endothelial growth factor receptor-2,” *EMBO J.*, vol. 18, no. 4, pp. 882–892, 1999, doi: 10.1093/emboj/18.4.882.

[192] B. Masson-Gadais, F. Houle, J. Laferrière, and J. Huot, “Integrin αvβ3 requirement for VEGFR2-mediated activation of SAPK2/p38 and for Hsp90-dependent phosphorylation of focal adhesion kinase in endothelial cells activated by VEGF,” *Cell Stress Chaperones*, vol. 8, no. 1, pp. 37–52, 2003, doi: 10.1379/1466-1268(2003)8<37:IVRFVA>2.0.CO;2.

[193] R. E. Nisato, J. C. Tille, A. Jonczyk, S. L. Goodman, and M. S. Pepper, “Avβ3 and Avβ5 Integrin Antagonists Inhibit Angiogenesis in Vitro,” *Angiogenesis*, vol. 6, no. 2, pp. 105–119, 2003, doi: 10.1023/B:AGEN.0000011801.98187.f2.

[194] S. Yamada, X. Y. Bu, V. Khankaldyyan, I. Gonzales-Gomez, J. G. McComb, and W. E. Laug, “Effect of the angiogenesis inhibitor Cilengitide (EMD 121974) on glioblastoma growth in nude mice,” *Neurosurgery*, vol. 59, no. 6, pp. 1304–1312, 2006, doi: 10.1227/01.NEU.0000245622.70344.BE.

[195] R. Stupp *et al.*, “Cilengitide combined with standard treatment for patients with newly diagnosed glioblastoma with methylated MGMT promoter (CENTRIC EORTC 26071-22072 study): a multicentre, randomised, open-label, phase 3 trial,” *Lancet. Oncol.*, vol. 15, no. 10,

pp. 1100–1108, 2014, doi: 10.1016/S1470-2045(14)70379-1.

[196] A. R. Reynolds *et al.*, "Stimulation of tumor growth and angiogenesis by low concentrations of RGD-mimetic integrin inhibitors," *Nat. Med.*, vol. 15, no. 4, pp. 392–400, 2009, doi: 10.1038/nm.1941.

[197] V. Steri *et al.*, "Acute depletion of endothelial β3-integrin transiently inhibits tumor growth and angiogenesis in mice," *Circ. Res.*, vol. 114, no. 1, pp. 79–91, 2014, doi: 10.1161/CIRCRESAHA.114.301591.

[198] A. R. Reynolds *et al.*, "Elevated Flk1 (vascular endothelial growth factor receptor 2) signaling mediates enhanced angiogenesis in β3-integrin-deficient mice," *Cancer Res.*, vol. 64, no. 23, pp. 8643–8650, 2004, doi: 10.1158/0008-5472.CAN-04-2760.

[199] S. D. Robinson, L. E. Reynolds, L. Wyder, D. J. Hicklin, and K. M. Hodivala-Dilke, "β3-integrin regulates vascular endothelial growth factor-A-dependent permeability," *Arterioscler. Thromb. Vasc. Biol.*, vol. 24, no. 11, pp. 2108–2114, 2004, doi: 10.1161/01.ATV.0000143857.27408.de.

[200] H. B. Schiller *et al.*, "β 1 - And α v -class integrins cooperate to regulate myosin II during rigidity sensing of fibronectin-based microenvironments," *Nat. Cell Biol.*, vol. 15, no. 6, pp. 625–636, 2013, doi: 10.1038/ncb2747.

[201] S. J. Atkinson *et al.*, "The β3-integrin endothelial adhesome regulates microtubule-dependent cell migration," *EMBO Rep.*, vol. 19, no. 7, pp. 1–14, 2018, doi: 10.15252/embr.201744578.

[202] S. I. Aota, M. Nomizu, and K. M. Yamada, "The short amino acid sequence Pro-His-Ser-Arg-Asn in human fibronectin enhances cell-adhesive function," *J. Biol. Chem.*, vol. 269, no. 40, pp. 24756–24761, 1994.

[203] J. T. Yang, H. Rayburn, and R. O. Hynes, "Embryonic mesodermal defects in α5 integrin-deficient mice," *Development*, vol. 119, no. 4, pp. 1093–1105, 1993.

[204] L. E. Stephens *et al.*, "Deletion of β1 integrins in mice results in inner cell mass failure and peri-implantation lethality," *Genes Dev.*, vol. 9, no. 15, pp. 1883–1895, 1995, doi: 10.1101/gad.9.15.1883.

[205] R. Fässler and M. Meyer, "Consequences of lack of β1 integrin gene expression in mice," *Genes Dev.*, vol. 9, no. 15, pp. 1896–1908, 1995, doi: 10.1101/gad.9.15.1896.

[206] C. Brakebusch, E. Hirsch, A. Potocnik, and R. Fässler, "Genetic analysis of β1 integrin function: Confirmed, new and revised roles for a crucial family of cell adhesion molecules," *J. Cell Sci.*, vol. 110, no. 23, pp. 2895–2904, 1997.

[207] S. E. Francis *et al.*, "Central roles of α5β1 integrin and fibronectin in vascular development in mouse embryos and embryoid bodies," *Arterioscler. Thromb. Vasc. Biol.*, vol. 22, no. 6, pp. 927–933, 2002, doi: 10.1161/01.ATV.0000016045.93313.F2.

[208] H. L. Goel, B. Pursell, C. Standley, K. Fogarty, and A. M. Mercurio, "Neuropilin-2 regulates α6β1 integrin in the formation of focal adhesions and signaling," *J. Cell Sci.*, vol. 125, no. 2, pp. 497–506, 2012, doi: 10.1242/jcs.094433.

[209] J. J. Ou *et al.*, "Neuropilin-2 mediates lymphangiogenesis of colorectal carcinoma via a VEGFC/VEGFR3 independent signaling," *Cancer Lett.*, vol. 358, no. 2, pp. 200–209, 2015, doi:

10.1016/j.canlet.2014.12.046.

[210] Y. Cao *et al.*, "Neuropilin-2 promotes extravasation and metastasis by interacting with endothelial α5 integrin," *Cancer Res.*, vol. 73, no. 14, pp. 4579–4590, 2013, doi: 10.1158/0008-5472.CAN-13-0529.

[211] A. Walz, I. Rodriguez, and P. Mombaerts, "Aberrant Sensory Innervation of the Olfactory Bulb in Neuropilin-2 Mutant Mice," *J. Neurosci.*, vol. 22, no. 10, pp. 4025–4035, 2002, doi: 10.1523/jneurosci.22-10-04025.2002.

[212] C. Gu *et al.*, "Neuropilin-1 conveys semaphorin and VEGF signaling during neural and cardiovascular development," *Dev. Cell*, vol. 5, no. 1, pp. 45–57, 2003, doi: 10.1016/S1534-5807(03)00169-2.

[213] S. Claxton, V. Kostourou, S. Jadeja, P. Chambon, K. Hodivala-Dilke, and M. Fruttiger, "Efficient, inducible cre-recombinase activation in vascular endothelium," *Genesis*, vol. 46, no. 2, pp. 74–80, 2008, doi: 10.1002/dvg.20367.

[214] L. Reynolds and K. Hodivala-Dilke, "Primary mouse endothelial cell culture for assays of angiogenesis.," *Methods Mol Med*, vol. 120, pp. 503–509, 2006.

[215] J. Lambert *et al.*, "ADAMTS-1 and syndecan-4 intersect in the regulation of cell migration and angiogenesis," *J. Cell Sci.*, vol. 133, no. 7, pp. 1–15, 2020, doi: 10.1242/jcs.235762.

[216] T. Xu *et al.*, "SOAX: A software for quantification of 3D biopolymer networks," *Sci. Rep.*, vol. 5, 2015, doi: 10.1038/srep09081.

[217] A. W. M. Van Weert, H. J. Geuze, B. Groothuis, and W. Stoorvogel, "Primaquine interferes with membrane recycling from endosomes to the plasma membrane through a direct interaction with endosomes which does not involve neutralisation of endosomal pH nor osmotic swelling of endosomes," *Eur. J. Cell Biol.*, vol. 79, no. 6, pp. 394–399, 2000, doi: 10.1078/0171-9335-00062.

[218] D. Krilleke *et al.*, "Molecular mapping and functional characterization of the VEGF164 heparin-binding domain," *J. Biol. Chem.*, vol. 282, no. 38, pp. 28045–28056, 2007, doi: 10.1074/jbc.M700319200.

[219] A. Remacle, G. Murphy, and C. Roghi, "Membrane type I-matrix metalloproteinase (MT1-MMP) is internalised by two different pathways and is recycled to the cell surface," *J. Cell Sci.*, vol. 116, no. 19, pp. 3905–3916, 2003, doi: 10.1242/jcs.00710.

[220] M. Tomayko, M and P. Reynolds, C, "Determination of subcutaneous tumour size in athymic (nude) mice," *Cancer Chemother Pharmacol*, vol. 24, no. 3, pp. 148–154, 1989.

[221] S. Payne, S. De Val, and A. Neal, "Endothelial-specific cre mouse models is your cre CREdibile?," *Arterioscler. Thromb. Vasc. Biol.*, vol. 38, no. 11, pp. 2550–2561, 2018, doi: 10.1161/ATVBAHA.118.309669.

[222] R. Feil, J. Wagner, D. Metzger, and P. Chambon, "Regulation of Cre Recombinase Activity by Mutated Estrogen Receptor Ligand-Binding Domains," *Biochem. Biophys. Res. Commun.*, vol. 237, pp. 752–757, 1997.

[223] P. Leneuve *et al.*, "Cre-mediated germline mosaicism: a new transgenic mouse for the selective removal of residual markers from tri-lox conditional alleles.," *Nucleic Acids Res.*, vol. 31, no. 5, pp. 1–8, 2003, doi: 10.1093/nar/gng021.

[224] C. Ni, S. Kumar, and C. Jo, “Development of immortalised mouse aortic endothelial cell lines,” *Vasc. Cell*, vol. 6, no. 1, 2014.

[225] A. A. A. Alghamdi, C. J. Benwell, S. J. Atkinson, J. Lambert, R. T. Johnson, and S. D. Robinson, “NRP2 as an Emerging Angiogenic Player; Promoting Endothelial Cell Adhesion and Migration by Regulating Recycling of α5 Integrin,” *Front. Cell Dev. Biol.*, vol. 8, no. May, pp. 1–16, 2020, doi: 10.3389/fcell.2020.00395.

[226] N. V. Goncharov, A. D. Nadeev, R. O. Jenkins, and P. V. Avdonin, “Markers and Biomarkers of Endothelium: When Something Is Rotten in the State,” *Oxid. Med. Cell. Longev.*, vol. 2017, 2017, doi: 10.1155/2017/9759735.

[227] V. Nikolova-Krstevski *et al.*, “ERG is required for the differentiation of embryonic stem cells along the endothelial lineage,” *BMC Dev. Biol.*, vol. 9, no. 1, pp. 1–14, 2009, doi: 10.1186/1471-213X-9-72.

[228] M. Markku, S. Maarit, and W. Zeng-Feng, “Claudin-5 as an Immunohistochemical Marker for Angiosarcoma and Hemangioendotheliomas,” *Am. J. Surg. Pathol.*, vol. 35, no. 12, pp. 1848–1856, 2011.

[229] M. Gröger *et al.*, “IL-3 Induces Expression of Lymphatic Markers Prox-1 and Podoplanin in Human Endothelial Cells,” *J. Immunol.*, vol. 173, no. 12, pp. 7161–7169, 2004, doi: 10.4049/jimmunol.173.12.7161.

[230] C. J. Benwell, J. A. G. E. Taylor, and S. D. Robinson, “Endothelial neuropilin-2 influences angiogenesis by regulating actin pattern development and α5-integrin-p-FAK complex recruitment to assembling adhesion sites,” *FASEB J.*, vol. 35, no. 8, pp. 1–19, 2021, doi: 10.1096/fj.202100286R.

[231] H. B. Schiller, C. C. Friedel, C. Boulegue, and R. Fässignssler, “Quantitative proteomics of the integrin adhesome show a myosin II-dependent recruitment of LIM domain proteins,” *EMBO Rep.*, vol. 12, no. 3, pp. 259–266, 2011, doi: 10.1038/embor.2011.5.

[232] R. H. Adams and K. Alitalo, “Molecular regulation of angiogenesis and lymphangiogenesis,” *Nat. Rev. Mol. Cell Biol.*, vol. 8, no. 6, pp. 464–478, 2007, doi: 10.1038/nrm2183.

[233] J. Keuschnigg *et al.*, “PV-1 is recognized by the PAL-E antibody and forms complexes with NRP-1,” *Blood*, vol. 120, no. 1, pp. 232–235, 2012, doi: 10.1182/blood-2012-01-406876.

[234] L. Herrnberger, K. Ebner, B. Junglas, and E. R. Tamm, “The role of plasmalemma vesicle-associated protein (PLVAP) in endothelial cells of Schlemm’s canal and ocular capillaries,” *Exp. Eye Res.*, vol. 105, pp. 27–33, 2012, doi: 10.1016/j.exer.2012.09.011.

[235] J. Keuschnigg *et al.*, “Plasticity of Blood- and Lymphatic Endothelial Cells and Marker Identification,” *PLoS One*, vol. 8, no. 9, pp. 1–14, 2013, doi: 10.1371/journal.pone.0074293.

[236] S. Park, C. Sorenson, and N. Sheibani, “PECAM-1 isoforms, eNOS and endoglin axis in regulation of angiogenesis,” *Clin. Sci.*, vol. 129, no. 3, pp. 217–234, 2015.

[237] G. Jacquemet *et al.*, “Rac1 is deactivated at integrin activation sites through an IQGAP1-filamin-A-RacGAP1 pathway,” *J. Cell Sci.*, vol. 126, no. 18, pp. 4121–4135, 2013, doi: 10.1242/jcs.121988.

[238] S. A. Langhans, “Three-dimensional in vitro cell culture models in drug discovery and drug repositioning,” *Front. Pharmacol.*, vol. 9, no. JAN, pp. 1–14, 2018, doi:

10.3389/fphar.2018.00006.

[239] W. J. Ho *et al.*, “Incorporation of multicellular spheroids into 3-D polymeric scaffolds provides an improved tumor model for screening anticancer drugs,” *Cancer Sci.*, vol. 101, no. 12, pp. 2637–2643, 2010, doi: 10.1111/j.1349-7006.2010.01723.x.

[240] Y. H. Kim *et al.*, “A MST1–FOXO1 cascade establishes endothelial tip cell polarity and facilitates sprouting angiogenesis,” *Nat. Commun.*, vol. 10, no. 1, pp. 1–17, 2019, doi: 10.1038/s41467-019-08773-2.

[241] G. Genet *et al.*, “Endophilin-A2 dependent VEGFR2 endocytosis promotes sprouting angiogenesis,” *Nat. Commun.*, vol. 10, no. 1, pp. 1–15, 2019, doi: 10.1038/s41467-019-10359-x.

[242] T. S. Malinova *et al.*, “A junctional PACSIN2/EHD4/MICAL-L1 complex coordinates VE-cadherin trafficking for endothelial migration and angiogenesis,” *Nat. Commun.*, vol. 12, no. 1, 2021, doi: 10.1038/s41467-021-22873-y.

[243] T. Uruno *et al.*, “Activation of Arp2/3 complex-mediated actin polymerization by cortactin,” *Nat. Cell Biol.*, vol. 3, no. 3, pp. 259–266, 2001, doi: 10.1038/35060051.

[244] A. Fantin *et al.*, “NRP1 Regulates CDC42 Activation to Promote Filopodia Formation in Endothelial Tip Cells,” *Cell Rep.*, vol. 11, no. 10, pp. 1577–1590, 2015, doi: 10.1016/j.celrep.2015.05.018.

[245] M. K. Woo and V. M. Fowler, “Identification and characterization of tropomodulin and tropomyosin in the adult rat lens,” *J. Cell Sci.*, vol. 107, no. 5, pp. 1359–1367, 1994.

[246] Y. Yamakita, S. Ono, F. Matsumura, and S. Yamashiro, “Phosphorylation of human fascin inhibits its actin binding and bundling activities,” *J. Biol. Chem.*, vol. 271, no. 21, pp. 12632–12638, 1996, doi: 10.1074/jbc.271.21.12632.

[247] P. M. Benz *et al.*, “Differential VASP phosphorylation controls remodeling of the actin cytoskeleton,” *J. Cell Sci.*, vol. 122, no. 21, pp. 3954–3965, 2009, doi: 10.1242/jcs.044537.

[248] S. Jalal *et al.*, “Actin cytoskeleton self-organization in single epithelial cells and fibroblasts under isotropic confinement,” *J. Cell Sci.*, vol. 132, no. 5, pp. 1–14, 2019, doi: 10.1242/jcs.220780.

[249] M. R. Holt, D. R. Critchley, and N. P. J. Brindle, “The focal adhesion phosphoprotein, VASP,” *Int. J. Biochem. Cell Biol.*, vol. 30, no. 3, pp. 307–311, 1998, doi: 10.1016/S1357-2725(97)00101-5.

[250] H. L. Goel, D. Bae, B. Pursell, L. M. Gouvin, S. Lu, and A. M. Mercurio, “Neuropilin-2 promotes branching morphogenesis in the mouse mammary gland,” *Development*, vol. 138, no. 14, pp. 2969–2976, 2011, doi: 10.1242/dev.051318.

[251] M. Nagano, D. Hoshino, N. Koshikawa, T. Akizawa, and M. Seiki, “Turnover of focal adhesions and cancer cell migration,” *Int. J. Cell Biol.*, no. June 2014, 2012, doi: 10.1155/2012/310616.

[252] R. Zaidel-Bar, R. Milo, Z. Kam, and B. Geiger, “A paxillin tyrosine phosphorylation switch regulates the assembly and form of cell-matrix adhesions,” *J. Cell Sci.*, vol. 120, no. 1, pp. 137–148, 2007, doi: 10.1242/jcs.03314.

[253] Y. L. Hu *et al.*, “FAK and paxillin dynamics at focal adhesions in the protrusions of migrating cells,” *Sci. Rep.*, vol. 4, pp. 1–7, 2014, doi: 10.1038/srep06024.

[254] K. E. Michael, D. W. Dumbauld, K. L. Burns, S. K. Hanks, and A. J. García, “Focal adhesion kinase modulates cell adhesion strengthening via integrin activation,” *Mol. Biol. Cell*, vol. 20, no. 9, pp. 2508–2519, 2009, doi: 10.1091/mbc.E08-01-0076.

[255] K. A. Kragtorp and J. R. Miller, “Regulation of somitogenesis by Ena/VASP proteins and FAK during Xenopus development,” *Development*, vol. 133, no. 4, pp. 685–695, 2006, doi: 10.1242/dev.02230.

[256] V. A. Bernusso *et al.*, “Imatinib restores VASP activity and its interaction with Zyxin in BCR-ABL leukemic cells,” *Biochim. Biophys. Acta - Mol. Cell Res.*, vol. 1853, no. 2, pp. 388–395, 2015, doi: 10.1016/j.bbamcr.2014.11.008.

[257] Y. Wang *et al.*, “Neuropilin-1 modulates interferon-γ-stimulated signaling in brain microvascular endothelial cells,” *J. Cell Sci.*, vol. 129, no. 20, pp. 3911–3921, 2016.

[258] C. J. Burckhardt, J. D. Minna, G. Danuser, C. J. Burckhardt, J. D. Minna, and G. Danuser, “Article SH3BP4 promotes neuropilin-1 and a 5-integrin endocytosis and is inhibited by Akt Article SH3BP4 promotes neuropilin-1 and a 5-integrin endocytosis and is inhibited by Akt,” *Dev. Cell*, pp. 1–18, 2021, doi: 10.1016/j.devcel.2021.03.009.

[259] M. Kaksonen, C. P. Toret, and D. G. Drubin, “Harnessing actin dynamics for clathrin-mediated endocytosis,” *Nat. Rev. Mol. Cell Biol.*, vol. 7, no. 6, pp. 404–414, 2006, doi: 10.1038/nrm1940.

[260] F. Shi and J. Sottile, “Caveolin-1-dependent β1 integrin endocytosis is a critical fibronectin.pdf,” *J. Cell Sci.*, vol. 121, no. Pt 14, pp. 2360–2371, 2009, doi: 10.1242/jcs.014977.Caveolin-1-dependent.

[261] A. Benmerah, M. Bayrou, N. Cerf-Bensussan, and A. Dautry-Varsat, “Inhibition of clathrin-coated pit assembly by an Eps15 mutant,” *J. Cell Sci.*, vol. 112, no. 9, pp. 1303–1311, 1999.

[262] L. Das *et al.*, “Novel regulation of integrin trafficking by rab11-FIP5 in aggressive prostate cancer,” *Mol. Cancer Res.*, vol. 16, no. 8, pp. 1319–1331, 2018, doi: 10.1158/1541-7786.MCR-17-0589.

[263] K. L. Sheung *et al.*, “Rice SCAMP1 defines clathrin-coated, trans-Golgi-located tubular-vesicular structures as an early endosome in tobacco BY-2 cells,” *Plant Cell*, vol. 19, no. 1, pp. 296–319, 2007, doi: 10.1105/tpc.106.045708.

[264] J. Vadakekolathu *et al.*, “MTSS1 and SCAMP1 cooperate to prevent invasion in breast cancer,” *Cell Death Dis.*, vol. 9, no. 3, 2018, doi: 10.1038/s41419-018-0364-9.

[265] E. J. Ezratty, M. A. Partridge, and G. G. Gundersen, “Microtubule-induced focal adhesion disassembly is mediated by dynamin and focal adhesion kinase,” *Nat. Cell Biol.*, vol. 7, no. 6, pp. 581–590, 2005, doi: 10.1038/ncb1262.

[266] L. Brinas, S. Vassilopoulos, G. Bonne, P. Guicheney, and M. Bitoun, “Role of dynamin-2 in the disassembly of focal adhesions,” *J. Mol. Med.*, vol. 91, pp. 803–809, 2013.

[267] M. Y. Lee, A. Skoura, E. J. Park, S. Landskroner-eiger, and L. Jozsef, “Dynamin 2 regulation of integrin endocytosis , but not VEGF signaling , is crucial for developmental angiogenesis,” no. March, 2014, doi: 10.1242/dev.104539.

[268] M. C. Jones, P. T. Caswell, and J. C. Norman, “Endocytic recycling pathways: emerging regulators of cell migration,” *Curr. Opin. Cell Biol.*, vol. 18, no. 5, pp. 549–557, 2006, doi:

10.1016/j.ceb.2006.08.003.

[269] E. Schonteich *et al.*, “The Rip11/Rab11-Fip5 and Kinesin II Complex Regulates Endocytic Protein Recycling,” *J. Cell Sci.*, vol. 121, no. 22, pp. 3824–3833, 2008, doi: 10.1242/jcs.032441.The.

[270] L. Kao and W. Chao, “Rab11-mediated focal adhesion turnover in sarcoma cell migration,” *Chin J Physiol*, vol. 64, pp. 43–50, 2021.

[271] S. Dutta *et al.*, “Neuropilin-2 regulates endosome maturation and EGFR trafficking to support cancer cell pathobiology,” vol. 76, no. 2, pp. 418–428, 2016, doi: 10.1158/0008-5472.CAN-15-1488.Neuropilin-2.

[272] A. Sundararaman, Y. Fukushima, J. C. Norman, A. Uemura, and H. Mellor, “RhoJ Regulates α5β1 Integrin Trafficking to Control Fibronectin Remodeling during Angiogenesis,” *Curr. Biol.*, vol. 30, no. 11, pp. 2146-2155.e5, 2020, doi: 10.1016/j.cub.2020.03.042.

[273] A. Arjonen, J. Alanko, S. Veltel, and J. Ivaska, “Distinct Recycling of Active and Inactive β1 Integrins,” *Traffic*, vol. 13, no. 4, pp. 610–625, 2012, doi: 10.1111/j.1600-0854.2012.01327.x.

[274] D. R. Bielenberg *et al.*, “Increased smooth muscle contractility in mice deficient for neuropilin 2,” *Am. J. Pathol.*, vol. 181, no. 2, pp. 548–559, 2012, doi: 10.1016/j.ajpath.2012.04.013.

[275] A. Fantin, Q. Schwarz, K. Davidson, E. M. Normando, L. Denti, and C. Ruhrberg, “The cytoplasmic domain of neuropilin 1 is dispensable for angiogenesis, but promotes the spatial separation of retinal arteries and veins,” *Development*, vol. 138, no. 19, pp. 4185–4191, 2011, doi: 10.1242/dev.070037.

[276] A. Plein, A. Fantin, and C. Ruhrberg, “Neuropilin regulation of angiogenesis, arteriogenesis, and vascular permeability,” *Microcirculation*, vol. 21, no. 4, pp. 315–323, 2014, doi: 10.1111/micc.12124.

[277] H. Zhu *et al.*, “Neuropilin-1 regulated by miR-320 contributes to the growth and metastasis of cholangiocarcinoma cells,” *Liver Int.*, vol. 38, no. 1, pp. 125–135, 2018, doi: 10.1111/liv.13495.

[278] B. Chaudhary, Y. Khaled, B. Ammori, and E. Elkord, “Neuropilin 1: function and therapeutic potential in cancer,” *Cancer Immunol. Immunother.*, vol. 63, pp. 81–99, 2014.

[279] S. Kim, K. Bell, S. A. Mousa, and J. A. Varner, “Regulation of angiogenesis in vivo by ligation of integrin (alpha5 beta1 wi ...,” *Heal. (San Fr.*, vol. 5, no. 4, pp. 1345–1362, 2000.

[280] A. Borkowetz *et al.*, “Neuropilin-2 is an independent prognostic factor for shorter cancer-specific survival in patients with acinar adenocarcinoma of the prostate,” *Int. J. Cancer*, vol. 146, no. 9, pp. 2619–2627, 2020, doi: 10.1002/ijc.32679.

[281] S. J. Lord, K. B. Velle, R. Dyche Mullins, and L. K. Fritz-Laylin, “SuperPlots: Communicating reproducibility and variability in cell biology,” *J. Cell Biol.*, vol. 219, no. 6, 2020, doi: 10.1083/JCB.202001064.

[282] D. Hanahan and R. A. Weinberg, “Hallmarks of cancer: The next generation,” *Cell*, vol. 144, no. 5, pp. 646–674, 2011, doi: 10.1016/j.cell.2011.02.013.

[283] J. Holash *et al.*, “Vessel Cooption, Regression, and Growth in Tumors Mediated by Angiopoietins and VEGF,” *Science (80-.).*, vol. 284, no. 5422, pp. 1994–1998, 1999.

[284] L. E. Benjamin, D. Golijanin, A. Itin, D. Pode, and E. Keshet, “Selective ablation of immature blood vessels in established human tumors follows vascular endothelial growth factor withdrawal,” *J. Clin. Invest.*, vol. 103, no. 2, pp. 159–165, 1999, doi: 10.1172/JCI5028.

[285] V. M. Golubovskaya, M. Zheng, L. Zhang, J. L. Li, and W. G. Cance, “The direct effect of Focal Adhesion Kinase (FAK), dominant-negative FAK, FAK-CD and FAK siRNA on gene expression and human MCF-7 breast cancer cell tumorigenesis,” *BMC Cancer*, vol. 9, 2009, doi: 10.1186/1471-2407-9-280.

[286] Jianliang Zhang and Steven N. Hochwald, “The role of FAK in tumor metabolism and therapy,” *Pharmacol Ther*, vol. 142, no. 2, pp. 154–163, 2014, doi: 10.1016/j.pharmthera.2013.12.003.

[287] C. Gao, G. Chen, S. F. Kuan, D. H. Zhang, D. D. Schlaepfer, and J. Hu, “FAK/PYK2 promotes the Wnt/β-catenin pathway and intestinal tumorigenesis by phosphorylating GSK3β,” *Elife*, vol. 4, no. AUGUST2015, pp. 1–17, 2015, doi: 10.7554/eLife.10072.

[288] F. L. Lenzo and W. G. Cance, “From tumorigenesis to microenvironment and immunoregulation: The many faces of focal adhesion kinase and challenges associated with targeting this elusive protein,” *Transl. Cancer Res.*, vol. 6, no. 17, pp. S957–S960, 2017, doi: 10.21037/tcr.2017.06.05.

[289] H. Haskell *et al.*, “Focal Adhesion Kinase Is Expressed in the Angiogenic Blood Vessels of Malignant Astrocytic Tumors in Vivo and Promotes Capillary Tube Formation of Brain Microvascular Endothelial Cells 1,” vol. 9, no. June, pp. 2157–2165, 2003.

[290] V. Bhaskar *et al.*, “A function blocking anti-mouse integrin α5β1 antibody inhibits angiogenesis and impedes tumor growth in vivo,” *J. Transl. Med.*, vol. 5, pp. 1–11, 2007, doi: 10.1186/1479-5876-5-61.

[291] X. Su *et al.*, “Antagonizing integrin beta3 increases immune suppression in cancer,” vol. 76, no. 12, pp. 3484–3495, 2017, doi: 10.1158/0008-5472.CAN-15-2663.Antagonizing.

[292] P. P. Deshpande, S. Biswas, and V. P. Torchilin, “Current trends in the use of liposomes for tumor targeting,” *Nanomedicine*, vol. 8, no. 9, pp. 1509–1528, 2013, doi: 10.2217/nnm.13.118.

[293] D. Ghosh Dastidar, D. Ghosh, and G. Chakrabarti, “Tumour vasculature targeted anti-cancer therapy,” *Vessel Plus*, vol. 2020, 2020, doi: 10.20517/2574-1209.2019.36.

[294] M. Pitulescu, I. Schmidt, R. Benedito, and R. Adams, “Inducible gene targeting in the neonatal vasculature and analysis of retinal angiogenesis in mice,” *Nat. Protoc.*, vol. 5, pp. 1518–1534, 2010.

[295] A. Stahl, K. Connor, P. Sapiepha, J. Chen, R. Dennison, and N. Krah, “The mouse retina as an angiogenesis model,” *Investig. Opthalmology Vis. Sci.*, vol. 51, no. 6, pp. 2813–2826, 2010.

[296] M. Simons, K. Alitalo, B. Annex, H. Augustin, C. Beam, and B. Berk, “State-of-the-art methods of evaluation of angiogenesis and tissue vascularisation,” *A Sci. statement from Am. Hear. Assoc.*, 2015.

[297] I. Zaitoun, R. Johnson, N. Jamali, R. Almomani, S. Wang, and N. Sheibani, “Endothelium expression of Bcl-2 is essential for normal and pathological ocular vascularisation,” *PLoS One*, vol. 10, no. 10, pp. 1–17, 2015.

[298] F. Milde, S. Lauw, P. Koumoutsakos, and M. L. Iruela-Arispe, “The mouse retina in 3D: Quantification of vascular growth and remodeling,” *Integr. Biol. (United Kingdom)*, vol. 5, no. 12, pp. 1426–1438, 2013, doi: 10.1039/c3ib40085a.

[299] D. R. Bielenberg, C. A. Pettaway, S. Takashima, and M. Klagsbrun, “Neuropilins in neoplasms: Expression, regulation, and function,” *Exp. Cell Res.*, vol. 312, no. 5, pp. 584–593, 2006, doi: 10.1016/j.yexcr.2005.11.024.

[300] L. Alarcon-Martinez *et al.*, “Capillary pericytes express α-smooth muscle actin, which requires prevention of filamentous-actin depolymerization for detection,” *Elife*, vol. 7, pp. 1–17, 2018, doi: 10.7554/eLife.34861.

[301] D. Stenzel *et al.*, “Integrin-dependent and -independent functions of astrocytic fibronectin in retinal angiogenesis,” *Development*, vol. 138, no. 20, pp. 4451–4463, 2011, doi: 10.1242/dev.071381.

[302] C. Korn and H. G. Augustin, “Mechanisms of Vessel Pruning and Regression,” *Dev. Cell*, vol. 34, no. 1, pp. 5–17, 2015, doi: 10.1016/j.devcel.2015.06.004.

[303] C. Prahst *et al.*, “Mouse retinal cell behaviour in space and time using light sheet fluorescence microscopy,” *Elife*, vol. 9, pp. 1–29, 2020, doi: 10.7554/eLife.49779.

[304] L. Schimmel *et al.*, “C-Src controls stability of sprouting blood vessels in the developing retina independently of cell-cell adhesion through focal adhesion assembly,” *Dev.*, vol. 147, no. 7, 2020, doi: 10.1242/dev.185405.

[305] K. Okabe *et al.*, “Neurons limit angiogenesis by titrating VEGF in retina,” *Cell*, vol. 159, no. 3, pp. 584–596, 2014, doi: 10.1016/j.cell.2014.09.025.

[306] Q. Pan *et al.*, “Blocking Neuropilin-1 Function Has an Additive Effect with Anti-VEGF to Inhibit Tumor Growth,” *Cancer Cell*, vol. 11, no. 1, pp. 53–67, 2007, doi: 10.1016/j.ccr.2006.10.018.

[307] C. Raimondi, J. T. Brash, A. Fantin, and C. Ruhrberg, “NRP1 function and targeting in neurovascular development and eye disease,” *Prog. Retin. Eye Res.*, vol. 52, pp. 64–83, 2016, doi: 10.1016/j.preteyeres.2016.02.003.

[308] B. Jiang, I. Liou, G, A. Behzadian, M, and B. Caldwell, R, “Astrocytes modulate retinal vasculogenesis: effects on fibronectin expression,” *J Cell Sci*, vol. 107, pp. 2499–2508, 1994.

[309] B. A. Corliss *et al.*, “Pericyte bridges in homeostasis and hyperglycemia,” *Diabetes*, vol. 69, no. 7, pp. 1503–1517, 2020, doi: 10.2337/db19-0471.

[310] M. G. Dallinga *et al.*, “IGF2 and IGF1R identified as novel tip cell genes in primary microvascular endothelial cell monolayers,” *Angiogenesis*, vol. 21, no. 4, pp. 823–836, 2018, doi: 10.1007/s10456-018-9627-4.

[311] B. Tavora *et al.*, “Endothelial FAK is required for tumour angiogenesis,” *EMBO Mol. Med.*, vol. 2, no. 12, pp. 516–528, 2010, doi: 10.1002/emmm.201000106.

[312] G. Yu *et al.*, “Nicastrin modulates presenilin-mediated notch/glp-1 signal transduction and βAPP processing,” *Nature*, vol. 407, no. 6800, pp. 48–54, 2000, doi: 10.1038/35024009.

[313] F. Demircioglu and K. Hodivala-Dilke, “aVb3 integrin and tumour blood vessels- learning from the past to shape the future,” *Curr. Opin. Cell Biol.*, vol. 42, pp. 121–127, 2016.

[314] S. D. Liu, L. P. Zhong, J. He, and Y. X. Zhao, “Targeting neuropilin-1 interactions is a promising

anti-Tumor strategy," *Chin. Med. J. (Engl).*, vol. 134, no. 5, pp. 508–517, 2021, doi: 10.1097/CM9.0000000000001200.

[315] L. E. Jimenez-Hernandez *et al.*, "NRP1-positive lung cancer cells possess tumor-initiating properties," *Oncol. Rep.*, vol. 39, no. 1, pp. 349–357, 2018, doi: 10.3892/or.2017.6089.

[316] R. Islam *et al.*, "Role of Neuropilin-2-mediated signaling axis in cancer progression and therapy resistance," *Cancer Metastasis Rev.*, vol. 41, no. 3, pp. 771–787, 2022, doi: 10.1007/s10555-022-10048-0.

[317] W. C. Lim, M. Olding, E. Healy, and T. M. Millar, "Human endothelial cells modulate CD4+ T cell populations and enhance regulatory T cell suppressive capacity," *Front. Immunol.*, vol. 9, no. MAR, 2018, doi: 10.3389/fimmu.2018.00565.

[318] J. Powell *et al.*, "Small Molecule Neuropilin - 1 Antagonists Combine Antiangiogenic and Antitumor Activity with Immune Modulation through Reduction of Transforming Growth Factor Beta (TGF β) Production in Regulatory T - Cells," 2018, doi: 10.1021/acs.jmedchem.8b00210.

[319] A. M. Said, M. W. Parker, and C. W. Vander, "Bioorganic Chemistry Design , synthesis , and evaluation of a novel benzamidine-based inhibitor of VEGF-C binding to Neuropilin-2," *Bioorg. Chem.*, vol. 100, no. March, p. 103856, 2020, doi: 10.1016/j.bioorg.2020.103856.

[320] W. Parker, M and W. Vander Kooi, C, "Microplate-based screening for small molecule inhibitors of Neuropilin-2/VEGF-C interactions," *Anal Biochem*, vol. 15, no. 453, pp. 4–6, 2014.

[321] M. Potez *et al.*, "Characterization of a B16-F10 melanoma model locally implanted into the ear pinnae of," pp. 1–19, 2018.

[322] A. Dumond and G. Pagès, "Neuropilins, as Relevant Oncology Target: Their Role in the Tumoral Microenvironment," *Front. Cell Dev. Biol.*, vol. 8, no. July, pp. 1–10, 2020, doi: 10.3389/fcell.2020.00662.

[323] A. G. Sorensen *et al.*, "Increased survival of glioblastoma patients who respond to antiangiogenic therapy with elevated blood perfusion," *Cancer Res.*, vol. 72, no. 2, pp. 402–407, 2012, doi: 10.1158/0008-5472.CAN-11-2464.

[324] R. T. Tong, Y. Boucher, S. V. Kozin, F. Winkler, D. J. Hicklin, and R. K. Jain, "Vascular normalization by vascular endothelial growth factor receptor 2 blockade induces a pressure gradient across the vasculature and improves drug penetration in tumors," *Cancer Res.*, vol. 64, no. 11, pp. 3731–3736, 2004, doi: 10.1158/0008-5472.CAN-04-0074.

[325] H. G. Augustin and G. Y. Koh, "Antiangiogenesis: Vessel Regression, Vessel Normalization, or Both?," *Cancer Res.*, vol. 82, no. 1, pp. 15–17, 2022, doi: 10.1158/0008-5472.can-21-3515.

9 Appendices

Appendix 1: Full LFQ mass spectrometry peptide hit data

Gene name (Andromeda peptide database)	Average fold-change (Log2* LFQ Ctrl siRNA-NRP2 siRNA (N=1)	Average fold-change (Log2* LFQ Ctrl siRNA-NRP2 siRNA (N=2)
Rik	0.00000	13.65657
Ktn1	16.17446	0.00000
Ly6c1	0.00000	13.82277
Tardbp	17.06016	0.00000
Shank3	17.82211	18.26145
Sptbn1	0.00000	14.65428
Cyb5r3	16.04488	0.00000
Marcks	0.00000	15.88345
Flg	0.00000	14.15221
Stx6	0.00000	17.08659
Adamts	14.85673	0.00000
Itgav	12.75036	17.41807
Lrrfip2	0.00000	18.91836
Eif4e	0.00000	17.40088
Tspan9	0.00000	16.83734
Hist1h2ak	0.00000	17.50595
Eif4g1	0.00000	16.55687
Hist1h2ah;Hist1h2aa;Hist1h2ad;Hist3h2a;H2afj	23.24967	0.00000
H2afx	0.00000	11.49547
Gng12	0.00000	17.68437
Rab11fip5	0.00000	18.07134
Specc1l	0.00000	15.30421
Cdc42ep1	0.00000	17.34617
Dab2	0.00000	20.85650
Bst1	0.00000	16.05558
Sorbs2	20.95983	0.00000
Syncrip	18.74471	0.00000
Atxn2l	16.26792	0.00000
Bub3	0.00000	12.64183
Adam9	0.00000	17.10370
Eif3k	16.67751	17.44238
Rpl23a	0.00000	22.26155
Tsg101	0.00000	16.96867
Ctsd	0.00000	16.25454
Rpl18a	0.00000	21.54819
Zfp445;Znf445	14.77876	0.00000

Rps25	0.00000	19.53817
Ldlr	16.65608	17.01857
Higd1a	0.00000	16.06900
Tmod2	0.00000	17.90464
Actn4	15.90556	0.00000
Slc44a2	0.00000	13.85006
Atp6v1b2	0.00000	15.62945
Paxbp1	0.00000	13.55367
Pcnt	18.77577	0.00000
Hist1h3e;H3f3a;Hist1h3i;Hist2h3b;Hist1h3b;Hist1h3a;H3f3c	23.44484	0.00000
Rps12	0.00000	16.60983
Hist1h2bj;Hist1h2bk;Hist1h2bm;Hist1h2br;Hist1h2bp;Hist1h2bc;Hist2h2bb;Hist1h2bh;Hist1h2bb;Hist1h2bf;Hist1h2ba;Hist3h2ba;Hist3h2bb;Hist2h2be	23.71975	0.00000
Krt24	0.00000	14.36785
Ddx5	0.00000	0.00000
Hspa1l;Hsc70t	0.00000	0.00000
Tgfbi	0.00000	0.00000
Gatad2b	0.00000	0.00000
Rpl19	0.00000	21.06246
Ywhab	0.00000	0.00000
Stau1	0.00000	0.00000
Fam171a2	0.00000	15.67513
Hist1h2af	0.00000	16.43193
Srrm1	0.00000	16.43600
Gosr2	0.00000	15.44065
M21Rik	0.00000	16.50479
Rpn2	18.26759	0.00000
Soga1	0.00000	0.00000
Ebna1bp2	0.00000	0.00000
Magt1	0.00000	0.00000
Morf4l2	0.00000	0.00000
Tfe3	0.00000	0.00000
Eftud2	0.00000	0.00000
Map7d1	0.00000	18.96572
Snap23	0.00000	17.80331
Cntrl	0.00000	0.00000
Agps	0.00000	13.50283
Surf6	0.00000	0.00000
Hp1bp3	0.00000	0.00000
Emd	17.48906	0.00000
Rpl10;Rpl10l	0.00000	18.24748
Cds2	0.00000	0.00000
Mrto4;mg684	0.00000	0.00000

Ubap2	15.22819	17.27588
Atp8b4	0.00000	0.00000
Ndufb6	15.12283	0.00000
Ttll9	0.00000	0.00000
Akap2;Pakap	16.08348	0.00000
Slc1a2	0.00000	0.00000
Cd44	18.60012	0.00000
Neb	15.42565	0.00000
Tfpi	15.94133	17.69823
Plcb4	0.00000	14.69073
Fam171a1	0.00000	0.00000
Myef2	0.00000	0.00000
Raly	0.00000	0.00000
Rrbp1	16.64409	0.00000
Ubtf	0.00000	0.00000
Dpm1	0.00000	0.00000
CD59A;Cd59a	0.00000	17.32445
Rab12	0.00000	0.00000
Coro1b	0.00000	0.00000
Tmed5	0.00000	0.00000
Cox4i1	17.10908	0.00000
Olfr727	0.00000	0.00000
Pabpc4	18.36122	0.00000
Casc5	0.00000	0.00000
H13;Hm13	0.00000	0.00000
Sptan1	0.00000	17.10353
Ywhaq	0.00000	0.00000
Atp6v0c	0.00000	0.00000
Rps16	0.00000	20.71663
Mmrn2	0.00000	17.95231
Cd109	0.00000	20.08026
Fhad1	0.00000	0.00000
Lgals8	14.48788	14.66178
Hbat1;Hba	0.00000	0.00000
Ywhag	11.42696	15.19255
Slc29a1	0.00000	0.00000
Chp1	0.00000	0.00000
Pecam1	21.15972	23.34476
Msi2	0.00000	0.00000
Grb2	0.00000	16.43816
Arhgap15	0.00000	0.00000
Clta	0.00000	15.45988
Rragd;Rragc	0.00000	16.55913

Dnaja1	0.00000	0.00000
Itgb6	0.00000	0.00000
Baiap2	0.00000	0.00000
Prdx4	0.00000	0.00000
Rpsa	0.00000	20.48526
Hnrnpk	18.46310	0.00000
Pcbp2;Pcbp3	14.98385	0.00000
Rab5b	0.00000	0.00000
Dsg1b;Dsg1a;Dsg1c	0.00000	13.88700
Map1b	0.00000	14.83246
Akap12	0.00000	0.00000
Myo18a	0.00000	11.90463
Cd2ap	0.00000	0.00000
Actb;Actg1	26.74492	27.96095
Nedd4	0.00000	15.66335
Hist2h4;Hist1h4a	24.11347	0.00000
Ddx18	0.00000	0.00000
H2afv;H2afz	0.00000	0.00000
Hist2h2aa1;H2A	0.00000	0.00000
Ppp1r18	0.00000	18.63242
Myo1d	0.00000	0.00000
Hnrnpa3	18.86831	0.00000
Rbm25	0.00000	0.00000
Flna	0.00000	17.30314
Anxa1	14.97204	16.41720
Alpl	0.00000	0.00000
Ncoa5	0.00000	0.00000
Acp2	0.00000	14.26427
Rgs19	0.00000	0.00000
Abi1	0.00000	0.00000
Lmo7	21.62931	0.00000
Sntb2	0.00000	11.92308
Ddx3x;D1Pas1	16.13370	18.40222
Ankrd11	0.00000	0.00000
Tjp1	0.00000	22.57389
Sltm	0.00000	0.00000
Ppil1	0.00000	0.00000
Rasip1	0.00000	19.11505
Wwp1	0.00000	0.00000
Tnks1bp1	0.00000	15.24646
Ptp4a1;Ptp4a2	0.00000	0.00000
Gm597	0.00000	0.00000
Usp27x;Usp27	17.28819	0.00000

Serpine1	0.00000	0.00000
GAPDH	0.00000	20.38680
Cers2	0.00000	0.00000
Hnrnpdl	0.00000	0.00000
Rps15	0.00000	0.00000
Sec11a	14.91563	0.00000
Ncln	0.00000	0.00000
Exoc3l2	0.00000	0.00000
Eif4e2	14.85250	16.96642
Mov10	0.00000	0.00000
Golim4	14.59475	0.00000
Ttll5	0.00000	0.00000
Slco3a1	0.00000	0.00000
Safb;Safb2	0.00000	0.00000
Ccdc61	0.00000	13.09628
Smtn	0.00000	12.48062
Tmed7	0.00000	0.00000
Tmbim1	0.00000	0.00000
Tmem106b	0.00000	14.72418
Gnb2;Gnb4	0.00000	18.10707
Ctnnd1	0.00000	15.38476
Tnip1	16.59310	0.00000
Cope	12.94733	13.11721
Mest	0.00000	17.76098
Fip1l1	0.00000	0.00000
Cisd2	0.00000	0.00000
Fmr1	12.05212	16.94615
Hmha1	0.00000	0.00000
Hdhd2;Ier3ip1	0.00000	0.00000
Dmpk	21.90561	0.00000
Raet1e;Raet1c	0.00000	17.37597
Ctnna2	0.00000	0.00000
Gulp1	0.00000	0.00000
Cyb5a	0.00000	0.00000
Stab1	0.00000	17.58984
Cul5	0.00000	15.84549
Myo6	0.00000	17.50802
Nap1l1	0.00000	0.00000
Csnk1a1	0.00000	0.00000
Dpysl3	0.00000	0.00000
Farsa	0.00000	13.14317
Nedd4l	0.00000	0.00000
Rsl24d1	0.00000	0.00000

Rpl11	0.00000	21.05212
Tnfrsf12a	0.00000	0.00000
Srprb	0.00000	0.00000
Sipa1	16.50711	17.93118
Cct3	12.96404	0.00000
Hist2h2ac	0.00000	15.46871
Trim24	0.00000	0.00000
4732456N10Rik	0.00000	23.23259
Gigyf2	0.00000	0.00000
Synpo	0.00000	16.99803
Tpm1	0.00000	21.71132
Dsp	0.00000	0.00000
Myo1b;Myo1a	0.00000	16.71633
Hnrnpd	0.00000	0.00000
Actb	0.00000	0.00000
Tpm3	0.00000	0.00000
Ahnak	0.00000	20.08667
Myo1e	0.00000	18.50094
Ctnnb1	14.04132	16.01054
Luc7l2	17.25008	0.00000
Arf4	0.00000	0.00000
P4ha1	0.00000	0.00000
Bahcc1	0.00000	0.00000
Rbms2	0.00000	0.00000
Nnt	0.00000	0.00000
Ablim1	0.00000	18.72782
Nos3	0.00000	13.34369
Cald1	15.64976	19.31011
Rpl15	0.00000	21.85366
Cenpe	14.63530	0.00000
Vps13b	0.00000	14.86762
Inf2	0.00000	0.00000
Zfhx3	0.00000	0.00000
Ikbip	0.00000	0.00000
Triobp	0.00000	17.00441
Eef1d	16.83129	0.00000
Nop2	17.97481	0.00000
Lrrcc1	0.00000	0.00000
Col18a1	0.00000	18.94963
Ubr3	0.00000	0.00000
Rpl29	0.00000	19.85503
Rps7	0.00000	22.06393
Ermp1	0.00000	12.60262

Fxyd5	0.00000	0.00000
Tmx1	0.00000	0.00000
Oasl2	0.00000	0.00000
Eps15	13.49852	17.56639
Ppp1r12c	0.00000	16.29832
Rps18	0.00000	20.35201
Tpr	0.00000	0.00000
Eng	13.63594	16.63320
Gpx4;PHGPx	0.00000	0.00000
Hnrnpr	15.48766	0.00000
Pcdh1	0.00000	17.46153
Ahnak2	15.62247	17.44713
Gypc	0.00000	0.00000
Erc1	0.00000	16.08726
Glg1	0.00000	0.00000
Tmem55b	0.00000	16.00814
Kmt2c	15.89297	0.00000
Tpm1	0.00000	16.56535
Dnm2	0.00000	18.22985
Rps15a	0.00000	20.02459
Tra2b	0.00000	0.00000
Vkorc1	0.00000	0.00000
Vdac2	20.09072	0.00000
Prrc2a	0.00000	15.91856
Ptbp3	0.00000	0.00000
Fus;Taf15	0.00000	0.00000
Hnrnpl	0.00000	0.00000
Pabpn1	0.00000	0.00000
Rragb;Rraga	0.00000	0.00000
Flot1	0.00000	16.23650
Rps28	0.00000	15.78851
Plvap	8.19640	15.66909
Rpf2	0.00000	13.73344
Atp5h	15.21950	0.00000
Usp10	0.00000	0.00000
Fis1	0.00000	0.00000
Lrrc32	0.00000	0.00000
Cct4	17.25002	0.00000
Gprc5a	17.11871	0.00000
Lrrfip1	0.00000	18.16921
Tpm1	0.00000	19.57410
Slc25a3	21.37767	0.00000
Las2	15.23532	0.00000

Stx5a;Stx5	14.56250	0.00000
Cpsf6	0.00000	0.00000
Pou2f3	0.00000	13.34337
Ap2b1	0.00000	17.88544
Gnb1	0.00000	19.17637
Tcof1	0.00000	0.00000
Cxcl12	0.00000	0.00000
Tpi1	0.00000	0.00000
Ccdc179	0.00000	0.00000
Irgm1	16.45705	0.00000
Bsg	0.00000	0.00000
Myh14	0.00000	21.00138
Atp6v0a1	0.00000	16.78093
Rac1;Rac3;Rac2	0.00000	20.33898
S1pr1	0.00000	0.00000
Zfp207;Znf207	0.00000	13.93188
Csnk2b;Csnk2b-Ly6g5b	0.00000	18.01946
Cacna2d1	0.00000	13.64250
Sec22b	16.56748	0.00000
Dpysl2;Crmp1	0.00000	0.00000
Lgals9	0.00000	20.84202
Alyref	16.31678	0.00000
Bak1	16.30527	0.00000
Sdcbp	16.56674	17.01283
Degs1	18.65215	0.00000
Sypl;Sypl1	0.00000	18.46365
Ptgis	0.00000	0.00000
Scarb2	0.00000	18.57612
Phb2	20.86027	0.00000
Purb	0.00000	17.30326
Nrp2	0.00000	18.74602
Myadm	14.62495	19.32868
Hnrnph1;Hnrnph2	17.93959	0.00000
Slc1a4	0.00000	16.25535
Lsm2	0.00000	0.00000
Ptrf	0.00000	19.77045
Ddost	19.22294	0.00000
Il16	0.00000	0.00000
Bysl	0.00000	0.00000
Csnk2a2	0.00000	0.00000
Itgb3	0.00000	16.55691
Reps1	0.00000	18.68034
Dnajb6	13.79394	0.00000

Banf1	0.00000	0.00000
Pgrmc1	17.72045	0.00000
Eif6	0.00000	0.00000
Rpl35a	0.00000	18.09836
Atp2a2	0.00000	0.00000
Nmt1	0.00000	0.00000
Tspan6	0.00000	17.04296
Stx7	0.00000	18.63148
Vamp4	0.00000	0.00000
Snrpn;Snrpb	0.00000	0.00000
Hsd17b12	0.00000	0.00000
rps14;Rps14	0.00000	0.00000
H2-D1;H-2D;H2-L	13.28290	16.61588
Wdr1	0.00000	18.12918
Vti1b	0.00000	17.23260
Hnrnpa2b1	19.96470	0.00000
Lamtor3	0.00000	0.00000
F11r	0.00000	0.00000
Adam15	0.00000	0.00000
Yme1l1	0.00000	0.00000
Stx8	15.25820	0.00000
Leprot	0.00000	0.00000
Itm2b	0.00000	0.00000
Rbm3	0.00000	0.00000
Cd93	15.91579	0.00000
Vti1a	0.00000	0.00000
H2-K1;H2-K	16.32234	0.00000
Tgfb1	0.00000	0.00000
Prnp;Prnpb	0.00000	0.00000
Tuba1b;Tuba4a	17.77056	18.55225
Ly6a	0.00000	0.00000
Gap43	0.00000	0.00000
Anxa2	0.00000	16.54764
Gnai2	0.00000	20.76285
Itgb1	19.58851	20.40907
P4hb	0.00000	0.00000
Ncl	0.00000	21.06338
Calm1;Calml3	0.00000	0.00000
Eef1a1	0.00000	19.79223
Rras	0.00000	16.78979
Slc3a2	17.34863	0.00000
H1f0	0.00000	0.00000
Lamp1	0.00000	0.00000

Hsp90ab1	0.00000	0.00000
Itga5	17.63318	19.69024
Oas1g;Oas1a	0.00000	0.00000
Tcp1	17.39188	0.00000
Rpl7a	0.00000	23.12624
Icam1	0.00000	19.91639
Rpl27a	0.00000	20.96350
Rpl7	22.96149	23.20262
Lmnb1	17.09757	0.00000
Rplp0	0.00000	22.36984
Hmox1	0.00000	16.27561
Thbd	18.25425	0.00000
Hist1h1c	20.18422	0.00000
Lamp2	0.00000	0.00000
Hmga1	0.00000	0.00000
Fam167b	0.00000	17.95016
Ap2a1	15.59941	16.89696
Ap2a2	0.00000	16.04031
Slc2a1	17.65790	16.96909
Cfl1	0.00000	20.52987
Rpl13a	19.60422	21.64278
Serpinh1	15.89178	0.00000
Hspa5	0.00000	0.00000
Vim	26.34357	0.00000
Tpm3	0.00000	22.65905
Gna11	0.00000	16.97436
Gnaq	0.00000	16.42762
Mfge8	0.00000	0.00000
Tgm2	0.00000	0.00000
Eif3a	0.00000	15.82642
Cbx3	0.00000	0.00000
Prkch	0.00000	16.73057
Ppib	0.00000	0.00000
Capg	0.00000	0.00000
M6pr	0.00000	0.00000
Mcm3	0.00000	0.00000
Rps2;Gm6576	15.22003	0.00000
Lyn	0.00000	15.97415
Msn	0.00000	18.52815
Rdx	0.00000	15.48895
Ctnna1	14.46956	15.58295
U2af2	0.00000	0.00000
Man2a1	0.00000	0.00000

Map4	0.00000	20.29954
Rpl3	0.00000	21.63688
Pdia3	17.34392	0.00000
Marcksl1	0.00000	16.49389
Grn	0.00000	0.00000
Ptprm	0.00000	16.42099
Pabpc1	21.00949	21.25427
Ppic	0.00000	18.02105
Ssb	0.00000	0.00000
Drg1	0.00000	17.58258
Pvrl2	0.00000	0.00000
Kras;Hras	15.32720	16.14503
Rab5c	16.27054	0.00000
Rab6a;Rab6b	17.70230	0.00000
Rab18	17.37967	0.00000
Icam2	13.61156	0.00000
Plaur	19.75714	0.00000
Fbl	17.04834	0.00000
Canx	18.40000	0.00000
Prdx1	0.00000	19.13042
Cd81	0.00000	13.31628
Rpl12	0.00000	20.97227
Rpl18	21.38325	21.41876
Por	17.46353	0.00000
Hspa9	0.00000	0.00000
Timp3	0.00000	0.00000
Rpl28	0.00000	21.02817
Eif4a1	18.15594	18.91559
Pura	18.42197	17.23809
Cct8;Cctq	0.00000	0.00000
Hist1h1e	20.71638	0.00000
Hist1h1a	16.47938	0.00000
Hist1h1b	19.17525	0.00000
Hist1h1d	20.35200	0.00000
Cfl2	0.00000	0.00000
Capza2	21.93517	22.74181
Capzb	0.00000	21.04462
Emp1	0.00000	0.00000
Rpl6	0.00000	23.70332
Rplp1	20.45834	0.00000
Rpl5	0.00000	20.91649
Rpl13	0.00000	22.95402
Lmna	23.46976	0.00000

Slc25a4	18.78924	0.00000
Hnrnpa1	18.07508	0.00000
Hcls1	0.00000	15.55255
Psen1	0.00000	11.01495
Cav1	0.00000	19.57003
Cav1	21.52741	0.00000
Srp9	0.00000	0.00000
Atp6v1e1	0.00000	17.16546
Pa2g4	0.00000	18.99418
Rab7;Rab7a	17.02443	0.00000
Rpl9	20.84547	21.25882
Atp6v0d1	10.89936	16.93522
Slc25a5	21.79900	0.00000
Kpna2	0.00000	0.00000
Tmem165	0.00000	0.00000
Hmga2	0.00000	0.00000
Slc16a1	0.00000	15.53655
Rab2a;Rab2b	0.00000	0.00000
Cnbp	0.00000	16.44060
Stom	0.00000	19.21300
Ddx6	0.00000	17.82861
Cdh5	0.00000	16.83820
Entpd1	15.66521	18.09918
Cox6b1	0.00000	0.00000
Atp5b	23.26738	0.00000
Cckbr	0.00000	0.00000
Cd38;CD38	0.00000	17.58346
Ncstn	0.00000	17.05162
Atp6v1d	0.00000	0.00000
Snrpa1	0.00000	0.00000
Slc16a3	0.00000	0.00000
Acot8	15.01396	16.48170
Smpdl3b	0.00000	18.32567
Eef2	0.00000	0.00000
Tpm1	0.00000	17.04772
Arpc4	0.00000	21.86602
Ruvbl1	0.00000	0.00000
Eif3e	0.00000	15.72973
Cdc42	0.00000	0.00000
Cirbp	0.00000	0.00000
Eif4a2	13.80137	17.49214
Rps20	0.00000	19.70365
Dnajc5	0.00000	15.59164

Rab10	0.00000	0.00000
Rab8b	0.00000	0.00000
Actr2	0.00000	20.16754
Actr1a	15.16257	15.92509
Arf3;Arf1;Arf2	0.00000	0.00000
Rap2b	0.00000	0.00000
Rpl26	0.00000	22.14801
Magoh;Magohb	12.49519	0.00000
Rpl27	0.00000	21.25738
Rpl37a	21.42535	18.72089
Sec61a1	0.00000	0.00000
Dad1	16.04687	0.00000
Rras2	15.13464	0.00000
Ppp1ca	0.00000	16.45030
Ppp1cb	0.00000	0.00000
Rps8	0.00000	22.46398
Ywhae	0.00000	16.18760
Rps23	0.00000	19.04322
Rps29	0.00000	0.00000
Rps11	0.00000	21.62945
Rps13	0.00000	21.41493
Snrpe	0.00000	0.00000
Snrpf	0.00000	0.00000
Snrpd1	0.00000	0.00000
Snrpd2	0.00000	0.00000
Snrpd3	18.01690	0.00000
Rps4x;Rps4l	0.00000	21.05101
Ppp2cb;Ppp2ca	0.00000	0.00000
Ap2s1	0.00000	18.87728
Rps6	0.00000	22.73980
Rasl2-9	14.77331	0.00000
Rpl23	0.00000	18.86282
Rps24	16.96428	17.11952
Rps26	21.66345	18.11942
Fau	0.00000	0.00000
Rpl30	0.00000	20.82778
Rpl39	0.00000	18.40624
Rpl31	0.00000	20.93462
Rps3	0.00000	22.29005
Rpl32	0.00000	20.17637
Rpl8	0.00000	21.79994
Fbxo40	0.00000	0.00000
Ybx1	0.00000	20.60850

Rps27a	21.95719	0.00000
Hspa8	0.00000	20.25311
Vamp3;Vamp2	0.00000	16.97365
Ppp1cc	0.00000	0.00000
Gnas	0.00000	15.91579
Ywhaz	0.00000	18.22572
Dynll1	0.00000	0.00000
Actg1	21.38089	18.84251
Rps17	20.37613	0.00000
Rala	17.51902	18.64505
Rps10	0.00000	19.76598
Phb	20.17270	0.00000
Rpl22	20.79656	20.80591
Actc1;Acta2;Actg2;Acta1	16.71621	20.74104
Gnb2l1	0.00000	15.36412
Tuba1c;Tuba1a;Tuba3a;Tuba8	0.00000	0.00000
Ywhah	16.12161	16.34551
Kpnb1	0.00000	0.00000
Vamp7	0.00000	17.12582
Elavl1	18.12851	0.00000
Stx4	0.00000	16.54558
Vasp	0.00000	18.36514
Naca	0.00000	17.75881
Cct2	17.23135	16.06967
Cct5	0.00000	0.00000
Cct6a	17.71187	0.00000
Rpl36a	0.00000	19.12187
Ap2m1	0.00000	19.94502
Rhog	0.00000	0.00000
Srsf3	17.07309	0.00000
Nptn	0.00000	17.30243
Csrp2	0.00000	17.23251
Csrp1	0.00000	0.00000
Rps3a1;Rps3a	0.00000	21.47234
Atp1b3;atp1b3	0.00000	18.33772
Frg1	0.00000	16.27574
G3bp2	0.00000	19.58770
G3bp1	0.00000	21.27812
Brca2	0.00000	0.00000
Tubb5;Tubb2b;Tubb2a;Tubb3	16.61827	14.75881
Rplp2	0.00000	15.72734
Col8a1	0.00000	21.45704
Hnrnpul2	0.00000	0.00000

Top2a	0.00000	0.00000
Notch1	0.00000	12.79969
Rsu1	13.95432	17.09032
Vcp	16.31599	0.00000
Jup	0.00000	0.00000
Epha2	16.21529	0.00000
Atp5a1	23.00326	0.00000
Eif2ak2	0.00000	16.25991
Yes1;Lck;Fyn;Src	0.00000	13.31628
LOC72520	0.00000	0.00000
Eif5b	0.00000	0.00000
Utp3	0.00000	0.00000
Add3	0.00000	0.00000
Atp5k;Atp5i	0.00000	0.00000
Cnn2;Cnn3	0.00000	16.02162
Tgm3	0.00000	13.25808
Slc7a1;SLC7A1	0.00000	12.65508
Rab1b	14.23007	0.00000
Rpl22l1	0.00000	0.00000
Ccdc47	15.70250	0.00000
Plp2	0.00000	0.00000
Jdp2	0.00000	0.00000
Ehd4	0.00000	17.67049
Rsl1d1	16.96871	0.00000
Atp6ap2	0.00000	0.00000
Hnrnpab	15.48138	0.00000
Plcb1	0.00000	0.00000
Klra4;Klra15;Klra20;Klra16;Klra7;Klra18;Ly-49A;Klra1;Klra23	0.00000	14.52383
Gsdma3;Gsdma2;Gsdma	0.00000	15.63218
Ptbp1	19.94273	0.00000
Plscr3	0.00000	0.00000
Wasf2	0.00000	0.00000
Fxr2	0.00000	0.00000
Hs3st3b1;Hs3st3a1	0.00000	0.00000
Npm3	0.00000	0.00000
Scamp2	0.00000	16.37087
Appl2	0.00000	0.00000
Arpc1b	0.00000	20.82736
Ppp1r13l	0.00000	0.00000
Picalm	0.00000	17.13025
Scamp1	14.12918	16.03603
Stx12	0.00000	20.84521
Mfge8	0.00000	19.72949

Rcn2	0.00000	0.00000
Coro1c	0.00000	17.30652
Atp5o	20.06205	0.00000
Nono	14.25020	0.00000
Lrrc59	17.09987	15.07779
Tmod3	19.75966	23.26303
Dnaja2	0.00000	15.50339
Tmed9	17.71900	0.00000
Atp6v1c1	0.00000	0.00000
Ehd1	16.74583	0.00000
Actr3	0.00000	18.68072
Srsf7	17.34352	0.00000
Eif4b	0.00000	15.50256
Hnrnpm	17.90638	0.00000
Pdia6	12.67655	17.01683
Dkc1	16.91959	0.00000
Uqcrc1	17.55500	0.00000
Ndufs1	0.00000	0.00000
Zc3h15	0.00000	15.97634
Golm1	0.00000	16.21048
Rtcb	0.00000	0.00000
Dnaja3	0.00000	0.00000
Atp5f1	0.00000	0.00000
Pdlim7	16.62921	0.00000
Gnai3	0.00000	0.00000
Gnl3	0.00000	0.00000
Arpc5	0.00000	18.14685
Rps2	0.00000	21.36771
Skp1a	0.00000	14.73591
Eif2s3y	0.00000	0.00000
Mybbp1a	0.00000	0.00000
Cdk5rap3	0.00000	0.00000
Eif2s3x	0.00000	15.47548
Utp15	0.00000	0.00000
Tmpo	19.06423	0.00000
Ppp2r2a	0.00000	0.00000
Maoa	0.00000	0.00000
Hmgcll1	0.00000	15.21561
Dctn2	0.00000	10.31817
Dctn4	0.00000	0.00000
Sh3gl1	0.00000	15.05388
Dbn1	0.00000	21.52365
Snd1	0.00000	19.70235

Tomm70a	0.00000	0.00000
Vdac3	16.17771	0.00000
Gdf15	0.00000	0.00000
Trim25	0.00000	0.00000
Ssr1	14.93572	0.00000
Ssr4	18.17383	0.00000
Sf3a1	16.60302	0.00000
Hnrnpu	19.15010	0.00000
Srsf6;Srsf4	0.00000	0.00000
Vat1	14.47970	15.24995
Epn3	0.00000	0.00000
Snx9	0.00000	19.04328
Rab35	0.00000	17.06830
Esam	17.52096	0.00000
Tnfrsf23	0.00000	0.00000
Ppfibp1;Ppfibp2	0.00000	14.05861
Sfxn3	16.36692	0.00000
Mapre1	0.00000	15.64087
Rpl10a	0.00000	22.86180
Ifit1	15.52517	0.00000
Rbm14;p16	17.42043	0.00000
Hnrnpc	19.83284	0.00000
Ddx17	0.00000	0.00000
Atp6v1g1	0.00000	17.87600
Esyt1	14.65247	0.00000
Rpl7l1	0.00000	0.00000
Poldip3	0.00000	0.00000
Eif3f	16.42773	17.25752
Rpn1	18.83142	0.00000
Lman1	0.00000	14.75168
Sh3bgrl	0.00000	0.00000
Lbr	0.00000	0.00000
Bcap31	17.78541	0.00000
Slc31a2	0.00000	0.00000
Mtch2	0.00000	0.00000
Capza1	0.00000	23.21312
Vim	0.00000	0.00000
Actb	0.00000	23.11712
Actb	0.00000	0.00000
Eif1a;Eif1ax	15.54834	0.00000
Cdc5l	0.00000	0.00000
Nmes1	0.00000	0.00000
Atp5c1	20.01599	0.00000

Txlna	0.00000	16.58880
Plscr1	0.00000	0.00000
Hgsnat	0.00000	15.28675
Puf60	17.96668	0.00000
Flot2	0.00000	15.32638
Slc1a5	17.80950	0.00000
Derl1	0.00000	0.00000
Wdr19	0.00000	0.00000
Rasa3	0.00000	14.40219
Wasl	0.00000	0.00000
Clint1	0.00000	15.28675
Ttc21b	0.00000	0.00000
Parvb	0.00000	0.00000
Myh10	0.00000	22.79844
Tln1	0.00000	0.00000
Ewsr1	0.00000	18.71649
Maged1	0.00000	14.78982
Btf3	17.55739	16.72103
Cmtm6	0.00000	0.00000
Ddx21	17.39087	0.00000
Eif2s2	0.00000	18.72222
Serbp1	0.00000	18.78337
Mcu	0.00000	0.00000
Ythdf2	0.00000	14.99472
Endod1	0.00000	0.00000
Slc7a5	0.00000	0.00000
Aatf	0.00000	0.00000
Nop56	0.00000	0.00000
Abcf2	0.00000	0.00000
Vwa3a	0.00000	0.00000
Rpl24	0.00000	20.63821
Ilf2	0.00000	0.00000
Scamp3;Tu52	16.18946	17.89125
Podxl	0.00000	0.00000
Adrbk2	16.05579	0.00000
Lrrfip1	0.00000	17.33705
Aimp1	14.01198	0.00000
Stx3	0.00000	14.23619
Eef1a1	0.00000	0.00000
Gm906	14.81916	0.00000
Spag8	0.00000	0.00000
Ddx1	17.00690	13.54432
Dstn	0.00000	0.00000

Ssr3	17.67457	0.00000
Eef1g	15.96780	0.00000
Gm8765	0.00000	17.58049
Ndufb4	0.00000	0.00000
Rab14	17.70072	0.00000
Rpl38	0.00000	0.00000
Rap1b	0.00000	14.92447
Rheb	0.00000	0.00000
Exosc4	0.00000	0.00000
Tfrc	0.00000	17.66236
Cd34	0.00000	18.17047
Rpl4	0.00000	21.66806
Thrap3	0.00000	17.93587
Zkscan3	0.00000	0.00000
Trim28	0.00000	0.00000
Nufip2	0.00000	18.58858
Tmem2	0.00000	17.13397
Prdx2	0.00000	15.57163
Epn2	0.00000	16.55035
Abcf1	0.00000	17.81205
Igf2bp2	16.95587	16.34851
Npm1	19.79588	0.00000
Tom1l2	0.00000	0.00000
Tom1l2	16.79732	0.00000
Rab1;Rab1A	0.00000	0.00000
Slc25a11	0.00000	0.00000
Cltc	15.11689	15.77486
Jagn1	0.00000	0.00000
Cttn	0.00000	18.84761
Csnk2a1	0.00000	15.48138
Khdrbs1	0.00000	0.00000
Caprin1	0.00000	20.72886
Eps15l1	0.00000	19.98542
Zfp317	0.00000	0.00000
Vdac1	21.01198	0.00000
Ybx1	0.00000	0.00000
Rbbp4	0.00000	0.00000
Hras;Nras	0.00000	0.00000
Fscn1	0.00000	16.16555
Fxr1	0.00000	20.27810
Cd47	0.00000	17.54498
Itga6	0.00000	20.04820
H2-D1	0.00000	0.00000

Rnps1	0.00000	0.00000
Rhoc;Rhoa;Rhob	15.73653	0.00000
Itga2	0.00000	0.00000
Itga3	19.19916	0.00000
Sdpr	0.00000	18.27245
Utp14a	0.00000	0.00000
Sqstm1	17.00005	0.00000
Sdc3	0.00000	14.67728
Procr	0.00000	0.00000
Cr1l	0.00000	17.64508
Jmjd1c	0.00000	14.91202
Tbc1d30	0.00000	0.00000
Emc2	0.00000	0.00000
Rftn1	0.00000	17.06608
Nomo1	0.00000	0.00000
Tpm4	0.00000	22.57404
Fam3c	0.00000	0.00000
Dusp11	0.00000	0.00000
Fxr2	17.69423	17.33225
Nes	20.45531	0.00000
Ccdc148	0.00000	0.00000
Ano6	0.00000	13.14147
Rpl17	0.00000	20.82832
Ppp1r9b	0.00000	16.89936
Plec	18.63159	0.00000
Larp1	0.00000	0.00000
Matr3	0.00000	0.00000
Lsm8	0.00000	0.00000
Rps9	0.00000	21.93576
Spcs3	0.00000	0.00000
Myl12a	0.00000	16.95068
Rpl35	18.36439	20.53602
Eif2s1	0.00000	17.22396
Rps27l	0.00000	17.96422
Rpl36	0.00000	0.00000
Mgat5b	0.00000	0.00000
Usmg5	0.00000	0.00000
Apool	0.00000	0.00000
Tmed3	0.00000	0.00000
Vma21	0.00000	0.00000
Ostc	0.00000	0.00000
Dek	0.00000	0.00000
Rrs1	0.00000	0.00000

Pgrmc2	14.84875	0.00000
Iqgap1	0.00000	16.32632
Fam98b	0.00000	0.00000
Epn1	0.00000	16.21974
Mtdh	0.00000	0.00000
Tspan18	0.00000	0.00000
Fbll1	0.00000	0.00000
Ddrgk1	0.00000	0.00000
Ubap2l;lig-2a	0.00000	18.99664
Flnb	0.00000	0.00000
Pdcd6ip	0.00000	17.17114
Tnc	0.00000	17.48901
Wbscr25	15.64573	0.00000
Actbl2	25.99547	27.82845
Erlin2	15.13022	0.00000
Ppp1r12b	0.00000	17.39473
Bcam	0.00000	17.20623
Samm50	0.00000	0.00000
U2af1l4;U2af1	0.00000	0.00000
Ccny	0.00000	12.95189
Slc25a12	18.02317	0.00000
Ehd2	16.04132	14.69171
Rtn4	18.27337	18.64878
Vapb	17.26688	0.00000
Lyve1	0.00000	0.00000
Add3	15.54402	19.90345
Fbxo30	15.00358	15.07755
Sun2	0.00000	0.00000
Eif2a	0.00000	0.00000
Thyn1	0.00000	0.00000
Ptk7	0.00000	15.70356
Slc25a24	14.30302	0.00000
Dlat	0.00000	0.00000
Ckap4	21.97439	0.00000
Rbfox2	16.54729	0.00000
Tollip	5.29768	14.48283
Cdh13	0.00000	18.36345
She	0.00000	0.00000
Timmdc1	0.00000	0.00000
Pvr	17.71934	0.00000
Gimap3	0.00000	0.00000
Gimap5	0.00000	18.10180
Ythdf3	0.00000	0.00000

Tor1aip2	0.00000	0.00000
Ttc39b	0.00000	0.00000
Prkd2	0.00000	0.00000
Add2	13.89125	17.71187
Slc25a13	13.64641	0.00000
Tmem14c	0.00000	0.00000
C130021I20	0.00000	0.00000
Rps19bp1	0.00000	0.00000
Usp20	0.00000	0.00000
Tpm3	0.00000	0.00000
Kctd12b	0.00000	0.00000
Efhd2	0.00000	20.26633
Immt	18.61037	0.00000
Palm	0.00000	16.74272
Prpf31	0.00000	0.00000
Ralb	17.80305	18.13320
Ccdc150	0.00000	0.00000
Lamtor4	0.00000	0.00000
Slc38a2	0.00000	17.62635
Pcdh1	0.00000	19.81745
Myl6b	0.00000	0.00000
Eif3b	17.45488	0.00000
Apol9b	0.00000	0.00000
Timm23	0.00000	0.00000
Slc25a1	14.96924	0.00000
Lmbrd1	0.00000	15.16021
Spats2	0.00000	0.00000
Add1	0.00000	20.48766
Mmgt1	0.00000	0.00000
Colgalt1	0.00000	0.00000
Eva1b	0.00000	0.00000
Colec12	0.00000	17.85844
Eif3l	0.00000	15.23717
Sf3b4	0.00000	0.00000
Vps37c	0.00000	0.00000
Eif3c	0.00000	0.00000
Tmed4	0.00000	0.00000
Dnttip2	0.00000	0.00000
Bst2	0.00000	22.24278
Mcam	20.20144	21.80630
Ptrh2	0.00000	0.00000
Gle1	0.00000	0.00000
Myct1	13.76763	16.90254

Nup35	0.00000	0.00000
C1qbp	0.00000	0.00000
Rbpms2	12.70585	0.00000
Cald1	0.00000	0.00000
Myh9	0.00000	24.38293
Atp1a1	0.00000	19.28350
Apol9a	17.27797	0.00000
Mitd1	0.00000	0.00000
Pdcd10	17.15686	18.14309
Tmem30a	0.00000	17.54525
Oasl1	15.05965	0.00000
Sfpq	0.00000	0.00000
Plcb4	0.00000	18.86502
Rps5	19.15041	18.00470
Eif4a3	18.07370	0.00000
Nifk	16.47351	0.00000
Chchd3	16.77567	0.00000
Prkcdbp	0.00000	0.00000
Rbmxl1;Rbmx	18.70958	0.00000
Tcirg1	0.00000	19.78660
Golga7	0.00000	12.51175
Ubtd1	0.00000	0.00000
Rrp9	0.00000	0.00000
Basp1	0.00000	19.22678
Twf1	0.00000	22.19763
Tmem63a	0.00000	15.32848
Ppan	0.00000	0.00000
Bmp2k	0.00000	15.29302
Ddx27	0.00000	0.00000
Tor1aip1	16.54411	0.00000
Imp3	0.00000	0.00000
Atad3;Atad3a	0.00000	0.00000
Myo5a	0.00000	16.95829
Dhx58	16.65261	0.00000
Ifitm2	0.00000	0.00000
Stoml2	16.25551	0.00000
Homer3	0.00000	16.94081
Sfxn1	16.03433	0.00000
Eif3m	0.00000	0.00000
Ppap2b	0.00000	16.58964
Emc3	14.52260	0.00000
Prpf19	0.00000	0.00000
Dnajb11	0.00000	16.78213

Itfg1	0.00000	0.00000
Tspan13	0.00000	0.00000
Cox6c	0.00000	0.00000
Tomm22	17.11678	0.00000
Atp5l	17.13377	0.00000
Myl9	0.00000	0.00000
Lamtor1	16.09562	16.52925
Tspan31	0.00000	15.66696
Rab5a	0.00000	0.00000
Nudt21	17.82993	0.00000
Snrpb2	0.00000	0.00000
Ndufb9	0.00000	0.00000
Rpl21	0.00000	21.62309
Sec61b	0.00000	0.00000
Rer1	12.78545	0.00000
Pam16	0.00000	0.00000
Ykt6	0.00000	0.00000
Ifitm3	20.41724	0.00000
Cyb5b	18.99162	0.00000
Ndufa6	0.00000	0.00000
Ndufb3	0.00000	0.00000
Rpl14	0.00000	22.57544
Nhp2	0.00000	0.00000
Arpc2	0.00000	22.09911
Rbm8a	0.00000	0.00000
Yif1b	0.00000	0.00000
Hnrnpa0	16.30474	0.00000
Grap	0.00000	0.00000
Nip7	0.00000	0.00000
Rpl14-ps1	0.00000	16.38037
Napa	14.99170	15.09713
Glipr2	13.76242	0.00000
Nde1	0.00000	0.00000
Utp11l	0.00000	0.00000
Hspa12b	0.00000	0.00000
Tmem206	0.00000	16.74724
Tmem55a	0.00000	16.07284
Rps19	0.00000	18.84537
Emc4	0.00000	0.00000
Dynll2	0.00000	0.00000
Tmem88	0.00000	0.00000
Lsm12	16.51124	15.23132
Nhp2l1	0.00000	0.00000

Vps28	0.00000	0.00000
Tmed10	18.03238	0.00000
Cxx1a	18.34495	0.00000
Fkbp11	0.00000	0.00000
Rpl34;Gm2178	0.00000	21.35344
Coa3	0.00000	0.00000
Plgrkt	0.00000	0.00000
Ndufb8	16.79810	0.00000
Ndufv2	0.00000	0.00000
Timm50	0.00000	0.00000
Arpc5l	0.00000	19.19293
Chmp2a	0.00000	0.00000
Uqcrc2	18.21776	0.00000
Ngdn	0.00000	0.00000
Ftsj3	0.00000	0.00000
Lman2	14.67801	0.00000
Ppp1r12a	0.00000	19.65549
Tmem43	19.32007	0.00000
Ikbip	0.00000	0.00000
Ndufs7	0.00000	0.00000
Ndufa8	0.00000	0.00000
Ndufb10	16.88240	0.00000
Ndufs3	16.42706	0.00000
Rai14	0.00000	0.00000
Rp2	0.00000	17.23067
Snap29	0.00000	0.00000
Lima1	0.00000	21.59035
Ndufa13	0.00000	0.00000
Plac8	15.63915	19.11841
Raet1d	0.00000	17.24507
Praf2	0.00000	0.00000
Flii	16.09678	16.73463
Grasp	0.00000	13.39968
Tmem191c	0.00000	14.94413
Ybx3;Igf2bp3	0.00000	19.06616
Arpc3	0.00000	16.54422
Gkap1	0.00000	0.00000
Edf1	0.00000	0.00000
Clca3a1;Clca3a2	0.00000	15.98608
Tomm40	0.00000	0.00000
Actg1	0.00000	13.11146
Eif3i	0.00000	15.47136
H2afy	17.10421	0.00000

Pex14	16.47985	0.00000
Ak1	0.00000	17.09624
Htra1	0.00000	14.88820
Tmem176b	0.00000	0.00000
Myo1c	0.00000	20.41087
Prkra	0.00000	0.00000
Vapa	17.45271	0.00000
Cav2	0.00000	20.05977
Twf2	16.10847	17.78743
Tjp2	0.00000	22.24607
Hnrnpf	0.00000	0.00000
Gm17087	17.05240	0.00000
Abcg2	0.00000	17.64024

Appendix 2: Ingenuity Pathway Analysis results

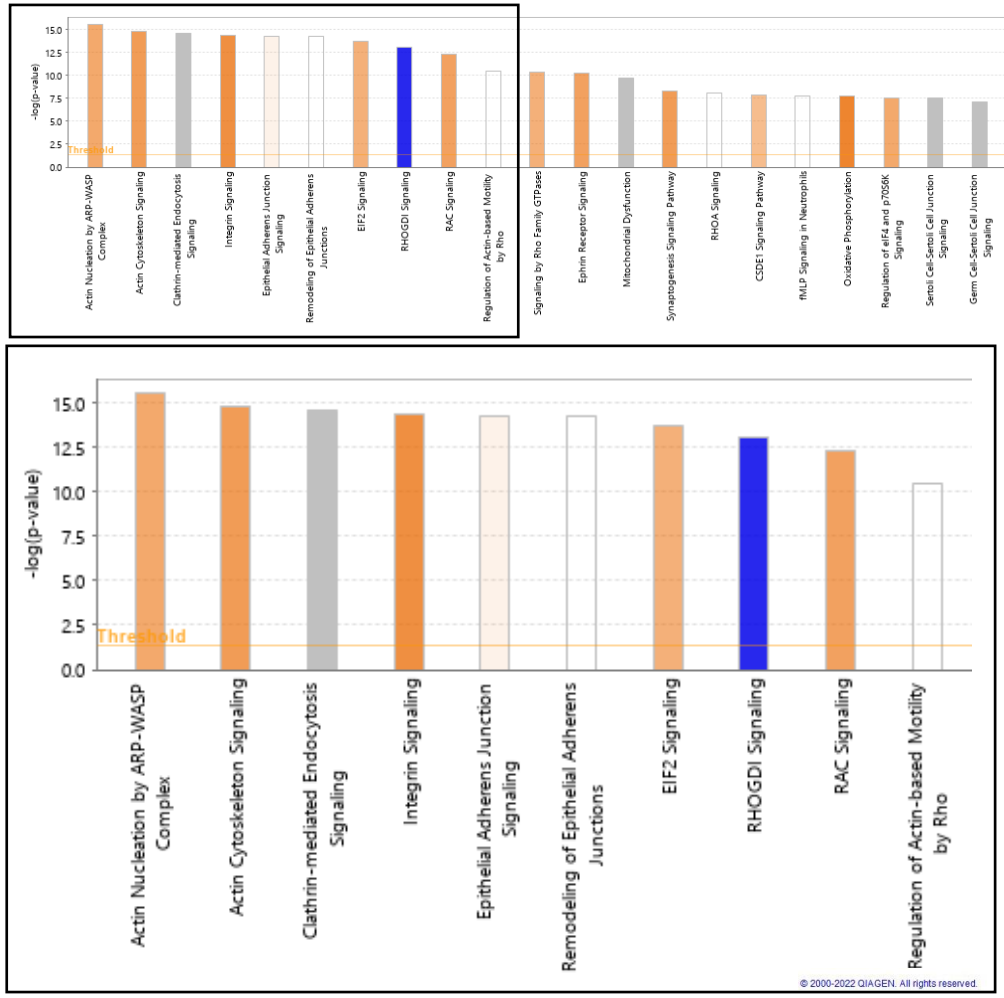

Figure 1: Top 10 highest confidence cellular pathways by Log2 (fold-change).

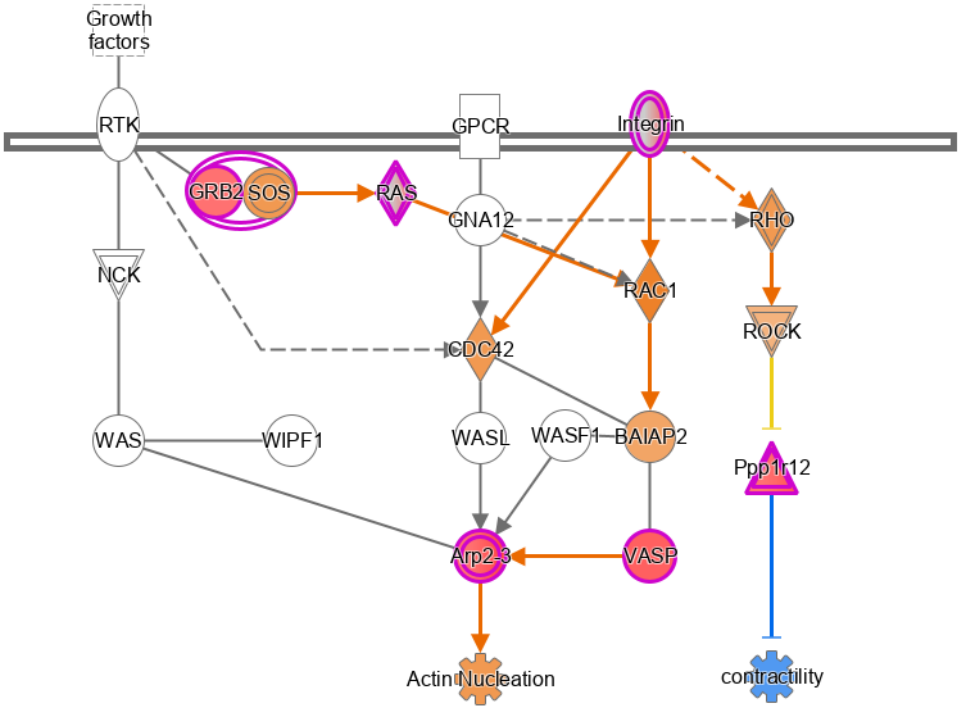

Figure 2: Actin nucleation by ARP/WASP complex.

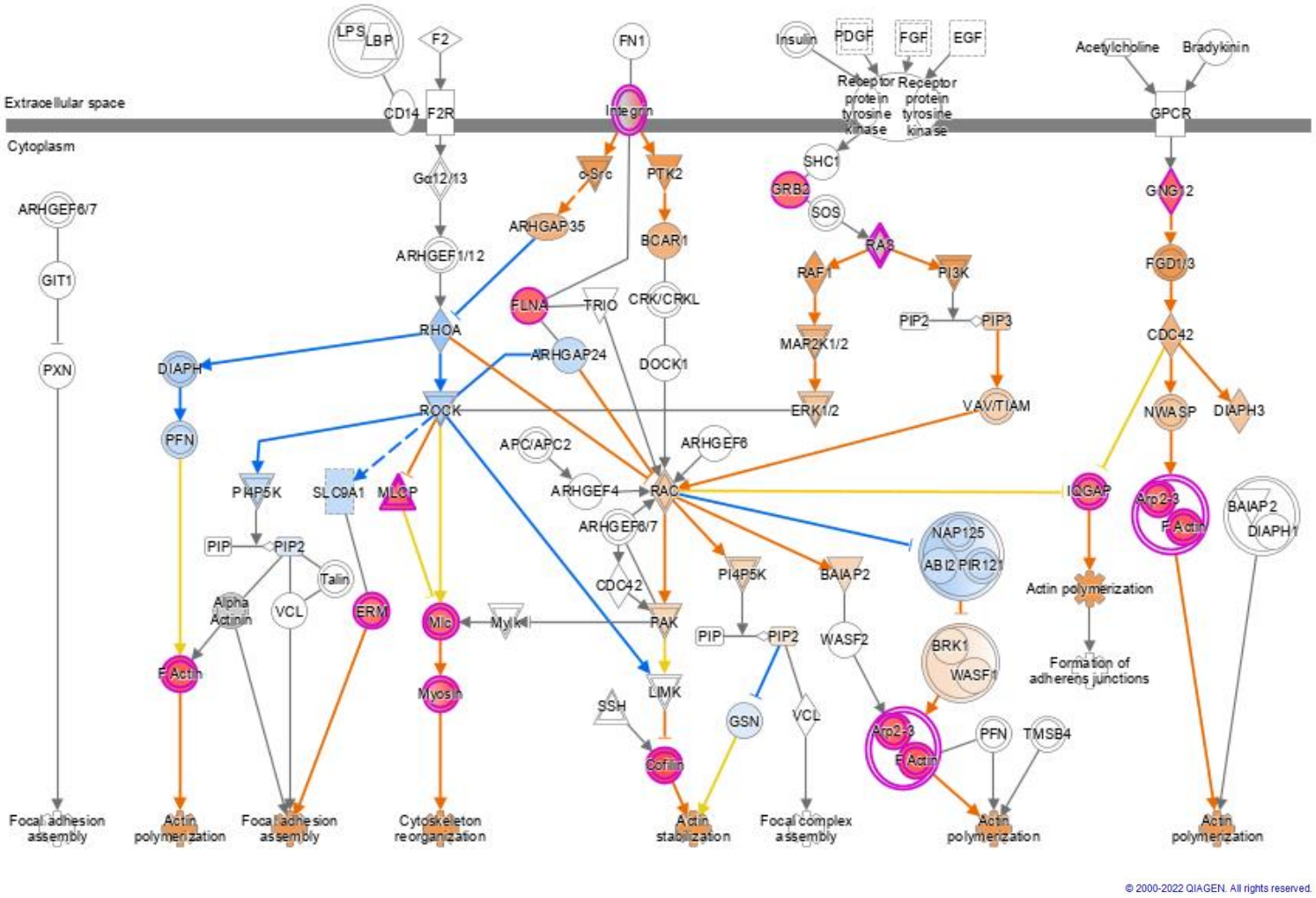

Figure 3: Actin cytoskeleton signalling.

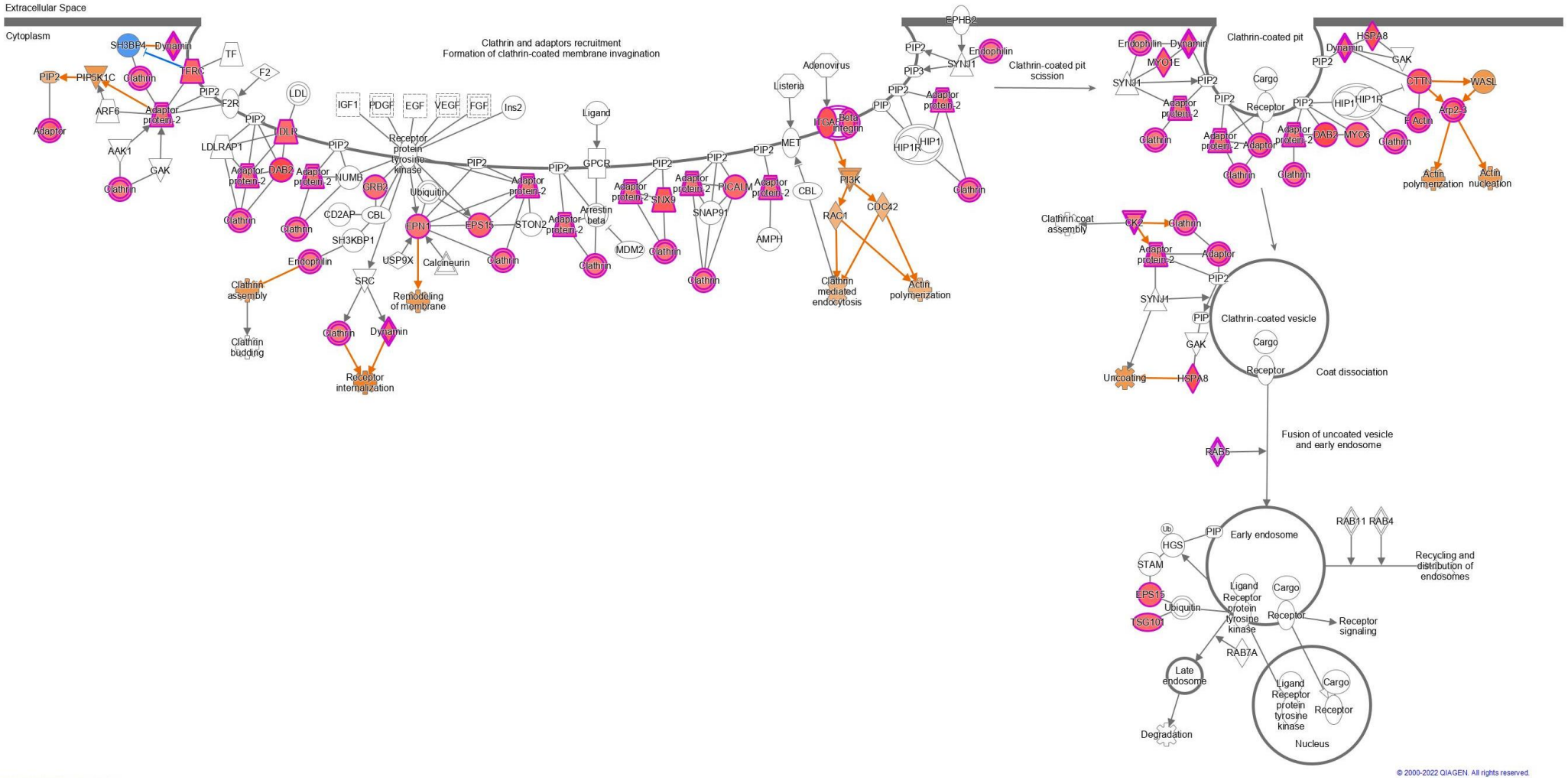

Figure 4: Clathrin-mediated endocytosis.

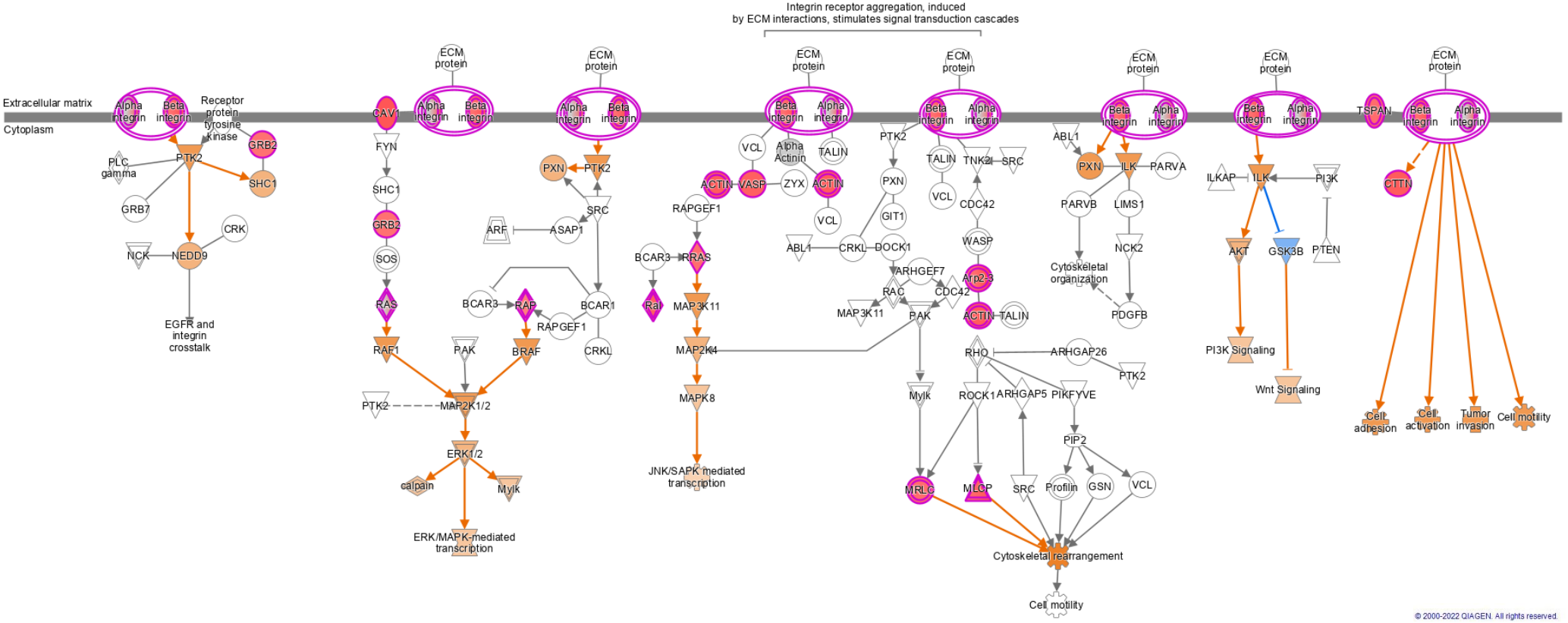

Figure 5: Integrin signalling.

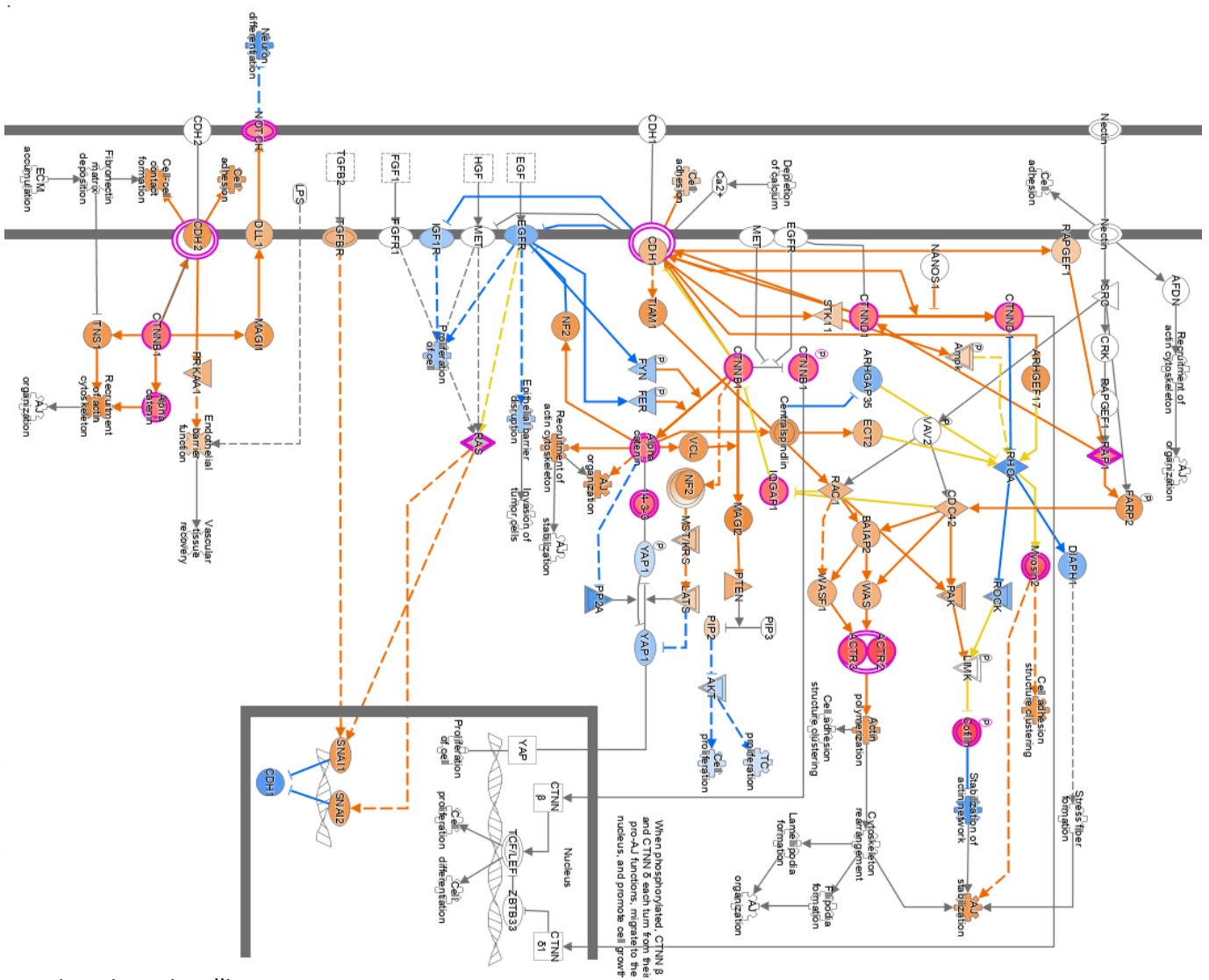

Figure 6: Epithelial adherens junctions signalling.

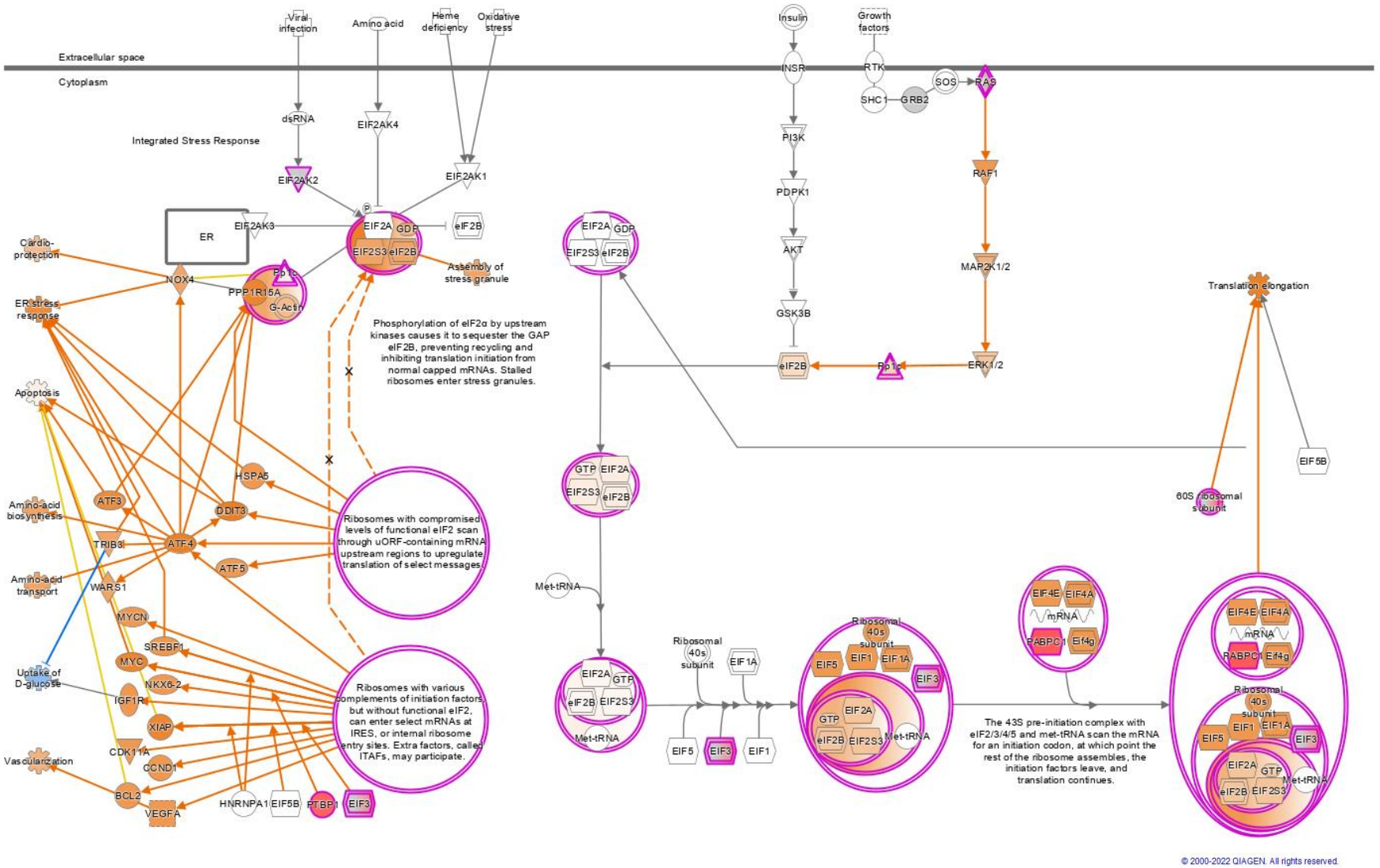

Figure 7: EIF2 signalling.

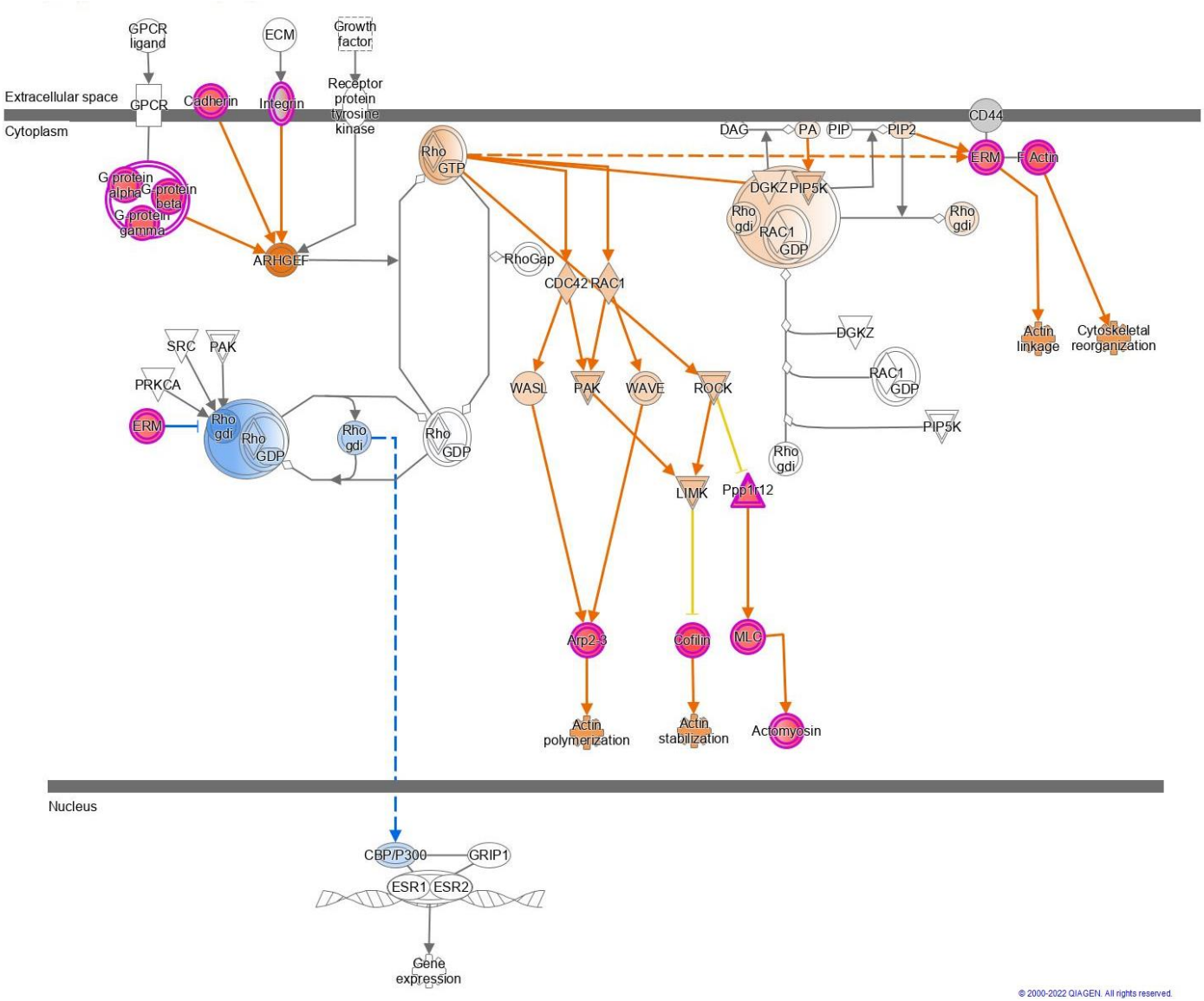

Figure 8: Rho-GDI signalling.

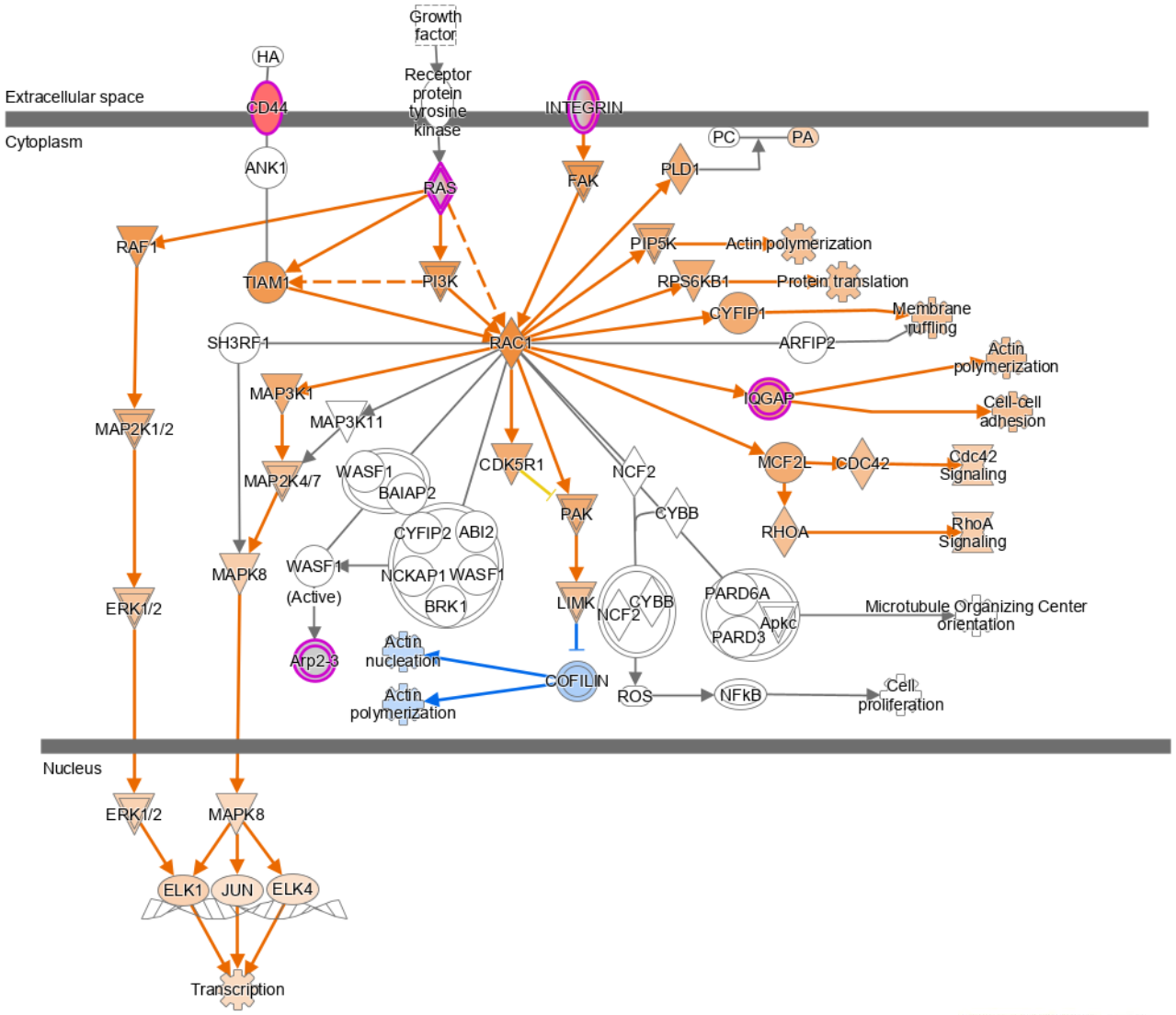

Figure 9: Rac signalling.

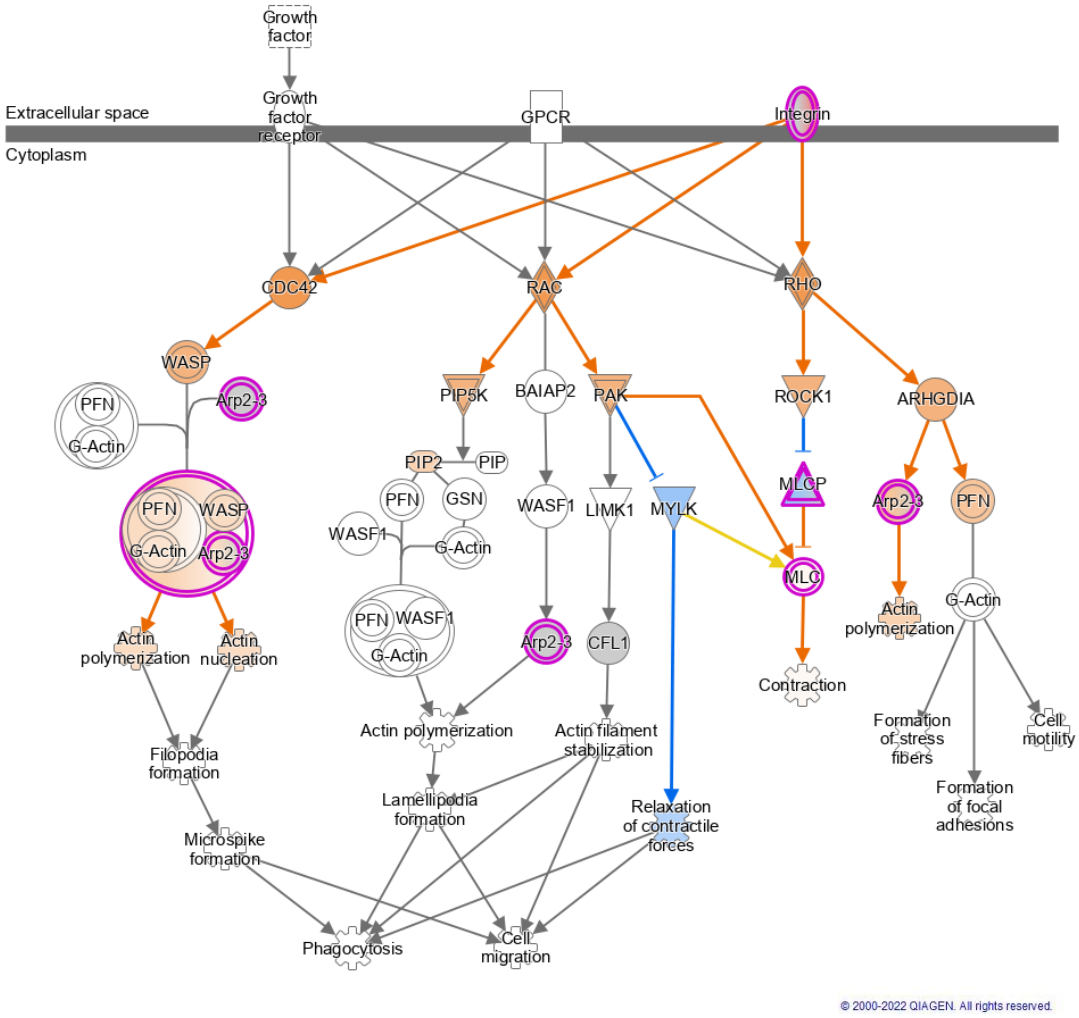

Figure 10: Regulation of actin-based motility by Rho.